

**Uncovering correlates of protection of attenuated *Francisella tularensis* vaccines**

by

**Jennifer Bowling**

B.S. Biology, Coastal Carolina University, 2010

M.P.H., University of Pittsburgh, 2016

Submitted to the Graduate Faculty of the  
Graduate School of Public Health in partial fulfillment  
of the requirements for the degree of  
Doctor of Philosophy

University of Pittsburgh

2021

UNIVERSITY OF PITTSBURGH

GRADUATE SCHOOL OF PUBLIC HEALTH

This dissertation was presented

by

**Jennifer Bowling**

It was defended on

August 10, 2021

and approved by

Moses T. Bility, PhD, Assistant Professor, Department of Infectious Diseases and Microbiology,  
Graduate School of Public Health, University of Pittsburgh

Robbie B. Mailliard, PhD, Assistant Professor, Department of Infectious Diseases and  
Microbiology, Graduate School of Public Health, University of Pittsburgh

Joshua T. Mattila, PhD, Assistant Professor, Department of Infectious Diseases and  
Microbiology, Graduate School of Public Health, University of Pittsburgh

Thesis Advisor:

Douglas S. Reed, PhD, Associate Professor, Department of Immunology, School of Medicine,  
University of Pittsburgh

Copyright © by Jennifer Bowling

2021

## Uncovering correlates of protection of attenuated *Francisella tularensis* vaccines

Jennifer Bowling, PhD

University of Pittsburgh, 2021

### Abstract

Tularemia is a severe zoonotic infection caused by the gram-negative bacterium, *Francisella tularensis*. Because of the potential for *F. tularensis* to be weaponized, vaccines and therapeutics are needed. The Live Vaccine Strain (LVS), a type B strain of *F. tularensis*, was developed as a potential vaccine. Though LVS is able to protect non-human primates and humans against low-dose aerosol exposure to a highly virulent *F. tularensis* strain, SchuS4 (S4), it is ineffective against high-dose exposure. Due to the unknown mechanism of attenuation, there are concerns that reversion to virulence or batch variation could affect LVS efficacy. We have demonstrated that type A strain S4-based vaccines with mutations in genes encoding metabolic enzymes (S4 $\Delta$ aroD and S4 $\Delta$ guaBA) produce a range of protective efficacy (75% and 50%, respectively) against respiratory challenge with wild type S4 in rabbit model. The mechanisms by which these vaccines provide protection are currently unclear. We have assessed several factors that can influence the interpretation of *F. tularensis* studies, the role of persistence and dissemination on vaccine efficacy of LVS, S4 $\Delta$ aroD, and S4 $\Delta$ guaBA, and the immune response following vaccination. We have demonstrated sex, growth medium used for challenge material, vaccine schedule, and strain selection are factors that can influence vaccine efficacy studies. S4 $\Delta$ aroD was able to disseminate to the spleen, while LVS and S4 $\Delta$ guaBA were not, though S4 $\Delta$ guaBA persisted in the lung the longest. Microarray analysis of lung, liver, and spleen tissue

of S4 infected rabbits show extensive immune suppression, which is consistent with S4 infection in other animal models. In addition to immune suppression, pathways involved in wound healing were suppressed. Cell death pathways, including the inflammasome, were not upregulated following exposure to attenuated *F. tularensis* strains. These data demonstrate that persistence and dissemination are an important factor in vaccine efficacy while inflammasome activation is not. This work will benefit public health by contributing to the knowledge of immune correlates of protection and rational vaccine design to protect against *F. tularensis* and other intracellular bacteria.

## Table of Contents

Preface.....	xix
1.0 Introduction.....	1
1.1 <i>F. tularensis</i> .....	2
1.1.1 Epidemiology .....	2
1.1.2 Tularemia.....	3
1.1.2.1 <i>F. tularensis</i> life cycle.....	5
1.1.2.2 <i>F. tularensis</i> actively suppresses host immune response .....	5
1.1.3 Current state of vaccine development .....	8
1.1.4 Potential mechanisms of protection.....	10
1.1.4.1 Early innate immune response .....	10
1.1.4.2 B cells and antibody response.....	11
1.1.4.3 T cells .....	12
1.2 Animal models are vital for <i>F. tularensis</i> vaccine development.....	14
1.2.1 FDA Animal Rule.....	14
1.2.2 Disease in humans .....	15
1.2.3 Non-human primates .....	16
1.2.3.1 African green monkey ( <i>Chlorocebus aethiops</i> ).....	16
1.2.3.2 Rhesus macaque ( <i>Macaca mulatta</i> ) .....	17
1.2.3.3 Marmoset ( <i>Callithrix jacchus</i> ) .....	18
1.2.3.4 Cynomolgus macaque ( <i>Macaca fascicularis</i> ).....	18
1.2.4 Small animal models .....	19

1.2.4.1 Mice.....	19
1.2.4.2 Rats.....	20
1.2.5 Large animal models.....	21
1.2.5.1 Rabbits.....	21
1.3 Factors affecting vaccine efficacy.....	22
1.3.1 Sexual dimorphism can affect the immune response.....	22
1.3.2 Growth conditions of challenge material alter protein expression.....	23
1.3.3 Strain selection and gene mutations.....	24
1.3.3.1 LVS.....	25
1.3.3.2 S4 $\Delta$ aroD.....	26
1.3.3.3 S4 $\Delta$ guaBA.....	27
1.3.3.4 S4 $\Delta$ clpB.....	27
1.3.4 Dissemination and persistence.....	28
1.3.5 Inflammasome activation.....	30
2.0 Hypothesis and Specific Aims.....	33
2.1 Aim 1.....	34
2.1.1 Aim 1a.....	35
2.1.2 Aim 1b.....	35
2.1.3 Aim 1c.....	35
2.2 Aim 2.....	36
2.2.1 Aim 2a.....	37
2.2.2 Aim 2b.....	37
2.2.3 Aim 2c.....	37

<b>2.3 Aim 3.....</b>	<b>38</b>
<b>2.3.1 Aim 3a .....</b>	<b>38</b>
<b>2.3.2 Aim 3b .....</b>	<b>38</b>
<b>3.0 Materials and Methods.....</b>	<b>40</b>
<b>3.1 Biosafety and regulatory information .....</b>	<b>40</b>
<b>3.2 Animals .....</b>	<b>40</b>
<b>3.2.1 Vaccine efficacy studies .....</b>	<b>41</b>
<b>3.2.2 Dissemination studies.....</b>	<b>41</b>
<b>3.2.3 Clinical observations.....</b>	<b>42</b>
<b>3.2.4 Necropsy .....</b>	<b>43</b>
<b>3.3 Bacteria.....</b>	<b>43</b>
<b>3.3.1 Challenge strain.....</b>	<b>43</b>
<b>3.3.2 Vaccine strains.....</b>	<b>44</b>
<b>3.4 Aerosol exposures .....</b>	<b>45</b>
<b>3.5 Laboratory Tests: ESR, CBCs, and chemistries.....</b>	<b>45</b>
<b>3.6 Tissue titers .....</b>	<b>46</b>
<b>3.7 Hematoxylin and eosin staining .....</b>	<b>46</b>
<b>3.8 Lung space analysis .....</b>	<b>47</b>
<b>3.9 Gene expression .....</b>	<b>47</b>
<b>3.9.1 RNA extraction.....</b>	<b>47</b>
<b>3.9.2 Microarray.....</b>	<b>48</b>
<b>3.9.3 cDNA synthesis for PCR.....</b>	<b>49</b>
<b>3.9.4 PCR .....</b>	<b>49</b>

3.10 ELISAs.....	51
3.11 Statistical analysis.....	51
<b>4.0 Results .....</b>	<b>53</b>
<b>4.1 Aim 1.....</b>	<b>53</b>
<b>4.1.1 Aim 1a .....</b>	<b>53</b>
<b>4.1.1.1 Sex does not play a significant role in primary S4 infection.....</b>	<b>53</b>
<b>4.1.1.2 Sex is not a significant factor for vaccine efficacy of S4<math>\Delta</math>aroD.....</b>	<b>58</b>
<b>4.1.1.3 Sex is not a significant factor for vaccine efficacy for LVS .....</b>	<b>66</b>
<b>4.1.2 Aim 1b .....</b>	<b>70</b>
<b>4.1.2.1 Growth conditions for challenge material affect vaccine efficacy.....</b>	<b>70</b>
<b>4.1.3 Aim 1c.....</b>	<b>76</b>
<b>4.1.3.1 S4<math>\Delta</math>aroD protects better than other attenuated <i>F. tularensis</i> strains</b>	<b>76</b>
<b>4.2 Aim 2.....</b>	<b>89</b>
<b>4.2.1 Aim 2a .....</b>	<b>89</b>
<b>4.2.1.1 Virulent S4 does not result in leukocyte expansion despite induction of inflammatory processes .....</b>	<b>89</b>
<b>4.2.1.2 Virulent S4 infection causes massive hemorrhaging and necrosis in the lung .....</b>	<b>97</b>
<b>4.2.1.3 Virulent S4 disseminates rapidly from the primary site of infection to the liver and spleen .....</b>	<b>107</b>
<b>4.2.2 Aim 2b .....</b>	<b>113</b>
<b>4.2.2.1 S4<math>\Delta</math>guaBA results in a more severe clinical presentation compared to LVS and S4<math>\Delta</math>aroD.....</b>	<b>113</b>

4.2.3 Aim 2c.....	122
4.2.3.1 S4 $\Delta$ aroD is able to disseminate from the lungs to a secondary site of infection .....	122
4.3 Aim 3.....	135
4.3.1 Aim 3a .....	135
4.3.1.1 Lungs exhibit limited alterations in gene expression during early infection .....	135
4.3.1.2 Limited alteration of gene expression in the liver of S4 infected rabbits.....	141
4.3.1.3 Spleen exhibits upregulation of immune genes during virulent S4 infection .....	145
4.3.1.4 NZW rabbits recapitulate widespread immune suppression observed in other animal models .....	149
4.3.1.5 Death of S4 infected rabbits is not a result of a cytokine storm event .....	154
4.3.1.6 Virulent S4 infection results in upregulation of damaging inflammatory pathways and downregulation of wound healing pathways	160
4.3.2 Aim 3b .....	167
4.3.2.1 Cell death pathways are not activated by attenuated <i>F. tularensis</i> strains.....	167
4.3.2.2 Protective cytokines induced by vaccine strains .....	170
5.0 Discussion.....	172
5.1 Future directions .....	178

<b>5.2 Public health significance.....</b>	<b>180</b>
<b>5.2.1 Bioterrorism defense.....</b>	<b>180</b>
<b>5.2.2 Vaccine development .....</b>	<b>181</b>
<b>Appendix A Glossary and Abbreviations .....</b>	<b>183</b>
<b>Appendix B Supplementary Figures and Tables .....</b>	<b>187</b>
<b>Appendix B.1 Aim 2 .....</b>	<b>187</b>
<b>Appendix B.1.1 Aim 2a .....</b>	<b>187</b>
<b>Appendix B.1.2 Aim 2b.....</b>	<b>192</b>
<b>Appendix B.1.3 Aim 2c .....</b>	<b>193</b>
<b>Appendix B.2 Aim 3 .....</b>	<b>194</b>
<b>Appendix B.2.1 Aim 3a .....</b>	<b>194</b>
<b>Bibliography .....</b>	<b>227</b>

## List of Tables

<b>Table 1. Clinical scoring criteria for S4 infected NZW rabbits.....</b>	<b>42</b>
<b>Table 2. Primer sequences for gene targets in NZW rabbits.....</b>	<b>50</b>
<b>Table 3. Mixed effects analysis between sexes following challenge of naïve rabbits .....</b>	<b>55</b>
<b>Table 4. Mixed effects analysis between sexes following vaccination of naïve rabbits with S4<math>\Delta</math>aroD .....</b>	<b>60</b>
<b>Table 5. Mixed effects analysis between sexes following challenge of S4<math>\Delta</math>aroD vaccinated rabbits .....</b>	<b>63</b>
<b>Table 6. Mixed effects analysis between sexes following vaccination of naïve rabbits with LVS.....</b>	<b>66</b>
<b>Table 7. Mixed effects analysis between sexes following challenge of LVS vaccinated rabbits .....</b>	<b>69</b>
<b>Table 8. Mixed effects analysis between LVS vaccinated rabbits challenged with S4 grown in MHb or BHI.....</b>	<b>73</b>
<b>Table 9. Mixed effects analysis between S4<math>\Delta</math>aroD and S4<math>\Delta</math>guaBA vaccinated rabbits.....</b>	<b>82</b>
<b>Table 10. Mixed effects analysis between S4<math>\Delta</math>aroD and S4<math>\Delta</math>clpB vaccinated rabbits.....</b>	<b>87</b>
<b>Table 11. Mixed effects modeling of vaccine strains over time.....</b>	<b>118</b>
<b>Table 12. Biological class of DEGs in the lung.....</b>	<b>139</b>
<b>Table 13. Biological class of DEGs in the liver.....</b>	<b>143</b>
<b>Table 14. Biological class of DEGs in the spleen.....</b>	<b>147</b>
<b>Table 15. Top 10 upregulated and downregulated genes at 3 DPE in the lung .....</b>	<b>163</b>
<b>Table 16. Predicted activation states in the lungs .....</b>	<b>166</b>

Appendix Table 1. Dunn’s multiple comparison of lung titers for each lobe compared to baseline.....	190
Appendix Table 2. Tukey’s multiple comparison of clinical signs for vaccine strains over time.....	192
Appendix Table 3. Kruskal Wallis comparison of tissue titers between vaccine groups over time.....	193
Appendix Table 4. Top 10 upregulated and downregulated genes at 5 DPE in the lung...	198
Appendix Table 5. GO analysis of lung at 3 DPE .....	199
Appendix Table 6. GO analysis of lung 5 DPE .....	200
Appendix Table 7. Predicted activation states in the lung tissue of S4 infected rabbits ....	203
Appendix Table 8. Top 10 upregulated and downregulated genes at 3 DPE in the liver ..	207
Appendix Table 9. Top 10 upregulated and downregulated genes at 5 DPE in the liver ..	208
Appendix Table 10. GO analysis of liver at 3 DPE .....	209
Appendix Table 11. GO analysis of liver at 5 DPE.....	210
Appendix Table 12. Predicted activation states in the liver tissue of S4 infected rabbits..	213
Appendix Table 13. Top 10 upregulated and downregulated genes at 3 DPE in the spleen .....	217
Appendix Table 14. Top 10 upregulated and downregulated genes at 5 DPE in the spleen .....	218
Appendix Table 15. GO analysis of spleen at 3 DPE .....	219
Appendix Table 16. GO analysis of spleen at 5 DPE.....	220
Appendix Table 17. Predicted activation states in the spleen.....	223
Appendix Table 18. Fold change of immune genes in the lung .....	226

## List of Figures

<b>Figure 1. Sex does not result in differences in SchuS4 clinical disease in naïve NZW rabbits</b>	
.....	<b>54</b>
<b>Figure 2. No differences seen in in vitro diagnostic blood tests between sexes in naïve rabbits</b>	
.....	<b>57</b>
<b>Figure 3. S4<math>\Delta</math>aroD vaccination of rabbits results in different clinical signs between males and females</b>	
.....	<b>59</b>
<b>Figure 4. Sex does not play a significant role in S4<math>\Delta</math>aroD vaccine efficacy following SchuS4 challenge</b>	
.....	<b>62</b>
<b>Figure 5. No differences seen in in vitro diagnostic blood tests between sexes in vaccinated rabbits</b>	
.....	<b>65</b>
<b>Figure 6. Sex does not affect LVS vaccine efficacy in challenge NZW rabbits</b>	
.....	<b>68</b>
<b>Figure 7. Rabbits exhibit clinical signs of more severe disease when challenged with S4 grown in BHI</b>	
.....	<b>72</b>
<b>Figure 8. MHb S4 challenged rabbits exhibit less severe loss of lymphocytes and increase in ESR compared to BHI S4 challenged rabbits</b>	
.....	<b>75</b>
<b>Figure 9. Prime/boost vaccination resulted in higher <i>F. tularensis</i> specific antibodies</b>	
.....	<b>78</b>
<b>Figure 10. S4<math>\Delta</math>aroD vaccinated rabbits exhibit better vaccine efficacy compared to S4<math>\Delta</math>guaBA vaccinated rabbits</b>	
.....	<b>81</b>
<b>Figure 11. No differences observed in clinical blood parameters during challenge between vaccine strains</b>	
.....	<b>83</b>

<b>Figure 12. S4<math>\Delta</math>aroD vaccinated rabbits exhibit better vaccine efficacy compared to S4<math>\Delta</math>clpB vaccinated rabbits .....</b>	<b>86</b>
<b>Figure 13. No differences observed in blood parameters during challenge between S4<math>\Delta</math>aroD and S4<math>\Delta</math>clpB vaccinated rabbits .....</b>	<b>88</b>
<b>Figure 14. Time to death is dependent on challenge dose .....</b>	<b>89</b>
<b>Figure 15. NZW rabbits begin to exhibit clinical symptoms of infection at 3 DPE .....</b>	<b>92</b>
<b>Figure 16. Uncontrolled infection results in a decrease of total lymphocytes .....</b>	<b>93</b>
<b>Figure 17. Loss of RBCs suggests internal bleeding .....</b>	<b>95</b>
<b>Figure 18. NZW rabbits infected with virulent S4 exhibit thrombocytopenia .....</b>	<b>96</b>
<b>Figure 19. Uncontrolled infection leads to extensive pulmonary hemorrhaging .....</b>	<b>98</b>
<b>Figure 20. Uncontrolled virulent S4 infection leads to consolidation of alveolar spaces and necrotizing pneumonia .....</b>	<b>99</b>
<b>Figure 21. S4 infection results in decreased alveolar space .....</b>	<b>100</b>
<b>Figure 22. Virulent S4 infection results in visible bacterial foci on the liver .....</b>	<b>102</b>
<b>Figure 23. Necrotic lesions were found in the liver by the time the animal reached the moribund period .....</b>	<b>103</b>
<b>Figure 24. S4 infection results in splenomegaly with visible bacterial foci.....</b>	<b>105</b>
<b>Figure 25. S4 infection results in necrotizing splenitis .....</b>	<b>106</b>
<b>Figure 26. <i>F. tularensis</i> spreads throughout lung lobes as infection progresses .....</b>	<b>108</b>
<b>Figure 27. Bacteria disseminates from the lung to the spleen and liver at 3 DPE .....</b>	<b>111</b>
<b>Figure 28. Bacteria is not detected in the blood until animals become moribund.....</b>	<b>112</b>
<b>Figure 29. Rabbits received aerosolized vaccine doses greater than 108 CFU .....</b>	<b>114</b>

<b>Figure 30. S4ΔguaBA is more clinical severe than either LVS or S4ΔaroD based on clinical signs .....</b>	<b>117</b>
<b>Figure 31. Characteristic loss of lymphocytes at 3 DPE is seen with all vaccine strains....</b>	<b>121</b>
<b>Figure 32. S4ΔguaBA results in hemorrhage and bacterial lesions .....</b>	<b>123</b>
<b>Figure 33. S4ΔaroD and S4ΔguaBA result in severe pneumonia .....</b>	<b>124</b>
<b>Figure 34. Attenuated <i>F. tularensis</i> strains result in decreased alveolar space.....</b>	<b>125</b>
<b>Figure 35. No macroscopic changes in liver with any vaccine strain.....</b>	<b>126</b>
<b>Figure 36. S4ΔaroD infected rabbits exhibit more severe leukocyte infiltration and hepatic cell death .....</b>	<b>127</b>
<b>Figure 37. S4ΔaroD and S4ΔguaBA exposed rabbits exhibit splenomegaly .....</b>	<b>129</b>
<b>Figure 38. S4ΔaroD and S4ΔguaBA exposed rabbits exhibit disruption in splenic organization.....</b>	<b>130</b>
<b>Figure 39. S4ΔguaBA replicates to high titers and can be detected in the lung longer than LVS and S4ΔaroD.....</b>	<b>132</b>
<b>Figure 40. S4ΔaroD is able to escape the lung and spread to the spleen but not the liver.</b>	<b>134</b>
<b>Figure 41. Number of DEGs in lung tissue over time.....</b>	<b>137</b>
<b>Figure 42. Top 10 downregulated and upregulated DEG in lung at 3 DPE.....</b>	<b>138</b>
<b>Figure 43. Gene ontology enrichment analysis of lung tissue at 3 and 5 DPE compared to baseline.....</b>	<b>140</b>
<b>Figure 44. Number of DEGs in liver tissue over time.....</b>	<b>142</b>
<b>Figure 45. Gene ontology enrichment analysis of liver tissue.....</b>	<b>144</b>
<b>Figure 46. Number of DEGs in spleen tissue over time.....</b>	<b>146</b>
<b>Figure 47. Gene ontology enrichment analysis of spleen tissue.....</b>	<b>148</b>

<b>Figure 48. Appropriate acute phase reactant response produced by the liver at 3 DPE ....</b>	<b>152</b>
<b>Figure 49. No upregulation in genes related to pattern recognition pathways or interferon response in the lung at 3DPE .....</b>	<b>153</b>
<b>Figure 50. No evidence of pyroptotic septic event during S4 infection .....</b>	<b>157</b>
<b>Figure 51. No significant changes in apoptic pathway in the lung .....</b>	<b>158</b>
<b>Figure 52. Necrosis and necroptosis pathways are not upregulated in the lung of S4 infected rabbits .....</b>	<b>159</b>
<b>Figure 53. The top 10 genes that trended downwards or upwards over time in the lung..</b>	<b>164</b>
<b>Figure 54. Pathway analysis of DEGs that shared a trend over time in the lungs of S4 infected NZW rabbits .....</b>	<b>165</b>
<b>Figure 55. IFN<math>\beta</math> gene expression differs between vaccine strains in the lung, liver, and spleen.....</b>	<b>168</b>
<b>Figure 56. STAT1 gene expression correlates with observed vaccine efficacies.....</b>	<b>169</b>
<b>Figure 57. Trend in upregulation of IFN<math>\gamma</math> and CXCL10 in rabbits exposed to attenuated <i>F. tularensis</i> strains.....</b>	<b>171</b>
<b>Appendix Figure 1. No significant differences were observed in alveolar space analysis between technicians .....</b>	<b>188</b>
<b>Appendix Figure 2. Infection primarily starts in lower lungs and then spreads to upper lungs .....</b>	<b>189</b>
<b>Appendix Figure 3. Titers taken at necropsy corroborate bacterial growth in tissues seen from frozen tissue pieces .....</b>	<b>191</b>
<b>Appendix Figure 4. QC and PCA plot for lung gene expression of S4 infected NZW rabbits .....</b>	<b>196</b>

<b>Appendix Figure 5. Hierarchical clustering reveals significant differences in gene expression at different times post infection .....</b>	<b>197</b>
<b>Appendix Figure 6. Pathway analysis of DEGs in the lung at 3 DPE .....</b>	<b>201</b>
<b>Appendix Figure 7. Pathway analysis of DEGs in the lung at 5 DPE .....</b>	<b>202</b>
<b>Appendix Figure 8. QC and PCA plot for liver gene expression of S4 infected NZW rabbits .....</b>	<b>205</b>
<b>Appendix Figure 9. Significant differences in gene expression at different times post infection.....</b>	<b>206</b>
<b>Appendix Figure 10. Pathway analysis of DEGs in the liver at 3 DPE.....</b>	<b>211</b>
<b>Appendix Figure 11. Pathway analysis of DEGs in the liver at 5 DPE.....</b>	<b>212</b>
<b>Appendix Figure 12. QC and PCA plot for spleen gene expression of S4 infected NZW rabbits .....</b>	<b>215</b>
<b>Appendix Figure 13. Significant differences in gene expression at different times post infection.....</b>	<b>216</b>
<b>Appendix Figure 14. Pathway analysis of DEGs in the spleen at 3 DPE.....</b>	<b>221</b>
<b>Appendix Figure 15. Pathway analysis of DEGs in the spleen at 5 DPE.....</b>	<b>222</b>
<b>Appendix Figure 16. Gene expression of PRR pathways in the liver .....</b>	<b>224</b>
<b>Appendix Figure 17. Interferon and HMGB1 signaling gene expression in the spleen .....</b>	<b>225</b>

## Preface

The journey I have been on since the beginning of my doctoral work has been filled with many ups and downs. From learning to balance work and life, overcoming personal obstacles, and living through a global pandemic, I have grown a great deal not only as a scientist, but as a person. This journey would not have been possible without the mentorship and support of my lab and friends.

I would whole-heartedly like to thank Dr. Douglas Reed for being my mentor throughout this endeavor. I have been with Dr. Reed for seven years, and it amazes me how the time feels like it flew by. I will always remember when he offered me a position as a PhD student in his lab after I successfully completed my Master's thesis defense.

I would especially like to thank the members my dissertation committee, Drs. Moses Bility, Robbie Mailliard, Joshua Mattila, and Douglas Reed, for their time and consideration of my work. I chose several members following my experience with them on the comprehensive exam, which was emotionally and mentally challenging, but I appreciated the time they took to prepare for the exam and the choice of questions to challenge me. It definitely left a scar, Dr. Mattila, but one I can look back on and appreciate.

Completion of my thesis would not have been possible without the support and friendship of the wonderful members of my lab. I want to give a special thank you to Katie Willett, the lone lab tech that was hired after I first joined the Reed lab. She has been invaluable for her help with the rabbit work and avid emotional support. I would also like to thank the former and current members of the Reed lab: Morgan Midget, Jeneveve Lundy, Tabitha Schmer, Connor Williams, Amanda Laughlin, Henry Ma, Emily Olsen, Sohaib Khan, Naveen Suresh Babu, Summer Xia,

Jennifer Burwinkle, and Megan Beary. Mentoring new lab members helped keep my love of the lab alive as I struggled through my doctoral work. I hope they know how much I value all of them and the work they have done to make the Reed lab function efficiently.

Finally, I would like to thank my friends and family. My friends have supported me throughout the emotional journey I have been on during my doctoral work. My family always believed I could do more and have always been proud of me as I have completed my academic endeavors. I want to give a special thank you to Thomas Jageman. Though he entered my life at the end of my academic journey, his love and support helped get me out of the pandemic isolation funk and was crucial to helping me complete my dissertation.

## 1.0 Introduction

*F. tularensis* is a pathogen able to cause severe disease in humans and has been developed as a potential agent for use in biological warfare (1). While the Biological Weapons Convention prohibits the development of biological weapons, ongoing efforts in defensive biological research remain strong (2). The goal of this defense research is to develop therapeutics and vaccines to protect against a potential bioterrorism attack. Vaccination is one of the most cost-effective public health interventions and is largely responsible for the reduction in infectious diseases, such as polio and measles (3). The benefits of developing vaccines against biological weapons are not so obvious due to the low risk and smaller affected population of a biowarfare attack in the U.S. Nevertheless, as the “anthrax letters” demonstrated, a small number of infected individuals can have a large impact on the country in regards to health care, environmental, and psychological costs. Effective vaccines against bioterrorism agents are essential in the deterrence and management of an attack (3).

A vaccine is composed of an agent that resembles the target infectious disease to stimulate the body’s immune system to replicate this process. Development of acquired immunity is dependent on both the innate and adaptive immune response of the host. The innate immune response recognizes foreign microbes and mounts a non-specific immune response that does not result in long-lasting immunity against the pathogen. The innate immune response is necessary for activation of the adaptive immune response. The adaptive immune response provides a more targeted response to the invading microbe and results in immunological memory. To date, there is no FDA approved vaccine available to protect against a potential bioterrorism attack with *F. tularensis*.

## 1.1 *F. tularensis*

### 1.1.1 Epidemiology

*F. tularensis* is a small, pleomorphic, gram-negative coccobacillus responsible for the zoonotic disease tularemia. Edward Francis first described the epidemiology and clinical symptoms of tularemia in humans. The bacterium was isolated from ground squirrels in Tulare County, California in 1911. There are three subspecies of *F. tularensis*: *tularensis*, *holarctica*, and *mediasiatica*. *Francisella novicida* (*F. novicida*) was formally classified as a *F. tularensis* subspecies based on a 99.8% sequence identity in 16s ribosomal DNA but has recently been reclassified as its own species due to distinct phenotypic traits (4). *F. tularensis* subsp. *tularensis* is highly virulent, is the dominant species found in the United States (U.S.), and can be further broken down into four genotypes with differing rates of infection, severity of disease, and distribution (5). As few as 10 colony-forming units (CFU) are sufficient to cause disease in humans. *F. tularensis* subsp. *holarctica* is less virulent than subspecies *tularensis* and is prevalent in the U.S. and Europe (5). *F. tularensis* subsp. *mediasiatica* and *F. novicida* are rarely associated with human disease and are of little clinical importance.

In the U.S., tularemia has been reported in all states except Hawaii but is mainly found in the Midwest and Southwest. The highest prevalence occurs in Arkansas, Illinois, Missouri, Texas, Oklahoma, Virginia, Tennessee, and the New England region. The U.S. has had an average of 257 cases of tularemia per year from 2015 to 2019, which is 1.5 times higher than the average number of cases the previous five years. The most recent outbreak of tularemia in the U.S. was in Colorado and resulted in 175 cases in nine months with 48 hospitalizations and one death (6). The bacterium is associated with a terrestrial and aquatic cycle and is able to infect

more than 250 mammals, birds, cold blood animals, and arthropods (7). Animals associated with the terrestrial cycle often succumb to disease. Rodents and hares are the most important reservoir as circulation continues in these reservoirs in endemic areas. Asymptomatic carrier animals can spread disease to other animals through arthropod vectors, such a ticks, flies, and mosquitoes. Ticks are extremely important for persistence in nature as they can be lifetime carriers of the bacteria and spread the bacteria to mammals through bites or feces, thus serving as both a reservoir and vector. *F. tularensis holarctica* is primarily circulated through the aquatic cycle. Water rodents, such as beavers, muskrats, and voles, carry the bacteria and infect surface waters. *F. tularensis* can survive for years in external environment conditions. Humans and pets are incidental hosts, and high numbers of infected rodents often correlate with high rates of cases in humans. Disease incidence is highest in foresters, hikers, hunters, butchers, farmers, veterinarians, and lab workers. To date, there has been no person-to-person transmission of *F. tularensis*.

### **1.1.2 Tularemia**

Up to 19% of *F. tularensis* infected humans can be asymptomatic depending on subspecies (8). In those that do exhibit symptoms, patients exhibit flu-like symptoms after a three-to-five-day incubation period (9, 10). Febrile illness can progress to systemic dissemination and death in up to 30% of cases without treatment (11). Dr. Edward Francis was the first person to recognize that symptoms vary depending on virulence, mode of entry and exposed dose of the bacterium, as well as individual immunity. Oropharyngeal tularemia is more common in areas with the aquatic cycle of *F. tularensis* and is characterized by ulcers on the pharynx, tonsils, and soft palette. Humans contract the disease by eating or drinking contaminated food or water. In

2016, a small outbreak of oropharyngeal tularemia occurred in Germany due to grape must that had been pressed accidentally along with *F. tularensis* infected mice (12). Ulceroglandular tularemia is the most common form of tularemia and is characterized by cutaneous ulcers. This is most often caused by blood-sucking arthropods or handling of infected animal carcasses. Pneumonic tularemia is characterized by hemorrhagic inflammation of the airways and systemic dissemination, with the spleen and liver being the primary location of pathological changes. “Lawnmower tularemia” is a pulmonary tularemia infection associated with aerosolization of bacteria after mowing over rabbit carcasses or rabbit dens (13). Typhoidal tularemia is used to describe *F. tularensis* infections that do not follow any of the previously described pathologies of disease (14). Of all clinical disease presentations, pneumonic is the most severe form. All disease presentations can progress to pneumonic forms of disease.

Fortunately, *F. tularensis* infection is treatable with antibiotics, which can reduce fatalities to 2%. The antibiotics most used to treatment are streptomycin and gentamicin, though doxycycline and chloramphenicol can be used (10, 15, 16). Antibiotic treatment must be initiated early during infection, and the full course of antibiotics must be followed as early antibiotic termination can result in relapse of infection. The long treatment course may not be feasible in all cases as the approved antibiotics are often nephrotoxic (17). Early diagnosis of *F. tularensis* infection is important for starting antibiotic treatment early during infection and can be achieved via blood tests, cultures, or PCR in conjunction with clinical symptoms. Rapid diagnostic tests are not widely available, so detection often relies on recognition by public health authorities. The low frequency of disease and lack of widely available rapid diagnostics tests can delay diagnosis of *F. tularensis* infection, and thus affect the success of antibiotic therapy.

### **1.1.2.1 *F. tularensis* life cycle**

*F. tularensis* is an intracellular pathogen capable of infecting a broad range of cell types, including macrophages, dendritic cells, epithelial cells, hepatocytes, and fibroblasts (18). The receptor used for entry depends on opsonization conditions. Non-opsonized bacteria have been shown to use the mannose receptor in human and mouse macrophages, though additional receptors are also thought to be involved as well (19-21). Serum opsonized bacteria mostly use complement receptor 3 (CR3) in human and mouse macrophages, but the scavenger receptor A, FC $\gamma$  receptors, nucleolin, and lung surfactant protein A have also been implicated in bacterial uptake. (19, 20, 22-24). FC $\gamma$  receptors are the primary receptors for antibody opsonized *F. tularensis* (19, 21). Binding of *F. tularensis* to host cell receptors initiates asymmetrical looping phagocytosis, allowing entry into the host cell (25). The *Francisella* containing phagosome (FCP) matures into a late endosome but does not bind with lysosomes. Opsonized *F. tularensis* results in non-acidified FCPs while non-opsonized *F. tularensis* results in acidified FCPs, which can affect efficiency of phagosomal escape. For non-opsonized bacteria, acidification of the FCP occurs within 15 to 30 minutes of uptake and subsequent phagosomal escape occurs within one hour (26, 27). For opsonized *F. tularensis*, phagosomal escape occurs two to four hours after uptake (28). Phagosomal escape is mediated by a type VI secretion like system, which is also necessary for bacterial replication (27, 29-37). Intracellular replication of *F. tularensis* in the cytoplasm induces apoptosis of the infected cell within 24 hours (38, 39). The released *F. tularensis* continue the infection cycle by infecting new cells.

### **1.1.2.2 *F. tularensis* actively suppresses host immune response**

*F. tularensis* evades the host immune response through a variety of means. CR3 and the mannose receptor are the primary receptors used for entry of opsonized and non-opsonized *F.*

*tularensis*; neither receptors activate pro-inflammatory signaling cascades (40). *F. tularensis* possesses a lipopolysaccharide (LPS) that is not biologically active compared to *E. coli* (41). This is largely due to the tetra-acylation of the lipid A with longer acyl chains and the absence of phosphates at the 1' and 4' which affect the overall charge and prevent recognition by the toll-like receptor 4 (TLR 4) receptor (42). The O-antigen of LPS is also important for subverting host immune responses. Mutations in the O-antigen have been shown to induce early cell death in human macrophages and *F. tularensis* mutants lacking the O-antigen are significantly more sensitive to complement lysis compared to wildtype (43). Analysis of *F. tularensis* transposon mutants indicate the O-antigen is also important in avoiding xenophagic recognition and clearance (44). *F. tularensis* lipoproteins are able to engage TLR 2 receptors, resulting in stimulation of proinflammatory cytokines (45-47). *F. tularensis* actively dampens this proinflammatory response and can antagonize activation by other stimulants. This is largely thought to be due to crosstalk between CR3 and TLR 2 receptors resulting in blockade of NFκB signaling (48, 49). As early production of pro-inflammatory cytokines is critical for initial control of infection, this delay in inflammation allows for unrestricted replication of *F. tularensis* for the first few days of infection.

Many proteins necessary for phagosomal escape and replication are clustered in a 30 kilobase (kb) region within *F. tularensis* circular DNA, known as the *Francisella* pathogenicity island (FPI) (23, 30, 31). Virulent strains of *F. tularensis* contain two copies of the FPI, while *F. novicida* only contains one copy. The FPI encodes several proteins that comprise the Type VI secretion system used during phagosomal escape. Mutations in any of the genes encoded in the FPI results in attenuation of the bacterium, indicating the FPI is an important mediator of *F. tularensis* virulence and host immune evasion.

Since *F. tularensis* infects many cells important for host immune response, it has developed strategies to subvert innate immune mechanisms within these cells. *F. tularensis* is able to evade host reactive oxygen species (ROS) by disrupting NADPH oxidase assembly at the phagosomal membrane in neutrophils (33, 50, 51). *F. tularensis* also produces proteins that can directly neutralize ROS, such as catalase and superoxide dismutase (52, 53). Dendritic cells (DCs) are necessary for antigen presentation and are used as a replicative niche for *F. tularensis*. *F. tularensis* prevents DC activation and their production of TNF $\alpha$  and IL-6 (54). *F. tularensis* infection also stimulates secretion of TGF $\beta$ , an anti-inflammatory cytokine, through upregulation of MHC II and CD86.

*F. tularensis* also utilizes nutritional virulence, which manipulates the host nutrient supply to support the robust replication that occurs in the cytoplasm. The *F. tularensis* genome encodes for 15 ATP-binding cassette (ABC)-type transporters which are predicted to participate in amino acid and ion uptake (55). Mutations in ABC transporters have been identified in attenuated mutants, indicating defects in nutrient uptake systems can alter virulence of *F. tularensis* (56, 57). Cysteine is a necessary amino acid for *F. tularensis* growth and serves as a carbon and energy source (58). *F. tularensis* encodes proteins to exploit host glutathione, which is a primary source of cysteine in the cytoplasm of eukaryotic cells. Glutathione plays a major role in cell homeostasis and its deficiency has been associated with severe disease (59). *F. tularensis* induces autophagy through an Atg-5 independent pathway to harvest amino acids and bulk carbon, which is necessary for *F. tularensis* replication (60).

*F. tularensis* has also developed strategies to alter the development of an adaptive immune response. Macrophages infected with *F. tularensis* secrete PGE2 which suppresses host T cell response through inhibition of IL-2 secretion and production of IL-5. This results in

decreased T cell proliferation and a shift to a T helper 2 response (61). PGE2 production also induces ubiquitin dependent MHC II degradation, which would inhibit efficient activation of CD4 T cells. (62). The ability of *F. tularensis* to evade the host immune response has made developing an effective vaccine difficult.

### **1.1.3 Current state of vaccine development**

*F. tularensis* has been studied as a potential biological weapon by Japan, the U.S., and the Union of Soviet Socialist Republics (USSR) (1). During World War II, Japan used human subjects to study the infectivity of *F. tularensis* (63). In the 1950s the U.S. developed weapons capable of dispersing *F. tularensis* aerosol and exposed humans to virulent *F. tularensis* to test therapeutics and vaccines during Operation White Coat(1). The Soviet Union developed *F. tularensis* strains that were resistant to antibiotics and capable of causing disease in vaccinated individuals (1). Despite the disbandment of offensive biological research programs, the threat of potential bioterrorism attacks highlights the need for defensive biological research. In the U.S., *F. tularensis* is classified by the Center for Disease Control (CDC) as a Category A biothreat due to its high infectivity, ease of dissemination, and its ability to cause severe illness. Bioterrorism experts predict the most likely mode of attack would be through aerosolized infectious agents. Thus, the pneumonic form of tularemia is of the most concern. The World Health Organization estimated that 50kg of virulent *F. tularensis* dispersed over a large city would result in an estimated 250,000 infections and 19,000 deaths (64). Estimated costs for such an attack would exceed 5 billion per 100,000 persons exposed (65). Thus, development of vaccines and therapeutics is a long-term goal of defensive bioterrorism research in the U.S.

There are currently no vaccines approved by the Food and Drug Administration (FDA) available against *F. tularensis*, despite ongoing vaccine efforts since the 1940s. Early vaccine attempts utilized killed whole-cell *F. tularensis* which resulted in limited efficacy in human and animal studies with many adverse side effects. The Foshay vaccine was developed by oxidation of virulent *F. tularensis* by nitrous acid and preservation in phenol (66). This vaccine was shown to be less reactogenic when it was tested in humans from 1933 to 1941. Effectiveness could not be determined due to low infection rates in the population. The Foshay vaccine was shown to prevent death, but not illness following challenge in NHPs (67). In mice, the vaccine only offered low levels of protection against highly virulent strains for *F. tularensis*.

Subunit vaccines have not yielded significant protection against challenge with virulent *F. tularensis*. LPS subunit vaccines only provide limited protection against high dose Type A challenge (68-70). Antigens that stimulate an in vitro response in T cells result in poor vaccine efficacy (71). Proteomic analyses of mice, rabbits, and humans infected with *F. tularensis* have failed to identify a common set of antigen targets (72-74). Vaccines utilizing a mixture of outer membrane proteins have been shown to protect against low dose aerosol challenge, suggesting that subunit vaccines remain a viable vaccine design (75).

Live vaccines must strike a balance between attenuation of the pathogen and stimulation of the immune response. Over-attenuation may result in poor immunity, while under-attenuation may fail to reduce virulence. The most well-known vaccine against *F. tularensis* is known as the Live Vaccine Strain (LVS) which was derived from a holarctica strain isolated from Russia. LVS was given to the US in 1956 and further attenuated through multiple passages in mice. The FDA approved LVS as an investigational new drug in the early 1960s. Evaluation in humans shows LVS can protect against high dose subcutaneous and low dose aerosol challenge when given by

scarification. Improved efficacy has been observed when the vaccine is administered by aerosol, but this attenuated strain was still able to cause tularemia in a small subset of volunteers. Additionally, passaging of the bacteria can result in a batch variant that expresses an altered LPS that result in poorer vaccine efficacy. The unknown nature of attenuation, the residual virulence following vaccination, and risk for batch variants resulted in the removal of LVS from use as an investigational new drug. LVS is the most well characterized *F. tularensis* vaccine to date, and thus remains the gold standard when comparing other *F. tularensis* vaccines.

Only one study utilizing a *F. novicida* mutant resulted 80% protection in Fisher 344 rats and cynomolgus macaques against pulmonary tularemia(76). Holarctica mutants can protect against wild type (WT) LVS, but often have variable efficacy against virulent Type B and Type A strains. Tularensis derived mutants can provide low to modest levels of protection against virulent *F. tularensis* strains. Heterologous vaccines have shown limited protection against challenge but development of these vaccines have the same difficulties as subunit vaccines. While the carrier agent would result in a robust immune response, no set of antigens necessary for protection against *F. tularensis* have been identified.

#### **1.1.4 Potential mechanisms of protection**

##### **1.1.4.1 Early innate immune response**

*F. tularensis* is able to overwhelm the host quickly by delaying the host immune response. Increases in cytokines occur in mice starting at 3 days post exposure (DPE), which allows *F. tularensis* to establish high bacterial burdens in key organs (77, 78). The upregulation of cytokines at this time point resembles a cytokine storm associated with severe sepsis. Many studies indicate IFN $\gamma$  and TNF $\alpha$  are vital for combating *F. tularensis* infection (79, 80).

Peripheral blood leukocytes from tularemia patients showed production of IFN $\gamma$ , TNF $\alpha$ , and IL-2 within two weeks of infection (81, 82). In humans infected with ulceroglandular tularemia, there was an increase in expression of genes regulated by IFN $\gamma$  and related to apoptosis as well as downregulation of many genes related to innate and adaptive immune responses (83). In mice, early production of IFN $\gamma$  dictates the course and outcome of *F. tularensis* infection (79, 80, 84). IFN $\gamma$  is produced by natural killer cells, neutrophils, and DCs (85-87). IFN $\gamma$  activates infected macrophages resulting in the production of TNF $\alpha$  and iNOS, an antimicrobial effector molecule important in controlling *F. tularensis* replication (88, 89). Treatment of LVS infected macrophages with IFN $\gamma$  inhibits growth of the bacterium. At sublethal doses, iNOS deficient mice do not survive LVS infection compared to WT mice (90). While DCs and neutrophils play important roles in controlling *F. tularensis* infection, only monocytes are absolutely required for survival. Neutrophil depleted mice experience rapid bacterial growth in the liver, spleen, and lungs while infection was controlled in WT mice (79, 91, 92). Inflammasome activation is also thought to be a key mediator of *F. tularensis* clearance. *F. tularensis* infection has been shown to cause cleavage of IL-1 $\beta$  and IL-18 and to induce host cell death. AIM2, Asc, or caspase-1 knockout (KO) mice exhibited higher bacterial burdens in tissues and higher mortality compared to WT mice (93, 94).

#### **1.1.4.2 B cells and antibody response**

Many vaccines used today induce a B and T cell response that result in the production of protective antibodies. For *F. tularensis*, the ability of passive administration of *F. tularensis* specific antibodies to neutralize infection against infection is unclear due to the differences in animal models, treatment doses and schedules, and bacterial strains used. Despite induction of high levels of IgG, *F. tularensis* antibodies have not been shown to produce life-long protection

as there have been documented cases of reinfection in humans (95, 96). In our lab, assessment of total IgG antibody response to heat killed SchuS4 (S4), a type A strain, corresponds with vaccination status, but not survival, though it can predict time to death. This finding was corroborated by a study in wild caught cottontail rabbits which concluded that antibody titers were similar among subjects regardless of time of death (5). Additionally, proteomic analysis of the human antibody response to natural tularemia infection did not reveal any common antigens that were immunoreactive among all subjects (72, 73). Analysis of the antibody response in mice and rabbits also revealed no common antibodies among subjects, though in each study, several antibody targets were identified with a high incidence (74, 97). Thus, *F. tularensis* antibodies likely play a small and redundant protective mechanism in secondary immunity to *F. tularensis* infection.

C57BL/6J B cell KO mice are slightly defective in immune responses to primary infection, but severely impaired during secondary infection (98, 99). Further reconstitution experiments revealed this defect was due to the lack of B cells and not the lack of *F. tularensis* specific antibodies. The spleen of B cell KO mice reflected a marked neutrophil influx early after LVS challenge, while B cell KO mice rescued with naïve B cells prior to secondary challenge exhibited decreased bacterial titers and neutrophils in the spleen (100). The spleens of B cell KO mice were lacking germinal centers. Taken together, B cells play a more important role in secondary infection rather than primary infection and are linked to controlling bacterial burden and neutrophil recruitment.

#### **1.1.4.3 T cells**

Depletion of both CD4 and CD8 T cells allows for the establishment of a chronic *F. tularensis* infection in mice exposed to sublethal doses of infection (101). This control of

infection has been attributed to a double negative (DN) T cell population (102). CD4, CD8, and DN T cells can produce IFN $\gamma$  and IL-17a (101, 103). Mice treated with neutralizing anti-TNF $\alpha$  or anti-IFN $\gamma$  antibodies during secondary infection were highly susceptible to infection (104). To distinguish the role of these cytokines produced by T cells versus the innate immune response, an *in vitro* co-culture system was developed to measure the ability of LVS-immune T cells to control LVS replication within macrophages. LVS-immune CD4 cells were shown to control LVS replication in an IFN $\gamma$ -dependent, but TNF $\alpha$ -independent manner (105-107). LVS-immune CD8 and DN T cells controlled LVS intramacrophage growth in an IFN $\gamma$ -independent, but TNF $\alpha$ -dependent manner. In secondary *F. tularensis* infection, CD4, CD8, and DN T cells are individually able to clear *F. tularensis* infection in mice (108-110). Full resistance to secondary pulmonary tularemia requires both CD4 and CD8 T cells.

Peripheral blood leukocytes (PBLs) from LVS vaccination and natural infection in humans produced a typical T helper 1 response upon restimulation (81, 111). Assessment of cytokine production in the lung and spleen following vaccination with two strains of LVS showed increases in IFN $\gamma$ , IL-6, TNF $\alpha$ , IL-12, MIP-1 $\alpha$ , MIP-1 $\beta$ , KC, RANTES, and MCP-1 (112). No significant differences were observed in cytokine levels in the lungs between vaccine strains. In the spleen, the more virulent strain of LVS resulted in higher levels of IFN $\gamma$  and MCP 1. Another study assessing cytokines upregulated in the lungs following vaccination identified TNF $\alpha$ , Cox2, IL-1 $\beta$ , iNOS, CXCL1, and MCP-1 (113). Following vaccination of mice, PBLs exhibited increased gene expression for CCR5, IL-18, IL-27, CXCL11, GZMB, and Socs-1 (5). Upon restimulation, PBLs exhibited increased gene expression for IFN $\gamma$ , IL-1ra, MCP-5, and MIG. Genes from the *in vivo* assays did not match *ex vivo* assays, highlighting the difficulty in identifying correlates of protection following *F. tularensis* vaccination. In the study conducted

by Brown et al., key genes that overlapped between the *in vivo* and *ex vivo* assays were CCR5, GZMB, CXCL11, IL-12, IFN $\gamma$ , and CCL5. These studies highlight the difficulty not only in identifying correlates of protection for *F. tularensis*, but also in developing a clinically useful assay. Utilizing tissues to identify if an individual has been successfully vaccinated is unfeasible, and there is a high level of discrepancy in the identification of protective cytokine responses. This difference is likely due to differences in vaccine preparations, vaccine schedule, and animal models used.

## **1.2 Animal models are vital for *F. tularensis* vaccine development**

Vaccine efficacy must be determined for each new candidate vaccine. In human clinical trials, vaccine efficacy is defined as the percentage reduction of disease between unvaccinated and vaccinated individuals, which relies on a certain amount of uncertainty in the infectious disease attack rate. In key animal studies, vaccine efficacy is synonymous with survival in vaccinated animals following challenge with the infectious outcome of interest. Both human and animal studies rely on rigorous study design as there are many factors that can affect vaccine efficacy.

### **1.2.1 FDA Animal Rule**

The Food and Drug Administration Animal Efficacy Rule, termed Animal Rule for short, was authorized by Congress in 2002 following the terrorist attacks on September 11, 2001 to aid in the development of therapeutics and vaccines to combat potential bioterrorism (114, 115). The

Animal Rule allows the use of animals for efficacy testing of drugs or vaccines where human trials are not ethical or feasible, such as when the pathogen causes serious health complications or the disease incidence is low (115, 116). *F. tularensis* is able to cause severe disease or death in humans, and less than 300 cases if tularemia occurs each year. Thus, the FDA animal rule applies to therapeutic and vaccine development for *F. tularensis*.

There are four main requirements for biologics developed under the Animal Rule. The animal study end point must correlate with the desired outcome in humans; there must be sufficient pharmacokinetic and pharmacodynamics data to determine required doses in humans; the pathophysiology of disease and mechanism of protection must be well defined in the animal; the desired effect must be shown in relevant animal models (114-117). These requirements are necessary to predict the response of the biologic in humans and often, multiple animal models are needed to satisfy these requirements. The Animal Rule, however, does not negate the need for clinical trials to demonstrate safety. In addition to the four main requirements, the animal's immune response must be similar to the response in humans and the natural history of the disease should be similar to human disease (115).

### **1.2.2 Disease in humans**

A study conducted in humans under Operation White Coat determined the lethal dose (LD50) of *F. tularensis* is 10-15 CFU. Greater than 50 CFU resulted in 100% of exposed participants to develop tularemia. Less than 50 CFU had a 70% infection rate (11). Onset of tularemia in humans typically occurs 2 to 6 DPE (10, 11, 16, 72, 96, 118-125). Patients experience a flu-like illness characterized by fever, headache, chills, myalgia, cough, dyspnea, and chest pain. Patients also experience splenomegaly and rarely hepatomegaly (10). Increase in

C-reactive protein (CRP) and erythrocyte sedimentation rates (ESR) occur within the first few days of infection and remain increased for up to 12 days. Positive bacterial cultures can be found in the sputum and pharyngeal and gastric washings. Bacteria are rarely recovered from the blood and if detected, only occur in cases of severe disease. Upon death, bacteria are found in the lung, spleen, liver, lymph node, kidney, intestine, central nervous system, and skeletal muscle. Time to death occurs at approximately 31 days in those with severe disease. Death is typically due to bronchopneumonia or lobar pneumonia, meningeal involvement, or peritonitis (124). Gross examination of affected lungs reveals plaques or small necrotic foci on the pleural surface. Microscopic examination of lungs shows thickening of alveolar walls and lesions of necrotic foci. Necrosis has also been found in the lymph node, spleen, and liver.

### **1.2.3 Non-human primates**

Several NHP models have proved suitable for use as a model of *F. tularensis* infection due to their ability to recapitulate human disease (126-130). Due to the similarity in disease susceptibility and presentation, as well as their phylogenetic similarity with humans compared to other animal models, non-human primate models represent a key model for developing effective therapeutics and vaccines.

#### **1.2.3.1 African green monkey (*Chlorocebus aethiops*)**

African green monkey monkeys exposed to *F. tularensis* begin to show clinical symptoms two to three days post infection. Typical infection is characterized by fever, anorexia, dyspnea, and nasal discharge (126, 131). This model also exhibits increased heart rate, increased cardiac pressure, and increased blood pressure two days following exposure to the bacteria. Early

infection was also characterized by decreases in iron and zinc, which is characteristic of infection with many bacterial pathogens. White blood cells increase up to 3 DPE and then dropped dramatically. There is a loss of circulating lymphocytes and platelets as infection progresses. Lactate dehydrogenase (LDH) levels increase through infection. Assessment of serum cytokines showed an increase in IL-8, IL-6, IFN $\gamma$ , MCP-1, and MCP-1 $\beta$ . Bacteria were able to be cultured from nasal swabs and the blood throughout infection. African green monkeys succumb to infection five to eleven days post infection. Histopathological changes within the lung included pleuritis with congestion, necrosis, granulomas, edema, and hemorrhage. Pyogranulomatous and necrotic lesions were found in the liver, spleen, respiratory tract, and lymph nodes of all affected animals. The course of disease in African green monkeys was more severe than in human tularemia, and thus they were not considered further for use as a model of infection.

#### **1.2.3.2 Rhesus macaque (*Macaca mulatta*)**

Rhesus monkeys exhibit clinical symptoms 2 to 3 DPE to *F. tularensis*. Clinical symptoms included fever, anorexia, sensitivity to light, and splenomegaly (127, 132). Time to death occurred 4 to 10 DPE. Gross lesions were apparent in the lung, liver, and spleen 3 DPE (133). Bacteria were recovered from the lung, spleen, lymph nodes, and liver. The liver was mottled and yellowish tan, while the spleen was enlarged. Affected tissues exhibited focal necrosis. The bronchiole was determined to be the primary site of infection based on fluorescent antibody staining for *F. tularensis* within the lung tissue. In more recent studies, rhesus monkeys were found to be resistant to lethal *F. tularensis* infection, requiring challenge doses greater than 250,000 CFU to induce lethal disease (129).

### **1.2.3.3 Marmoset (*Callithrix jacchus*)**

In marmosets, clinical symptoms of tularemia include fever, splenomegaly, and hepatomegaly. Typically symptoms began 3 DPE (128, 134). Animals exhibited increased serum alanine transaminase and bilirubin levels coinciding with observed hepatomegaly. Animals succumbed to disease 4 to 7 DPE. Bacteria were able to be recovered from the blood, lung, liver, spleen, and kidney. Gross pathological changes were observed in the lung, spleen, liver, and lymph nodes. The lungs were characterized by massive hemorrhaging.

### **1.2.3.4 Cynomolgus macaque (*Macaca fascicularis*)**

The LD50 of Cynomolgus macaques is less than 10 CFU (130). Clinical onset begins two to three DPE and is characterized by fever, increased heart rate, increased respiration rate, decreased blood pressure (129, 135, 136). There is an initial increase in circulating white blood cells 2 DPE followed by an immediate decrease due to loss of lymphocytes. Time to death was dose dependent with animals exposed to low dose succumbing 7-19 DPE, 6-17 days for medium dose exposures, and 6-8 days for high dose exposures (136). CRP levels were increased by two DPE, while albumin decreased three DPE. The hepatic damage biomarkers aspartate aminotransferase, alanine transaminase, and alkaline phosphatase were elevated. LDH and blood urea nitrogen (BUN) were also elevated, suggesting damage to kidneys and other organs. Hepatomegaly was found in 50% of infected animals, while splenomegaly occurred in all infected animals. Pathological changes were found in the lungs and lymph nodes, with the lung characterized by neutrophilic infiltrates.

Experiments utilizing non-human primates are costly and require specialized housing, making use of this animal model for proof-of-concept experiments unfeasible. Thus, smaller animal models capable recapitulating the human disease and immune response are needed.

## 1.2.4 Small animal models

### 1.2.4.1 Mice

Mice begin to exhibit clinical symptoms 2 DPE characterized by anorexia and lethargy (78, 137-139). The host response is upregulated four days post infection, but cellular killing mechanisms are downregulated one day post infection (83). TNF $\alpha$  is elevated in the bronchoalveolar lavage 4 DPE. IFN $\gamma$  is upregulated in the BAL as early as 2 DPE. Similar to other animal models, white blood cells decrease 4 to 5 DPE due to a loss in circulating lymphocytes. Mice succumb to infection 4 to 7 DPE to Type A, Type B, or *F. novicida* strains. Dissemination from the lungs to secondary tissues begins two DPE (140). Bacteria can be cultured from the blood, lung, liver, and spleen. Gross pathology is observed in the lungs, liver, and spleen, but the spleen and liver are more affected than the lungs. Mice were believed to succumb to infection due to liver failure, not pulmonary dysfunction. Lung pathology is characterized by pulmonary abscesses, bronchopneumonia, and foci of consolidation.

Mice have been extensively used for *F. tularensis* infection and vaccine studies due to the depth of knowledge, pathogenicity in this model, and availability of knockout and transgenic mice. Despite the similarities between mouse and human tularemia, mice are susceptible to both LVS and *F. novicida*, which are attenuated in humans (94). This extreme sensitivity of mice to *F. tularensis* hinders vaccine studies. Additionally, bacteremia is severe in mice, but is rarely observed in humans. Forestal et al. determined *F. tularensis* recovered from the blood of mice were primarily located in the plasma rather than intracellularly, which has not been observed in other animal models or humans (141). Despite the cost savings, availability of many reagents, and ease of use of this model, mice may not be the best small animal model available to assess *F. tularensis* vaccines.

#### 1.2.4.2 Rats

Fisher 344 rats have been assessed as a model for *F. tularensis* infection. These rats have been found to be highly sensitive to Type A and Type B strains, while highly resistant to *F. novicida* and LVS infection (142, 143). The LD50 of virulent Type A strains in Fischer rats is 500 CFU (142-144). Clinical symptoms include weight loss, decreased activity and responsiveness, splenomegaly, and enlarged lymph nodes. There is an increase in neutrophils and monocytes, but a decrease in lymphocytes and platelets during infection. There is an increase in liver enzymes AST, ALT, ALP, lactate dehydrogenase, and total bilirubin, and an increase in kidney analytes blood urea nitrogen and creatinine. Glucose, albumin, and calcium decrease throughout infection. Fischer rats succumb to infection 4 to 10 DPE. During the moribund period there is an increase in PT and PTT concomitant with a decrease in fibrinogen, suggestive of disseminated intravascular coagulation. Bacteria can be recovered from the blood, liver, and spleen as early as 2 DPE.

Assessment of ability of *F. tularensis* to infect rat cell types revealed that while *F. tularensis* was able to infect rat macrophages, hepatocytes were the primary replicative niche (143). This predilection for hepatocytes represents a key difference in *F. tularensis* infection between rats, other animal models, and humans. Macrophages have been shown to be essential for *F. tularensis* growth in multiple animal models. Additionally, humans do not consistently exhibit hepatomegaly and changes in liver enzymes during infections. These differences may prove to be significant when it comes to assessing vaccines and therapeutics.

## 1.2.5 Large animal models

### 1.2.5.1 Rabbits

New Zealand White (NZW) rabbits have also been assessed as a suitable animal model for virulent *F. tularensis* infection. The LD<sub>100</sub> is 10<sup>9</sup> for Type B strains and 1 CFU for Type A strains in NZW rabbits (145). Rabbits exhibit fever, weight loss, splenomegaly, and increased erythrocyte sedimentation rates two to three DPE (146). Additionally, the characteristic drop in lymphocytes was observed at four DPE. Rabbits succumb to disease four to seven days post infection. Bacteria are only found during the moribund period when rabbits begin exhibiting severe disease. Gross pathological changes have been observed in the lungs, spleen, liver, kidney, intestines, and lymph nodes. Histopathological examination of the lung shows lesions, parenchymal consolidation, loss of lung volume, hemorrhage, and subpleural areas of nodular consolidation (147)

NZW rabbits have been used to study a variety of diseases, including cancer, atherosclerosis, Alzheimer's disease, eye issues, and wound healing (148). Rabbits are also an accepted model for inhalational anthrax and shigella. They exhibit the desirable characteristics of rodents, ease of breeding, and short reproduction times. They are also phylogenetically closer to primates than are rodents (148, 149). Additionally, rabbits exhibit a lung structure more similar to humans than mice (149).

### **1.3 Factors affecting vaccine efficacy**

#### **1.3.1 Sexual dimorphism can affect the immune response**

Sex specific disease outcomes are linked to sex hormones, different copy numbers of immune, and disease-susceptibility X-linked genes. Sexual dimorphism in immune functions begins as early as embryonic development and is maintained postnatally via sex hormones (150-159). Females exhibit stronger humoral and cellular adaptive immune responses due to increased estrogen receptor activation on white blood cells (153, 154). Progesterone has been shown to suppress T cell cytotoxicity and regulatory T cell proliferation (155, 156). Testosterone in males regulates macrophage chemotaxis and limits the ability to produce antibodies compared with females, resulting in decreased innate and adaptive responses (157-159). Additionally, the number and function of innate immune cells is higher in females than males, contributing to higher responses to antigens, vaccines, and infections in females (150-163).

Literature examining the effect of sex differences has documented differences in pattern recognition receptors and composition of white blood cell populations which can affect the innate response to *F. tularensis*. Males have been shown to express higher levels of TLR-4 and TLR-2, which have been shown to react with bacterial pathogen-associated molecular patterns, such as LPS and lipoproteins (41, 45, 46, 164). Females also exhibit higher inflammatory T-helper 1 and anti-inflammatory T-helper 2 response compared to males (150-163). These differences have been shown to play a role in susceptibility to certain pathogens, outcomes of infection, and vaccine efficacy. Studies show influenza is more severe in females, while Coxsackieviruses, hantavirus, and SARS is more severe in males, indicating sexual dimorphism in immune response is disease specific (160-163).

Basic and preclinical research has primarily been done in male animals and male derived cell lines. Additionally, women have historically been underrepresented in clinical study trials. Thus, the National Institutes of Health has implemented a policy to consider sex as a biological variable in animal and human studies. Sexual dimorphism has not been well studied for *F. tularensis* or potential vaccines. Sunager et al. examined sex-based differences in C57BL/6Tac mice following challenge with LVS. They saw no difference in survival between unvaccinated male and female mice following challenge with LVS at doses ranging from 800 to 3200 CFU. Following vaccination with paraformaldehyde inactivated LVS (*iF. tularensis*) or an attenuated strain of LVS (LVS $\Delta$ SodB), improved survival in female mice compared to male mice following challenge with virulent LVS or S4 was observed (165). More studies are needed to confirm the role of sexual dimorphism on infection of vaccine efficacy for *F. tularensis*.

### **1.3.2 Growth conditions of challenge material alter protein expression**

Often, cell culture results do not correspond with *in vivo* results. These differences have partially been attributed to differences in growth conditions. Mueller Hinton broth (MHb) is the most common growth medium used to grow *F. tularensis*. Our lab utilizes brain heart infusion (BHI) broth for growth of *F. tularensis* as this growth medium resulted in better aerosol performance compared to growth in MHb (166). NZW rabbits have been considered a poor model for tularemia as LVS vaccination does not protect against pulmonary challenge while LVS vaccination resulted in 100% protection in Fisher 344 rats and cynomolgus macaques (76, 167). An important distinction between these studies is the use of BHI in the rabbit study and MHb in the rat and monkey study. Proteomic assessment of antigen expression of *Francisella* grown in MHb versus BHI broth shows growth in BHI results in upregulation of virulence

factors (168). Additionally, *F. tularensis* grown in MHb exhibited an impaired bacterial membrane (168). Faith et al. has shown that growth in MHb versus BHI does not significantly alter LD50, but growth in BHI decreases the LD99 by 1 log CFU (166, 169). The effects of growth conditions of challenge material on vaccine efficacy have not been assessed in our model.

### 1.3.3 Strain selection and gene mutations

*F. tularensis* exhibits a highly conserved genomic sequence among subspecies. *F. tularensis* subsp. *tularensis*, *holarctica*, and *mediasiatica*, and even *F. novicida*, are antigenically similar and have 99.8% shared identity among the 16s rRNA (170). Despite this similarity there is a large disparity in virulence seen between the different subspecies (145). *F. tularensis* subsp. *mediasiatica* and *F. novicida* are not associated with disease in healthy humans. Many *F. tularensis* studies utilize LVS or *F. novicida* because they are not considered select agents and can be used at BLS-2 conditions, but since these strains are non-virulent in humans, data from these studies should be interpreted with caution. LVS is often a good reference point as studies comparing host immune responses to LVS and S4 indicate LVS acts as a milder version of S4 with moderate immune suppression abilities (53, 171). *F. novicida* infection is distinctly different from S4 infection. The same genes have different roles in pathogenesis between the two species. *F. novicida* is also susceptible to complement and the inflammasome and secretes bacterial proteins that aid in recruitment of host leukocytes to the site of infection.

Type A strains can be further subdivided into genetically distinct clades with different case fatality rates in humans: Type A1a (4%), Type A1b (24%), Type A2 (0%) (172). This difference in virulence among subclades was also observed in the mouse model (173).

Differences in virulence could be due to genome rearrangements and gene loss (174). Additionally, differences in virulence have been observed between different isolates of the same strain. S4 strain NR-643 is highly attenuated in Fischer 344 and NZW rabbits compared to NR-10492 (175). This difference in virulence highlights the potential importance of subspecies selection for vaccine development.

### 1.3.3.1 LVS

Type B strains have been shown to be able to provide partial protection against Type A2, but not Type A1b strains in cottontail rabbits (5). The LVS is an attenuated Type B strain developed as a vaccine by the former Soviet Union in the 1950s (95). LVS has been shown to provide limited protection against some forms of tularemia. Antibody titers to whole *F. tularensis* are similar between survivors and non-survivors, making it difficult to establish the immune status of vaccinated individuals. In BALB/C, C3H/HeN, and C57BL/6 mice, a single intradermal vaccination with LVS resulted in no survival when challenged with aerosols containing virulent S4, the standard strain used for virulent Type A infections (108, 176). A single aerosol vaccination of mice boosted vaccine efficacy (VE) to 60% in BALB/C and C3H/HeN mice (108). A single scarification with LVS in NZW rabbits resulted in 0% survival following aerosol challenge with S4 (177, 178).

Due to its ability to be handled under biosafety level 2 laboratory conditions, much of what is known about *F. tularensis* pathogenesis is derived from studies of LVS in mice. The genetic basis of attenuation of LVS is unknown, and spontaneous phase shifting has been observed in the lipopolysaccharide, affecting its virulence and subsequent vaccine efficacy (112).

These factors have hindered FDA approval of this vaccine. Despite the pitfalls of LVS, it serves as proof of concept and a comparator for other *Francisella* vaccines.

### 1.3.3.2 S4 $\Delta$ aroD

Aro genes encode enzymes of the shikimate pathway. The shikimate pathway is responsible for synthesis of aromatic amino acids in plants and microbes. Mutations in aro genes have been shown to decrease virulence in other pathogens, such as *Salmonella enterica* (179). *F. tularensis* produces all of the enzymes of the shikimate pathway. *F. tularensis* strains with deletions in the aro genes do not require additional supplements to growth medium to grow. A single intranasal dose of S4 $\Delta$ aroD resulted in 80% protection against 100 CFU challenge of virulent *F. tularensis* in C57BL/6J mice. A prime/boost vaccination with S4 $\Delta$ aroD resulted in 100% protection up to 250 CFU, but not at higher doses (113). At 500 CFU, protection was 80%, and at 1000 CFU, protection was 40%. S4 infection results in minimal induction of cytokine transcription in the lungs. In S4 $\Delta$ aroD vaccinated mice, there was an increase in TNF $\alpha$ , Cox2, IL-1 $\beta$ , iNOS, CXCL1, and MCP1. Additionally, vaccination induced an IgG2 serum response suggestive of T helper 1 response.

Our lab has shown a prime/boost regimen of aerosolized S4 $\Delta$ aroD results in 66% protection in female NZW rabbits challenged with 2000 CFU of virulent S4 (180). Interestingly, S4 $\Delta$ aroC mutations and double deletion mutants of aroC and aroD did not result in vaccine efficacy as high as S4 $\Delta$ aroD in mice(113). In rabbits, S4 $\Delta$ aroC also did not result in vaccine efficacy as high as S4 $\Delta$ aroD. S4 $\Delta$ aroC and S4 $\Delta$ aroC/D are more attenuated compared to S4 $\Delta$ aroD. This could be due to redundant pathways in the shikimate pathway. In plants, DHQ, the substrate that interacts with aroD, is able to enter another pathway. This alternate pathway can re-enter the shikimate pathway at the same location or a few steps down. AroC is the last

step in the shikimate pathway and is necessary for chorismate synthesis. Thus, there is no way for this step to be bypassed.

### **1.3.3.3 S4 $\Delta$ guaBA**

The *guaBA* operon determines production of the two enzymes required to convert hypoxanthine to guanine at the nucleotide level during guanine nucleotide biosynthesis (181). Mutations in this gene requires growth medium to be supplemented with guanine to support bacterial replication. Mutations in *guaBA* genes have resulted in attenuation of other bacterial pathogens, including *Shigella flexniri*, *Yersinia pestis*, and *Salmonella enterica*. Mutations in *gua* genes of *F. tularensis* do not result in protection of mice against virulent *F. tularensis* (182). An intranasal prime/boost vaccination of C57BL/6 mice with S4 $\Delta$ guaBA resulted in 0% protection against challenge with 100 CFU of S4. The average time to death of vaccinated animals was five days. Thus, vaccination with S4 $\Delta$ guaBA did not even extend time to death compared to virulent S4. A single scarification vaccination with S4 $\Delta$ guaBA resulted in 27.3% survival in rabbits (177).

### **1.3.3.4 S4 $\Delta$ clpB**

ClpB is the chaperone for heatshock protein 100. It works in conjunction with DnaK and is crucial for the ability of bacteria to survive extreme heat stress, including *E. coli*, *S. aureus*, *H. pylori*, and *V. cholerae* (183, 184). ClpB solubilizes and refolds aggregated proteins and is a virulence factor in *S. enterica* and *L. monocytogenes*. In *F. tularensis*, the *clpB* gene contributes to intracellular growth as it is involved in type VI secretion system disassembly but is not essential (185). It is, however, required for replication in target organs and reactivation of aggregated proteins under heat stress conditions (57, 186). Intradermal vaccination of BALB/C

mice resulted in 100% survival following challenge with 2000 CFU of S4 administered intradermally, or 75 CFU administered intranasally (187). When challenged with low doses of aerosolized S4, survival was 60%. Vaccination induced IFN $\gamma$ , but did not result in sterilizing immunity.

### **1.3.4 Dissemination and persistence**

The primary goal of vaccination is to induce a protective immune response without inducing disease. Live attenuated vaccines (LAVs) are sufficiently immunogenic and persistent to promote a long lasting and protective adaptive immune response. LAVs can induce life-long protection with as few as one vaccine dose. In contrast, inactivated and subunit vaccines require multiple doses to elicit and sustain a protective immune response throughout the human life span. In adults, live attenuated influenza vaccine produced long lasting serum and local antibody responses compared to inactivated influenza vaccines (188). In 2004, a prospective study showed vaccination of children with live attenuated influenza resulted in 54.9% fewer cases of influenza in that cohort than vaccination of children with the inactivated influenza vaccine (189). The oral polio vaccine exhibits the same degree of intestinal protection as natural polio infection and results in higher serum and local geometric mean antibody titers than the inactivated polio vaccine (190). Hamsters vaccinated with LAV Venezuelan eastern encephalitis virus (VEEV) produce higher and longer lasting antibody titers compared to the same strain inactivated with formaldehyde (191). Subsequently, hamsters vaccinated with the LAV survived aerosol challenge with virulent VEEV, while hamsters vaccinated with the inactivated virus did not (191). In rhesus macaques, the live attenuated dengue-2 vaccine protected against virulent dengue infection better than component dengue-2 vaccines (192).

Studies suggest dissemination and persistence of *F. tularensis* vaccine strains in the tissue of mice may play a role in the development of protective immunity. Heat killed *F. tularensis* vaccines fail to induce complete protective immunity in animals and humans challenged with virulent S4 (193-195). Mice intranasally infected with S4 typically die within five days and exhibit high bacterial titers in the lung, liver, and spleen. Administration of levofloxacin at 3 DPE still results in high bacterial loads in the spleen and lung, but this primary infection is resolved by 19 DPE (196). Upon subsequent rechallenge of levofloxacin treated mice resulted in 100% protection up to 120 CFU and 80% protection at 1400 CFU. Vaccination of mice with the more immunogenic Rocky Mountain Lab (RML) strain of LVS resulted in better survival following challenge with virulent SchuS4 (S4) than vaccination of mice with ATCC 29684 strain of LVS (112). The virulence of the RML strain compared to the ATCC strain contributes to its superior immunogenicity. In BALB/C mice, the LVS-derived  $\Delta$ ClpB strain protected better than LVS, and produced 2-log-fold higher titers than LVS in the skin, spleen, liver, and lung (168). Additionally, S4 $\Delta$ ClpB mutants protect mice better than LVS derived  $\Delta$ ClpB mutants (168). In C57BL/6 mice, S4 $\Delta$ ClpB strains reached higher titers and persisted longer than LVS S4 $\Delta$ ClpB strains in the spleen and the liver (74). The role of bacterial dissemination and tissue persistence on the immune response to *F. tularensis* vaccine efficacy and the mechanisms controlling these differences is unknown but is critical for the development of a safe and effective human vaccine. I hypothesize that persistence and dissemination each play a role in vaccine efficacy in rabbits and is a function of early host-pathogen interactions.

### 1.3.5 Inflammasome activation

Caspases are cysteine proteases that signal host cell death. Caspase-3 is associated with apoptotic cell death, while caspase 1 is associated with pyroptotic cell death. Caspase-1 is classified as an inflammatory caspase as it results in the release of inflammatory cytokines through the formation of pores in the plasma membrane. The inflammasome is an intracellular multiprotein complex that mediates the cleavage of IL-1 $\beta$  and IL-18 via caspase-1. Inflammasome activation requires two distinct signals from pathogen pattern recognition and an intracellular danger signal, particularly Toll like receptors and NOD-like receptors (197, 198). IL-1 $\beta$  has a wide range of local and systemic effects, such as neutrophil/macrophage recruitment and induction of fever.

Alum, a commonly used vaccine adjuvant has been found to activate the inflammasome and skew the immune response towards a T helper 2 response and antibody production (197, 199). In mice, inflammasome dependent IL-1 $\beta$  has been shown to be important in the production of anti-LPS antibodies. The inflammasome has been linked to the development of a T helper 1 response in Candidiasis, though the specific downstream mechanisms following inflammasome activation have not been identified (200). Recombinant BCG vaccine releases DNA into the host cell cytoplasm resulting in activation of AIM2 and an increase in IL-1 $\beta$  and IL-18 (201, 202). Multiple inflammasome pathways have been implicated in *L. monocytogenes* infection (203). NLRP3 is activated upon escape from the phagosome through an unknown mechanism, NLRC4 is activated through recognition of bacterial flagellum, and AIM2 is activated by the release of DNA in host cytoplasm (203, 204). However, excessive activation of the inflammasome has been correlated with diminished T cell responses and decreased protective immunity (204).

*F. novicida* and LVS have been shown to induce the secretion of downstream inflammasome cytokines, IL-1 $\beta$  and IL-18, in mouse and human macrophages (93, 94, 205, 206). Studies indicate inflammasome activation is dependent on phagosomal escape by *F. tularensis*. For *F. novicida*, concomitant activation of Type I interferon receptor signaling and detection of cytosolic bacteria result in inflammasome activation (93, 205, 206). In ASC<sup>-/-</sup> KO C57BL/6 mice, animals succumbed to *F. novicida* infection faster than WT mice indicating the inflammasome is a key mediator of the innate response to *F. tularensis* (94, 206). In mice, inflammasome dependent IL-18 has been linked with IFN $\gamma$  production during LVS infection (207, 208). Additionally, inflammasome dependent IL-1 $\beta$  has been shown to be important in the production of anti-LPS antibodies following infection with LVS (208). The AIM2 has been implicated as the main inflammasome mediator in mouse macrophages during *F. novicida* infection. Both AIM2 and NLRP3 inflammasome pathways have been shown to contribute to the inflammatory response to LVS and *F. novicida* in human macrophages (209).

Despite the ability of *F. novicida* and LVS to activate the inflammasome, there is some question as to the relevance of these studies in understanding *F. tularensis* pathogenesis since these strains are attenuated in humans and other species. Also, several pathogens are capable of subverting inflammasome recognition. *Yersinia pestis* prevents recognitions of its Type III secretory components by NLRP3 and NLRC4. Salmonella is able to repress flagellin expression and modify its Type III secretory proteins to evade detection by NLRC4. *M. tuberculosis* expresses the zinc protease Zmp1 and *P. aeruginosa* expresses ExoU to prevent inflammasome activation. Similar to these pathogens, other research indicates both LVS and virulent S4 actively suppress AIM2 and NLRP3 activation (198). *F. novicida* has been shown to induce high levels of cleaved caspase-1 and IL-1 $\beta$  in macrophages. In contrast, LVS is only able to induce low

levels of activated caspase-1 and IL-1 $\beta$  in macrophages, and S4 infection little to no inflammasome activation is observed (198). This reduction in inflammasome activation impairs induction of cell death and has been largely attributed to impaired activation of TLR-2 during initial infection, allowing for the establishment of fulminant infection (198). The role of the inflammasome activation on vaccine efficacy has not been explored for attenuated *F. tularensis* vaccines.

## 2.0 Hypothesis and Specific Aims

Despite improved immune protection, LAVs pose several safety concerns. LAVs are reactogenic and can result in fever or disease specific symptoms (191). There are concerns of batch-to-batch variations and the potential of the attenuated organism to revert to a virulent form; spontaneous phase shifting has been observed in the lipopolysaccharide of *F. tularensis* strains which can alter the pathogens virulence (112, 190, 191). Immunocompromised individuals may lack the capacity to combat an attenuated pathogen. Understanding the mechanisms driving the superior vaccine efficacy seen with LAVs is vital to improving the quality and longevity of protection induced by inactivated or component vaccines.

An objective of this research was to assess different attenuated *F. tularensis* strains with the goal of understanding mechanisms related to relative success in protecting against tularemia. These studies utilize the attenuated *F. tularensis* strains LVS, S4 $\Delta$ aroD, S4 $\Delta$ guaBA, and S4 $\Delta$ clpB, which have been assessed in the mouse model. Due to the hyper susceptibility of mice to *Francisella*, the differences in tularemia presentation, and differences in the immune system compared to humans these strains needed to be tested in an intermediate animal model before moving into nonhuman primate studies. Our lab has reestablished the New Zealand White rabbit as a relevant model for studying potential *F. tularensis* therapeutics and vaccines. Rabbits are phylogenetically closer to humans than are rodents and exhibit similar lung structure to humans. Rabbits are also the natural host for *F. tularensis* and are important in the transmission cycle. NZW rabbits exhibit a similar susceptibility and disease presentation to humans. This model is also outbred and thus is able to recapitulate the range in responses to *F. tularensis* that would be observed in humans. Animal studies using NZW rabbits are typically have smaller sample size

due to their larger size and thus statistical significance can be hard to determine. There is also a lack of reagents available for use in the NZW rabbit model, which can make development of immunological assays difficult.

**I hypothesize that the protection conferred by attenuated *F. tularensis* strains is influenced by persistence and dissemination of the bacteria within host tissues and early activation of the inflammasome compared to virulent *F. tularensis*.**

Impact Statement: The proposed studies will contribute significantly to the understanding of persistence and dissemination of live attenuated tularemia vaccines on the host immune response and subsequent vaccine efficacy. Understanding the immune mechanisms behind vaccine efficacy will aid the development of an inactivated or component *F. tularensis* vaccine by providing a framework for possible adjuvants and antigens that drive a protective immune response in the absence of a productive infection

## **2.1 Aim 1**

**Determine how host and bacterial factors affect *F. tularensis* vaccine success.**

Hypothesis: Sex, growth conditions for challenge strain, and strain selection will each affect vaccine efficacy. These factors are variables that may compete with the variable of interest, which can affect the interpretation of the results of the study as well as comparison between studies working towards developing *F. tularensis* vaccines. In Aim 1, I will assess if sex, growth conditions, vaccine schedule, or strain selection affect survival following challenge with virulent S4 of vaccinated NZW rabbits.

### 2.1.1 Aim 1a

Determine the role of sex as a biological factor on disease course and disease outcome in naïve and vaccinated NZW rabbits following challenge with virulent *F. tularensis*. It has been well documented that sex can affect disease susceptibility, outcome, and vaccine efficacy. Females tend to have more robust cellular and humoral immune response compared to males. Since Th1 responses are thought to be important for protection against *F. tularensis*, I hypothesize female rabbits will have improved vaccine efficacy compared to male rabbits.

### 2.1.2 Aim 1b

Demonstrate that choice of growth medium (MHb or BHI) for challenge material can alter disease course and vaccine efficacy in rabbits vaccinated with LVS and then challenged with S4. Assessment of virulence protein expression of *F. tularensis* grown in different conditions show *F. tularensis* grown in BHI expresses more virulence proteins than when grown in MHb. Thus, I hypothesize vaccine efficacy will be higher when animals are challenged with *F. tularensis* grown in MHb compared to animals challenged with *F. tularensis* grown in BHI broth.

### 2.1.3 Aim 1c

Determine that S4 $\Delta$ aroD results in better vaccine efficacy compared to other attenuated *F. tularensis* strains. A single dose of aerosolized LVS in NZW rabbits extended time to death but no survival following virulent *F. tularensis* challenge. Assessment of S4 $\Delta$ guaBA in mice

resulted in no protection in mice, but scarification in NZW rabbits resulted in 27.3% survival. S4ΔclpB has been shown to result in significantly improved vaccine efficacy compared to LVS in BALB/C mice. Thus, I hypothesize S4ΔaroD results in better vaccine efficacy compared to LVS, S4ΔguaBA, and S4ΔclpB when given in a prime/boost schedule via aerosol.

## 2.2 Aim 2

**Determine the roles of persistence and dissemination on vaccine efficacy of attenuated *F. tularensis* vaccines.** Hypothesis: Dissemination and persistence of bacteria within tissues following vaccination will correlate with observed vaccine efficacies. Persistence of antigen within the host is critical for ensuring a robust immune response that results in immune memory. Additionally, dissemination of antigen to secondary lymphoid tissue is an important consideration in vaccine design. LAVs have the benefit of being able to persist and disseminate within the host and are considered the most immunogenic vaccine design. Though LAVs provide superior and long lasting immune protection, they are often contraindicated in immune suppressed individuals. There is also a concern about reversion with virulent forms, as has been observed with live attenuated polio vaccines. The development of alternative methods for vaccine administration and discovery of new adjuvants can greatly improve inactivated vaccines by modulating antigen deliver and persistence. Understanding the role of dissemination and persistence for attenuated *F. tularensis* strains can aid in the design of inactivated *F. tularensis* vaccines.

### 2.2.1 Aim 2a

Establish a baseline of clinical disease course in uncontrolled tularemia in NZW rabbits. I will fully characterize virulent S4 infection in the NZW rabbit model. Describing the natural history of virulent infection will aid in determining how attenuated vaccine strains are inducing vaccine efficacy and further validate the NZW rabbit as a suitable model for *F. tularensis* studies.

### 2.2.2 Aim 2b

Quantitatively compare clinical disease presentation between LVS, S4 $\Delta$ aroD, and S4 $\Delta$ guaBA vaccinated NZW rabbits. Clinical disease presentation will be assessed through measurement of weight, temperature, ESR, and CBC data. I hypothesize that S4 $\Delta$ aroD will be more clinically severe compared to LVS and S4 $\Delta$ guaBA due to a more robust immune response.

### 2.2.3 Aim 2c

Determine the relationship between vaccine efficacy and dissemination and persistence of LVS, S4 $\Delta$ aroD, and S4 $\Delta$ guaBA. Bacterial titers within tissues of serially sacrificed NZW rabbits will be measured. LAVs are thought to have superior vaccine efficacy compared to component or inactivated vaccines due to their ability to persist and replicate in tissues. I hypothesize that S4 $\Delta$ aroD will disseminate to the liver and spleen of NZW rabbits and persist in the tissues longer than LVS and S4 $\Delta$ guaBA.

## 2.3 Aim 3

**Elucidate the immunological mechanisms associated with disease course of virulent vs. attenuated *F. tularensis* strains.** Hypothesis: Inflammasome activation will associate with observed vaccine efficacies of attenuated *F. tularensis* strains and will occur earlier than in virulent *F. tularensis* infection. Protective immune responses rely on effective innate mechanisms. Understanding innate immune mechanisms that are important for the development of a protective immune response can aid in development of inactivated vaccines.

### 2.3.1 Aim 3a

Determine if a pyroptosis mediated sepsis response is cause of death in S4 infected NZW rabbits. This will be determined by microarray analysis of liver, lung and spleen at baseline, 3 DPE, and 5 DPE, confirmation of select genes via PCR, and measurement of serum cytokines via ELISA. Studies in mice indicate *F. tularensis* suppresses early inflammasome activation, but there is increase in inflammatory cytokine expression as infection progresses to death, suggesting a sepsis related event. I hypothesize NZW rabbits succumb to virulent S4 infection due to a pyroptosis mediated cytokine storm.

### 2.3.2 Aim 3b

Determine if cell death pathways are activated during infection with attenuated *F. tularensis* strains in NZW rabbits. Cell death pathways will be assessed through measurement of

caspase 3, caspase 9, IL-1 $\beta$ , STAT1, and IFN $\beta$  gene expression in lung tissue via PCR. LVS has been shown to possess immune suppression capabilities, though to a lesser extent than virulent S4, which most likely contributes to its virulence in mice. I hypothesize that attenuated *F. tularensis* strains induce pyroptosis at an earlier time point compared to virulent *F. tularensis*.

## **3.0 Materials and Methods**

### **3.1 Biosafety and regulatory information**

All work with live *F. tularensis* was conducted at biosafety level-3 (BSL-3) in the University of Pittsburgh Regional Biocontainment Laboratory (RBL). The University of Pittsburgh RBL is a Registered Entity with the CDC and United States Department of Agriculture (USDA) for work with *F. tularensis*. The University of Pittsburgh's Biohazards Committee approved these studies.

All personnel wore powered air purifying respirators (3M GVP-1 PAPR with L-series bump cap) or used a class III biological safety cabinet. Vesphene II SE (1:128 dilution; Steris Corporation, Erie, PA) was used to disinfect all liquid wastes and surfaces associated with *F. tularensis*. All solid wastes and caging were steam sterilized. Animal carcasses were digested via alkaline hydrolysis (Peerless Waste Solutions, Holland, MI).

### **3.2 Animals**

All animal work performed adhered to the Guide for the Care and Use of Laboratory Animals of the National Institutes of Health (NIH) and Animal Welfare Act (AWA). All studies were performed under protocols approved by the University of Pittsburgh's Institutional Animal Care and Use Committee (Protocols 16027669 and 19014220). The University of Pittsburgh is

fully accredited by the Association for Assessment and Accreditation of Laboratory Animal Care (AAALAC).

Juvenile male and female NZW rabbits were obtained from Robinson Services, Inc. Rabbits were housed in the RBL at BSL-3 for the duration of studies. IPTT-300 temperature/ID chips (BioMedic Data Systems, Seaford, DE) were implanted between the shoulder blades subcutaneously. Rabbits were monitored at least once daily prior to infection and at least twice daily after infection. Body weight was recorded once in the morning and body temperature at least twice per day using the DAS-7000 reader. Rabbits were anesthetized with 2-5% isoflurane and bled from the saphenous vein. For euthanasia, rabbits were first anesthetized with isoflurane and then euthanized by barbiturate overdose (100mg/kg given intravenously).

### **3.2.1 Vaccine efficacy studies**

For vaccine efficacy studies, rabbits were vaccinated via aerosol with a single prime dose or a prime dose with a boost 14 days later. Phlebotomy was performed every seven days following vaccination until challenge. Rabbits were challenged 30 days after the last vaccination with aerosolized virulent S4 and bled 4, 6, 8, 11, and 14 DPE. Animals were monitored and euthanized when moribund or at study endpoint, 28 days post challenge. At necropsy the following samples were taken: blood, lymph nodes, lungs, spleen, liver, and kidney.

### **3.2.2 Dissemination studies**

For virulent S4 dissemination studies, animals were serial sacrificed up to five days post infection with venipuncture performed on an alternating schedule to ensure rabbits were being

bled a maximum of every other day and that blood was collected on all days post exposure. For vaccine strain dissemination studies, animals were sacrificed 3, 7, and 14 DPE. Rabbits were bled on an alternating schedule up to seven days post vaccination. At necropsy the following samples were taken: blood, bronchoalveolar lavage (BAL), lymph nodes, lungs, spleen, liver, kidney, heart, and gastrointestinal tract.

### 3.2.3 Clinical observations

Clinical observations were performed once daily prior to exposure and at least twice a day after vaccination (for at least three days) or S4 exposure. Body weight was measured once per day in the morning. Temperature, behavior, and appearance were measured during each observation. All four criteria were used to assess severity of disease and need for immediate euthanasia (See Table 1). Monitoring was increased to every six hours if cumulative scores were greater than 6.

**Table 1. Clinical scoring criteria for S4 infected NZW rabbits**

Score	Weight loss	Temperature	Appearance	Behavior
1	Up to 5%	34-40°C	Normal	Normal
2	5-10%	40-41°C	Reduced grooming	Less peer interaction
3	10-15%	41-42°C	Ruffled fur	Huddled
4	15-20%	42-43°C	Hunched	Moving only when prodded
5	>20%	<34°C	Respiratory distress	No response

### **3.2.4 Necropsy**

Animals were anesthetized with isoflurane and consciousness assessed prior to any animal manipulation. Approximately 50 ml of blood was collected via cardiac puncture into K<sub>2</sub>EDTA tubes. Rabbits were euthanized by intravenous injection of 3.0 ml of sodium pentobarbital. Once death was confirmed rabbits were necropsied. A BAL was performed post euthanasia by threading tubing into the lungs through the exposed trachea and rinsing with PBS. Pictures were taken of organs removed from the rabbits using a Fujifilm FinePix XP90 camera. Tissue samples were placed in 37% formaldehyde for histology or frozen for bacterial titering and RNA collection.

## **3.3 Bacteria**

### **3.3.1 Challenge strain**

Virulent *F. tularensis* subsp. *tularensis* strain SchuS4 originally obtained from Dynport Vaccine Company (Frederick, MD) was grown in BHI and stored as single-passage stocks with 20% glycerol. For aerosol exposures, *F. tularensis* was streaked on cysteine heart agar (CHA) and incubated for two days at 37°C in 5% CO<sub>2</sub>. Individual colonies were suspended in phosphate buffered saline (PBS) to an OD<sub>600</sub> reading of 0.1. For virulent S4 challenge, 500 µl of the PBS slurry was used to inoculate 24.5 ml of BHI broth supplemented with ferric pyrophosphate and L-cysteine in a baffled 125 ml vented polycarbonate flask. The inoculum was incubated in an orbital shaker at 37°C, 200 RPM. After 18 hours, the broth culture was diluted to the desired

concentration in fresh BHI based on a growth curve from prior studies and the OD600. After aerosol exposures, nebulizer and all-glass impinger (AGI) contents were diluted 10-fold in PBS and plated on CHA in duplicate and incubated two days at 37°C, 5% CO<sub>2</sub> to determine titers and subsequent inhaled dose.

### **3.3.2 Vaccine strains**

S4ΔaroD and S4ΔguaBA was obtained from Eileen Barry (University of Baltimore-Maryland), LVS was obtained from ATCC (29684), and S4ΔclpB was obtained from Wayne Conlan (National Research Council of Canada). Stocks of each vaccine strain were prepared as described for virulent S4. For aerosol exposures, *F. tularensis* was streaked on CHA and incubated for two days at 37°C in 5% CO<sub>2</sub>. Individual colonies were suspended in PBS to an OD600 reading of 0.1. For vaccination, 12.5 ml of the PBS slurry was used to inoculate 200 ml of BHI in a 1 liter vented polycarbonate flask. One flask was prepared for every four rabbits exposed. The inoculum was incubated in an orbital shaker at 37°C, 200 RPM for 18 hours. The vaccine was centrifuged at 4000 x g for 10 minutes at 4°C and re-suspended in 10mls of fresh BHI per every two rabbits being exposed. After aerosol exposures, nebulizer and AGI contents were diluted 10-fold in PBS and plated on CHA in duplicate and incubated two days at 37°C, 5% CO<sub>2</sub> to determine titers and subsequent inhaled dose.

### **3.4 Aerosol exposures**

Aerosols of *F. tularensis* were generated inside a class III biological safety cabinet (Baker Co., Sanford, ME). Rabbits were exposed two at a time for 10-minutes in a nose-only exposure chamber (CH Technologies, Westwood, NJ) using a 3-jet Collison nebulizer and an AGI controlled by the AeroMP or Aero3G exposure control system (Biaera Technologies, Hagerstown, MD) (180). Plethysmography data were collected using Finepointe software (Buxco Research Systems, Wilmington, NC) during the exposure. Following exposures, nebulizer and AGI samples were quantified on CHA as described above. Aerosol concentration and inhaled dose were determined as previously described: aerosol concentration multiplied by the rabbit's minute volume and duration of the exposure (166, 210, 211).

### **3.5 Laboratory Tests: ESR, CBCs, and chemistries**

Whole blood was collected with a syringe from the saphenous vein at baseline, and then alternating every other day until euthanasia. Blood was transferred into K2EDTA tubes for ESR assessment, complete blood counts (CBC), and serum chemistries. For ESRs, whole blood was pipetted using glass Pasteur pipets into glass Wintrobe tubes. Tubes were placed vertically for one hour and degree of red blood cell settling was measured in millimeters. The VetScan HM2 (Abaxis, Union City, CA) was used to measure CBCs, and the VetScan VS2 (Abaxis) was used to measure blood chemistry, using a profile optimized for mammalian liver function.

### **3.6 Tissue titers**

Whole blood and BAL fluid was serially diluted in PBS and plated on CHA. To determine tissue bacterial titers, 0.5 g of tissue was homogenized in 5 ml of PBS with an Omni Tissue homogenizer. The homogenate was serially diluted in PBS and plated on CHA. Plates were incubated seven days at 37°C, 5% CO<sub>2</sub> and counted both two and seven days after plating. Bacterial counts were used to determine CFU/ml of fluid or CFU/g of tissue.

### **3.7 Hematoxylin and eosin staining**

Formaldehyde fixed tissues were paraffin embedded by the University of Pittsburgh McGowan Institute. Tissue sections were cut to 5 µm and mounted on positively charged glass slides. Standard regressive hematoxylin (Cat # MHS16-500ml) and eosin (Cat # E511-100) staining was used to stain for histopathology. Slides were mounted with glass coverslips using a 1:1 xylene/toluene mixture. Slides were imaged at 10X using the Olympus Provis AX70 with MagnaFire v2.1. The transmitted light was set to 9.0 and the exposure time was kept consistent for all slides. The microscope was white balanced, and a blank image was obtained to remove shading. NIS-ElementsAR v5.30.01 was used to remove background shading and scale images to 1.35 µm per pixel

### **3.8 Lung space analysis**

Alveolar space analysis was performed on H&E samples post imaging in FIJI v1.53c. Images were converted to 8-bit and Huang thresholding with dark background was used to distinguish between alveolar spaces and tissues. Regions of interest were selected and alveolar space was assessed using the 'Analyze Particles' function of the FIJI software with size set to 50  $\mu\text{m}^2$  to infinity to exclude nuclei.

### **3.9 Gene expression**

#### **3.9.1 RNA extraction**

For RNA extraction, 0.2 g of tissue was homogenized in 2 ml of TRIzol (Invitrogen Cat # 15596026) and then spun at 600 x g for 5 minutes. The supernatant was transferred to two new 1.5 ml microfuge tubes and stored at  $-20^{\circ}\text{C}$  until inactivation of samples was verified for removal from BSL-3 space. Once removed, samples were defrosted on ice and centrifuged at 12,000 x g at  $4^{\circ}\text{C}$  for 5 minutes to separate out the fatty portion. The clear supernatant was transferred to a new tube and 200  $\mu\text{l}$  of chloroform was added. The sample was shaken vigorously for 15 seconds and incubated at room temperature for three minutes. Samples were centrifuged at 21,000 x g at  $4^{\circ}\text{C}$  for 20 minutes; all centrifuged speeds were 21,000 x g unless otherwise stated. The aqueous phase was transferred to a new 1.5 ml centrifuge tube and 500  $\mu\text{l}$  of ice-cold isopropanol was added. Samples were incubated at  $-20^{\circ}\text{C}$  overnight and then centrifuged at  $4^{\circ}\text{C}$  for 15 minutes. The supernatant was discarded, and the pellet was suspended

in 1 ml of ice-cold 75% ethanol and vortexed. Samples was incubated at room temperature for 10 minutes and then centrifuged at 4°C for five minutes. The supernatant was discarded, and sample tubes were stored upside down for five to ten minutes until pellets dried. Pellets were then suspended with 50 µl of RNase free water.

Samples were read on the Nanodrop One to assess RNA quantity and quality. Samples with 260/280 and 260/230 ratios less than 2.0 were cleaned using Zymogen RNA clean up and concentrator kit (Cat # R1013) per protocol. Polymerase chain reaction (PCR) for rabbit GAPDH was performed on the RNA samples to ensure no DNA was present (sequence listed in Table 2). If positive amplification was seen, RNA clean-up was performed utilizing the Zymogen RNA clean and concentrator kit. RNA cleanup was performed on 5 µl of RNA diluted in 45 µl of RNase free water with on column DNase I treatment. Once samples were cleaned, sample quality was assessed again via Nanodrop One and GAPDH PCR.

### **3.9.2 Microarray**

RNA quantity and quality assessment, cDNA synthesis, and microarray testing (GeneChip™ Rabbit Gene 1.0 ST Array, ThermoFisher) was performed by the University of Pittsburgh's Genomics Core. Differentially expressed gene (DEG) analysis was performed using the Transcriptome Analysis Console (NetAffx). Gene ontology analysis was performed using Partek Genomics Suite and pathway analysis was performed using Ingenuity Pathway Analysis; software licenses were obtained through the Molecular Biology Information Service of the Health Sciences Library System, University of Pittsburgh. Gene ontology analysis utilized mouse gene annotation obtained from [geneontology.org](http://geneontology.org). Pathway analysis utilized mouse, rat, and human gene databases provided by the software.

### **3.9.3 cDNA synthesis for PCR**

RNA was diluted to 3000 ng per 10  $\mu$ l with RNase free water. RNA was incubated at 70°C for seven minutes with 1  $\mu$ l of Oligo (dT)<sub>12-18</sub> primer (Invitrogen Cat. # 18418012). dNTP mix (Thermo Scientific Cat. # R0181) was prepared with 1  $\mu$ l each of dATP, dTTP, dCTP, dGTP and 6  $\mu$ l of RNase free H<sub>2</sub>O. Samples were transferred to ice and 9  $\mu$ l of SuperScript II Kit (Invitrogen Cat. # 18064022) Master Mix utilizing RNasin (Promega Cat. # N2111) and dNTP mix was added. Samples were incubated at 42°C for one hour, followed by 70°C for five minutes to inactivate the enzyme. Samples were stored at -20°C until PCR.

### **3.9.4 PCR**

PCR was performed on the ABI 6 Flex/7 instrument with QuantStudio software in 384-well plates (Thermo Scientific AB1384). Primer sequences for gene targets are listed in Table 2. Master Mix was composed of 7.5  $\mu$ l of Power SYBR Green Master Mix (Applied Biosystems 4367659), 0.3  $\mu$ l each of forward and reverse primer (10 $\mu$ M), 0.9  $\mu$ l of nuclease free H<sub>2</sub>O, and 5  $\mu$ l of cDNA (diluted to 10ng/5 $\mu$ l). PCR cycle conditions were as follows: 60°C for two minutes, 95°C for ten minutes, 40 cycles of 95°C for 15 seconds, 60°C for 15 seconds, 72°C for 45 seconds. Parameters for the dissociation curve were 95°C for 15 seconds, 60°C for 60 seconds, and 95°C for 15 seconds. Temperature increases were set to 1.6 °C/s for PCR and 0.05 °C/s for the melt curve. Relative fold change was determined using the delta-delta CT method. Gene expression data were normalized to the housekeeping genes PPIA and GAPDH.

**Table 2. Primer sequences for gene targets in NZW rabbits**

Gene	NCBI Accession	Primer	Sequence
GAPDH(212)	NM_001082253	F	TGACGACATCAAGAAGGTGGTG
		R	GAAGGTGGAGGAGTGGGTGTC
PPIA(213)	NM_001082057.1	F	AGGGCATGAGCATTGTGGAA
		R	TCCACAGTTGGCAATGGTGA
Caspase 3(213)	NM_001082117.1	F	AAGCCGACTTCCTGTATGCA
		R	CGTACTCTTTCAGCATGGCA
Caspase 9(213)	XM_002722329.1	F	AAACGTGGATTTGGCGTACG
		R	TGCTGCTGAAGTTCACGTTG
IL-1 $\beta$ (212)	NM_001082201	F	TTGAAGAAGAACCCGTCCTCTG
		R	CTCATACGTGCCAGACAACACC
IFN $\beta$ (212)	XM_002707968	F	TCCAACATGGCACGGAAGTCT
		R	TTCTGGAGCTGTTGTGGTTCCT
STAT1(213)	XM_002712346.1	F	TTCAACATCCTGGGCACACA
		R	TGCCAGCGTTCCTCTGTTCT
TNF $\alpha$ (212)	NM_001082263	F	CTGCACTTCAGGGTGATCG
		R	CTACGTGGGCTAGAGGCTTG
IFN $\gamma$ (212)	NM_001081991	F	TGCCAGGACACACTAACCAGAG
		R	TGTCACTCTCCTCTTCCAATTCC
IL-6 (212)	NM_001082064	F	CTACCGCTTTCCCCACTTCAG
		R	TCCTCAGCTCCTTGATGGTCTC
IL-12p35 (212)	XM_002716291	F	AAGGCCAGACAAACTCTAGAATTC
		R	TTGGTAACTCCAGTGGTAAACAGG
CCL2 (214)	NM_001082294.1	F	GTCTCTGCAACGCTTCTGTGCC
		R	AGTCGTGTGTTCTTGGGTTGTGG
CCL4(212)	NM_001082196	F	GAGACCACCAGCCTCTGCTC
		R	TCAGTTCAGTTCCTCAAGTCATCCAC
CXCL10(213)	XM_002717106.1	F	ATAGAAGCATCCTGAGCCCA
		R	GAAGTGCCTCAACTGAGGCCAA
TGF $\beta$ (212)	NM_001082660	F	CAGTGGAAAGACCCACATCTC
		R	GACGCAGGCAGCAATTATCC

### 3.10 ELISAs

Plasma from NZW rabbits infected with S4 was evaluated for 6 cytokines/chemokines by ELISA for the following analytes: CRP, IL-6, C3a, TNF- $\alpha$ , serum amyloid A1, H4, IL-1 $\beta$  and IL-18. Rabbit CRP kits were purchased from Abcam (ab157726) and performed per protocol on plasma diluted to 1:500. All remaining kits were purchased through American Research Products, Inc, MA (CSB-E06903RB, CSB-E09283RB, CSB-E06998RB, CSB-EL020656RB, DL-H4-RB, E-EL-RB0013, E-EL-RB1974). All ELISA kits were performed per kit protocol with the following sample dilutions: CRP (1:500); IL-6 (undiluted); C3a (1:10); TNF- $\alpha$  (1:10); serum amyloid (1:100), H4 (1:10); IL-1 $\beta$  (undiluted); IL-18 (undiluted). Standards curves were generated using four parameter logistic curve in GraphPad Prism 8.

### 3.11 Statistical analysis

Data were collected and organized using spreadsheets in Microsoft Excel 2010; graphing and statistical analyses were conducted using GraphPad Prism 9. Data represent medians with interquartile ranges (IQR) unless otherwise stated. Due to small sample size, non-parametric tests were used for statistical analysis unless otherwise stated.

Differences between vaccine strains were analyzed by fitting a mixed-effects model with Geisser-Greenhouse correction. Sphericity was not assumed and  $\alpha=0.05$ . This mixed model uses a compound symmetry covariance matrix and is fit using Restricted Maximum Likelihood. This method gives the same  $p$  values and multiple comparisons tests as repeated measures

ANOVA in the absence of missing values. In the presence of missing values, the results can be interpreted like repeated measures ANOVA.

## 4.0 Results

### 4.1 Aim 1

Determine how host and bacterial factors affect *F. tularensis* vaccine success.

#### 4.1.1 Aim 1a

##### 4.1.1.1 Sex does not play a significant role in primary S4 infection

Naïve NZW rabbits were exposed to aerosols containing virulent S4 to study the role of sex on disease course of tularemia. Data were obtained from seven separate experiments for a total of eight unvaccinated control rabbits for both male and female groups. Rabbits were exposed via aerosol to a median dose of 4935 CFU of virulent SchuS4. No difference was seen in survival curves between male and female rabbits based on a Mantel-Cox test,  $p$  value  $>0.9999$  (Figure 1A). Rabbits of both sexes became moribund between 4 and 6 DPE. Time to onset of clinical symptoms was 2 DPE for both male and female rabbits (Figure 1B and 1C). Female rabbits exhibited more weight loss compared to male rabbits during the moribund period. Mixed-effect analysis was used to assess differences between sexes over time for clinical signs. Sex did affect weight change over time ( $p$  value = 0.0419 and  $<0.0001$ , respectively), but there was no interaction with time ( $p$  value = 0.0588) (Table 3). Sex did not affect temperature over time post challenge.

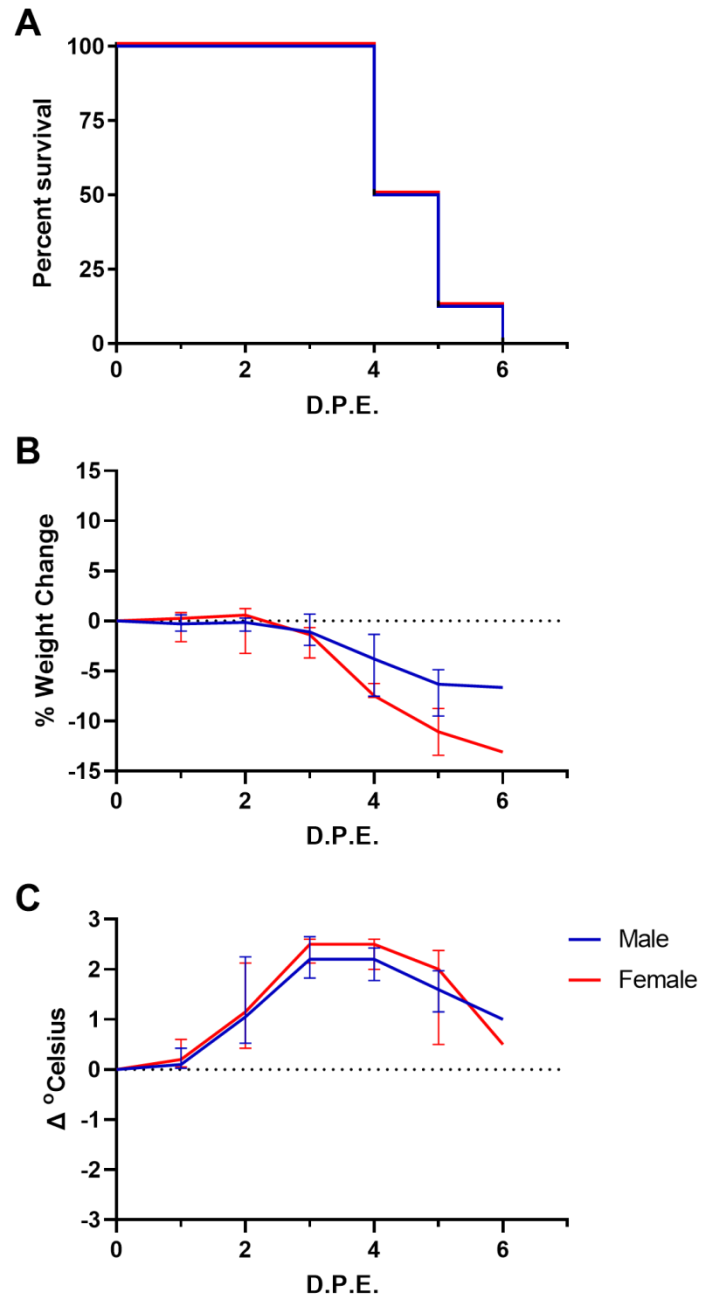


**Figure 1. Sex does not result in differences in SchuS4 clinical disease in naïve NZW rabbits**

Graphs show medians with IQR; males are represented by blue, females by red. Naïve rabbits were challenged with virulent S4 and A) survival, B) weight change, and C) temperature change were assessed. N=8 for each group.

**Table 3. Mixed effects analysis between sexes following challenge of naïve rabbits**

	Time	Sex	Time*Sex
Weight	<b>&lt;0.0001</b>	<b>0.0419</b>	0.0588
Temperature	<b>&lt;0.0001</b>	0.9028	0.8641
WBC	<b>0.0010</b>	0.5059	0.4422
Lymphocytes	<b>0.0433</b>	0.8200	0.5299
Granulocytes	0.2977	0.6344	0.9903
Monocytes	0.6140	0.6815	0.6712
Platelets	<b>0.0026</b>	0.7615	0.3766
ESR	<b>0.0005</b>	0.2238	0.3261

*P* values from mixed-effect modeling with Geisser-greenhouse correction of time and sex for clinical parameters. Significant *p* values (<0.05) indicated in bold.

Blood was collected -2, 4, and 6 DPE for complete blood counts and ESRs. Graphs show values for each subject with error bars representing median and IQR. Median totals of white blood cells (WBC) were higher for males at each time point but trended down throughout infection for both males and females (Figure 2A). Median lymphocyte levels decreased as infection progressed for both male and female rabbits (Figure 2B). Granulocytes and monocytes did not change over time for either sex (Figure 2C and 2D). Median platelet counts decreased over time for male and female rabbits (Figure 2E). Median ESR vales trended lower for males than females but increased over time for both sexes (Figure 2F). Mixed effects analysis indicated time, but not sex was a significant factor for WBCs, lymphocytes, platelets, and ESRs (Table 3). For granulocytes and monocytes, neither time nor sex had a significant effect. These data indicate that sex does not affect survival or clinical disease course of virulent S4 infection in NZW rabbits. It is unclear if sex has no effect or if the effect is masked by how quickly the animals succumb to disease.

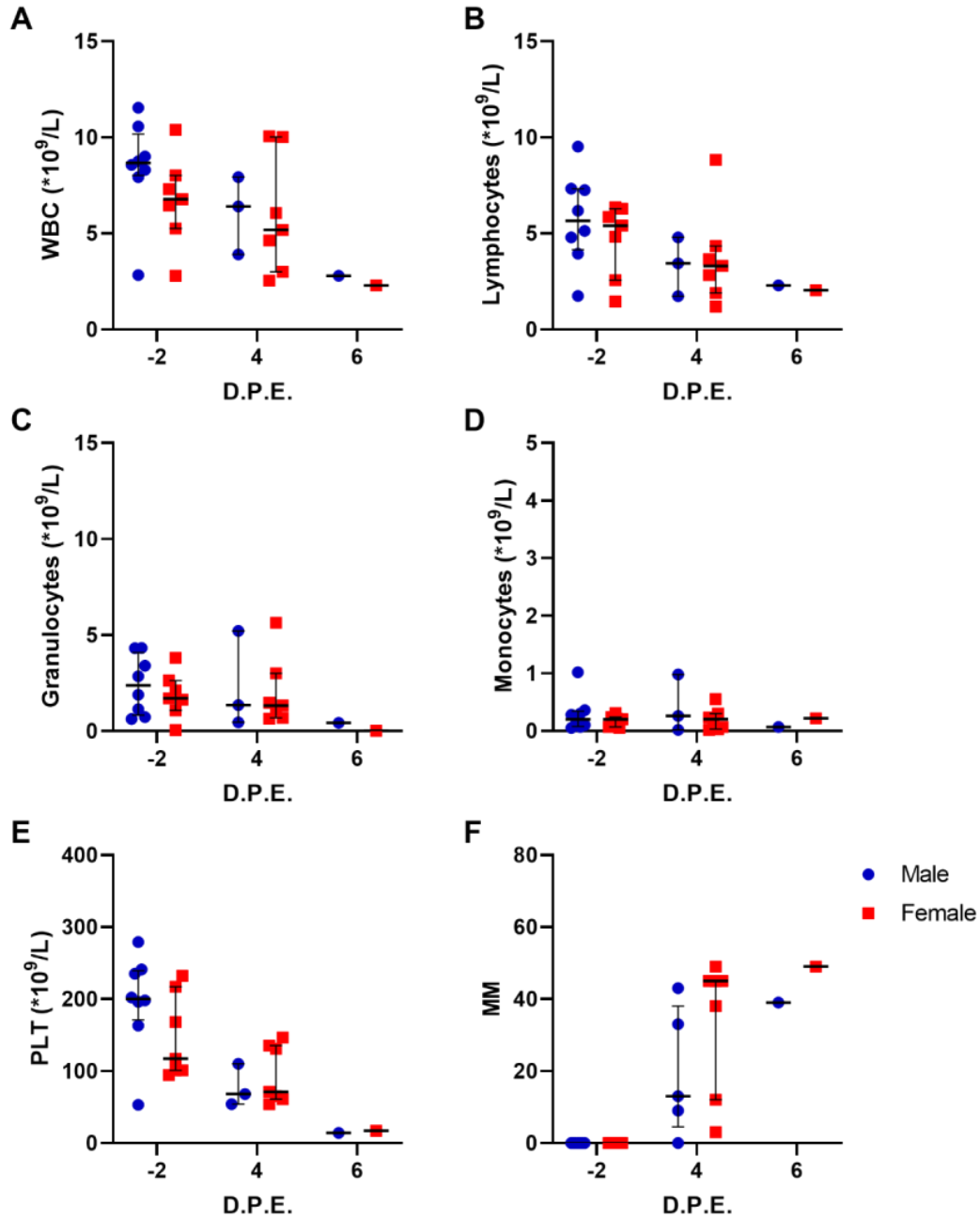


**Figure 2. No differences seen in in vitro diagnostic blood tests between sexes in naïve rabbits**

Graphs show value for each subject with error bars representing median and IQR. Males are represented by blue and females by red. Blood was drawn after exposure to virulent S4 to assess A) Total WBC, B) lymphocytes, C) granulocytes, D) monocytes, E) platelets, and F) ESR.

#### 4.1.1.2 Sex is not a significant factor for vaccine efficacy of S4ΔaroD

Naïve NZW rabbits were prime/boost vaccinated with aerosols containing  $10^8$  CFU of S4ΔaroD. Data were obtained from four separate experiments for a total of 17 females and 13 males. Clinical symptoms were monitored following vaccination and compared between male and female rabbits. Male rabbits exhibited more weight loss than female rabbits during prime vaccination, but both sexes exhibited similar fever profiles (Figure 3A and 3B). Little to no change in weight and fever response was seen in both males and females during boost vaccination (Figure 3C and 3D). Mixed-effects modeling of weight change during prime vaccination indicated sex affected weight change over time ( $p$  value $<0.0001$  and  $p=0.0040$ , respectively), and there is an interaction between sex and time ( $p$  value $<0.0001$ ) (Table 4). As females tend to produce a more robust immune response, it is possible the male NZW rabbits take longer to clear the infection and thus eat less due to a prolonged clinical syndrome resulting in more weight loss. Temperature following prime vaccination and boost vaccination was significantly affected by time, but not sex. Neither sex nor time was a significant factor for weight change during boost vaccination. Šídák's multiple comparison indicated weight change during prime vaccination was significantly different between males and females at 5 DPE. Temperature was significantly different between males and females during boost vaccination at 1 DPE.

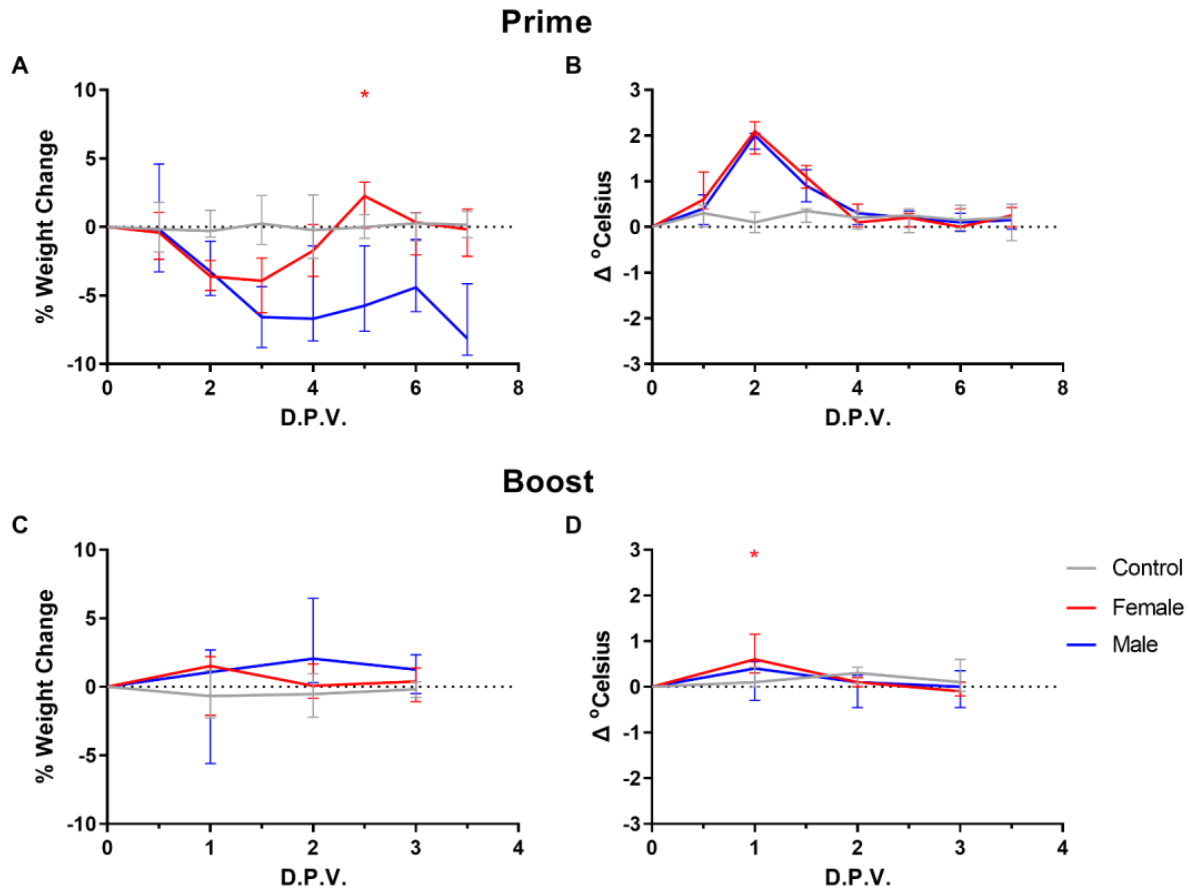


**Figure 3. S4 $\Delta$ aroD vaccination of rabbits results in different clinical signs between males and females**

Graphs show medians with IQR; males are represented by blue, females by red, and control rabbits by grey. A and B) Weight change and temperature was assessed following prime vaccination and C and D)boost vaccination. N=17 and 13 for females and males, respectively.

**Table 4. Mixed effects analysis between sexes following vaccination of naïve rabbits with S4ΔaroD**

		Time	Sex	Time*Sex
Prime	Weight	<b>&lt;0.0001</b>	<b>0.0040</b>	<b>&lt;0.0001</b>
	Temperature	<b>&lt;0.0001</b>	0.0602	0.8956
Boost	Weight	0.2235	0.3036	0.2144
	Temperature	<b>&lt;0.0001</b>	0.0592	<b>0.0052</b>

*P* values from mixed-effect modeling with Geisser-greenhouse correction of time and sex for clinical parameters. Significant *p* values (<0.05) indicated in bold.

Vaccinated rabbits were challenged with a median dose of 3025 CFU of aerosolized S4 30 days after boost vaccination. Vaccine efficacy was 84.6% for males and 64.7% for females (Figure 4A). No significant difference was seen in vaccine efficacy between male and female rabbits based on a one-sided Fisher's exact test ( $p$  value=0.2123). There was a trend for female rabbits to exhibit higher total *F. tularensis* antibody titers compared to males following vaccination (Figure 4B). Sex was found to affect *F. tularensis* antibody titer over time ( $p$  value=0.0099 and  $p$  value<0.0001, respectively), but there is no interaction with time based on mixed-effects modeling (Table 5). Šídák's multiple comparison indicated there was a significant difference between male and female antibody titers 35 days post prime vaccination ( $p$  value=0.0430). During late infection, there was a trend for females to exhibit more weight loss compared to males (Figure 4C). This trend in weight loss for females is associated with the lower vaccine efficacy observed for females and is likely due to persistent tularemia infection in the female rabbits. No difference in temperature was seen between male and female rabbits post challenge (Figure 4D). Mixed-effects analysis indicated sex does affect weight change over time ( $p$  value=0.0419 and  $p$  value<0.0001, respectively), but there is no interaction with time ( $p$  value 0.0588) (Table 4). Time but not sex significantly affected temperature change throughout infection. Temperature was significantly different between males and females 1 DPE based on Šídák's multiple comparison.

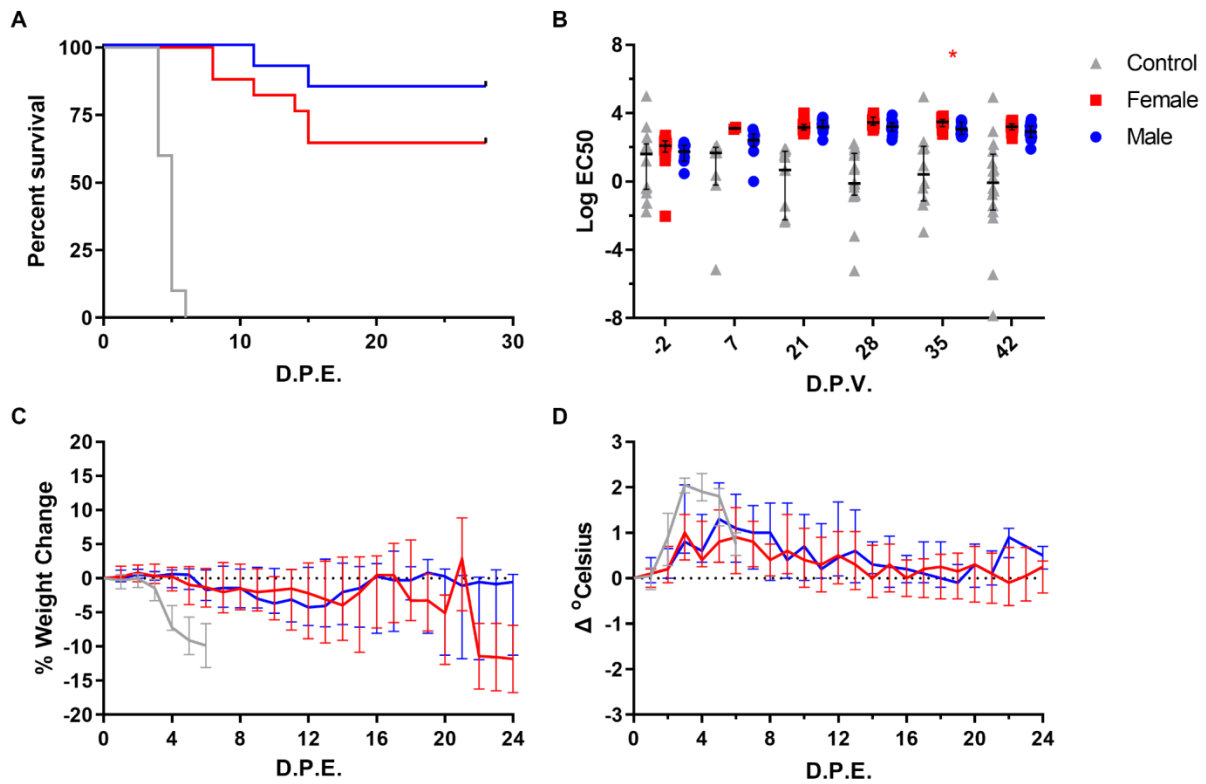


**Figure 4. Sex does not play a significant role in S4ΔaroD vaccine efficacy following SchuS4 challenge**

Graphs show medians with IQR; males are represented by blue, females by red, and control rabbits by grey. Rabbits were vaccinated with S4ΔaroD and then challenged with virulent S4 to determine A) vaccine efficacy, B) *F. tularensis* antibody titer, C) weight change, and D) temperature change.

**Table 5. Mixed effects analysis between sexes following challenge of S4ΔaroD vaccinated rabbits**

	Time	Sex	Time*Sex
Weight	<b>&lt;0.0001</b>	<b>0.0419</b>	0.0588
Temperature	<b>&lt;0.0001</b>	0.9028	0.8641
<i>F. tularensis</i> Ab	<b>&lt;0.0001</b>	<b>0.0099</b>	0.3036
WBC	<b>0.0010</b>	0.5059	0.4422
Lymphocytes	<b>0.0433</b>	0.8200	0.5299
Granulocytes	0.2977	0.6344	0.9903
Monocytes	0.6140	0.6815	0.6712
Platelets	<b>0.0026</b>	0.7615	0.3766
ESR	<b>0.0005</b>	0.2238	0.3261

*P* values from mixed-effect modeling with Geisser-greenhouse correction of time and sex for clinical parameters. Significant *p* values (<0.05) indicated in bold.

Figure 5 shows median CBC and ESR data for male and female rabbits following challenge. No difference was seen between males and females for total white blood cells, lymphocytes, granulocytes, monocytes, or platelets (Figure 5A-E). ESR is a nonspecific measure of inflammation. Red blood cells (RBC) have a net negative charge causing them to repel each other, and thus settle slowly. During inflammation, there is an increase in large, positively charged proteins in the plasma, which reduces the zeta potential between the red blood cells causing them to form rouleaux and settle out of plasma faster. There was a trend for males to exhibit higher ESR during infection compared to females (Figure 5F). Though females tend to produce a more robust immune response, males typically exhibit higher levels of pattern recognition receptors, such as TLR 2, which could explain the trend for elevated ESR in male NZW rabbits. Mixed effects analysis showed time but not sex significantly affected WBCs, lymphocytes, platelets, and ESR following challenge (Table 4).

Female rabbits exhibited a less pronounced clinical syndrome following initial exposure to S4 $\Delta$ aroD compared to males as measured by weight change. This difference was not observed during the boost vaccination. Similar to what has been observed in humans and other animal models, female rabbits exhibit a more robust antibody response compared to male rabbits. The robust antibody response seen in female NZW rabbits does not correlate with the observed vaccine efficacy. Within the limits of the study size there was a trend for males to exhibit a higher vaccine efficacy than females, though this difference was not significant. Thus, sex may play a role in vaccine efficacy of S4 $\Delta$ aroD.

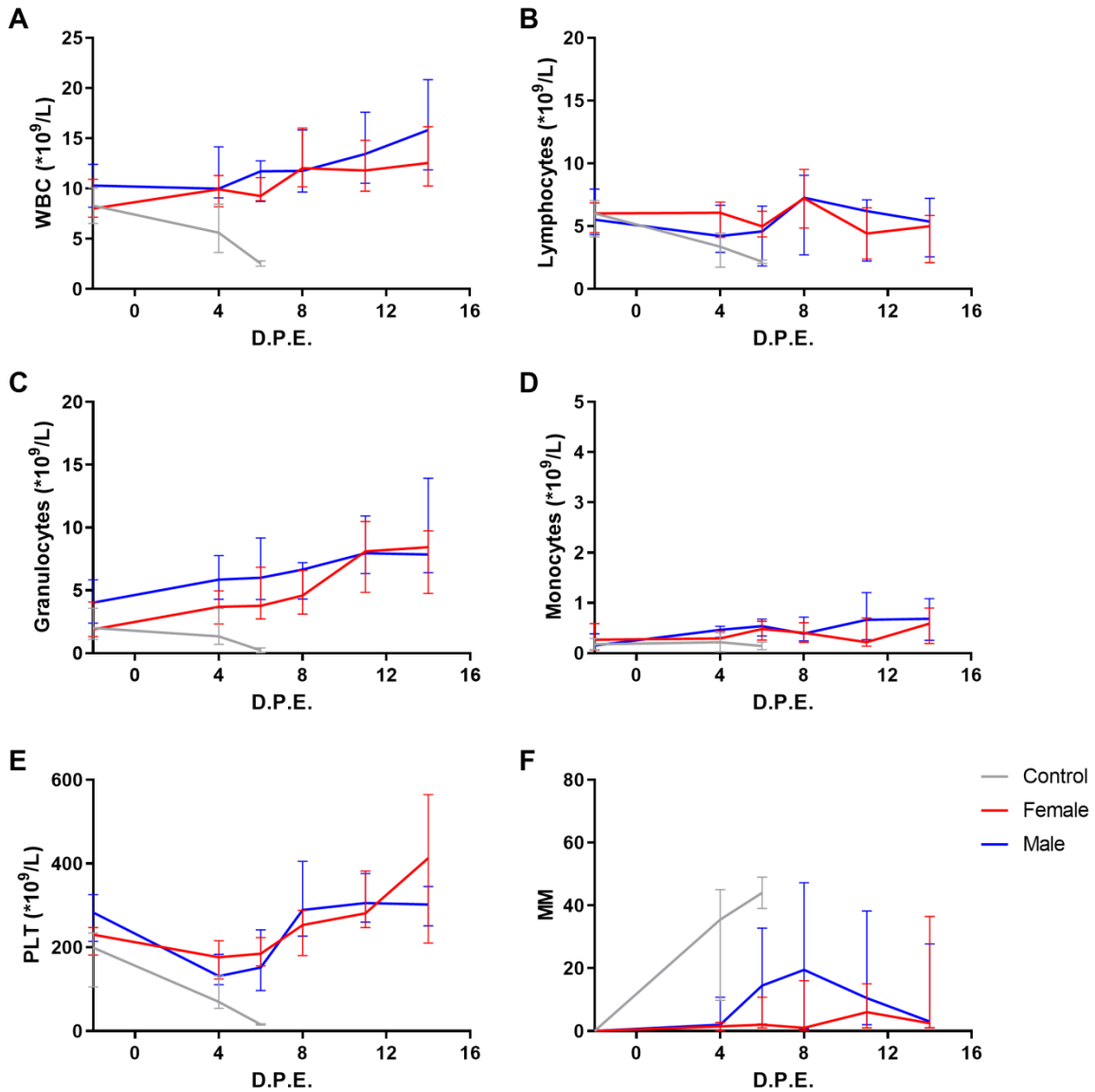


**Figure 5. No differences seen in in vitro diagnostic blood tests between sexes in vaccinated rabbits**

Graphs show medians with IQR; males are represented by blue, females by red, and control rabbits by grey. Rabbits were bled post exposure to assess A) Total WBC, B) lymphocytes, C) granulocytes, D) monocytes, E) platelets, and F) ESR.

#### 4.1.1.3 Sex is not a significant factor for vaccine efficacy for LVS

Sex was also assessed as a biological factor for vaccine efficacy of LVS, an attenuated Type B derived vaccine strain. Naïve rabbits were vaccinated following a prime/boost schedule with aerosols containing  $10^8$  CFU of LVS. Data were obtained from a single experiment with a total of two females and three males. No differences were seen in weight change following prime or boost vaccination between males and females. There was a trend for male rabbits to exhibit higher temperatures than females following exposure to LVS. Sex does not affect weight change over time (Table 6). Sex does affect temperature over time ( $p$  value=0.0360 and  $p$  value=0.0046, respectively), but there is no interaction with time ( $p$  value=0.1813) (Table 6).

**Table 6. Mixed effects analysis between sexes following vaccination of naïve rabbits with LVS**

		Time	Sex	Time*Sex
Prime	Weight	<b>0.0346</b>	0.6112	0.4960
	Temp	<b>0.0046</b>	<b>0.0360</b>	0.1813
Boost	Weight	0.1526	0.2560	0.2490
	Temp	0.1294	0.0540	0.9607

*P* values from mixed-effect modeling with Geisser-greenhouse correction of time and sex for clinical parameters. Significant *p* values (<0.05) indicated in bold.

Vaccinated rabbits were challenged with a median dose of 462 CFU of aerosolized S4. No difference was seen in weight change or temperature following challenge. Vaccine efficacy was 50.0% for females and 0% for males (Figure 6A). There was a trend for female rabbits to have higher vaccine efficacy compared to males, but due to study size limitations this difference was not significant based on a one-sided Fisher's exact test ( $p$  value=0.4000). Male and female rabbits exhibited similar antibody titers up to 28 days post vaccination (Figure 6B). Sex does not affect *F. tularensis* antibody titer over time ( $p$  value =0.4234 and  $p$  value =0.0366, respectively (Table 7). No difference was seen in CBC results between male and females following challenge. ESR peaks two days sooner in females compared to males. Mixed effects analysis indicate time, but not sex, was a significant factor for weight change and granulocytes following challenge (Table 7). Sex was not a significant factor for any parameter following challenge of LVS vaccinated rabbits.

The trend for differences in vaccine efficacy between male and female NZW rabbits for both S4ΔaroD and LVS highlights the importance of assessing the role of sex on vaccine efficacy. For S4ΔaroD, there was a trend for males to exhibit better vaccine efficacy, but for LVS, there was a trend for females to exhibit better vaccine efficacy. This difference in sex trends between two different vaccine strains suggests that sex dependent difference in vaccine efficacy are strain specific. Since vaccine efficacy between males and females was not significantly different, the remainder of data presented in this work will not be stratified by sex.

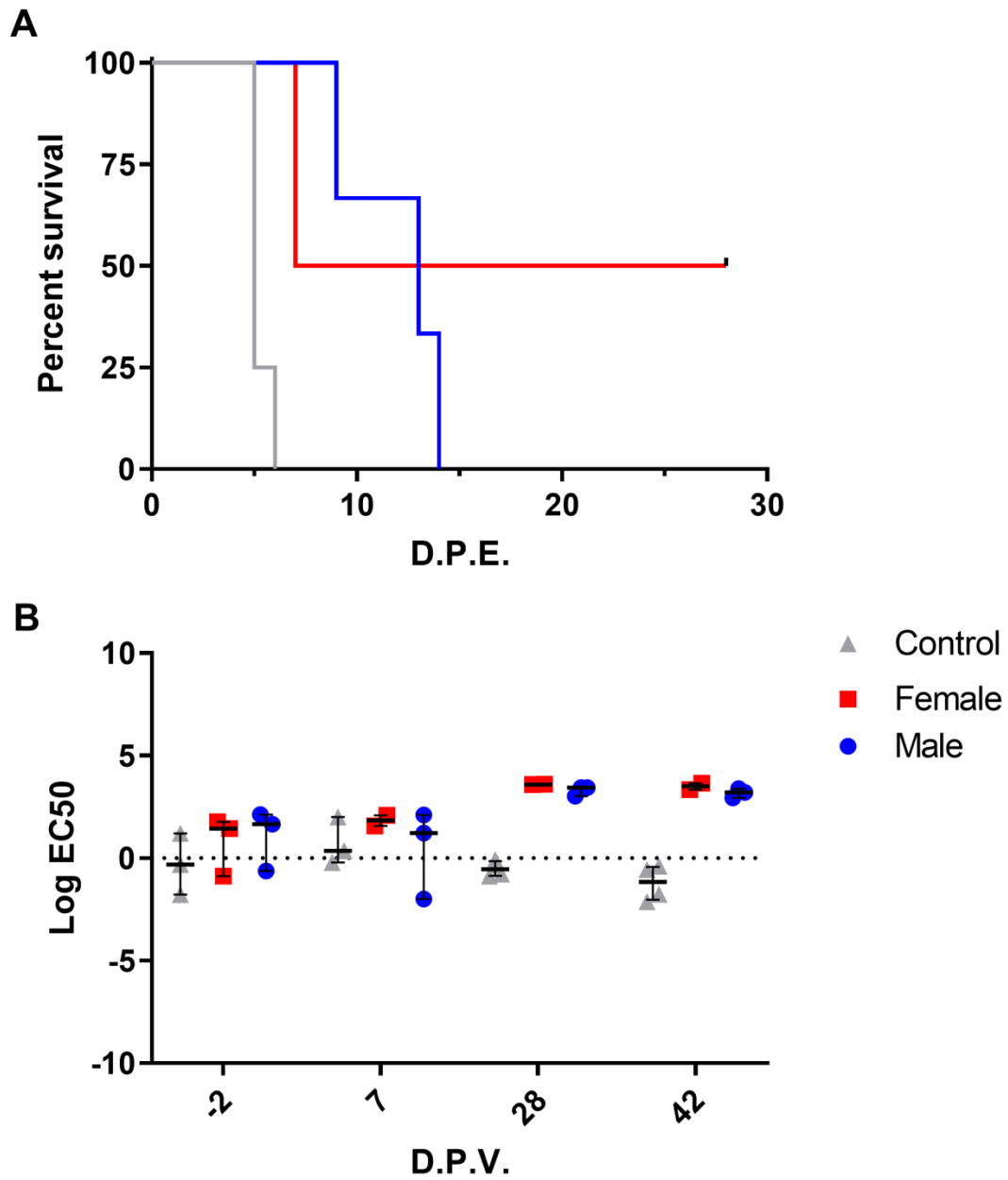


**Figure 6. Sex does not affect LVS vaccine efficacy in challenge NZW rabbits**

Graphs show medians with IQR; males are represented by blue, females by red, and control rabbits by grey. NZW rabbits were vaccinated with LVS and then challenge with virulent S4. A) Vaccine efficacy and B) *F. tularensis* antibody titer were assessed for each sex. N=2 and 3 for females and males, respectively.

**Table 7. Mixed effects analysis between sexes following challenge of LVS vaccinated rabbits**

	Time	Sex	Time*Sex
Weight	<b>0.0059</b>	0.5552	0.7056
Temperature	0.1265	0.1961	0.6957
<i>F. tularensis</i> Ab	<b>0.0366</b>	0.4234	0.7229
WBC	0.0556	0.7350	0.0799
Lymphocytes	0.1873	0.9350	0.2687
Granulocytes	<b>0.0455</b>	0.4530	<b>0.0270</b>
Monocytes	0.2717	0.3221	0.4252
Platelets	0.0818	0.4815	0.6899
ESR	0.0662	0.2694	0.1370

*P* values from mixed-effect modeling with Geisser-greenhouse correction of time and sex for clinical parameters. Significant *p* values (<0.05) indicated in bold.

### **4.1.2 Aim 1b**

Some of the work shown in Aim 1b has been published in *Infection and Immunity* in partial fulfillment of PhD requirements (215).

#### **4.1.2.1 Growth conditions for challenge material affect vaccine efficacy**

Our lab utilizes BHI to grow *F. tularensis* as growth in BHI resulted in better aerosol performance compared to growth in MHb (166). Most research groups studying *F. tularensis* utilize MHb. Proteomic analysis of *F. tularensis* grown in different culture mediums show BHI-grown *F. tularensis* has an increased expression of virulence proteins compared to MHb-grown *F. tularensis* (168). These differences have been shown to have effects within host cells. The LD<sub>99</sub> of mice exposed to BHI-grown *F. tularensis* is 1 log lower compared to mice exposed to MHb-grown *F. tularensis* (166). Naïve macrophages exposed to BHI-grown *F. tularensis* exhibit less secretion of proinflammatory cytokines compared to MHb-grown *F. tularensis* (168). Additionally, there has been some dispute regarding the appropriateness of the NZW rabbit model for studying *F. tularensis* due to the disparity seen with LVS vaccination compared to other animal models. In NZW rabbits, LVS only extended time to death following challenge, while LVS vaccination in Fisher 344 rats and NHPs resulted in 100% protection (76, 167). An important distinction between these studies is the choice of growth medium. The NZW rabbit study utilized BHI broth, while the rat and NHP studies used MHb.

To assess if growth condition of virulent S4 used in challenge can affect vaccine efficacy we vaccinated naïve NZW rabbits with aerosols containing 10<sup>8</sup> CFU of LVS grown in BHI following the prime/boost schedule described in the methods. Both groups had similar antibody titers 28 and 42 days post prime vaccination (days 14 and 28 post boost vaccination) suggesting

there was no difference in vaccination status between the two groups to account for any differences observed between the two groups (Figure 7B). Thirty days after the boost vaccination, LVS-vaccinated rabbits were challenged by aerosol exposure to SchuS4 grown in BHI broth or MHb. Data were obtained from a single experiment with six rabbits in the MHb group and five rabbits in the BHI group (one rabbit in the BHI group had died from complications with aerosol delivery of the prime vaccination resulting in uneven distribution of rabbits between groups). The MHb group received a median dose of 347 CFU of virulent S4 and the BHI group received a median dose of 462 CFU of virulent S4. There was no significant difference between these doses based on a Mann Whitney test ( $p$  value  $>0.9999$ ).

Fifty percent of LVS-vaccinated rabbits survived challenge with S4 grown in MHb while only 20.0% of LVS-vaccinated rabbits survived challenged with S4 grown in BHI (Figure 7A). This difference was suggestive but not statistically significant based on a one-sided Fisher's exact test ( $p$  value =0.3485). Rabbits challenged with BHI grown S4 exhibited more weight loss compared to rabbits challenged with MHb grown S4 (Figure 7C). There was a trend for rabbits exposed to BHI grown S4 to exhibit increased temperatures earlier and longer than rabbits exposed to the MHb grown S4 (Figure 7D). Mixed-effects analysis indicated growth condition did affect weight change over time ( $p$  value =0.0032 and  $p$  value  $<0.0001$ , respectively), and there is an interaction with time ( $p$  value  $<0.0001$ ) (Table 8). Growth condition was not a significant factor for temperature change (Table 8).

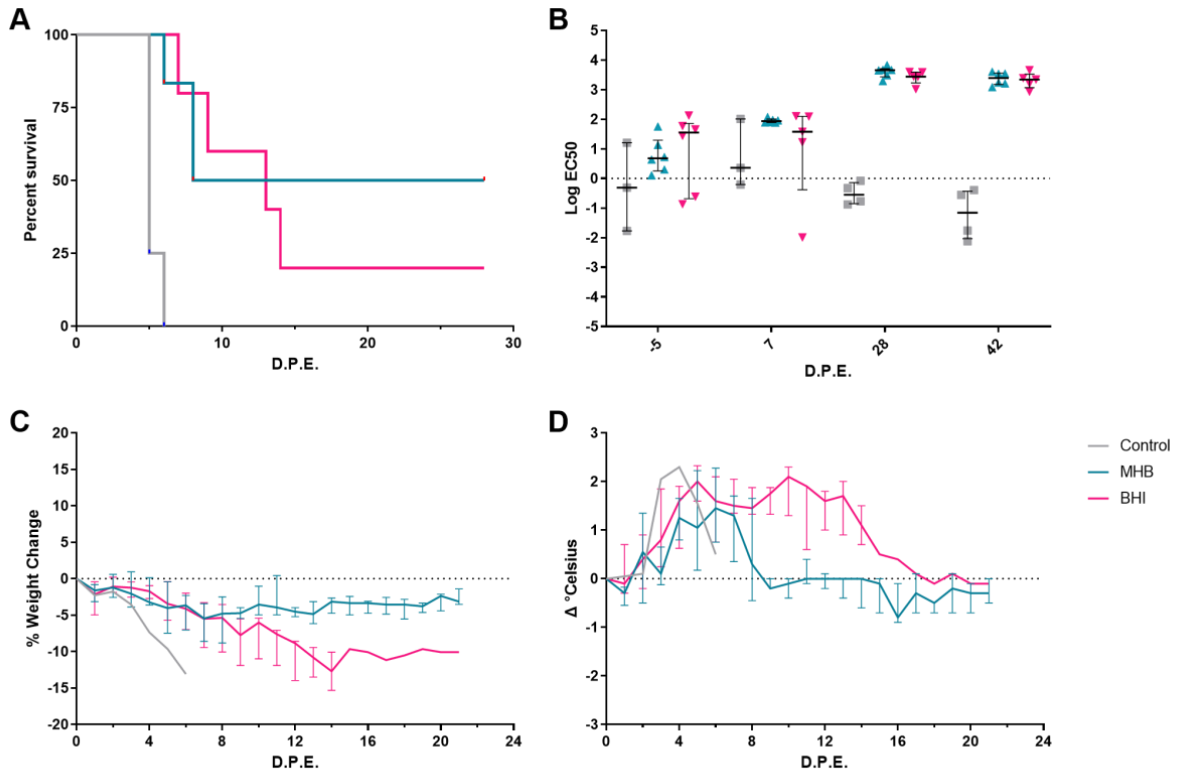


**Figure 7. Rabbits exhibit clinical signs of more severe disease when challenged with S4 grown in BHI**

Graphs show medians with IQR; MHB group is represented by teal, BHI group by pink, and control rabbits by grey. Rabbits were vaccinated with LVS and then challenged with virulent S4 grown in BHI or MHB to determine A) vaccine efficacy, B) *F. tularensis* antibody titer, C) weight change, and D) temperature change. N=6,5 for MHB and BHI groups, respectively (215).

**Table 8. Mixed effects analysis between LVS vaccinated rabbits challenged with S4 grown in MHb or BHI**

	Time	Broth	Time*Broth
Weight	<b>&lt;0.0001</b>	<b>0.0032</b>	<b>&lt;0.0001</b>
Temperature	<b>0.0014</b>	0.1541	<b>0.0166</b>
<i>F. tularensis</i> Ab	<b>&lt;0.0001</b>	0.2909	0.3990
WBC	<b>0.0101</b>	0.9818	0.0221
Lymphocytes	0.3386	0.2977	0.0569
Granulocytes	<b>0.0051</b>	0.1896	<b>0.0011</b>
Monocytes	0.1798	0.8736	0.0712
Platelets	<b>0.0001</b>	0.9765	0.6486
ESR	<b>0.0005</b>	0.0506	<b>0.0248</b>

*P* values from mixed-effect modeling with Geisser-greenhouse correction of time and broth for clinical parameters. Significant *p* values (<0.05) indicated in bold.

Figure 8 shows CBC and ESR data following challenge. LVS-vaccinated rabbits exposed to MHb grown S4 had higher total WBC counts during late infection than LVS-vaccinated rabbits exposed to BHI grown S4 (Figure 8A). No difference was observed between granulocytes, monocytes, and platelets following challenge in LVS-vaccinated rabbits (Figure 8C, 8D, and 8E). There was a trend for LVS-vaccinated rabbits exposed to BHI grown S4 to exhibit lower total lymphocytes counts compared to LVS-vaccinated rabbits exposed to MHb grown S4 during late infection (Figure 8B). Additionally, there was a trend for LVS-vaccinated rabbits challenged with BHI grown S4 to have higher ESRs compared to LVS-vaccinated rabbits challenged with MHb grown S4 starting 8 DPE (Figure 8F). Time but not growth condition was a significant factor for total WBCs, granulocytes, platelets, and ESR (Table 8). Broth choice did not affect granulocytes or ESR over time, but there was an interaction with time for both analytes. The trend in data for weight loss, fever, CBC results, and ESR indicates that choice of

broth media used for challenge material can affect vaccine efficacy. Based on clinical symptoms, BHI broth resulted in a more severe infection compared to MHB. Thus, BHI grown S4 represents a more robust challenge for use in vaccine efficacy studies. Additionally, choice of growth medium partially explains the differences in LVS vaccine efficacy between the NZW rabbit, Fisher 344 rat, and cynomolgus macaque models. NZW rabbits are a suitable model to assess vaccine efficacy of attenuated *F. tularensis* strain. The NZW rabbit model would be more useful than the rat and NHP model, which have 100% survival following vaccination with LVS, as they would allow for the detection of vaccines that protect better than LVS.

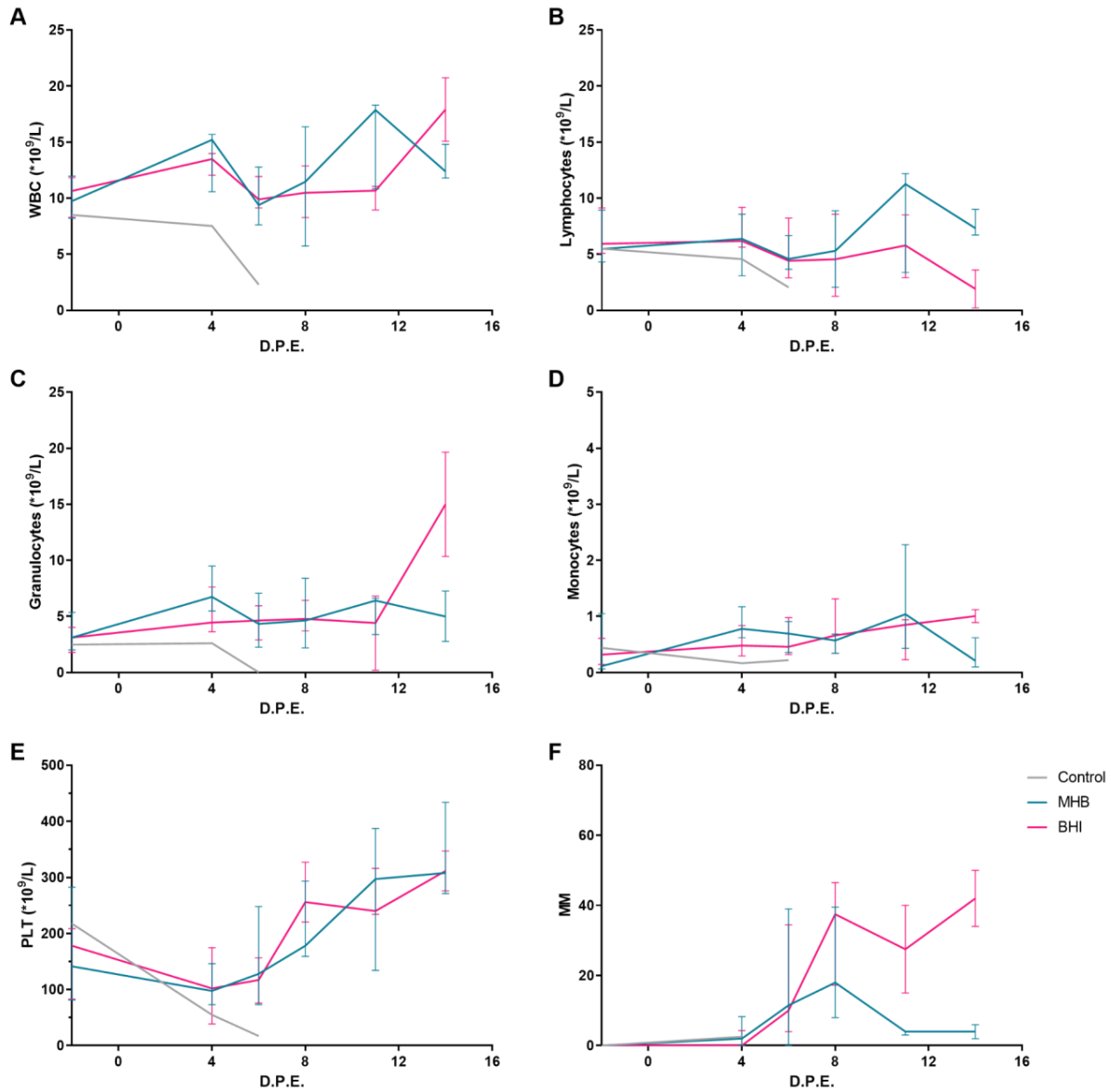


**Figure 8. MHB S4 challenged rabbits exhibit less severe loss of lymphocytes and increase in ESR compared to BHI S4 challenged rabbits**

Graphs show medians with IQR; MHB group is represented by teal, BHI group by pink, and control rabbits by grey. Rabbits were bled post exposure to assess A) Total WBC, B) lymphocytes, C) granulocytes, D) monocytes, E) platelets, and F) ESR.

### 4.1.3 Aim 1c

Some of the work shown in Aim 1c has been published in PLOS ONE in partial fulfillment of PhD requirements (180).

#### 4.1.3.1 S4ΔaroD protects better than other attenuated *F. tularensis* strains

##### 4.1.3.1.1 LVS

We have previously shown a prime/boost vaccine regimen improves vaccine efficacy of S4ΔaroD. A single aerosol dose of S4ΔaroD results in a vaccine efficacy of 16.7% in NZW rabbits, while a prime/boost regimen increases vaccine efficacy to 66% (177, 180). The prime/boost vaccine regimen had not been assessed for LVS in the NZW rabbit model. We have previously determined a single aerosol vaccination with LVS only extended time to death (Figure 9A) (216).

To determine the vaccine efficacy of LVS utilizing our standard study design, we vaccinated 5 NZW rabbits with aerosols containing  $10^8$  CFU of LVS following a prime/boost regimen. Rabbits were challenged via aerosol with a median inhaled dose of 316 CFU of virulent S4 30 days following the final vaccination. Data obtained from this experiment were compared with historical data from a single prime LVS vaccine study with 6 NZW rabbits. No difference was seen between prime vaccination doses and challenge doses between studies based on a Mann Whitney test ( $p$  value =0.1797 and  $p=0.1812$ , respectively).

A prime/boost regimen of LVS resulted in a vaccine efficacy of 20%. Difference in survival was not significantly different based on a one-sided Fisher's exact test ( $p=0.4545$ ).

Median survival time was 9 days for rabbits receiving a single vaccination and 13 days for rabbits receiving the prime/boost regimen. Assessment of antibody response to whole heat killed *F. tularensis* following vaccination showed antibody titers were elevated compared to naïve animals 14 and 28 days after the final vaccination (Figure 9B). Mixed effects analysis indicated vaccine schedule did affect antibody titers over time ( $p$  value =0.0222 and  $p$  value =0.0224, respectively) and there was an interaction with time ( $p$  value =0.0287). Antibody titers 28 days following the final vaccination were significantly different between the single prime and prime/boost vaccinated groups based on Šídák's multiple comparison ( $p$  value =0.0032). Both groups exhibited similar patterns in weight change following challenge (Figure 9C). Weight change began 1 DPE for both prime and prime/boosted animals, but prime vaccinated animals exhibited an overall larger median weight loss over time. Temperature increased for both groups starting 1 DPE with the single prime vaccinated group reaching higher elevations earlier during infection compared to the prime/boost vaccinated group (Figure 9D). Mixed effects analysis indicates time, but not schedule, affected weight and temperature change ( $p$  value <0.0001 and  $p$  value =0.0013, respectively).

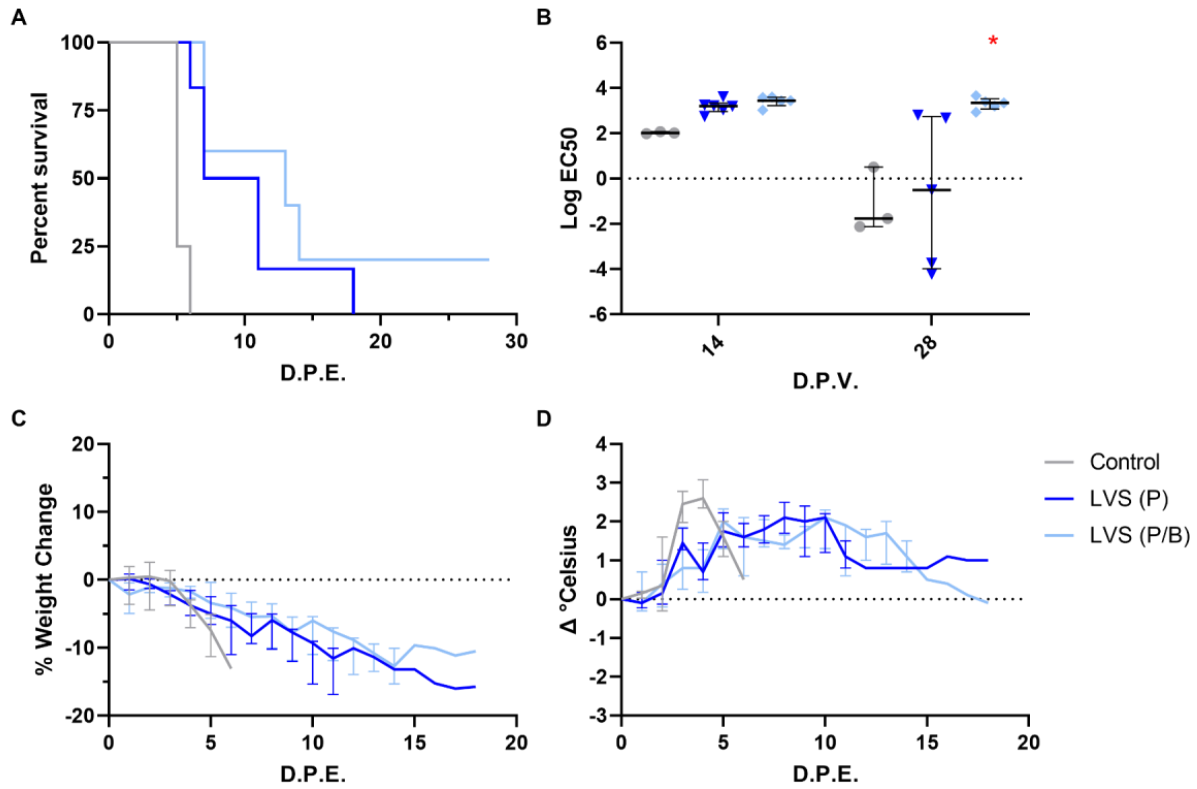


**Figure 9. Prime/boost vaccination resulted in higher *F. tularensis* specific antibodies**

Graphs show medians with IQR; single prime vaccination is represented by dark blue, prime/boost vaccination is represented by light blue, and control rabbits by grey. Rabbits were vaccinated with LVS and then challenged with virulent S4 to determine A) vaccine efficacy, B) *F. tularensis* antibody titer, C) weight change, and D) temperature change.

#### 4.1.3.1.2 S4ΔguaBA

An aerosol prime/boost vaccination with S4ΔguaBA did not protect mice from challenge, but a single scarification resulted in 27.3% survival in NZW rabbits (177, 182). We assessed the deletion mutant S4ΔguaBA in the NZW rabbits utilizing the aerosol prime/boost vaccination regimen. Twelve rabbits were exposed to aerosols containing  $10^7$  CFU of either S4ΔaroD or S4ΔguaBA. After 14 days, rabbits received a second dose of the same vaccine at a concentration of  $10^8$  CFU. No statistical difference was observed between vaccination doses for the prime or boost vaccination based on a Mann Whitney test ( $p=0.9372$  and  $p$  value  $=0.4134$ , respectively). Thirty days after the second vaccination NZW rabbits were challenged with a median dose of 1,310 CFU of virulent S4. No difference was observed in inhaled doses of S4 during challenge between vaccine groups ( $p$  value  $=0.8182$ ).

S4ΔaroD resulted in an observed vaccine efficacy of 66.7% while S4ΔguaBA resulted in a vaccine efficacy of 50.0% (Figure 10A). Due to the small study size this difference in vaccine efficacy was not significant based on a two-sided Fisher's exact test ( $p$  value  $>0.9999$ ). Antibody titer responses to whole heat-killed *F. tularensis* were elevated for both vaccine groups compared to naive NZW rabbits 21 to 42 days after the prime vaccination (Figure 10B). Time, but not vaccine strain, affected antibody responses based on a mixed-effects analysis (Table 9). No significant differences were observed in *F. tularensis* antibody titers between vaccine groups. Following exposure to virulent S4, there was a trend for S4ΔguaBA-vaccinated rabbits to exhibit more weight loss and elevated temperature during early infection compared to S4ΔaroD-

vaccinated rabbits (Figure 10C and 10D). Vaccine choice did not affect weight or temperature change during challenge over time (Table 10).

Results for clinical laboratory tests performed on the rabbits following challenge are shown in Figure 11. Total WBC count was similar between vaccine groups (Figure 11A). Rabbits vaccinated with S4ΔguaBA exhibited a decrease in total lymphocyte count (Figure 12B). Granulocytes increased overtime in both vaccine groups. There was a trend for total counts to be more elevated in S4ΔguaBA-vaccinated rabbits (Figure 11C). No significant changes over time were observed in total monocyte counts between vaccine groups (Figure 11D). There was a trend for S4ΔguaBA-vaccinated rabbits to exhibit lower platelet levels and elevated ESR compared to S4ΔaroD vaccinated rabbits (Figure 11E and 11F). Time, but not vaccine group, significantly affected WBCs, granulocytes, and platelets ( $p$  value =0.0004,  $p$  value =0.0127, and  $p$  value =0.0150, respectively) (Table 10). Platelet count was significantly different between vaccine groups 6 DPE based on Šídák's multiple comparison ( $p$  value =0.0071). Thus, both vaccines resulted in similar antibody titers and were able to protect against severe disease. There was a trend for S4ΔaroD vaccination to have better vaccine efficacy and protect against clinical symptoms compared to S4ΔguaBA in a head-to-head challenge.

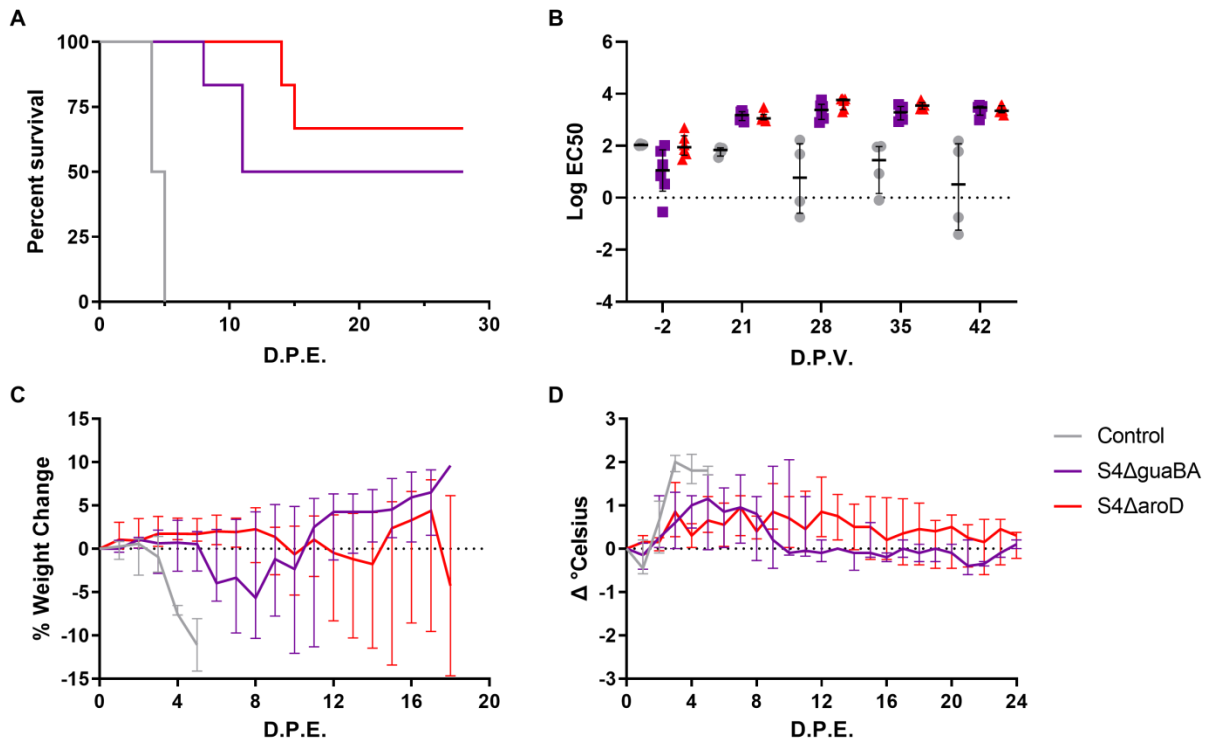


**Figure 10. S4ΔaroD vaccinated rabbits exhibit better vaccine efficacy compared to S4ΔguaBA vaccinated rabbits**

Graphs show medians with IQR; S4ΔaroD is represented by red, S4ΔguaBA is represented by purple, and control rabbits by grey. Rabbits were vaccinated with S4ΔaroD or S4ΔguaBA and then challenged with virulent S4 to determine A) vaccine efficacy, B) *F. tularensis* antibody titer, C) weight change, and D) temperature change.

**Table 9. Mixed effects analysis between S4 $\Delta$ aroD and S4 $\Delta$ guaBA vaccinated rabbits**

	Time	Vaccine	Time*Vaccine
Weight	0.3579	0.8509	<b>0.0320</b>
Temperature	<b>0.0384</b>	0.8506	0.6897
<i>F. tularensis</i> Ab	<b>&lt;0.0001</b>	0.0596	<b>0.0011</b>
WBC	<b>0.0004</b>	0.4007	0.9123
Lymphocytes	0.3847	0.6634	<b>0.0003</b>
Granulocytes	<b>0.0127</b>	0.3766	0.0958
Monocytes	0.0849	0.3320	0.1576
Platelets	<b>0.0150</b>	0.1849	0.3231
ESR	0.0683	0.7679	0.3394

*P* values from mixed-effect modeling with Geisser-greenhouse correction of time and vaccine for clinical parameters. Significant *p* values (<0.05) indicated in bold.

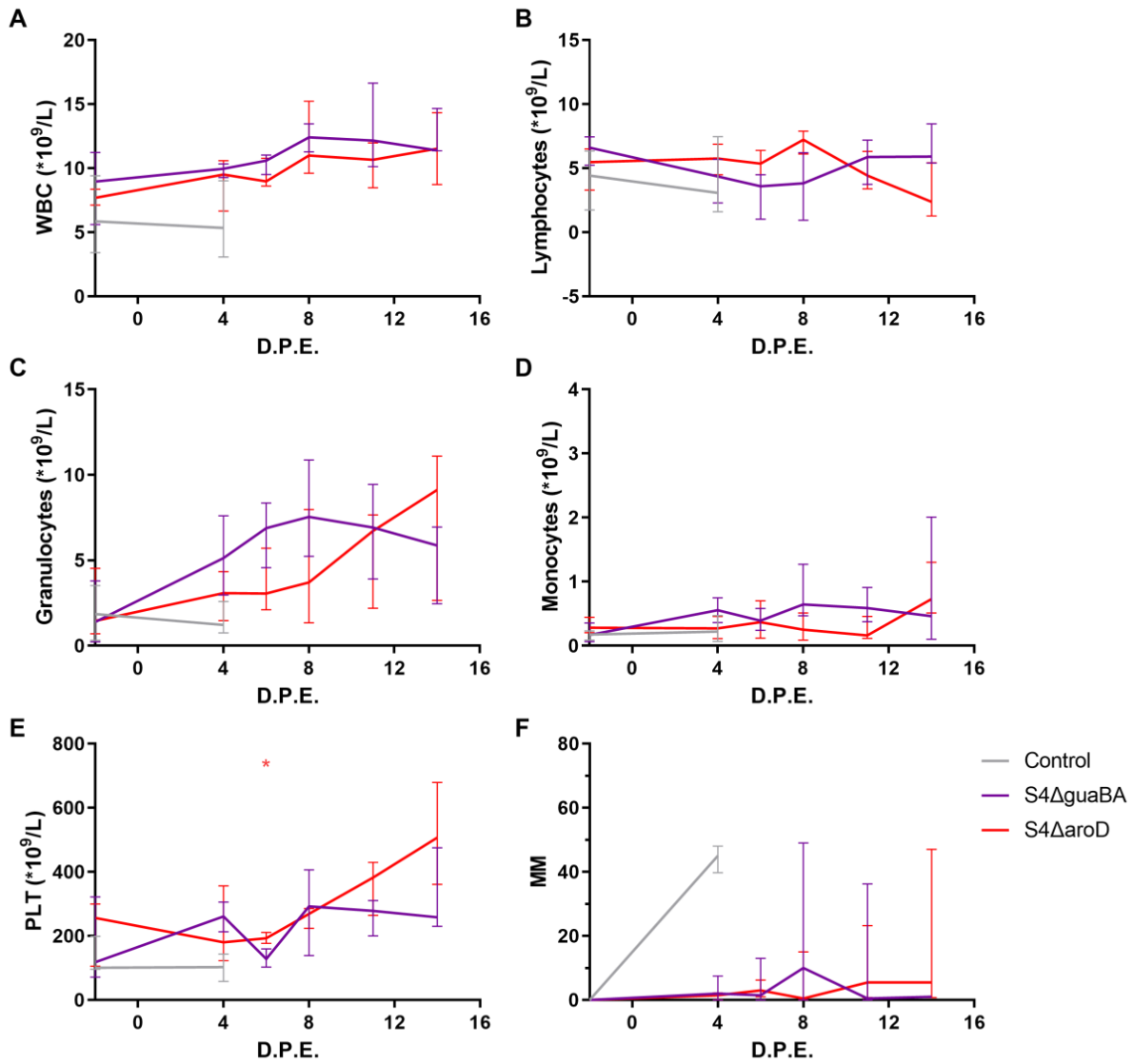


**Figure 11. No differences observed in clinical blood parameters during challenge between vaccine strains**

Graphs show medians with IQR; S4ΔaroD is represented by red, S4ΔguaBA is represented by purple, and control rabbits by grey. Rabbits were bled post exposure to assess A) Total WBC, B) lymphocytes, C) granulocytes, D) monocytes, E) platelets, and F) ESR.

#### 4.1.3.1.3 S4ΔclpB

S4ΔclpB is another SchuS4 derived vaccine strain that has shown promising vaccine efficacy in mouse and rat studies (187, 217). This mutant was assessed in a head-to-head challenge with S4ΔaroD. Twelve rabbits were vaccinated in a prime/boost regimen with aerosols containing  $10^8$  CFU of S4ΔaroD or S4ΔclpB. No significant difference in dose was observed between groups for prime vaccination based on a Mann Whitney test ( $p$  value=0.4199). Doses for boost vaccination were significantly different between vaccine groups ( $p$  value=0.0022) with the median dose being  $4.95 \times 10^8$  CFU for the S4ΔaroD group and  $1.03 \times 10^8$  CFU for the S4ΔclpB group. Thirty days after the final vaccination rabbits were challenged with a median dose of 1,750 CFU of virulent S4. No difference was observed in challenge dose between vaccine groups ( $p$  value=0.4848).

Vaccine efficacy for S4ΔaroD and S4ΔclpB was 66.7% and 33.3% respectively (Figure 12A). Due to study size limitations, this observed difference was not significant based on a two-sided Fisher's exact test ( $p$  value=0.5671). Vaccinated rabbits from both groups exhibited higher antibody titers compared to naïve rabbits, but no difference was observed between vaccine groups (Figure 12B). Vaccine group did not affect antibody titer over time (Table 10). There was a trend for S4ΔclpB-vaccinated rabbits to exhibit more weight loss and higher temperature during late infection compared to S4ΔaroD-vaccinated rabbits (Figure 12C and 12D). Mixed effects modeling indicated time, but not vaccine, affected weight and temperature ( $p$  value=0.0153 and  $p$  value=0.0230, respectively) (Table 10).

CBC analysis showed no significant differences between groups in WBC, lymphocyte, and granulocyte counts following challenge (Figure 13A, 13B, and 13C). There was a trend for

monocyte counts to be increased S4 $\Delta$ clpB-vaccinated rabbits, but not S4 $\Delta$ aroD-vaccinated rabbits (Figure 13D). Platelets decreased 4 DPE for both vaccine groups (Figure 13E). ESR rates increased 6 to 8 DPE for the S4 $\Delta$ aroD and S4 $\Delta$ clpB group, but there was a trend for ESR to remain elevated longer in the S4 $\Delta$ clpB-vaccinated group (Figure 14F). Mixed effects modeling indicated time, but not vaccine, affected WBC, granulocytes, platelets, and ESR ( $p$  value =0.0437,  $p$  value <0.0001,  $p$  value =0.0004, and  $p$  value =0.0033, respectively (Table 10). Taken together, S4 $\Delta$ aroD vaccinated rabbits exhibited better vaccine efficacy and were protected more from severe disease compared to S4 $\Delta$ clpB vaccinated rabbits when challenged with virulent S4.

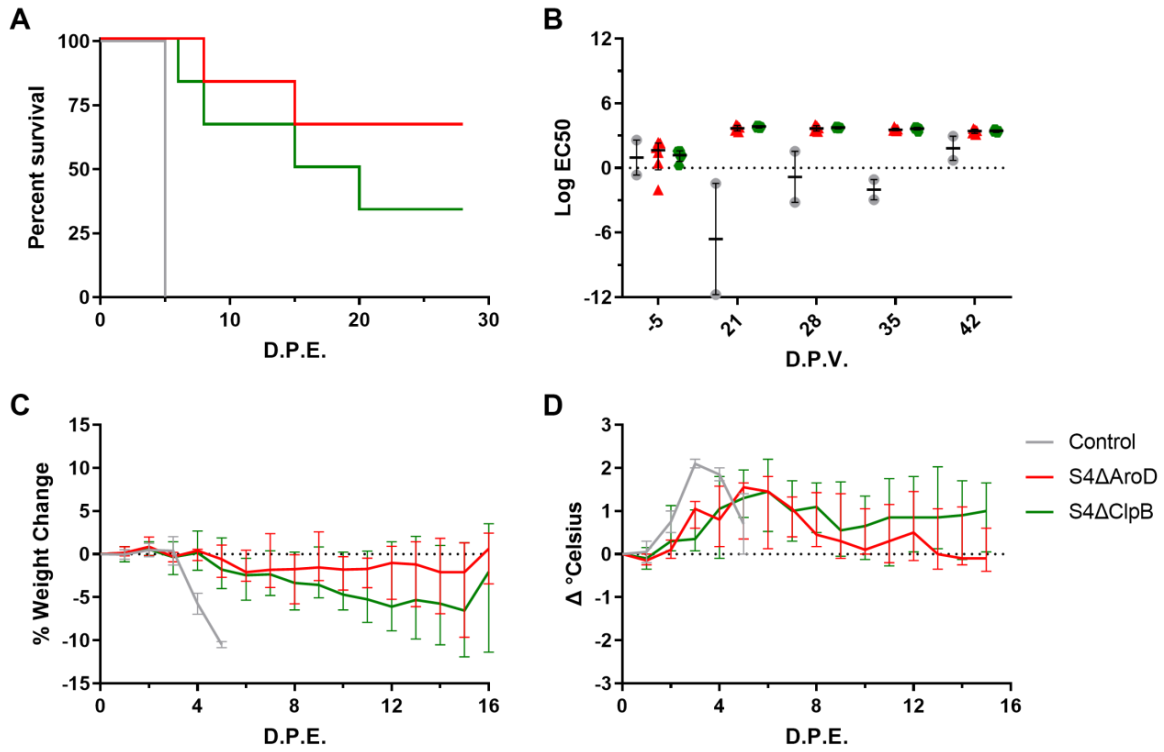


**Figure 12. S4ΔaroD vaccinated rabbits exhibit better vaccine efficacy compared to S4ΔclpB vaccinated rabbits**

Graphs show medians with IQR; S4ΔaroD is represented by red, S4ΔclpB is represented by green, and control rabbits by grey. Rabbits were vaccinated with S4ΔaroD or S4ΔclpB and then challenged with virulent S4 to determine A) vaccine efficacy, B) *F. tularensis* antibody titer, C) weight change, and D) temperature change.

**Table 10. Mixed effects analysis between S4ΔaroD and S4ΔclpB vaccinated rabbits**

	Time	Vaccine	Time*Vaccine
Weight	<b>0.0153</b>	0.3608	0.9553
Temperature	<b>0.0230</b>	0.2217	0.5896
<i>F. tularensis</i> Ab	<b>&lt;0.0001</b>	0.7625	0.9993
WBC	<b>0.0437</b>	0.2889	0.4991
Lymphocytes	0.3334	0.2480	0.7428
Granulocytes	<b>&lt;0.0001</b>	0.7649	0.7029
Monocytes	0.1201	0.4305	0.3792
Platelets	<b>0.0004</b>	0.6544	0.7857
ESR	<b>0.0033</b>	0.8287	0.9779

*P* values from mixed-effect modeling with Geisser-greenhouse correction of time and vaccine for clinical parameters. Significant *p* values (<0.05) indicated in bold.

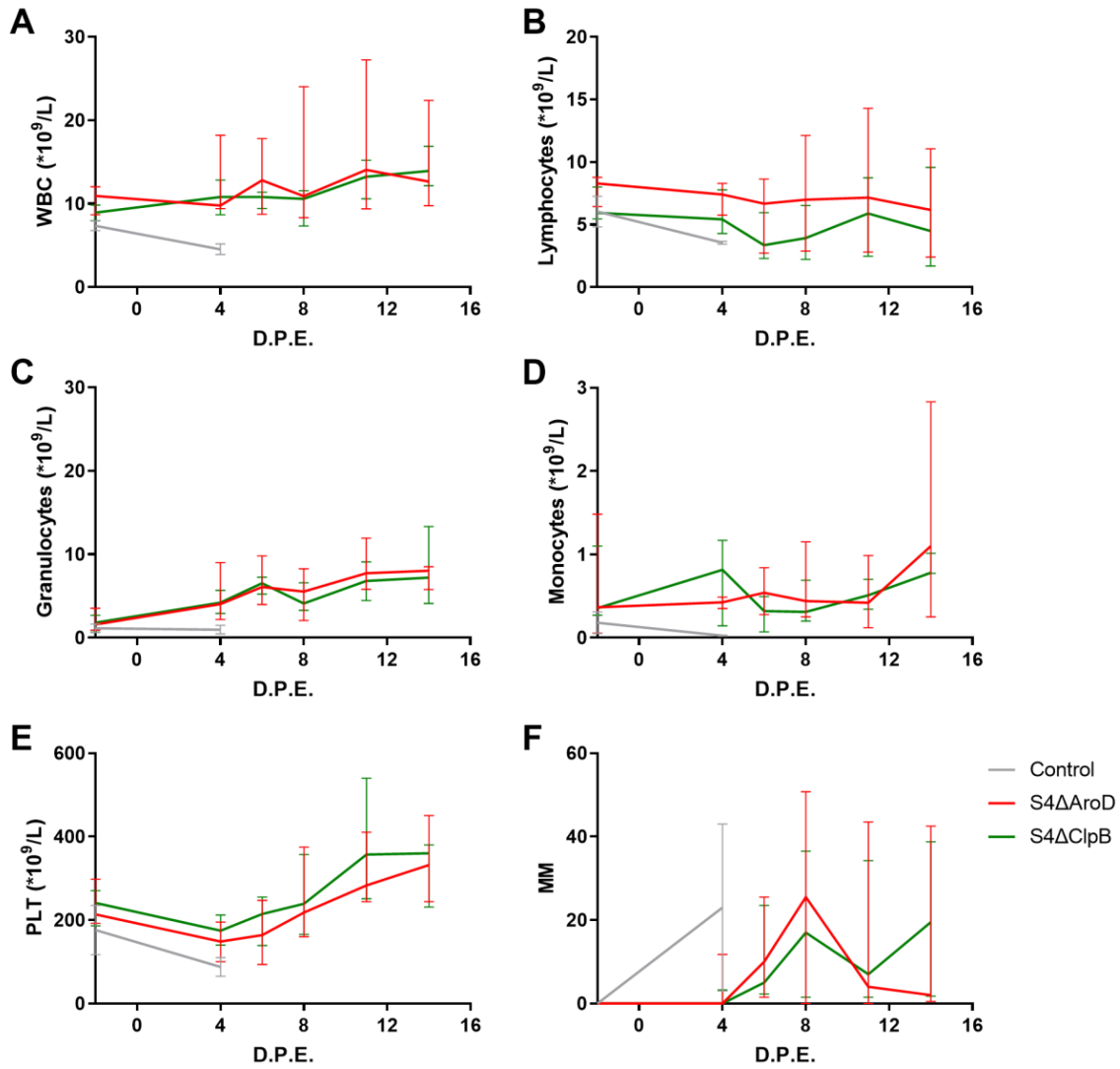


**Figure 13. No differences observed in blood parameters during challenge between S4ΔaroD and S4ΔclpB vaccinated rabbits**

Graphs show medians with IQR; S4ΔaroD is represented by red, S4ΔclpB is represented by green, and control rabbits by grey. Rabbits were bled post exposure to assess A) Total WBC, B) lymphocytes, C) granulocytes, D) monocytes, E) platelets, and F) ESR.

## 4.2 Aim 2

Determine the roles of persistence and dissemination on vaccine efficacy of attenuated *F. tularensis* vaccines.

### 4.2.1 Aim 2a

#### 4.2.1.1 Virulent S4 does not result in leukocyte expansion despite induction of inflammatory processes

We have previously established the NZW rabbit as a suitable model for virulent S4 infection, but outside of morbidity, weight loss, and temperature change, our understanding of the natural history of virulent S4 infection in the NZW rabbit model was limited. Pearson correlation of historical studies revealed time of death is dependent on dose and ranges from 4 to 7 DPE ( $p$  value =0.0067,  $R^2=0.1288$ ) (Figure 14). A moderate dose of virulent S4 was chosen to better understand the pathogenesis of infection as this is the dose we typically used for our vaccine efficacy studies.

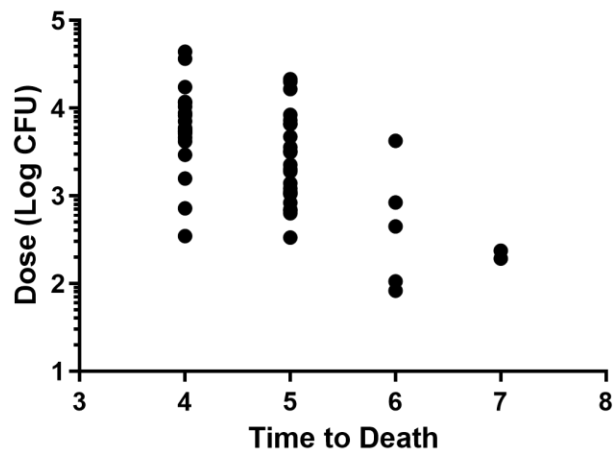
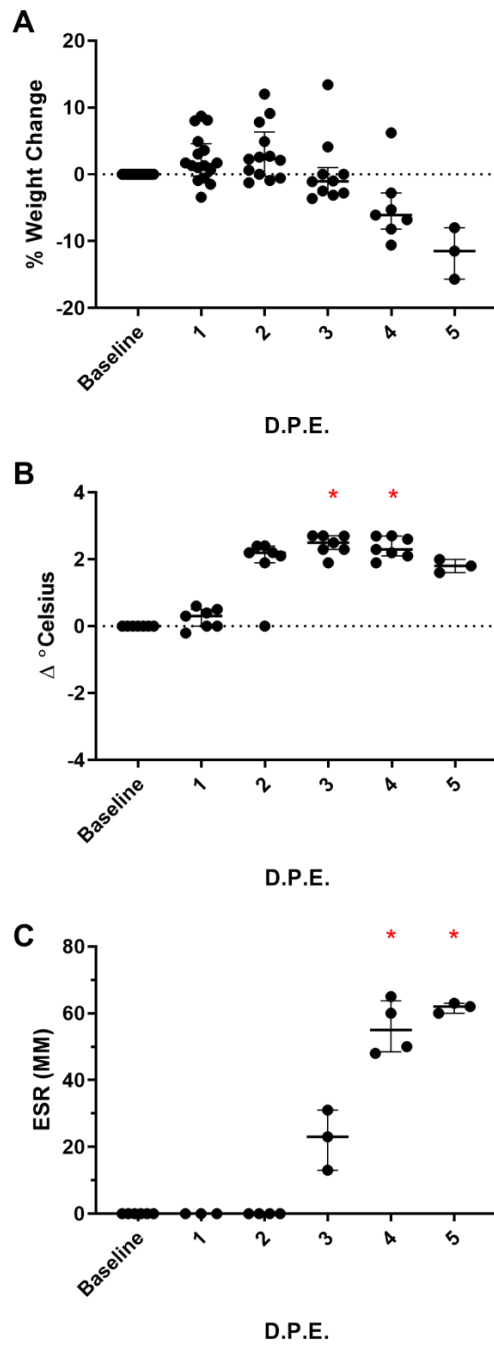


Figure 14. Time to death is dependent on challenge dose

Data were collected from two separate studies for a total of 19 NZW rabbits infected with virulent S4. No difference was observed in dose between studies based on a Mann Whitney test ( $p$  value =0.1416). Rabbits were exposed to a median dose of 4140 CFU of aerosolized virulent S4 and serial sacrificed up to 5 DPE. Weight loss was observed in rabbits beginning 4 DPE, when animals started to become moribund (Figure 15A). Weight change was not significant at any time point compared to baseline based on Dunn's multiple comparison; addition of historical data of S4 infected rabbits indicated weight change was significantly different from baseline at 4 and 5 DPE. Temperature begins to increase in rabbits as soon as 2 DPE, but the difference from baseline is not significant until 3 and 4 DPE (Figure 15B). Assessment of historical data confirms findings for temperature change in these studies, but also identifies 2 DPE as significantly different from baseline due to the increase in sample size. Erythrocyte sedimentation rate begins increasing 3 DPE with levels peaking during the moribund period. ESRs are significantly different from baseline on 4 and 5 DPE, and this trend is confirmed with historical data (Figure 15C). Based on these clinical parameters, we can determine that despite an active infection, the NZW rabbits do not begin exhibiting clinical symptoms of an immune response until two to three days after initial exposure.

Assessment of complete blood counts revealed a decrease in the total WBC count around 3 DPE (Figure 16A). Dunn's multiple comparison indicated this change was not significantly different from baseline levels, but inclusion of historical data revealed counts at 4 and 5 DPE are significantly different from baseline. Loss in total WBC count can be attributed to the loss in total circulating lymphocytes observed starting 3 DPE (Figure 16B). Total lymphocyte counts were significantly different from baseline 4 and 5 DPE, which was confirmed with historical

data. Granulocytes increased until 2 DPE followed by a decline until the moribund period (Figure 16C). Total granulocyte count was significantly different from baseline counts at 2 DPE; historical data suggested 5 DPE was also significantly different from baseline levels. Monocyte levels remained low throughout infection but decreased during the moribund period (Figure 16D). Total monocyte counts were not significantly different from baseline at any point during infection, which was confirmed with historical data. Taken together, these data suggest the innate leukocyte expansion typical of bacterial infection does not occur during virulent S4 infection. Lymphopenia is a typical response to viral infections. Since *F. tularensis* is an intracellular bacterium, it is possible the immune response is responding as it would to a viral infection. It is unclear if the loss in total lymphocytes is due to destruction due to the bacteria or migration into the tissue.



**Figure 15. NZW rabbits begin to exhibit clinical symptoms of infection at 3 DPE**

Graphs show medians with IQR with each symbol representing a single animal. Naïve NZW rabbits were exposed to aerosolized virulent S4 and A) weight change, B) temperature and C) ESR were assessed.

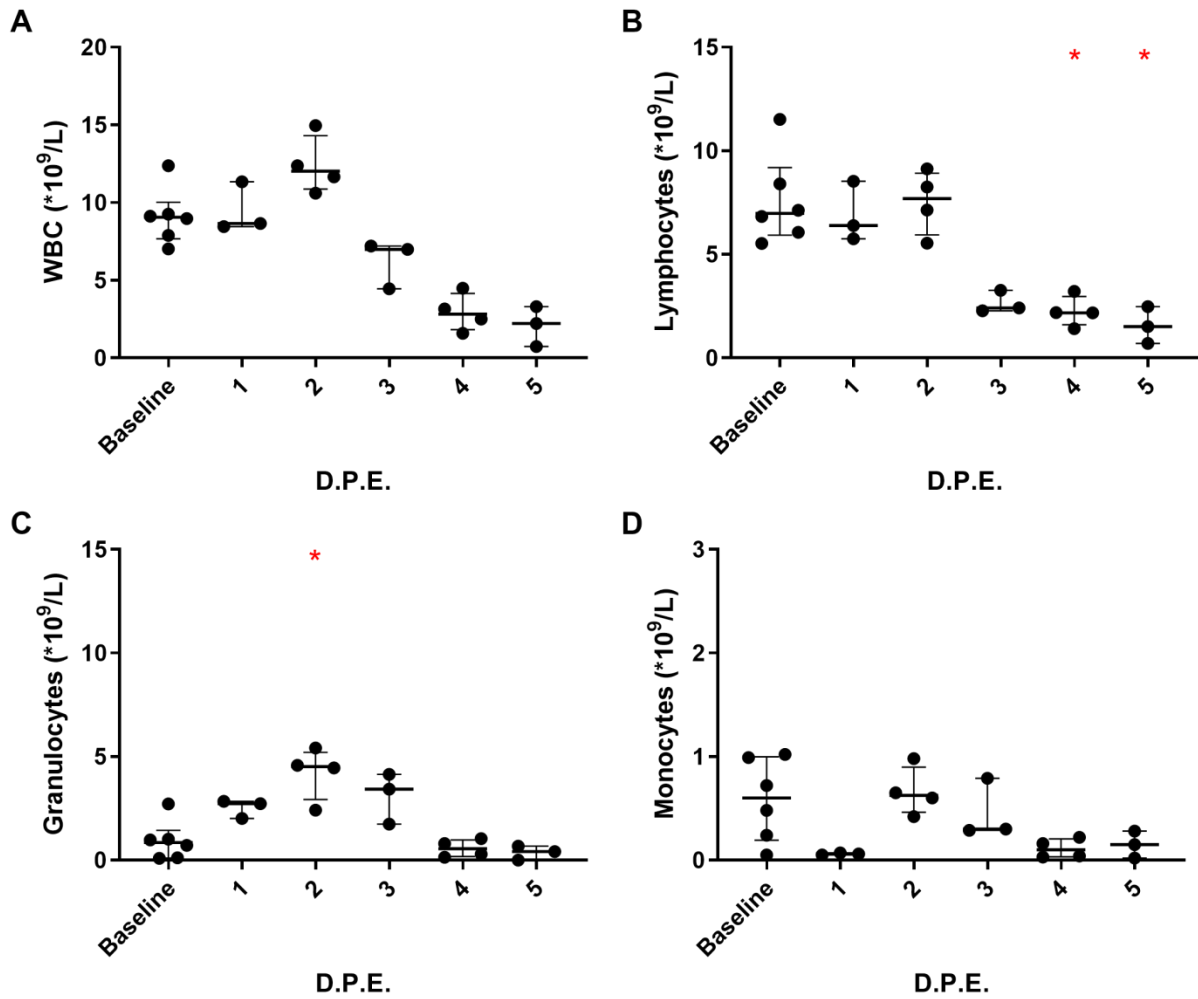


**Figure 16. Uncontrolled infection results in a decrease of total lymphocytes**

Graphs show medians with IQR with each symbol representing a single animal. Naïve NZW rabbits were exposed to aerosolized virulent S4. Rabbits were bled post exposure to assess A) Total WBC, B) lymphocytes, C) granulocytes, and D) monocytes.

Total red blood cells decreased starting at 3 DPE and continued until animals were moribund (Figure 17A). Dunn's multiple comparison indicated total RBCs were significantly different from baseline on 4 and 5 DPE, which was congruent with observation from historical data. There was a decrease in the hemoglobin and hematocrit 4 and 5 DPE (Figure 17B and 17C). Hemoglobin was significantly different 4 and 5 DPE, while hematocrit was significantly different 4 DPE; these trends were confirmed with historical data. No significant changes were observed in MCV, MCH, MCHC, and RDW (data not shown). The loss of RBCs, decrease in hemoglobin and hematocrit, and lack of change in other red cell indices suggest internal bleeding is occurring in the rabbits which has not resulted in anemia by time of death.

Platelets decreased as infection progressed, with total platelet counts at 4 and 5 DPE significantly different from baseline (Figure 18A). The plateletcrit followed a similar pattern as platelets with decreases being observed as soon as 1 DPE, with 4 and 5 DPE significantly different from baseline (Figure 18B). No significant changes were observed in MPV and PDW (data not shown). The observed thrombocytopenia correlated with the picture of internal bleeding observed in the RBC indices during late infection. Total platelet counts began to decrease as soon as 1 DPE, which was two days sooner than the observed loss of red blood cells. This pattern indicated the initial platelet decrease could be due to their role in mediating leukocyte movement from the bloodstream to the tissues. In humans exhibiting sepsis, often a low platelet count is observed due to production of cytokines, endothelial damage, and bone marrow suppression (218, 219). The inability of infected NZW rabbits to maintain WBC and platelet levels, the lack of increase in RDW and PDW suggest bone marrow suppression may be occurring during infection. Additionally, the combined decrease in platelet and plateletcrit is highly suggestive of a septic event.

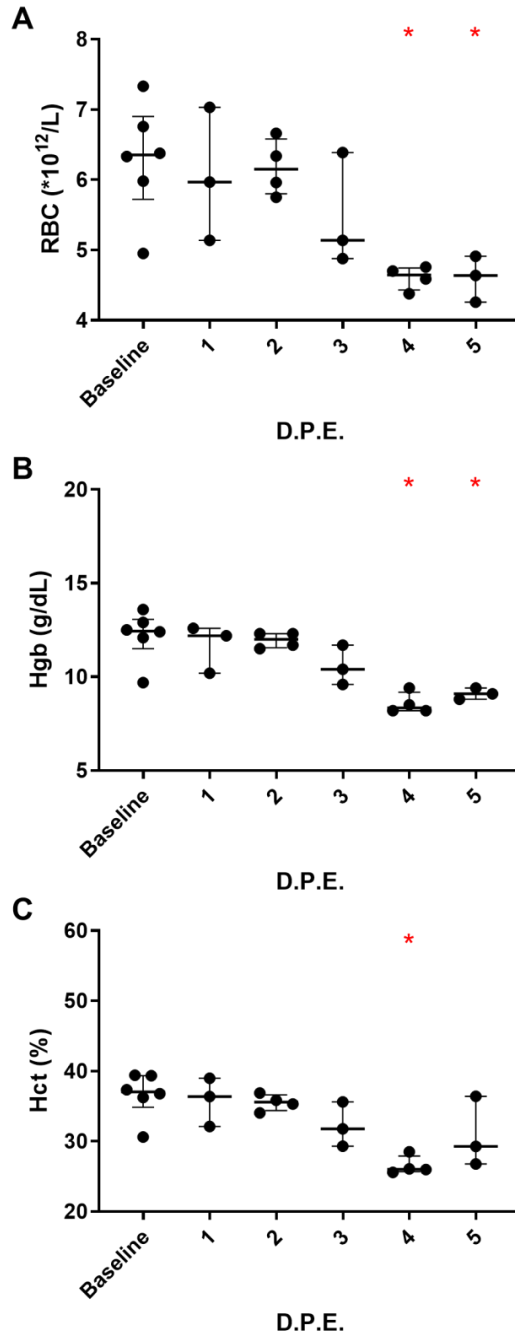


**Figure 17. Loss of RBCs suggests internal bleeding**

Graphs show medians with IQR with each symbol representing a single animal. Naïve NZW rabbits were exposed to aerosolized virulent S4. Rabbits were bled post exposure to assess A) RBC, B) hemoglobin, and C) hematocrit.

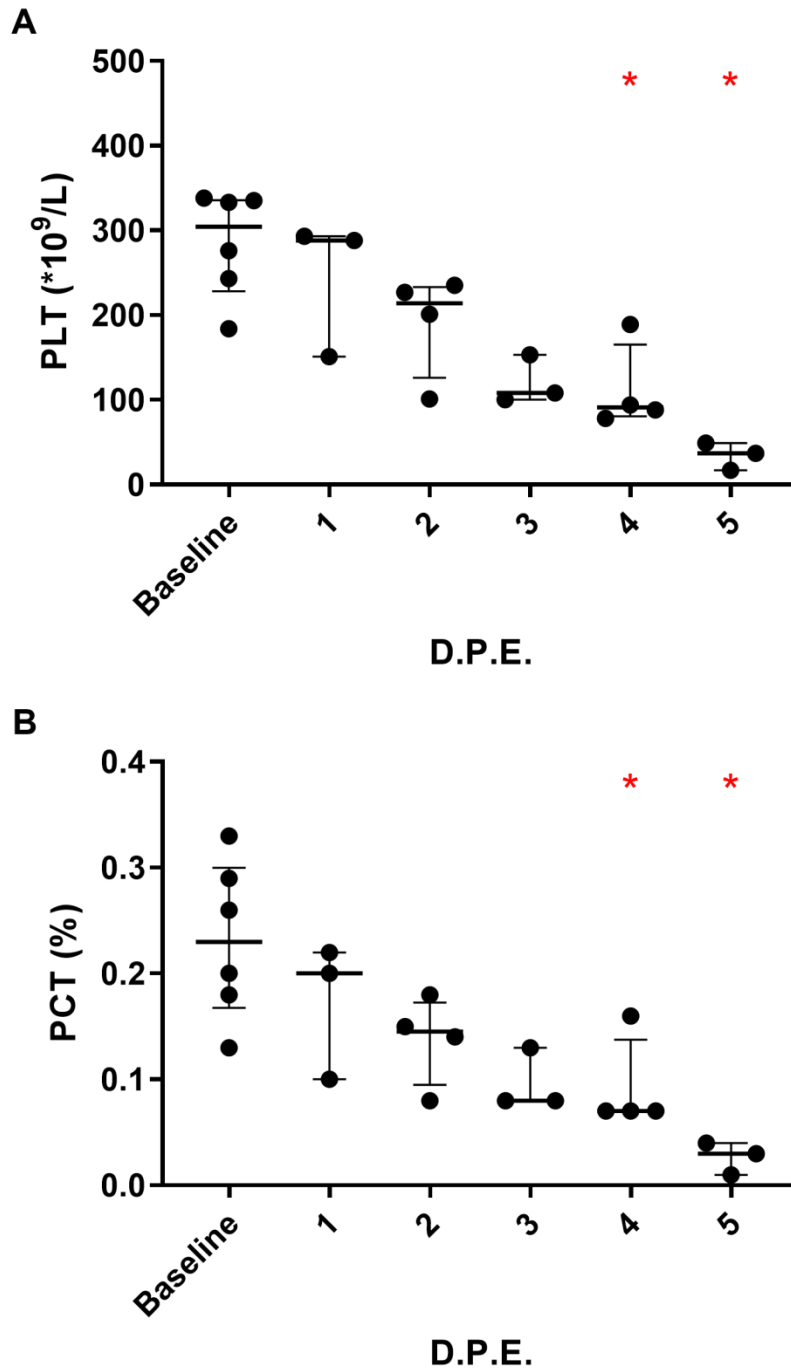


**Figure 18. NZW rabbits infected with virulent S4 exhibit thrombocytopenia**

Graphs show medians with IQR with each symbol representing a single animal. Naïve NZW rabbits were exposed to aerosolized virulent S4. Rabbits were bled post exposure to assess A) platelets and B) plateletcrit.

#### **4.2.1.2 Virulent S4 infection causes massive hemorrhaging and necrosis in the lung**

Figure 19A shows the lungs from an uninfected rabbit. Little to no gross changes were observed 1 DPE (Figure 19B). Examination of gross pathology of the lungs revealed pulmonary petechiae as early as 2 DPE (Figure 19C). As infection progressed, these lesions coalesced to form large patches of pulmonary hemorrhaging which appeared as dark red blotches (Figure 19D and 19E). Hemorrhagic lesions continued to coalesce resulting in severe, necrotizing pneumonia (Figure 19F). Lung size increased during infection indicating lung edema. During the moribund period, caseous necrotic lesions, approximately 2mm, in size could be visualized throughout the lung tissue.

Uninfected rabbits exhibited normal microscopic lung morphology characterized by no inflammation and normal alveolar spaces (Figure 20A). Small foci of leukocytes were scattered throughout the lung at 1 DPE (Figure 20B). At 2 DPE lesions were more numerous and fluid buildup was observed (Figure 20C). Isolated nodules of distended alveoli due to infiltrating leukocytes were observed. By 3 DPE, damaged lung tissue had increased but still exhibited patchy distribution (Figure 20D). Some areas exhibited normal morphology, while some areas of severe lung consolidation were observed. At 4 and 5 DPE, several caseous necrotic lesions consistent with pyogranulomatous inflammation were observed throughout the lung lobe (Figure 20E and 20 F). Percentage of alveolar space significantly decreased in S4 infected rabbits compared to uninfected animals based on an ANOVA ( $p$  value=0.0033) (Figure 21). Šídák's multiple comparisons shows significant changes in alveolar space occurred as early as 1 DPE.

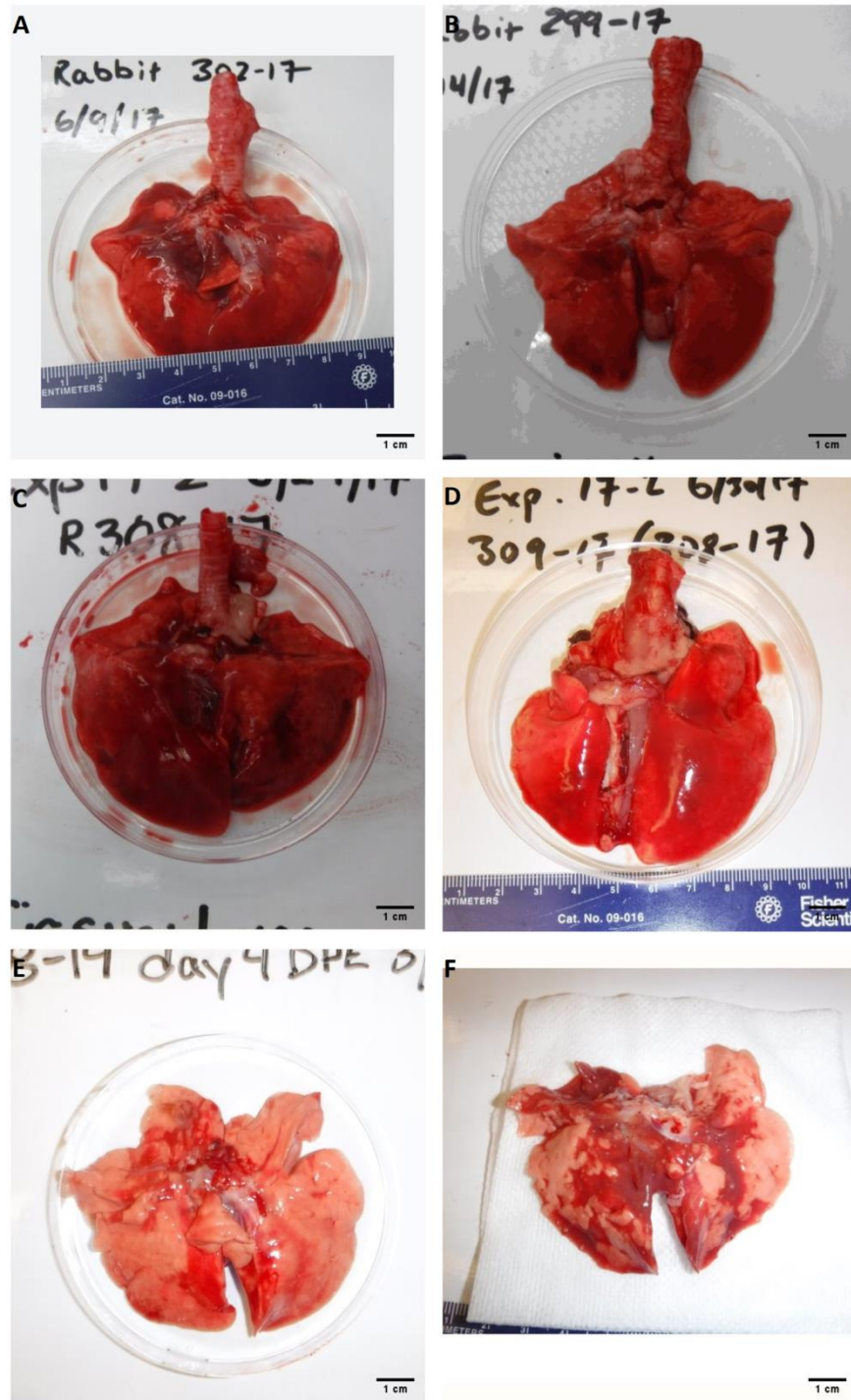


**Figure 19. Uncontrolled infection leads to extensive pulmonary hemorrhaging**

Rabbits were exposed to virulent S4 and serially sacrificed to observe gross pathological changes. One representative image of the lung was chosen for each time point: A) Uninfected; B) 1 DPE; C) 2 DPE; D) 3 DPE; E) 4 DPE; F) 5 DPE.

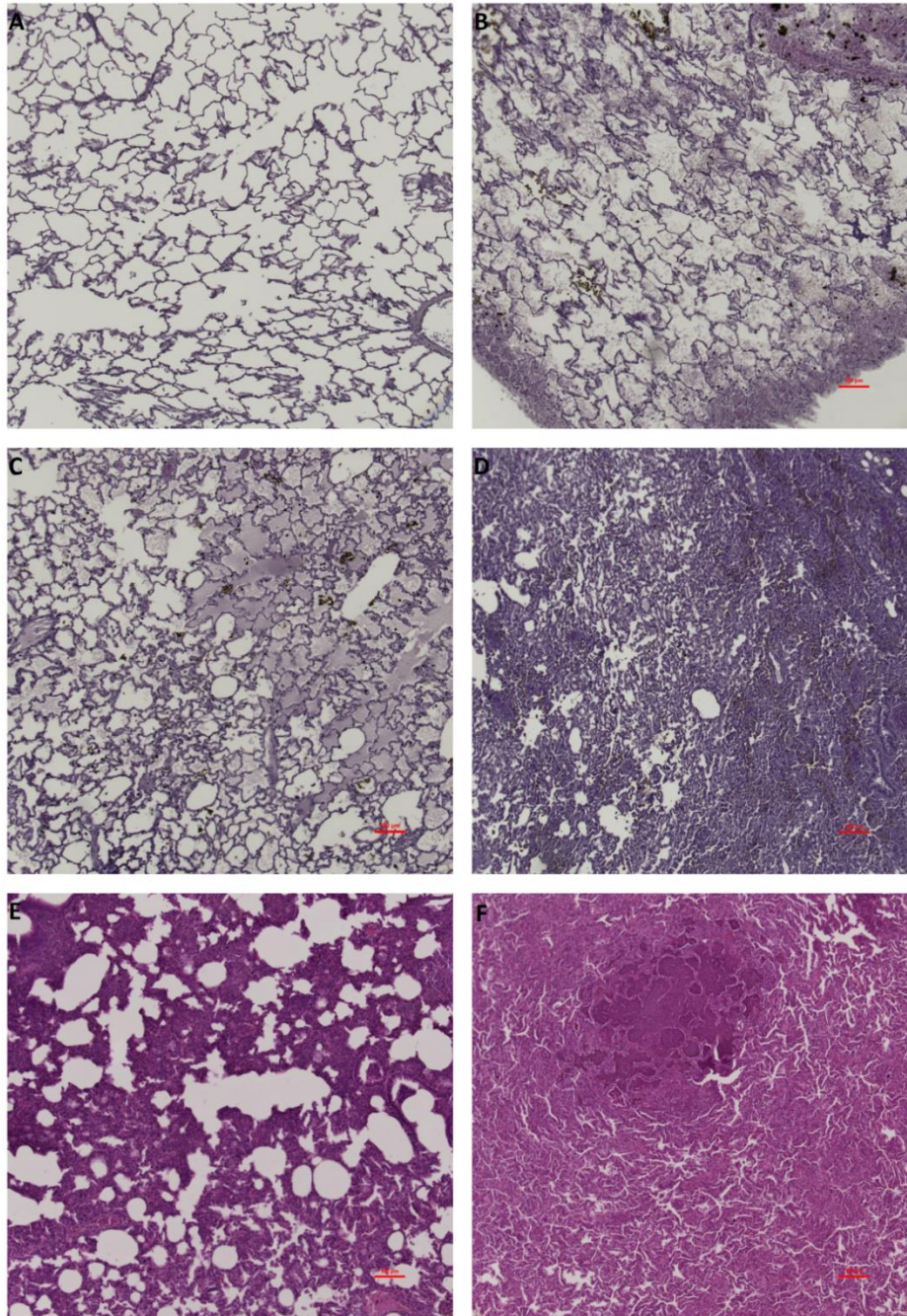


**Figure 20. Uncontrolled virulent S4 infection leads to consolidation of alveolar spaces and necrotizing pneumonia**

Rabbits were exposed to virulent S4 and serially sacrificed to observe microscopic pathological changes via H&E staining. One representative image of the lung was chosen for each time point: A) Uninfected; B) 1 DPE; C) 2 DPE; D) 3 DPE; E) 4 DPE; F) 5 DPE.

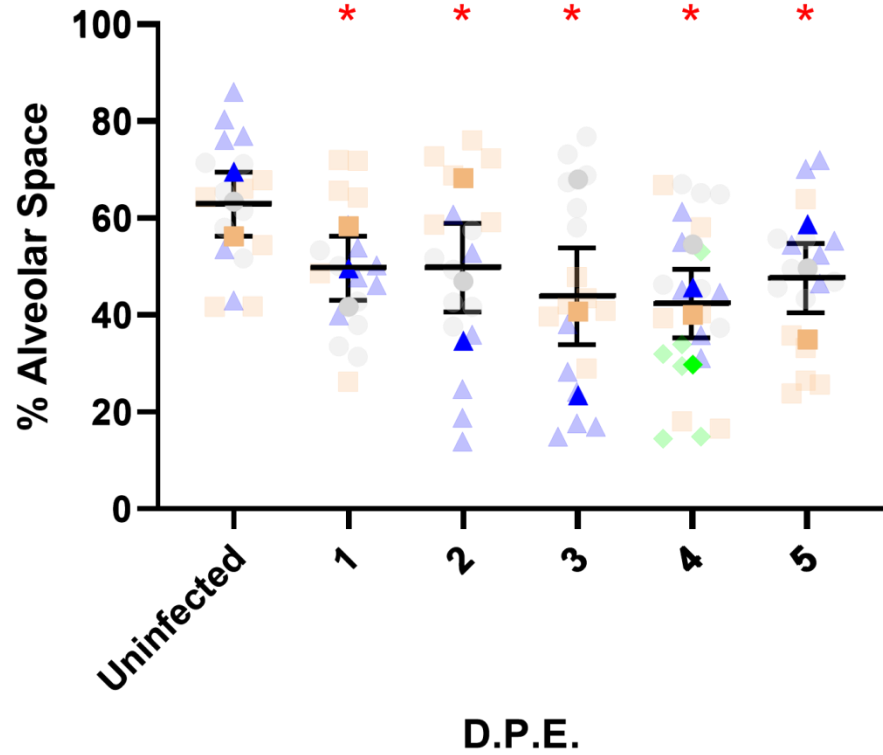


**Figure 21. S4 infection results in decreased alveolar space**

Each color represents a different animal. Each small, transparent symbol represents a region of interest that was assessed. Each large, solid symbol represents the mean alveolar space for an individual animal. Error bars represent the mean and 95% confidence interval.

Little to no change was observed in gross pathology of the liver up to 3 DPE compared to the liver of uninfected rabbits (Figure 22A-22D). Small bacterial foci could be observed on multiple lobes of the liver 4 and 5 DPE (Figure 22E and 22F). Consistent with gross pathology, little to no changes were observed in microscopic examination of liver sections up to 2 DPE (Figure 23A-23C). Leukocyte infiltrates were scattered throughout the liver at 3 DPE (Figure 23D). These lesions coalesced and became necrotic 4 to 5 DPE (Figure 23E and 23F). Hepatic cells have degenerated at the center of each lesion appearing as eosinophilic amorphous material.

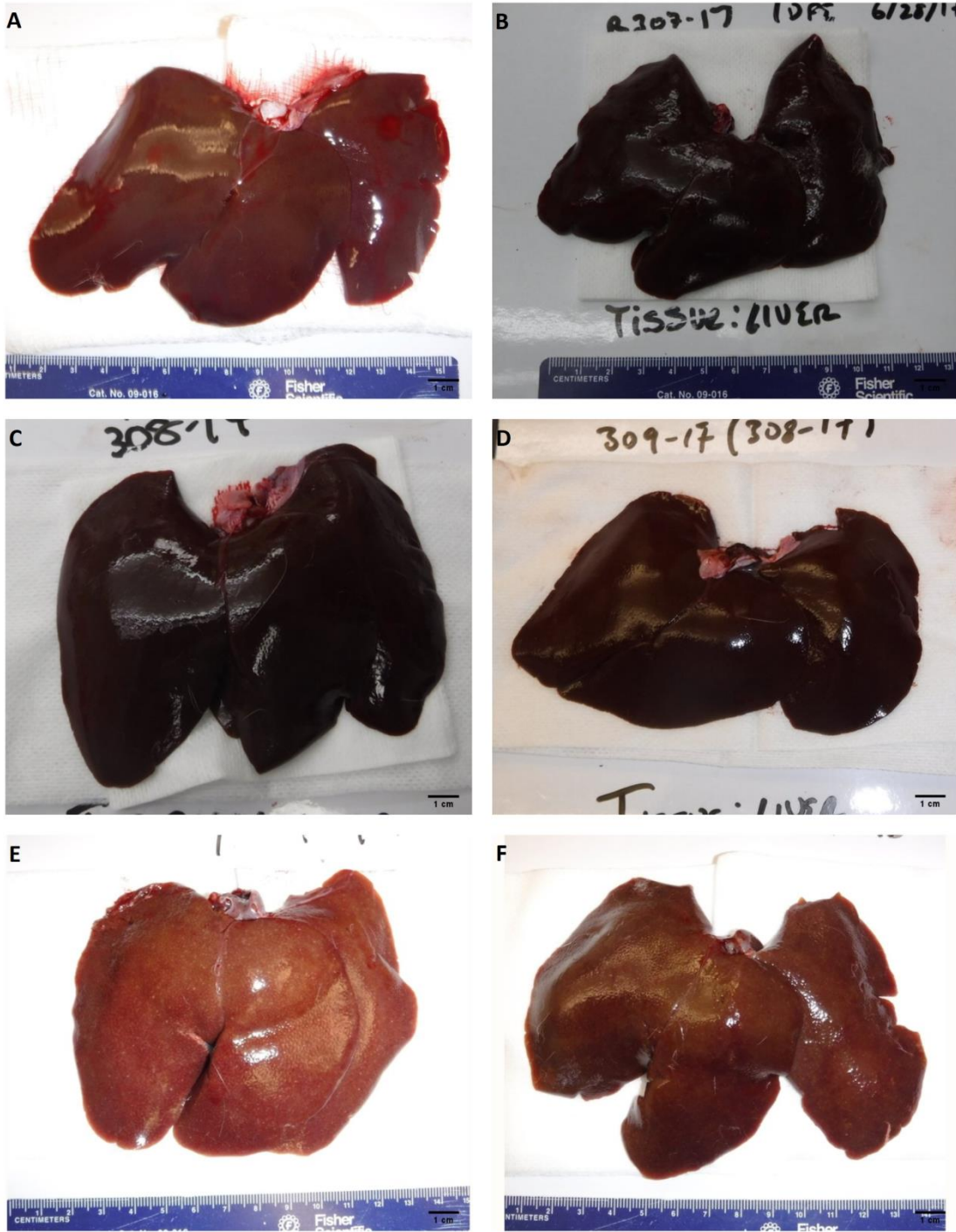


**Figure 22. Virulent S4 infection results in visible bacterial foci on the liver**

Rabbits were exposed to virulent S4 and serially sacrificed to observe gross pathological changes. One representative image of the liver was chosen for each time point: A) Uninfected; B) 1 DPE; C) 2 DPE; D) 3 DPE; E) 4 DPE; F) 5 DPE.

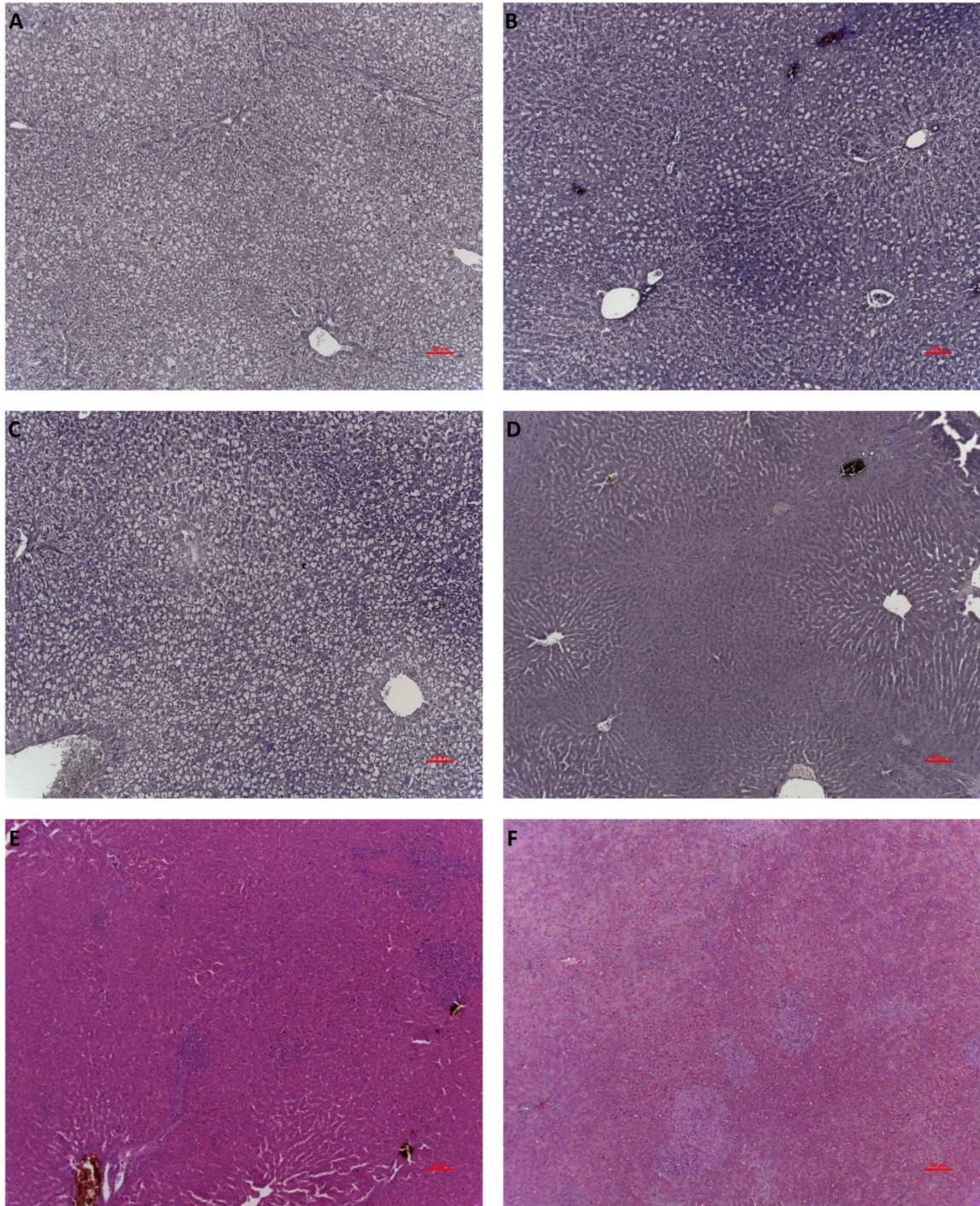


**Figure 23. Necrotic lesions were found in the liver by the time the animal reached the moribund period**

Rabbits were exposed to virulent S4 and serially sacrificed to observe microscopic pathological changes via H&E staining. One representative image of the liver was chosen for each time point: A) Uninfected; B) 1 DPE; C) 2 DPE; D) 3 DPE; E) 4 DPE; F) 5 DPE.

Splenomegaly was observed as early as 1 DPE (Figure 24B). Splenic size increased dramatically from 4cm at baseline to greater than 7cm in length by 4 DPE (Figure 24E). Bacterial foci were observed throughout the parenchyma and capsular surface of the spleen 4 and 5 DPE (Figure 24E and 24F). Spleens appeared dark-reddish brown and turgid, suggestive of diffuse congestion and hemorrhage. At 1 DPE, hyperplastic reactive lymphoid follicles and increased macrophages were observed compared to uninfected spleens (Figure 25A and 25B). At 2 DPE, these lymphoid follicles were disrupted resulting in functional disorganization (Figure 24C). Lesions extended into the red pulp early and there was reduced distinction between the red and white pulp 3 and 4 DPE (Figure 25D and 25E). Reduction in red pulp could be due to excessive antigen stimulation seeding B cell proliferation. Similar to the liver, coalescing necrotic lesions were found in the spleen at 5 DPE resulting in eosinophilic amorphous debris (Figure 25F).

Lymph nodes became enlarged and exhibited necrotizing lesions at 4 and 5 DPE. No changes were observed in the gross pathology of the kidney, heart, or GI tract. Occasionally bacterial foci were observed on the surface of the kidney during the moribund period, but microscopically kidney tissue was normal.

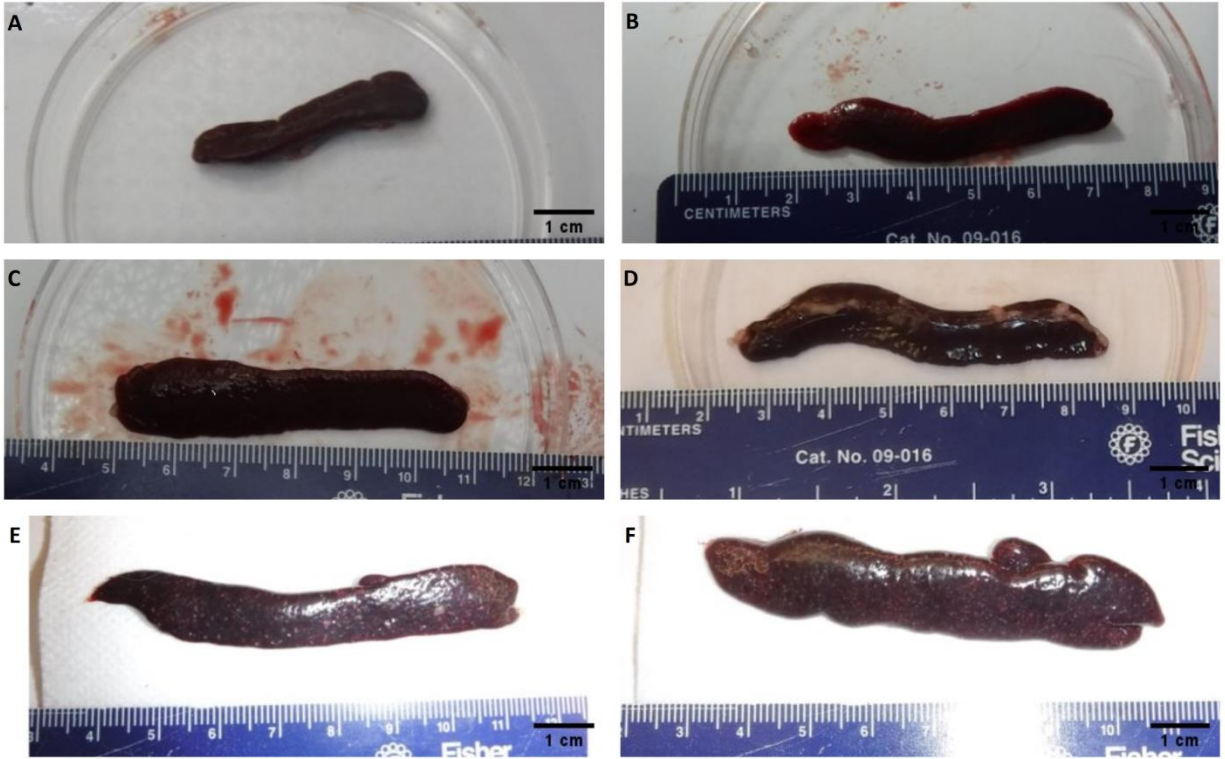


**Figure 24. S4 infection results in splenomegaly with visible bacterial foci**

Rabbits were exposed to virulent S4 and serially sacrificed to observe gross pathological changes. One representative image of the spleen was chosen for each time point: A) Uninfected; B) 1 DPE; C) 2 DPE; D) 3 DPE; E) 4 DPE; F) 5 DPE.

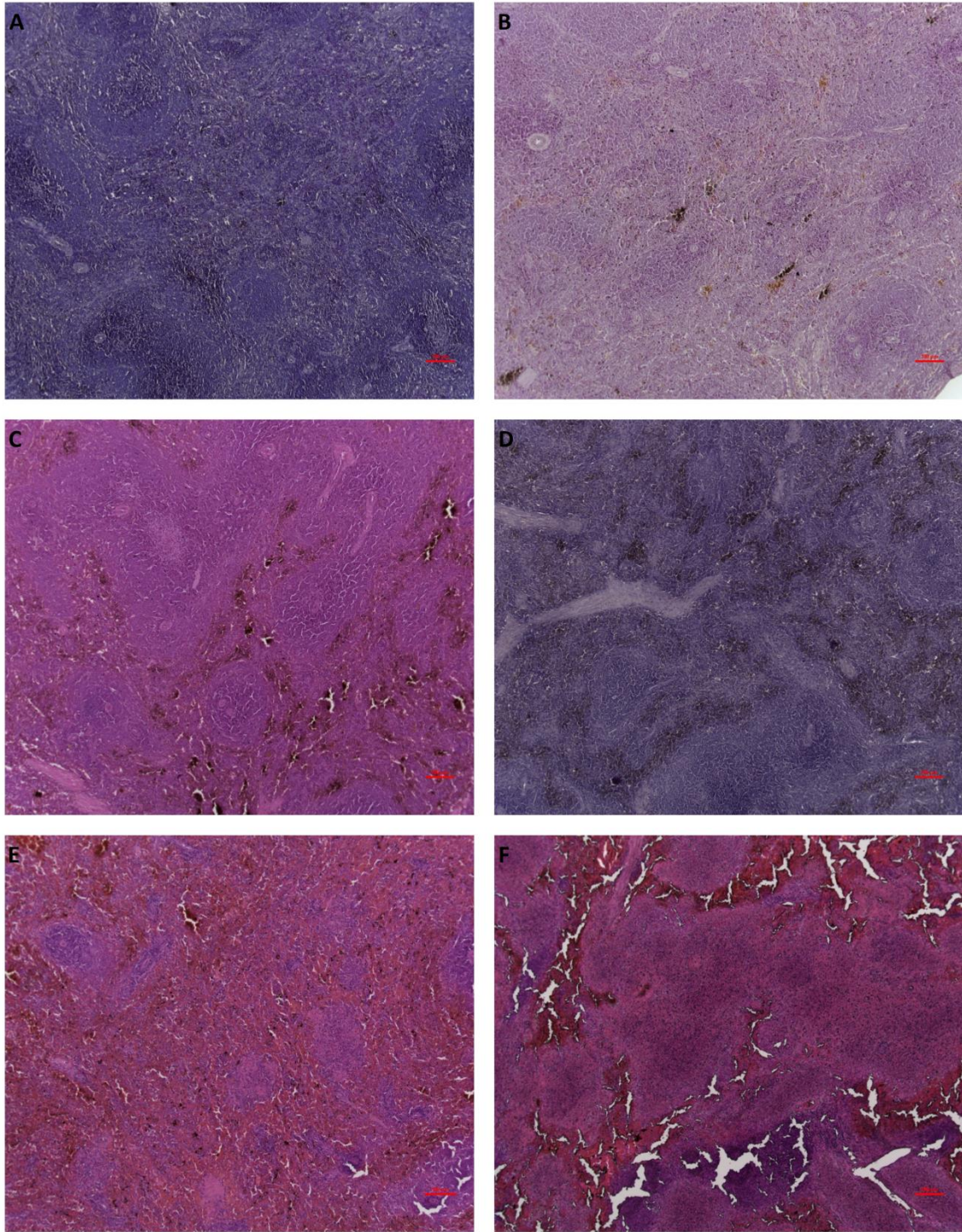


**Figure 25. S4 infection results in necrotizing splenitis**

Rabbits were exposed to virulent S4 and serially sacrificed to observe microscopic pathological changes via H&E staining. One representative image of the spleen was chosen for each time point: A) Uninfected; B) 1 DPE; C) 2 DPE; D) 3 DPE; E) 4 DPE; F) 5 DPE.

#### **4.2.1.3 Virulent S4 disseminates rapidly from the primary site of infection to the liver and spleen**

Figure 26 shows individual titers for each of 5 lobes collected from each rabbit in transparent symbols, with solid symbols indicating the median titer for each rabbit. Virulent S4 was culturable in at least one lung lobe of each of the three animals assessed 1 DPE with a median titer of  $1.1 \times 10^2$  CFU/g. Median titers increased 1 log each day post exposure reaching a median titer of  $7.0 \times 10^6$  CFU/g at 5 DPE. At 4 DPE, the bacteria had spread to infect all lobes of the lung for each animal. Median bacterial titers were significantly different from baseline titers at 5 DPE. Assessment of each lobe indicates the lower lobes were positive 1 DPE and infection spread to the upper lobes (Appendix Figure 2). Comparison of different lobe segments indicated median titers were significant from baseline 4 and 5 DPE for the upper right lung lobe, lower right lung lobe, and the lower left lobe, while only 5 DPE was significant for the upper left lobe and the middle lobe (Appendix Table 1). Bacterial titers in bronchoalveolar lavages corresponded with titers found in the lung (Appendix Figure 3A). Lung digests performed the same day as euthanasia also confirm bacterial titer trends observed in the lung (Appendix Figure 3B).

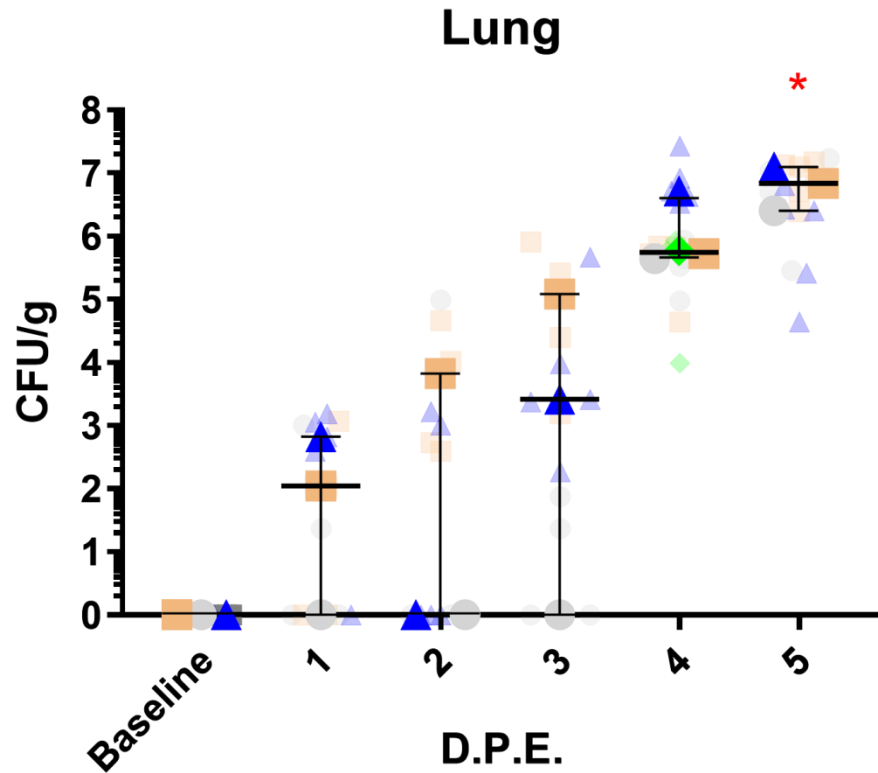


**Figure 26. *F. tularensis* spreads throughout lung lobes as infection progresses**

Each color represents a different animal. Each small, transparent symbol represents an individual lung lobe. Each large, solid symbol represents the median bacterial titer among all lobes for an individual animal. Error bars represent median and IQR of median bacterial titers for all animals.

Bacteria were detectable 3 DPE in the liver and spleen with median titers of  $4.2 \times 10^2$  CFU and  $1.1 \times 10^2$  CFU, respectively (Figure 27A and 27B). Titers increased by logs 4 DPE and an additional log 5 DPE in the liver. In the spleen, bacterial titers increased by 4 logs at 4 DPE and 1 log 5 DPE. Titers in the liver and spleen were significantly different from baseline 4 and 5 DPE. Spleen digests performed the same day as euthanasia confirm titers found in the spleen (Appendix Figure 3C). In the kidney, bacteria were detectable during the moribund period with a median titer of  $2.9 \times 10^2$  CFU/g 4 DPE and  $1.5 \times 10^4$  CFU/g at 5 DPE, which were significantly different from baseline based on Dunn's multiple comparison (Figure 27C). Lymph nodes remained small 1 to 3 DPE, making quantification of bacterial titers difficult during early time points (Figure 27D). Median bacterial titers of  $2.0 \times 10^4$  CFU/g and  $1.1 \times 10^5$  CFU/g were detected in the lymph nodes at 4 and 5 DPE, respectively. Bacteria were detectable in the heart during the moribund period with a median titer of  $2.2 \times 10^2$  CFU/g at 4 DPE and  $9.6 \times 10^2$  CFU/g at 5 DPE (Figure 27E). Titers at 5 DPE were significantly different from baseline titers in the heart. Liver bacteria were rarely found in the GI tract at any time point post exposure. Only one exhibited bacteria present in the GI tract with a titer of  $4.6 \times 10^2$  CFU/g at 4 DPE (Figure 27F). Only a small segment of one inch surrounding a Peyer's patch was collected for titer analysis of the GI tract which may have limited detection capabilities.

Consistent with humans, Fisher 344 rats, and cynomolgus macaques, virulent S4 was difficult to detect in the blood. Only one animal was positive at 4 DPE with a titer of  $7.5 \times 10^3$  CFU/ml of blood, but all animals assessed five days after exposure exhibited bacteremia with a median titer of  $5.5 \times 10^3$  CFU/ml (Figure 28). Titers at 5 DPE were significantly different from baseline titers. Thus, infection is able to spread to detectable levels in the liver and spleen within three days of primary exposure to virulent S4. Infection spreads to the kidney, lymph node, heart,

and GI tract by the time the animal reaches the moribund period. Interestingly, bacteremia is only detectable during the moribund period. These data indicates very few bacteria are needed to disseminate the infection to secondary sites through the blood.

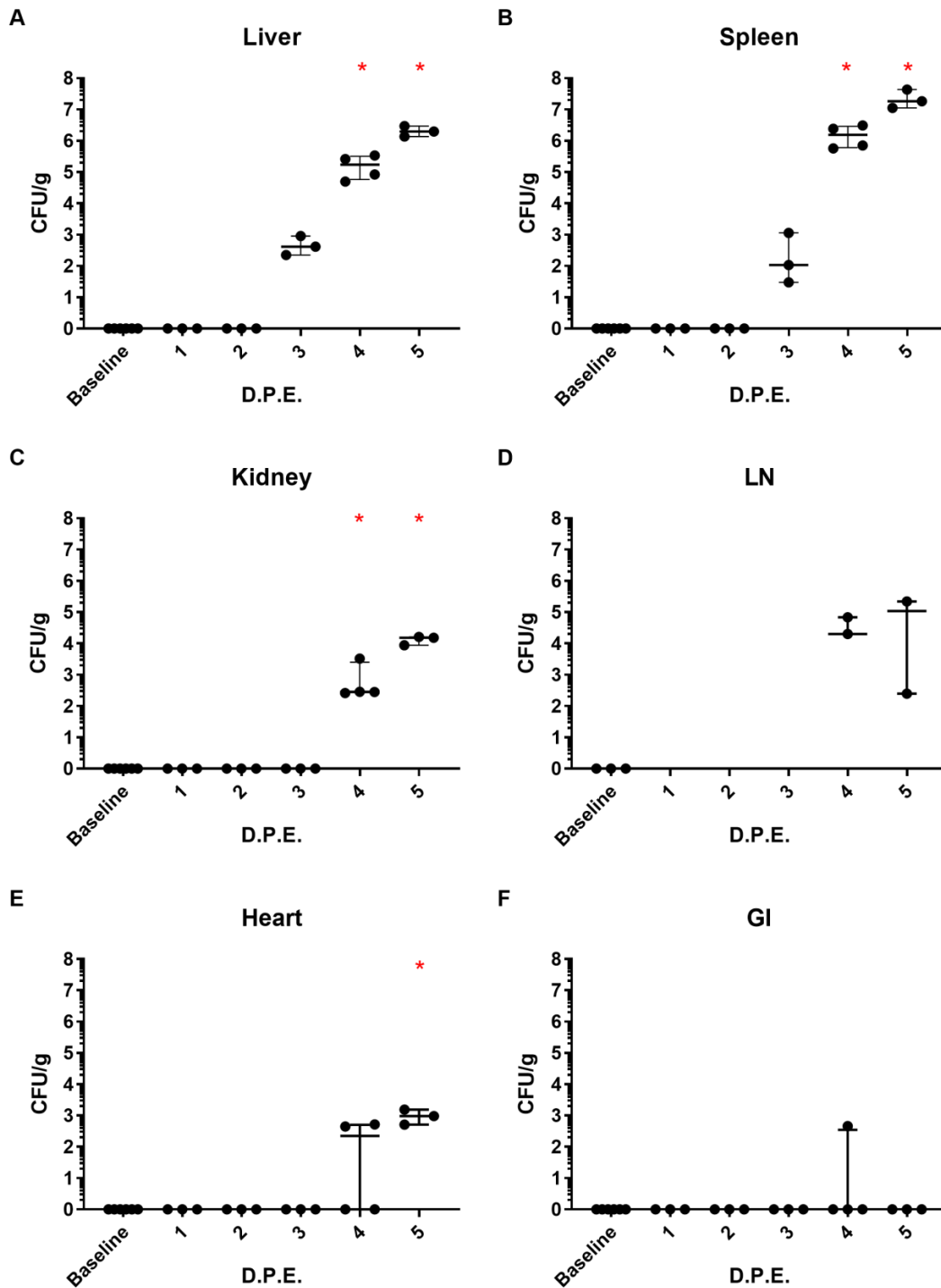


**Figure 27. Bacteria disseminates from the lung to the spleen and liver at 3 DPE**

Graphs show medians with IQR with each symbol representing a single animal. Naïve NZW rabbits were exposed to aerosolized virulent S4 and serially sacrificed to assess bacterial titers in A) liver, B) spleen, C) kidney, D) lymph node, E) heart, and F) GI tract.

# Bacteremia

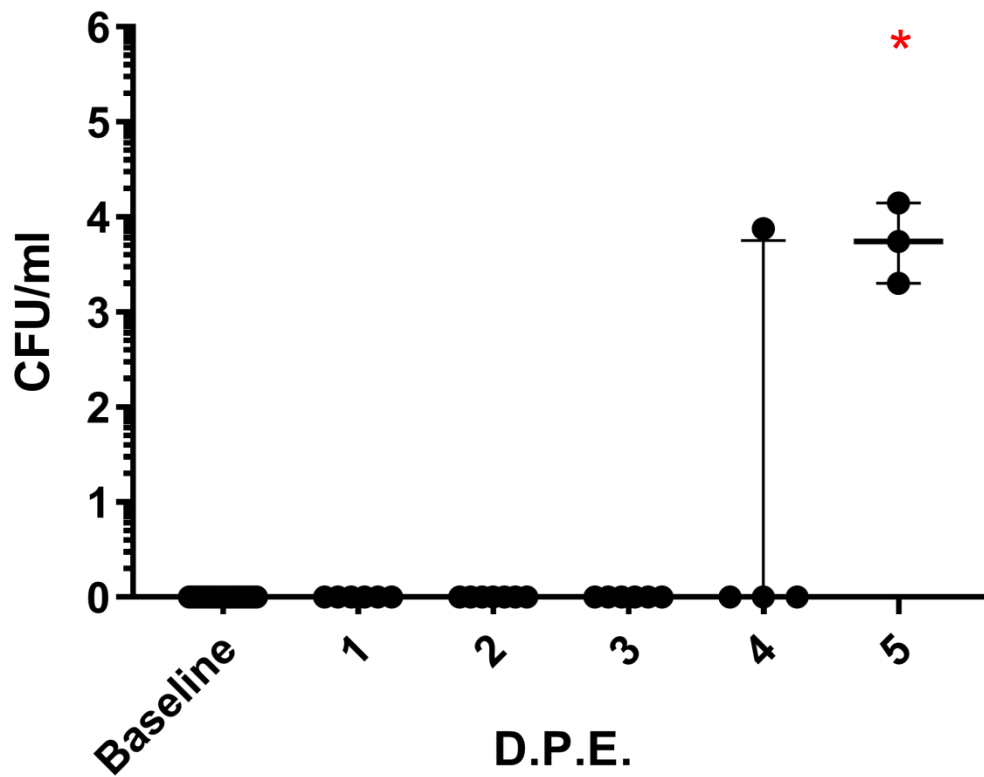


**Figure 28. Bacteria is not detected in the blood until animals become moribund**

Graphs show medians with IQR with each symbol representing a single animal. Naïve NZW rabbits were exposed to aerosolized virulent S4 and serially sacrificed to assess bacteremia.

## **4.2.2 Aim 2b**

### **4.2.2.1 S4ΔguaBA results in a more severe clinical presentation compared to LVS and S4ΔaroD**

Prime/boost vaccination with LVS, S4ΔaroD, and S4ΔguaBA results in a vaccine efficacy of 20%, 67.7%, and 50% respectively (Figure 9A, 10A, 11A). Rabbits were exposed to aerosols containing LVS, S4ΔaroD, or S4ΔguaBA to reach a dose comparable to that used in vaccine studies (Aim 1c). In the LVS group, 23 rabbits were exposed to a median dose of  $2.8 \times 10^8$  CFU. The S4ΔaroD group consisted of 16 rabbits and received a median dose of  $2.4 \times 10^8$  CFU. Nine rabbits were exposed to a median dose of  $1.2 \times 10^8$  CFU in the S4ΔguaBA group. Both LVS and S4ΔaroD groups had significantly different doses from S4ΔguaBA based on Dunn's multiple comparison, though all groups reached the minimum target dose (Figure 29).

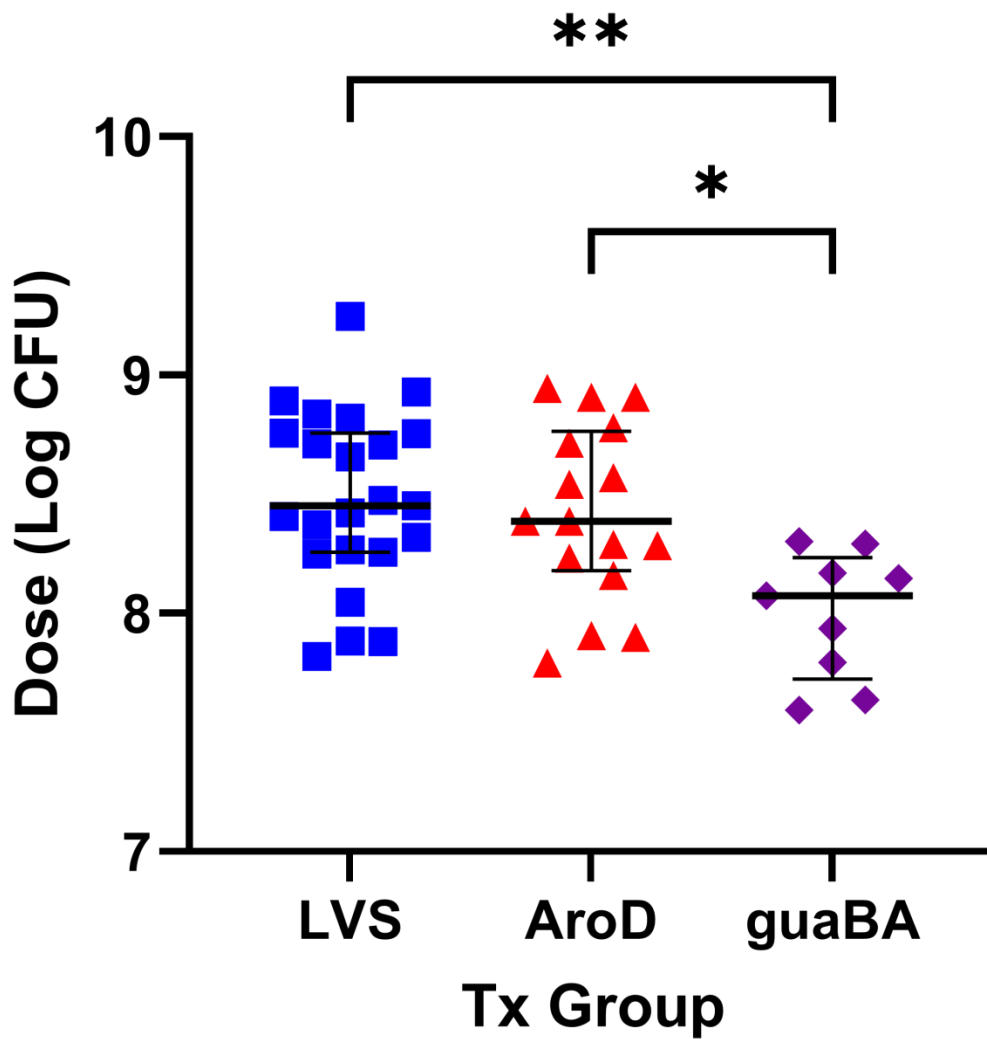


**Figure 29. Rabbits received aerosolized vaccine doses greater than 108 CFU**

Graphs show medians with IQR with each symbol representing a single animal. Animals were exposed to aerosols containing LVS, S4ΔaroD or S4ΔguaBA and dose was determined based on minute volume, Collision concentration, and length of aerosol.

Rabbits exposed to LVS and S4ΔguaBA exhibited weight loss as soon as 1 DPE, but rabbits in the LVS group began to regain weight by 2 DPE (Figure 30A). Weight change was significantly different from baseline levels 1 to 3 DPE in the LVS group. The S4ΔguaBA group continued to lose up to 10% of their body mass, with weight on days 4 through 7 DPE significantly different from baseline based on Dunn's multiple comparison. The S4ΔaroD group began to lose weight 2 DPE, but began to recover 4 DPE. Weight change was significantly different from baseline at 3 DPE in the S4ΔaroD group. Data for unvaccinated rabbits were pulled from historical data. Unvaccinated rabbits exposed only to BHI gained weight as they were young adult rabbits, which were still growing. Mixed effects analysis indicated vaccine strain did affect weight change over time ( $p$  value =0.0099,  $p$  value <0.0001, respectively), and there was an interaction with time ( $p$  value <0.0001) (Table 11).

Elevations in temperatures were observed 1 DPE in the LVS and S4ΔaroD group, though temperatures returned to baseline by 2 DPE in the LVS group (Figure 30B). Temperatures remained elevated in the S4ΔaroD group for 2 days before returning to baseline levels. Temperature change was significantly different from baseline readings 1 DPE in the LVS group, and days 1 through 3 post exposure in the S4ΔaroD group. Elevations in temperature were not observed until 2 DPE in the S4ΔguaBA group, similar to when fever response was observed in rabbits exposed to virulent S4. Temperatures remained elevated for several days, but returned to baseline levels 7 DPE. Temperature change was significantly different from baseline readings days 2 through 5 DPE. Vaccine strain did affect temperature over time ( $p$  value <0.0001,  $p$  value <0.0001, respectively), and there was an interaction with time ( $p$  value <0.0001) (Table 11).

ESRs increased to a median of 11mm at 2 DPE in the LVS exposed group and quickly began decreasing until levels returned to baseline 5 DPE (Figure 30C). At days 3 and 4 after

exposure, ESRs were significantly different from baseline in the LVS group. S4ΔaroD exposed rabbits exhibited an increase in ESR starting at 2 DPE with a peak occurring 3 DPE with a median of 41mm. ESRs started decreasing 4 DPE but remained elevated until 7 DPE. ESRs were significantly different from baseline in the S4ΔaroD group at 3 and 5 DPE. Again, similarly to virulent S4, S4ΔguaBA exposed rabbits showed elevations in ESRs at 3 DPE and peaked at 4 DPE with a median of 46mm. ESRs were still elevated at 7 DPE in S4ΔguaBA-exposed rabbits. All ESRs returned to baseline at 14 DPE in the S4ΔguaBA group. Dunn's multiple comparison showed ESRs were significantly different from baseline at 3 and 4 DPE in S4ΔguaBA exposed rabbits. Vaccine strain did affect ESR over time ( $p$  value <0.0001,  $p$  value <0.0001, respectively), and there was an interaction with time ( $p$  value <0.0001) (Table 11). Appendix Table 2 shows  $p$  values for Tukey's multiple comparisons between vaccine groups at each time point. Temperature was most frequently significantly different between groups over time.

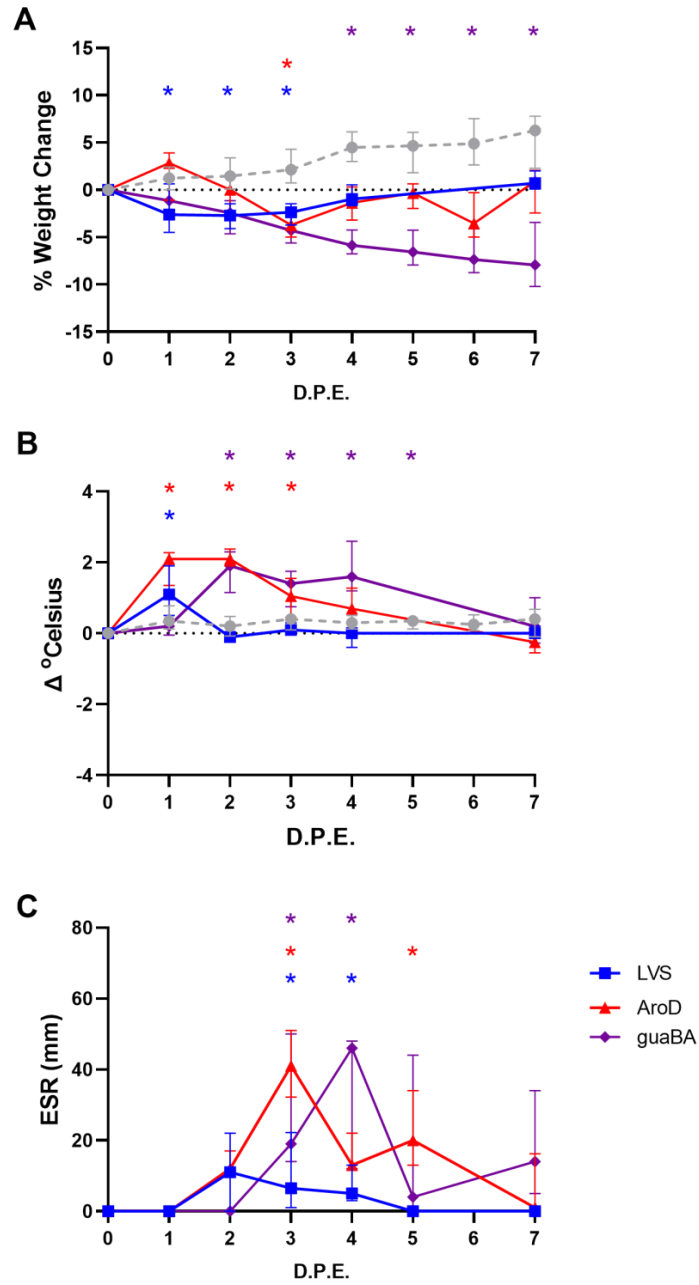


**Figure 30. S4ΔguaBA is more clinical severe than either LVS or S4ΔaroD based on clinical signs**

Graphs show median with IQR. Grey dotted line indicates data from uninfected rabbits over a period of 7 days. LVS is represented by blue, S4ΔaroD is represented by red, and S4ΔguaBA is represented by purple. Asterisks indicate significant changes from baseline values, with color correlating with the vaccine group. Naïve rabbits were exposed to aerosols containing LVS, S4ΔaroD, or S4ΔguaBA to assess A) weight change, B) temperature change, and C) ESRs.

**Table 11. Mixed effects modeling of vaccine strains over time**

	Time	Vaccine	Time*Vaccine
Weight	<b>&lt;0.0001</b>	<b>0.0099</b>	<b>&lt;0.0001</b>
Temperature	<b>&lt;0.0001</b>	<b>&lt;0.0001</b>	<b>&lt;0.0001</b>
WBC	<b>&lt;0.0001</b>	<b>0.0052</b>	<b>0.0199</b>
Lymphocytes	<b>0.0027</b>	0.1711	0.1598
Granulocytes	<b>&lt;0.0001</b>	0.0952	0.2065
Monocytes	<b>&lt;0.0001</b>	0.0952	0.2065
Platelets	<b>&lt;0.0001</b>	<b>&lt;0.0001</b>	0.1445
RBC	<b>0.0208</b>	0.9412	0.1567
ESR	<b>&lt;0.0001</b>	<b>&lt;0.0001</b>	<b>&lt;0.0001</b>

*P* values from mixed-effect modeling with Geisser-greenhouse correction of time and vaccine for clinical parameters. Significant *p* values (<0.05) indicated in bold.

Rabbits exposed to LVS, S4ΔaroD, or S4ΔguaBA exhibited a decrease in total white blood cell count at 3 DPE, similar to the trend seen in rabbits exposed to virulent S4 infection (Figure 31A). Though in contrast to what is observed with S4 infection, WBC counts rebounded by 4 DPE and continued to increase. Total WBC count was significantly different from baseline levels at 3 DPE in S4ΔaroD. Mixed effects analysis indicated vaccine strain did affect white blood cell counts over time ( $p$  value =0.0052,  $p$  value <0.0001, respectively), and there was an interaction with time ( $p$  value =0.0199) (Table 11). White blood cell counts were significantly different between S4ΔaroD and S4ΔguaBA at 1 DPE based on Šídák's multiple comparison (Appendix Table 2).

The decrease in WBC count observed with all vaccine strains is attributable to a decrease in circulating lymphocytes (Figure 31B). Lymphocyte counts were significantly different from baseline levels at 2 and 3 DPE in S4ΔaroD exposed rabbits. An increase in granulocytes began as soon as 1 DPE for LVS and S4ΔguaBA exposed rabbits (Figure 31C). This increase in granulocytes continued until 7 DPE. At 14 DPE, granulocyte counts were still elevated but had decreased with a median of  $2.39 \times 10^9$  cell per liter for the LVS group and  $4.74 \times 10^9$  cells per liter for the S4ΔguaBA group. Granulocyte counts at 7 DPE in the LVS exposed group and counts at 5 DPE in the S4ΔguaBA exposed group were significantly different from baseline levels. S4ΔaroD exposed rabbits exhibited an increase in granulocytes at 2 DPE, but counts plateaued at 4 DPE. At 14 DPE, granulocyte counts were still elevated at a median of  $3.35 \times 10^9$  cells per liter. A small increase in monocyte counts is observed for all vaccine strains at 2 DPE, followed by a decrease at 3 DPE (Figure 31D). A second peak in counts occurred at 4 DPE in LVS exposed rabbits, while the second peak in counts for the S4ΔaroD and S4ΔguaBA groups was seen at 5

DPE. Vaccine strain did not significantly affect lymphocyte, granulocyte, or monocyte counts over time (Table 11).

The characteristic drop in platelet count that occurred during virulent S4 infection was not observed in any of the vaccine groups (Figure 31E). Platelet counts began to increase at 4 DPE in the LVS group, 3 DPE in the S4 $\Delta$ aroD group, and 4 DPE in the S4 $\Delta$ guaBA group, concomitant with the increase observed in total WBC counts. The plateletcrit confirmed this trend (data not shown). Platelet counts were significantly different from baseline at 7 DPE in the S4 $\Delta$ aroD group as determined by Dunn's multiple comparison. Vaccine strain did affect platelet counts over time ( $p$  value <0.0001,  $p$  value <0.0001, respectively), but there was no interaction with time ( $p$  value =0.1445) (Table 11).

Red blood cell counts decreased as early as 1 DPE in all vaccine groups (Figure 31F). This decline was not as dramatic as what was observed during the moribund period in S4 infected rabbits. RBC counts were significantly different from baseline at 3 and 7 DPE in S4 $\Delta$ aroD exposed rabbits. Hemoglobin and hematocrit follow the same trend as RBCs in the vaccinated rabbits (data not shown). Šídák's multiple comparison indicated RBC counts were significantly different 1 DPE between the S4 $\Delta$ aroD and S4 $\Delta$ guaBA groups. In virulent S4 infection, the concomitant decrease in platelet and RBC indices were highly suggestive of internal bleeding. In rabbits exposed to attenuated strains, platelet counts remained steady prior to increasing while red blood cells decreased. Studies have shown *F. tularensis* is able to infect but not replicate within red blood cells (141, 220). The decrease in RBCs observed with vaccine strains may be attributed to culling of infected RBCs by the spleen. Mixed effects modeling indicated vaccine strain did not affect RBC count over time ( $p$  value =0.9412,  $p$  value =0.0208, respectively) (Table 11).

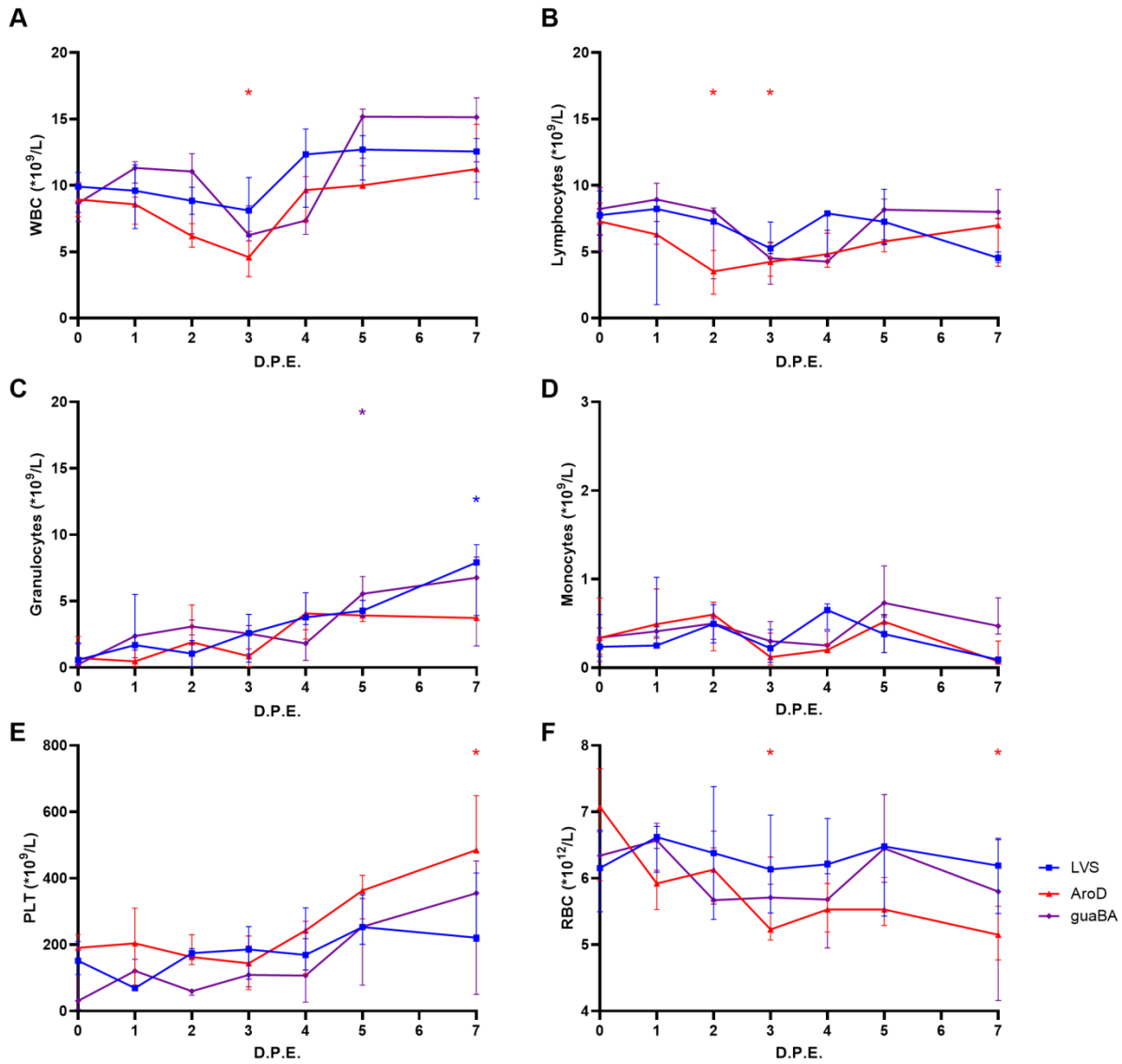


**Figure 31. Characteristic loss of lymphocytes at 3 DPE is seen with all vaccine strains**

Graphs show median with IQR. LVS is represented by blue, S4ΔaroD is represented by red, and S4ΔguaBA is represented by purple. Asterisks indicate significant changes from baseline values, with color correlating with the vaccine group. Naïve rabbits were exposed to aerosols containing LVS, S4ΔaroD, or S4ΔguaBA. Rabbits were bled post exposure to assess A) Total WBCs, B) lymphocytes, C) granulocytes, D) monocytes, E) platelets, and F) red blood cells.

### **4.2.3 Aim 2c**

#### **4.2.3.1 S4ΔaroD is able to disseminate from the lungs to a secondary site of infection**

Rabbits exposed to aerosols containing LVS, S4ΔaroD, or S4ΔguaBA were serially sacrificed 3, 7, and 14 DPE to determine bacterial titers within organs. Lungs from LVS exposed rabbits had little to no changes in gross pathology at 3, 7, and 14 DPE compared to uninfected lungs (Figure 19, Figure 32). Small areas of hemorrhaging could be seen in the lungs of S4ΔaroD infected rabbits at 3 DPE. Unlike in virulent S4 infection, the hemorrhages remained limited and did not coalesce over time. Lungs from S4ΔguaBA exposed rabbits showed extensive hemorrhaging and large bacterial foci at 3 DPE, a feature not observed until the moribund period in S4 infected rabbits. General morphology of the lungs deteriorated due to the spread of bacterial foci and scarring at 7 DPE. At 14 DPE, the lungs still exhibited massive trauma due to the infection.

Pockets of white blood cell infiltrates were found in the lungs of LVS exposed rabbits at 3 DPE. A progressive, mild pneumonia was observed in the LVS group characterized by small lesions and condensation of alveolar spaces (Figure 33). More severe progressive pneumonia characterized by necrotic lesions, condensation of alveolar space, and fluid occurred in animals exposed to S4ΔaroD and S4ΔguaBA. Exposure to LVS, S4ΔaroD, or S4ΔguaBA resulted in a significant decrease in alveolar space over time ( $p$  value < 0.0001 for all). This loss of alveolar space due to inflammation was not resolved by 14 DPE (Figure 34). No significant differences in loss of alveolar space were seen between vaccine strains based on Tukey's multiple comparison

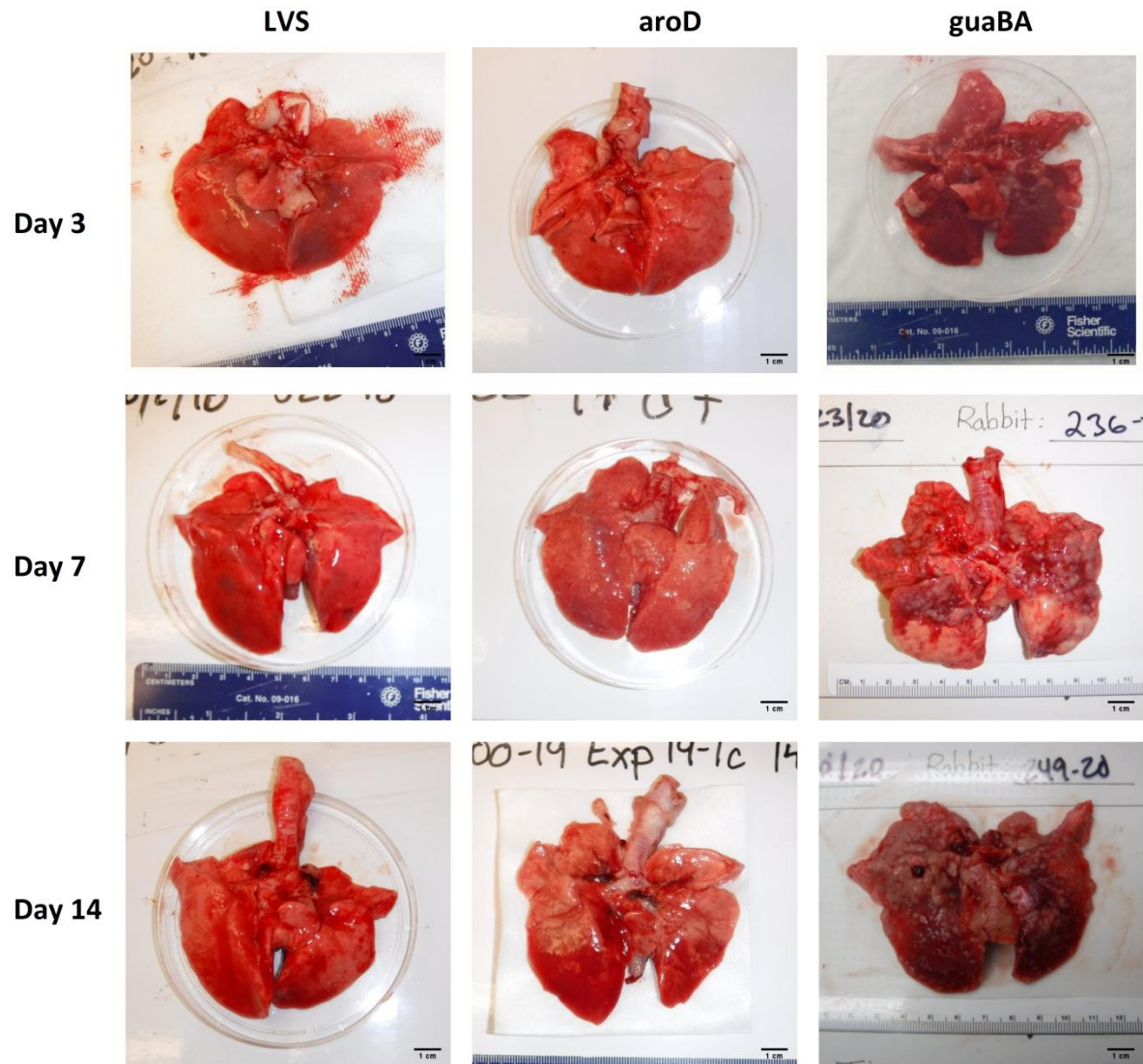


**Figure 32. S4ΔguaBA results in hemorrhage and bacterial lesions**

Rabbits were exposed to LVS, S4ΔaroD or S4ΔguaBA and serially sacrificed to observe gross pathological changes. One representative image of the lung was chosen for each time point: 3 DPE, 7 DPE, and 14 DPE.

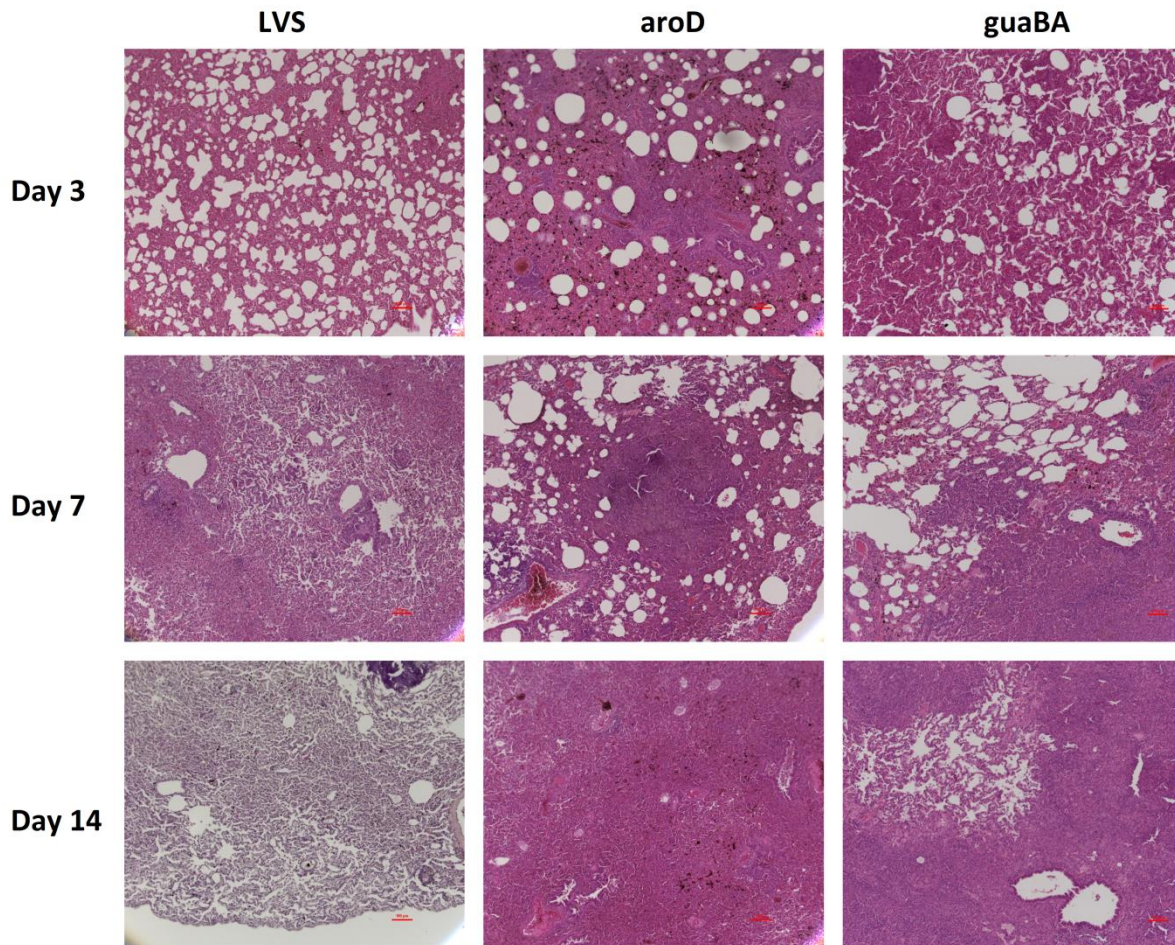


**Figure 33. S4 $\Delta$ aroD and S4 $\Delta$ guaBA result in severe pneumonia**

Rabbits were exposed to LVS, S4 $\Delta$ aroD or S4 $\Delta$ guaBA and serially sacrificed to observe microscopic pathological changes via H&E staining. One representative image of the lung was chosen for each time point: 3 DPE, 7 DPE, and 14 DPE.

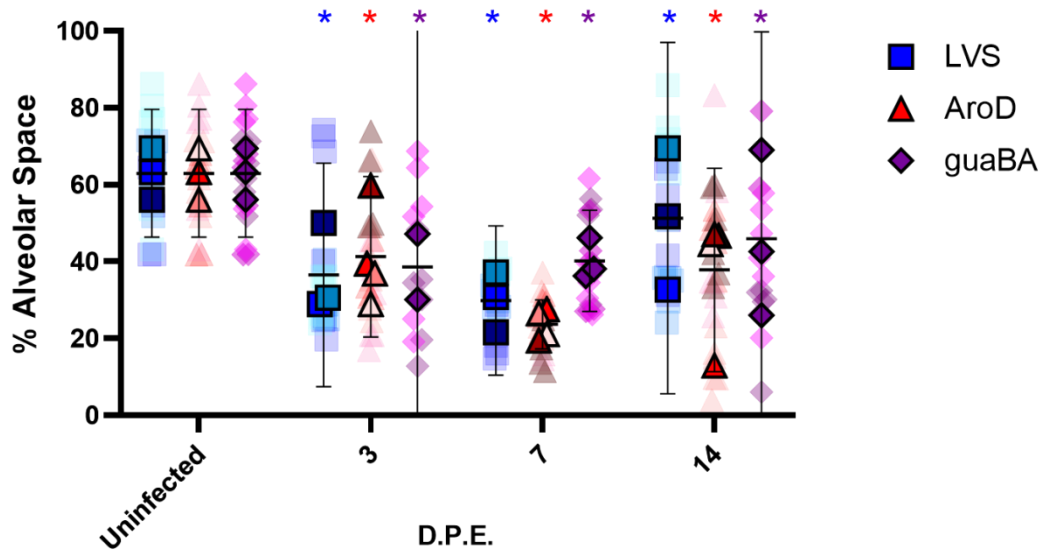


**Figure 34. Attenuated *F. tularensis* strains result in decreased alveolar space**

Each color represents a different animal. Each small, transparent symbol represents an individual lung lobe. Each large, solid symbol represents the median bacterial titer among all lobes for an individual animal. Error bars represent median and IQR of median bacterial titers for all animals.

As with virulent S4 infection, gross liver pathology appeared unremarkable for all vaccine strains (Figure 22, Figure 35). Livers had no visible changes on the tissue surface and were not enlarged or discolored. Rabbits from each vaccine group exhibited infiltration of leukocytes and pyknotic hepatocytes at 3 and 7 DPE (Figure 36). These pathological changes were more severe in S4 $\Delta$ aroD exposed rabbits. By 14 DPE, liver morphology was returning to normal.

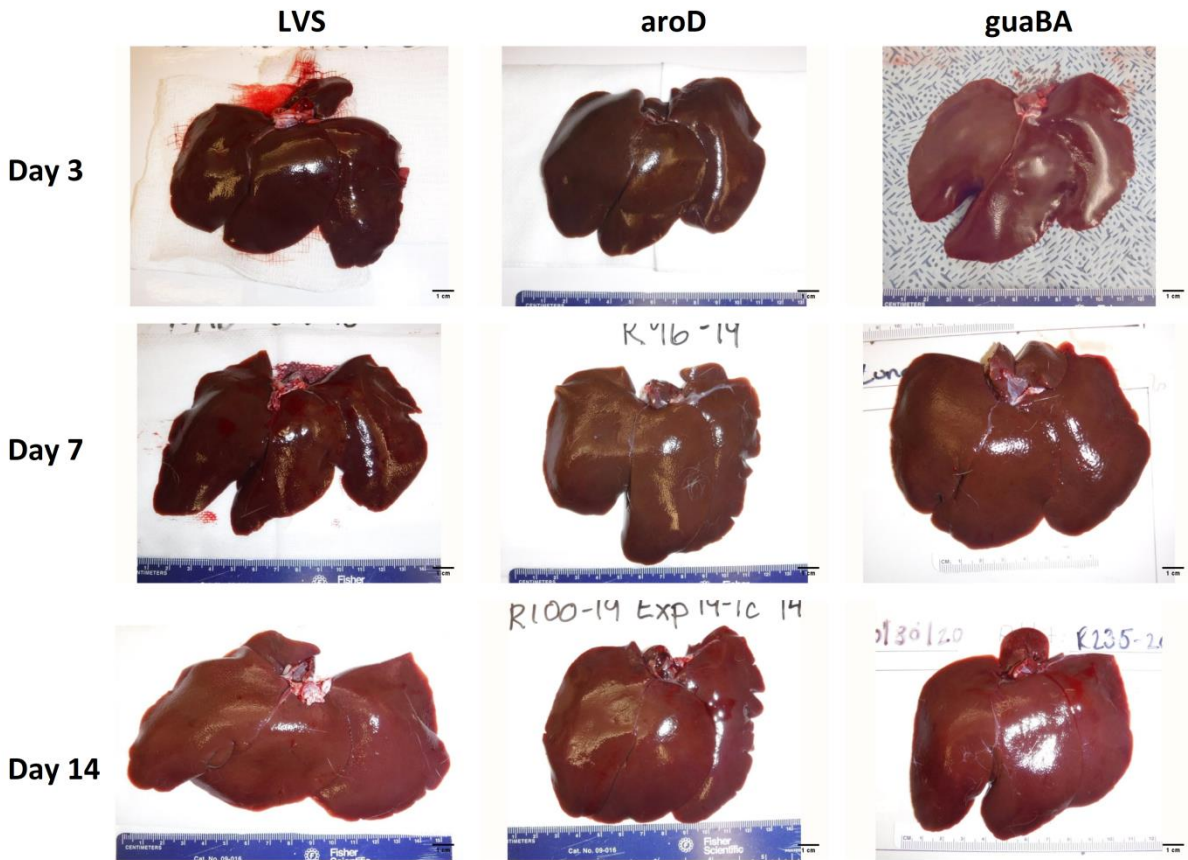


**Figure 35. No macroscopic changes in liver with any vaccine strain**

Rabbits were exposed to LVS, S4ΔaroD or S4ΔguaBA and serially sacrificed to observe gross pathological changes. One representative image of the liver was chosen for each time point: 3 DPE, 7 DPE, and 14 DPE.

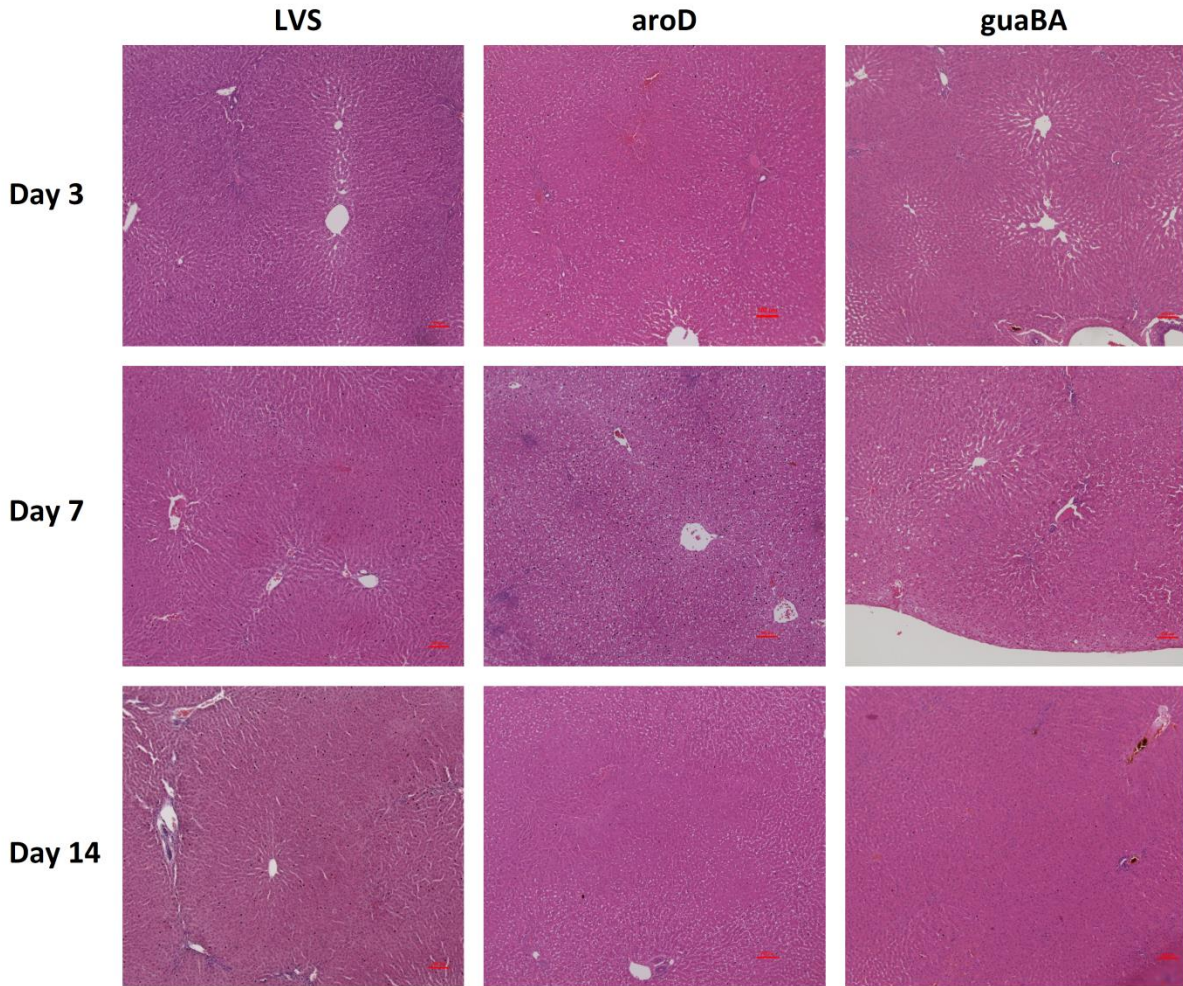


**Figure 36. S4 $\Delta$ aroD infected rabbits exhibit more severe leukocyte infiltration and hepatic cell death**

Rabbits were exposed to LVS, S4 $\Delta$ aroD or S4 $\Delta$ guaBA and serially sacrificed to observe microscopic pathological changes via H&E staining. One representative image of the liver was chosen for each time point: 3 DPE, 7 DPE, and 14 DPE.

LVS exposed rabbits did not exhibit splenomegaly throughout infection (Figure 37). S4ΔaroD exhibited an enlarged spleen 9cm in length at 7 DPE, but by 14 DPE the spleen returned to normal size. Rabbits from the S4ΔguaBA group exhibited splenomegaly with a length of approximately 7cm starting at 3 DPE. The splenomegaly was not resolved by 14 DPE in the S4ΔguaBA vaccine group. No bacterial foci were observed in the spleen at any time point for LVS, S4ΔaroD or S4ΔguaBA, which suggests the animals were able to control infection with attenuated *F. tularensis* strains. In LVS exposed rabbits, spleens exhibited hyperplastic reactive lymphoid follicles and increased macrophages, but returned to normal by 14 DPE (Figure 38). Hyperplastic reactive lymphoid follicles were observed at 3 DPE in the S4ΔaroD and S4ΔguaBA exposed rabbits. Reduced distinction between the red and white pulp, hemorrhage, and reduced red pulp were observed 7 and 14 DPE for both S4aroD and S4guaBA exposed rabbits.

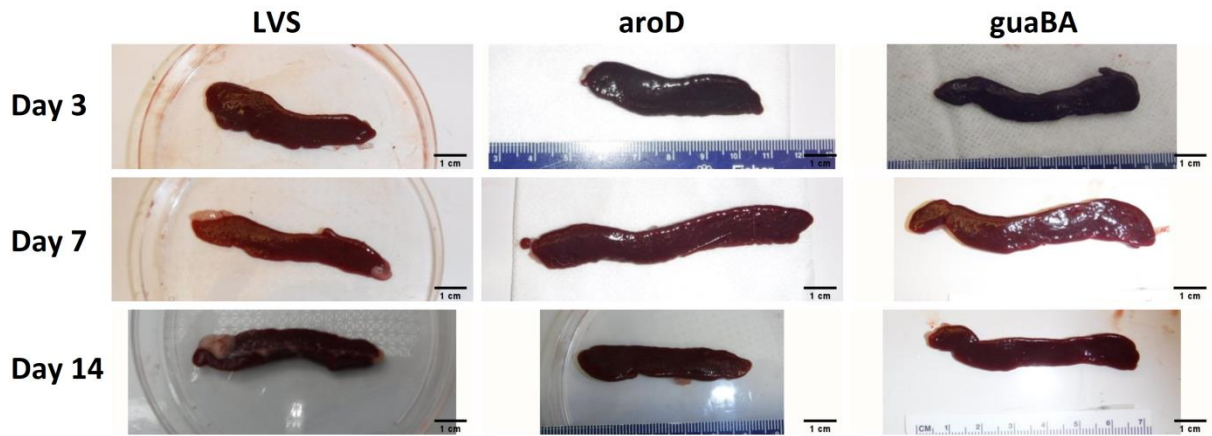


**Figure 37.  $S4\Delta aroD$  and  $S4\Delta guaBA$  exposed rabbits exhibit splenomegaly**

Rabbits were exposed to LVS,  $S4\Delta aroD$  or  $S4\Delta guaBA$  and serially sacrificed to observe gross pathological changes. One representative image of the spleen was chosen for each time point: 3 DPE, 7 DPE, and 14 DPE.

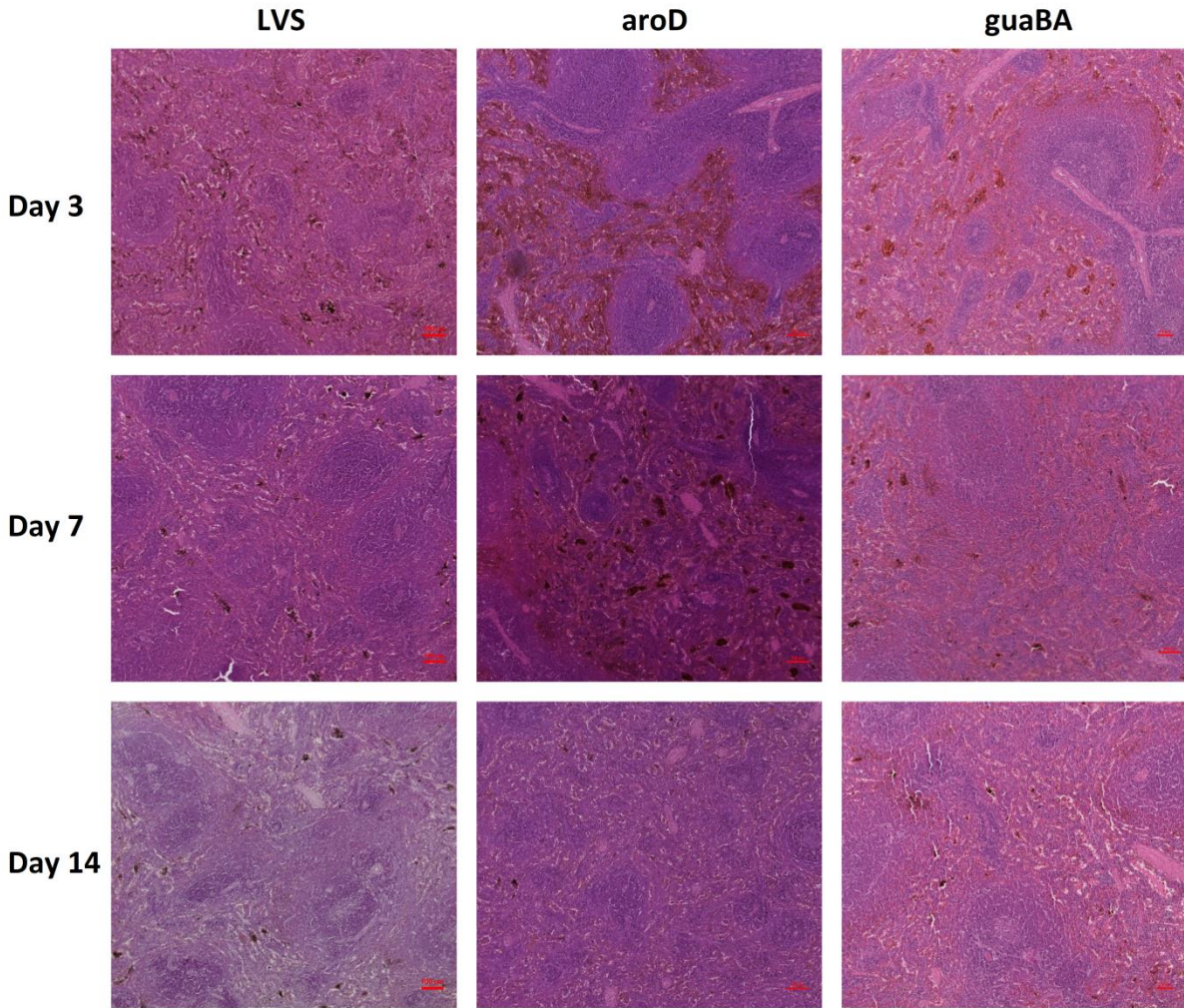


**Figure 38. S4 $\Delta$ aroD and S4 $\Delta$ guaBA exposed rabbits exhibit disruption in splenic organization**

Rabbits were exposed to LVS, S4 $\Delta$ aroD or S4 $\Delta$ guaBA and serially sacrificed to observe microscopic pathological changes via H&E staining. One representative image of the spleen was chosen for each time point: 3 DPE, 7 DPE, and 14 DPE.

Figure 39 shows titers of each of five lung lobes collected from each rabbit in the smaller transparent symbols. Larger, lined symbols represent the median lung lobe titer for each animal. At 3 DPE, the median lung lobe titer was  $5.3 \times 10^2$  CFU/g of tissue in LVS exposed rabbits. By 7 DPE, bacterial titers were beginning to decrease, with a median titer of  $7.2 \times 10^1$  CFU/g, and no bacterial was detected in the lungs at 14 DPE in the LVS group. Bacterial titers for the S4 $\Delta$ aroD at 3, 7, and 14 DPE were  $1.3 \times 10^4$ ,  $8.8 \times 10^2$ , and 0 CFU/g, respectively. Median lung lobe titers were significantly different from baseline at 3 DPE based on Dunn's multiple comparison. In the S4 $\Delta$ guaBA group, median lung titers were  $2.8 \times 10^5$ ,  $4.7 \times 10^5$ , and 0 CFU/g at 3, 7, and 14 DPE, though bacteria was present in at least one lobe of each animal at 14 DPE. S4 $\Delta$ guaBA median lung titers were significantly different from the LVS and S4 $\Delta$ aroD group at 3 DPE (Appendix Table 3). Relative lung titers corresponded with the clinical profile for each vaccine group. Based on weight change and temperature, S4 $\Delta$ guaBA appeared to be the most virulent of all the vaccine strains, and we find the highest bacterial titers in the lungs of S4 $\Delta$ guaBA. Likewise, LVS appeared to be the least virulent strain clinically and had the lowest median lung bacterial titers of the vaccine strains.

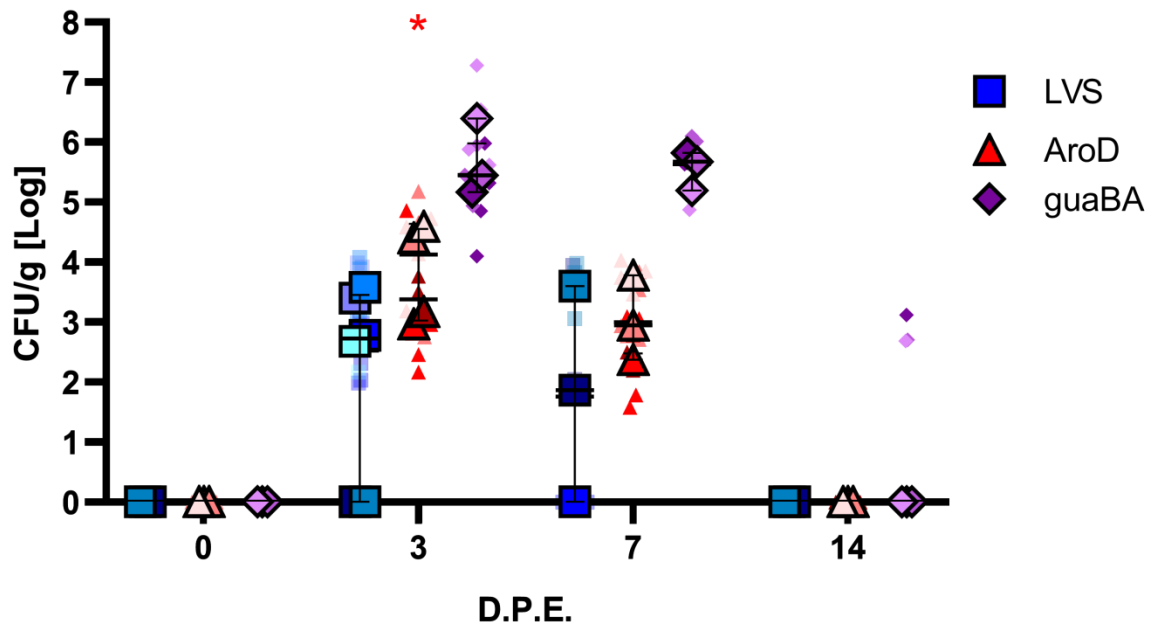


**Figure 39. S4ΔguaBA replicates to high titers and can be detected in the lung longer than LVS and S4ΔaroD**

Each color represents a different animal. Each small, transparent symbol represents an individual lung lobe. Each large, lined, solid symbol represents the median bacterial titer among all lobes for an individual animal. Error bars represent median and IQR of median bacterial titers for all animals.

No bacteria were detected in the liver of any animal at any time point for any of the vaccine strains (Figure 40A). In both LVS and S4 $\Delta$ guaBA exposed rabbits, no bacteria were detected in the spleen at any time point (Figure 40B). In the S4 $\Delta$ aroD group, bacteria were detected in two out of four rabbits euthanized at 7 DPE. Bacterial titers in the spleen were significantly different between vaccine groups at 7 DPE based on Tukey's multiple comparison. One rabbit at 3 DPE had detectable levels of bacteria in the heart (2500 CFU/g) and cervical lymph node (200 CFU/g) in the LVS group. One animal had bacteria in the lymph node (28.6 CFU/g) in the S4 $\Delta$ aroD group at 3 DPE. The heart of one rabbit had bacteria at 3 DPE in the S4 $\Delta$ guaBA group (909 CFU/g). No animal exhibited detectable bacteremia at any time point in the LVS, S4 $\Delta$ aroD, and S4 $\Delta$ guaBA groups. The heart and lymph node could have had bacteria incidentally due to their proximity to the primary site of infection, the lungs. Persistence of bacteria in the lung did not correlate with observed vaccine efficacy for attenuate strains, though it did correlate with clinical severity. Dissemination to the spleen did correlate with vaccine efficacy. S4 $\Delta$ aroD, which exhibited the best vaccine efficacy at 67.7%, was the only strain able to escape the primary site of infection. the activation of lymphoid follicles observed in the H&E of the spleen and the presence of bacteria in the spleen of S4 $\Delta$ aroD vaccinated rabbits suggest antigen presence within the spleen is important for vaccine efficacy of attenuated *Francisella* strains.

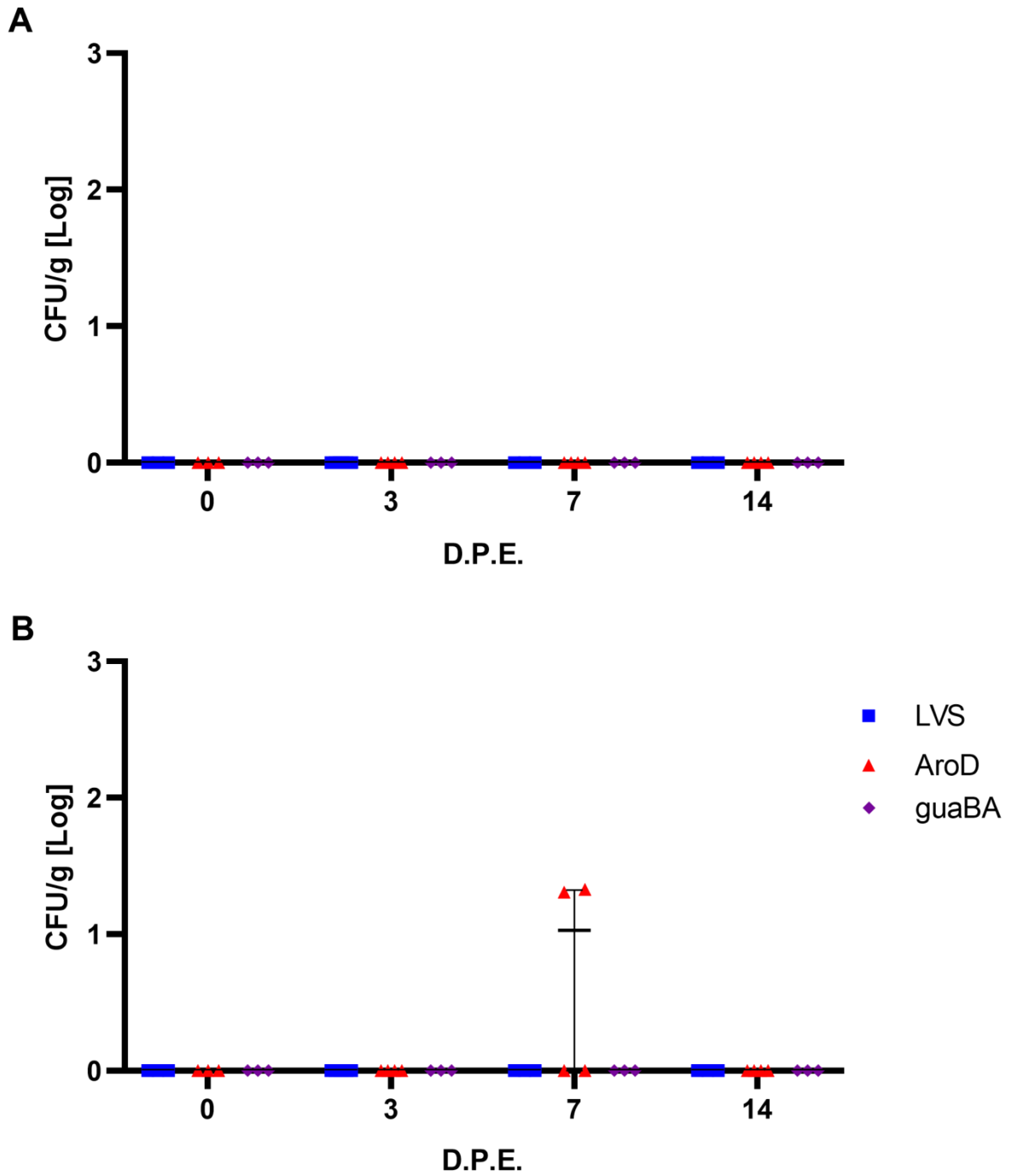


**Figure 40. S4ΔaroD is able to escape the lung and spread to the spleen but not the liver**

Graphs show medians with IQR with each symbol representing a single animal. Naïve NZW rabbits were exposed to aerosolized LVS, S4ΔaroD or S4ΔguaBA and serial sacrificed to assess bacterial titers in A) liver and B) spleen.

### 4.3 Aim 3

Elucidate the immunological mechanisms associated with disease course of virulent vs. attenuated *F. tularensis* strains.

#### 4.3.1 Aim 3a

##### 4.3.1.1 Lungs exhibit limited alterations in gene expression during early infection

The GeneChip<sup>TM</sup> Rabbit Gene 1.0 ST Array utilizes a median of 22 probes per gene. There are a total of 496,321 probes and 23,282 gene-level probe sets. Use of multiple probes across a gene ensures higher resolution and accuracy than classical 3'-biased microarray and detection of multiple isoforms. Rabbits were exposed to aerosols containing virulent S4 and serially sacrificed to collect RNA from lung, liver, and spleen for microarray analysis. The time points chosen for analysis were -2, 3 and 5 relative to exposure to capture baseline, onset of symptoms, and death, respectively. Three rabbits were used for each time point.

Microarray data was parsed to include genes with a fold change less than -1.5 and greater than 1.5 and a *p* value less than 0.05; genes meeting these criteria were considered differentially expressed between time points. Based on these criteria, a total of 4,959 genes were differentially expressed in the lung at either 3 or 5 DPE compared to baseline. At 3 DPE there were 253 (44.39%) upregulated genes and 317 (55.61%) down regulated genes with a filter criteria of fold change greater than 1.5 or less than -1.5 (Figure 41A). Differentially expressed genes (DEGs) at 3 DPE accounted for 2.44% of all genes, with 97.56% of genes expressing no change. At 5 DPE there were 2110 (44.37%) upregulated genes and 2645 (55.63%) down regulated genes. These DEGs accounted for 20.35% of all genes on the microarray with 79.65% expressing no change.

Between day 3 and day 5 post exposure there were 366 shared DEGs (Figure 41B). Figure 42 depicts a volcano plot of all genes at 3 DPE in relation to their fold change and p value. Significant DEGs are marked with green and red symbols indicating if they are upregulated or downregulated, respectively. The top 10 DEGs that are upregulated and downregulated are marked with their gene names. Appendix Table 4 shows the top 10 DEGs in the lung at 5 DPE. These will be discussed in more detail later.

Gene ontology enrichment analysis was performed on DEGs in the lung using Fisher's exact test (Table 12). Enrichment refers to the number of genes that are differentially expressed and does not give an indication in which direction those genes are altered. Biological processes accounted for 19.48% of DEGs at 3 DPE and 58.01% of DEGs at 5 DPE. Cellular component at 3 and 5 DPE was 10.03% and 6.69%, respectively. At 3 DPE, 70.49% of DEGs were involved with molecular function, while only 35.30% were involved at 5 DPE. Figure 43 depicts a heat map of enrichment scores of significantly affected functional groups; blocks that are grey were not significant and thus represent data not shown. At 3 DPE, genes involved in the extracellular region had the highest enrichment score at 59.41. In this group 64 genes were upregulated and 66 were downregulated (Appendix Table 5). At 5 DPE, genes involved with the nucleus had the highest enrichment score at 28.89; 306 genes in this group were upregulated and 1128 genes were downregulated (Appendix Table 6). Immune system processes were enriched at 3 DPE, but not 5 DPE. Within the immune system process functional group 45 genes were upregulated and 7 genes were downregulated. Genes related to cell death processes were enriched at 3 DPE with 4 genes downregulated.

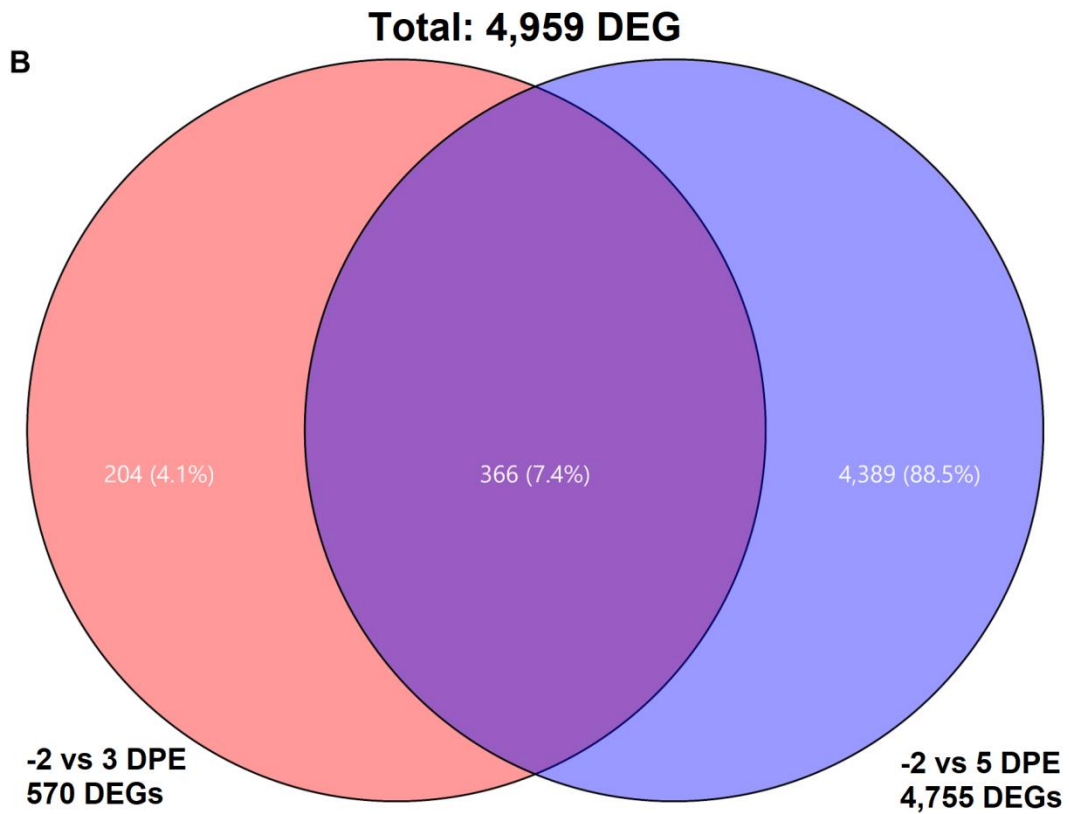
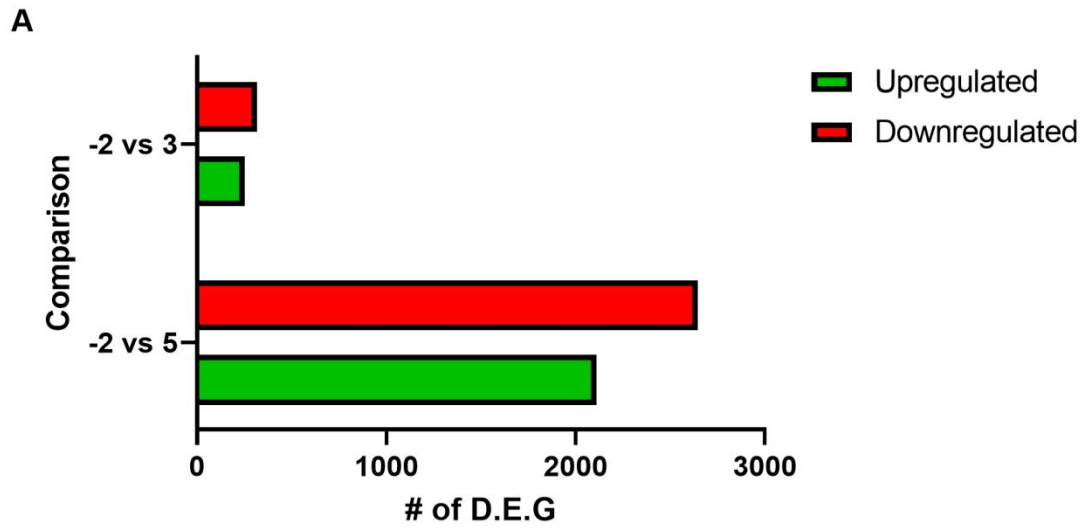


**Figure 41. Number of DEGs in lung tissue over time**

Microarray data was filtered to include samples with a gene-level fold change  $<-1.5$  or  $>1.5$  and a gene-level  $p$  value  $<0.05$  using the eBayes Anova method to determine A) DEGs at 3 and 5 DPE to virulent S4 and B) number of shared DEGs between 3 and 5 DPE compared to baseline.

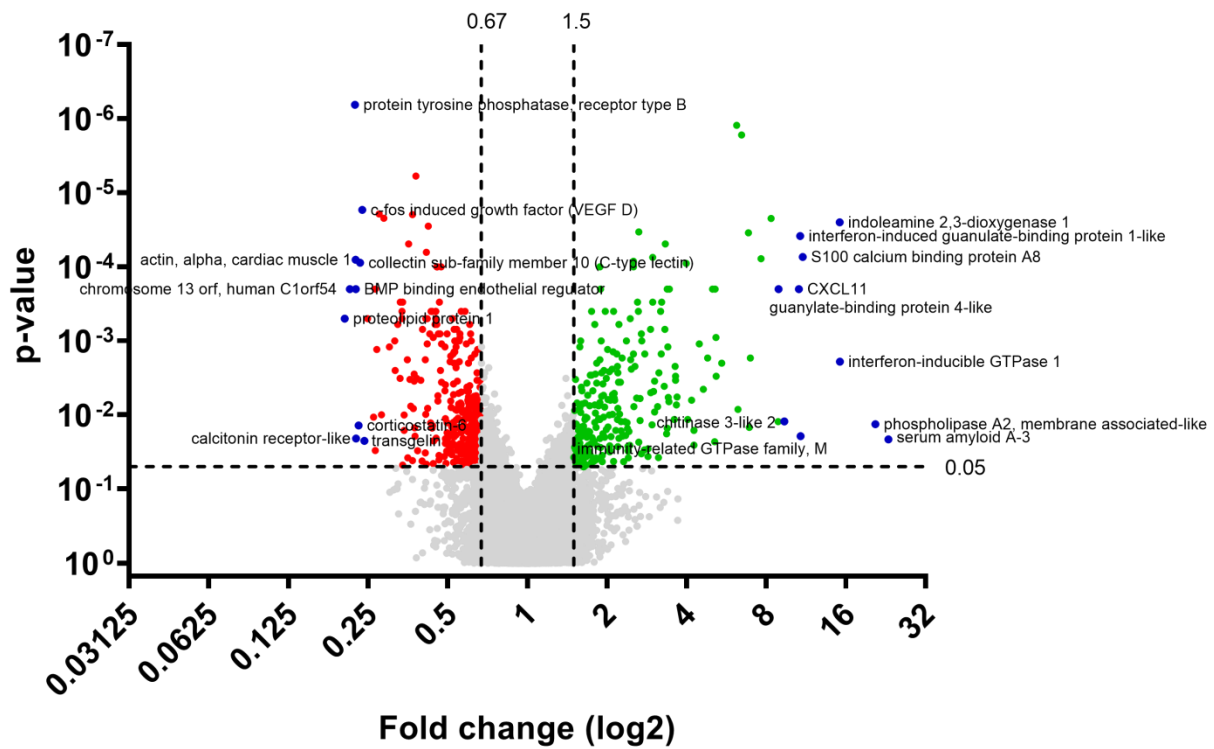


**Figure 42. Top 10 downregulated and upregulated DEG in lung at 3 DPE**

Volcano plot depicts all DEG in the lung at 3 DPE compared to baseline. The dotted horizontal line represents the  $p$  value cut off of 0.05. Dotted vertical lines represent the fold change limits of  $<-1.5$  (0.67) and  $>1.5$ . Negative fold changes were converted to fit on the log<sub>2</sub> scale. Grey symbols indicate values that are not significantly differentially expressed. Red symbols represent DEG that are downregulated. Green symbols represent DEG that are upregulated.

**Table 12. Biological class of DEGs in the lung**

Class	3 DPE	5 DPE
Biological process	19.48%	58.01%
Cellular component	10.03%	6.69%
Molecular function	70.49%	35.30%

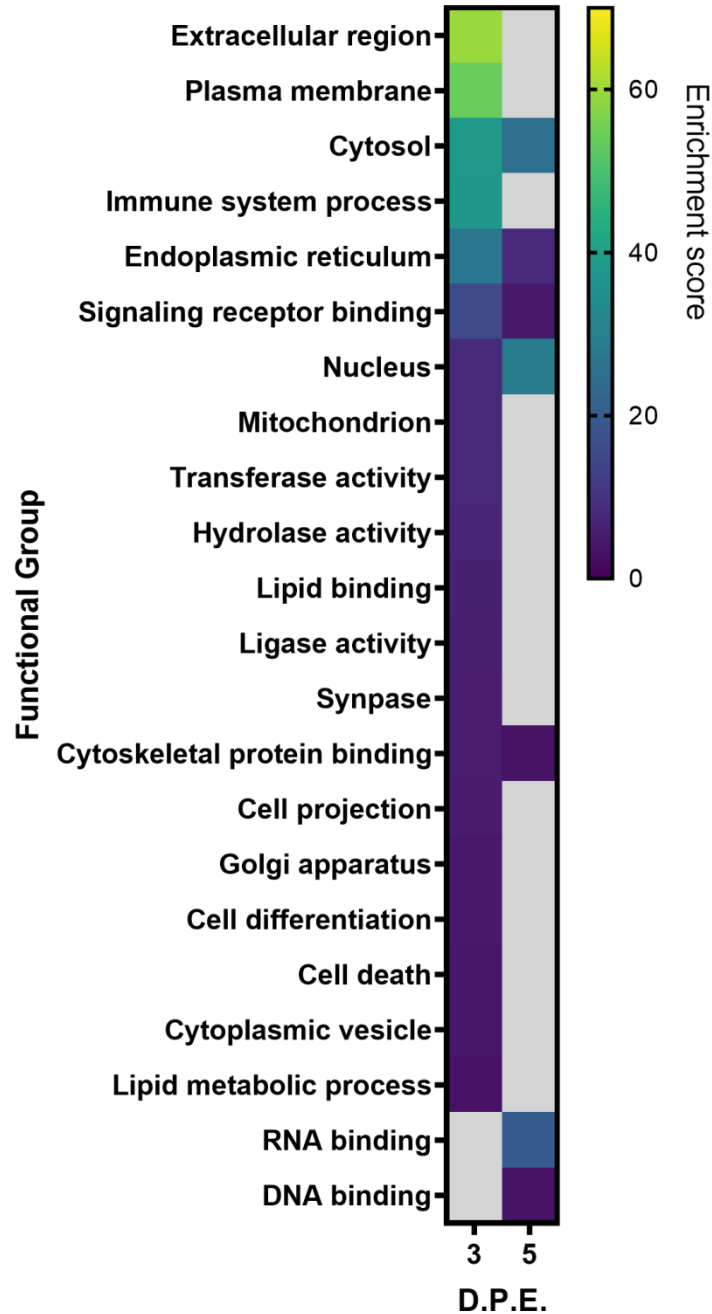


**Figure 43. Gene ontology enrichment analysis of lung tissue at 3 and 5 DPE compared to baseline**

Biological class was further broken down into function groups. Only statistically functional groups with statistically significant enrichment scores ( $p$  value  $<0.05$ ) are shown. Grey blocks indicate functional groups that were not enriched.

#### **4.3.1.2 Limited alteration of gene expression in the liver of S4 infected rabbits.**

A total of 2,946 genes were differentially expressed in the liver at 3 and 5 DPE compared to baseline. There were 768 (41.9%) upregulated genes and 1066 (58.1%) downregulated genes at 3 DPE (Figure 44A). At 5 DPE there were 1041 (46.9%) upregulated genes and 1177 (53.1%) downregulated genes. DEGs accounted for 7.85% and 9.49% of all genes at 3 and 5 DPE, respectively. There were 1,106 shared DEGs between 3 and 5 DPE (Figure 44B).

Gene ontology enrichment analysis showed biological processes accounted for 55.81% of DEGs at 3 DPE and 53.60% of DEGs at 5 DPE (Table 13). DEGs related to cellular components were 6.23% at 3 DPE and 7.34% at 5 DPE. Molecular function accounted for 37.96% and 39.06% of DEGs at 3 and 5 DPE, respectively. Oxidoreductase activity was the most affected functional group at 3 DPE and 5 DPE with an enrichment score of 67.86 and 55.69, respectively (Figure 45, Appendix Table 10, Appendix Table 11). Within this functional group, 22 genes were upregulated, and 146 genes were downregulated at 3 DPE. At 5 DPE, 36 genes were upregulated, and 119 genes were downregulated related to oxidoreductase activity. Immune system processes were enriched at both 3 and 5 DPE. At 3 DPE, 94 genes were upregulated, and 24 genes were downregulated related to immune system processes. Similar numbers were seen at 5 DPE with 87 genes being upregulated and 18 genes being down regulated within this functional group.

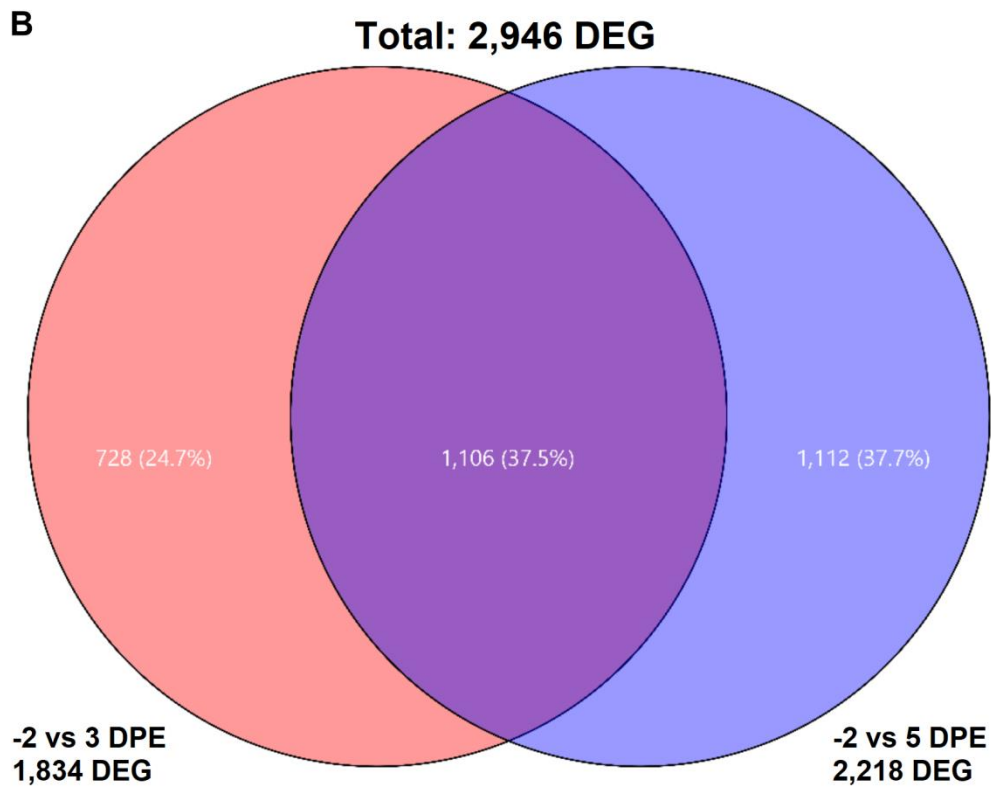
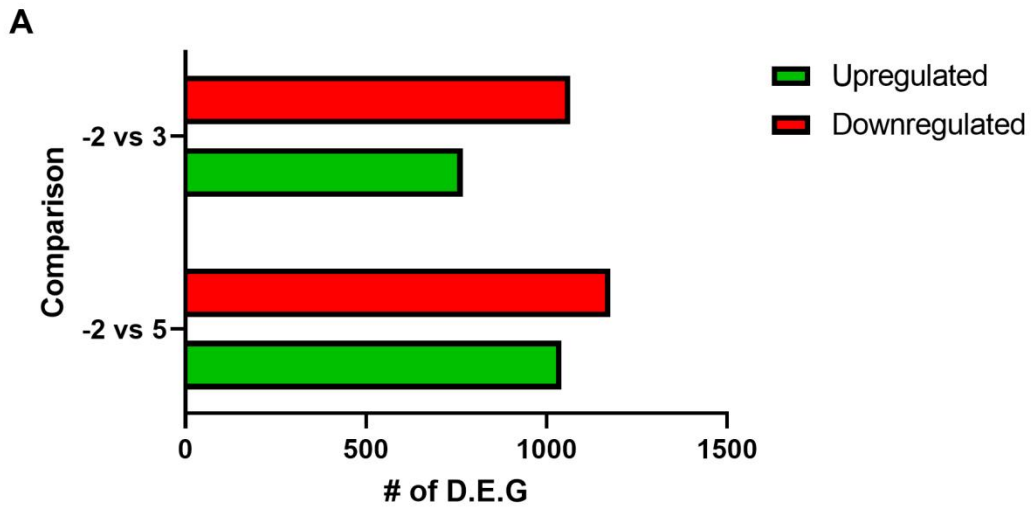


**Figure 44. Number of DEGs in liver tissue over time**

Microarray data was filtered to include samples with a gene-level fold change  $<-1.5$  or  $>1.5$  and a gene-level  $p$  value  $<0.05$  using the eBayes Anova method to determine A) DEGs at 3 and 5 DPE to virulent S4 and B) number of shared DEGs between 3 and 5 DPE compared to baseline.

**Table 13. Biological class of DEGs in the liver**

<u>Class</u>	<u>3 DPE</u>	<u>5 DPE</u>
Biological process	55.81%	53.60%
Cellular component	6.23%	7.34%
Molecular function	37.96%	39.06%

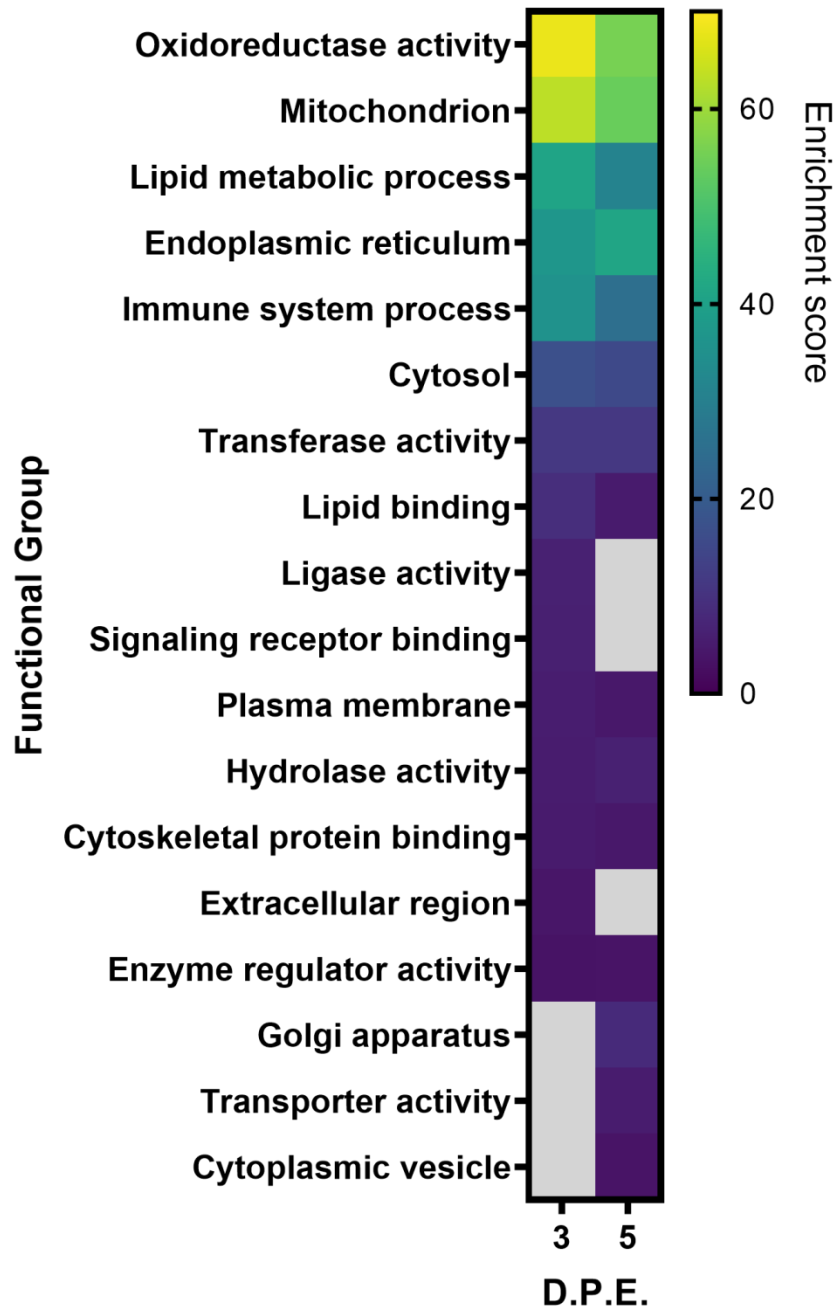


Figure 45. Gene ontology enrichment analysis of liver tissue

Biological class was further broken down into function groups. Only statistically functional groups with statistically significant enrichment scores ( $p$  value  $<0.05$ ) are shown. Grey blocks indicate functional groups that were not enriched.

#### **4.3.1.3 Spleen exhibits upregulation of immune genes during virulent S4 infection**

At 3 and 5 DPE, there was a total of 3,142 DEGs in the spleen compared to baseline. At 3 DPE there were 292 (39.2%) upregulated genes and 452 (60.8%) downregulated genes (Figure 46A). These DEGs accounted for 3.18% of all genes on the microarray. At 5 DPE, there were 1408 (51.0%) upregulated genes and 1353 (49.0%) downregulated genes, which accounted for 11.82% of all genes. There were 363 DEGs shared between 3 and 5 DPE (Figure 46B).

The class distribution of DEGs in the spleen at 3 DPE was 43.89% for biological process, 19.00% for cellular component, and 37.12% for molecular functions (Table 14). At 5 DPE, biological processes accounted for 85.64% of DEGs. Cellular component was 5.22% and molecular function was 9.13% of DEGs. Genes related to the extracellular region were the most affected at 3 DPE with an enrichment score of 21.79 (Figure 47, Appendix Table 15). Within this functional group, 49 genes were upregulated, and 45 genes were downregulated. Immune system process was the second most enriched group at 3 DPE. At 5 DPE, immune system process was the most enriched functional group with an enrichment score of 46.55 (Appendix Table 16). Within this group, 95 genes were upregulated while 22 genes were downregulated.

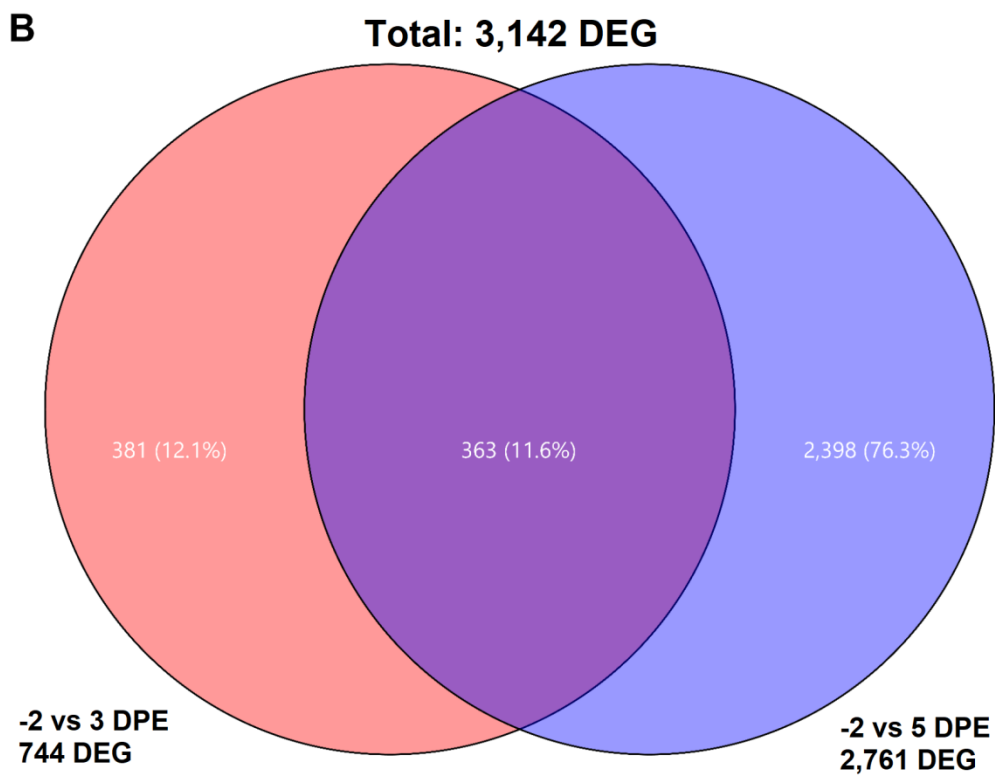
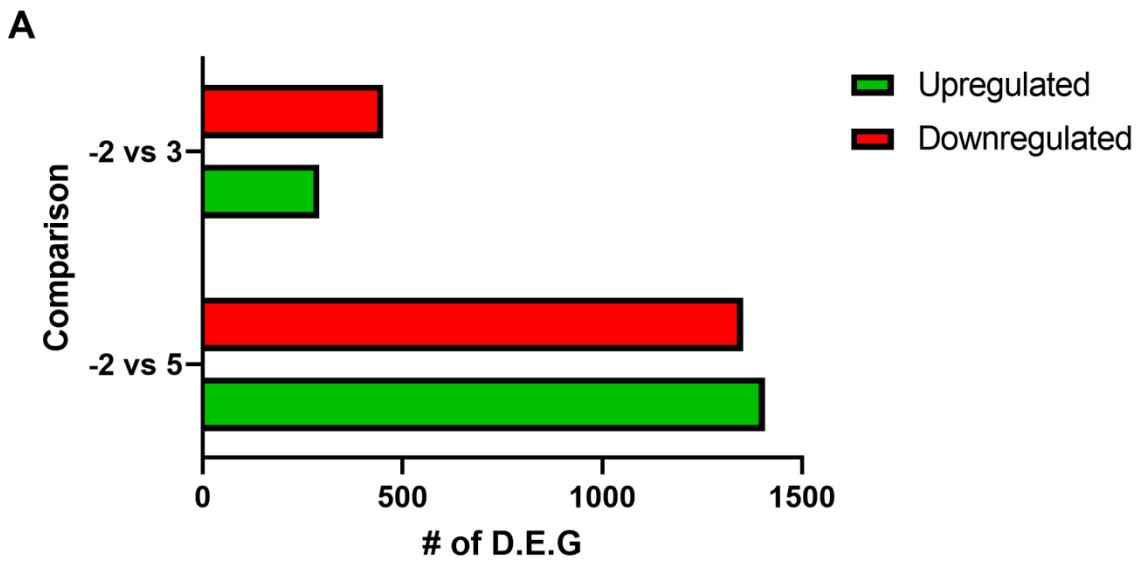


**Figure 46. Number of DEGs in spleen tissue over time**

Microarray data was filtered to include samples with a gene-level fold change  $<-1.5$  or  $>1.5$  and a gene-level  $p$  value  $<0.05$  using the eBayes Anova method to determine A) DEGs at 3 and 5 DPE to virulent S4 and B) number of shared DEGs between 3 and 5 DPE compared to baseline.

**Table 14. Biological class of DEGs in the spleen**

<u>Class</u>	<u>3 DPE</u>	<u>5 DPE</u>
Biological process	43.89%	85.64%
Cellular component	19.00%	5.22%
Molecular function	37.12%	9.13%

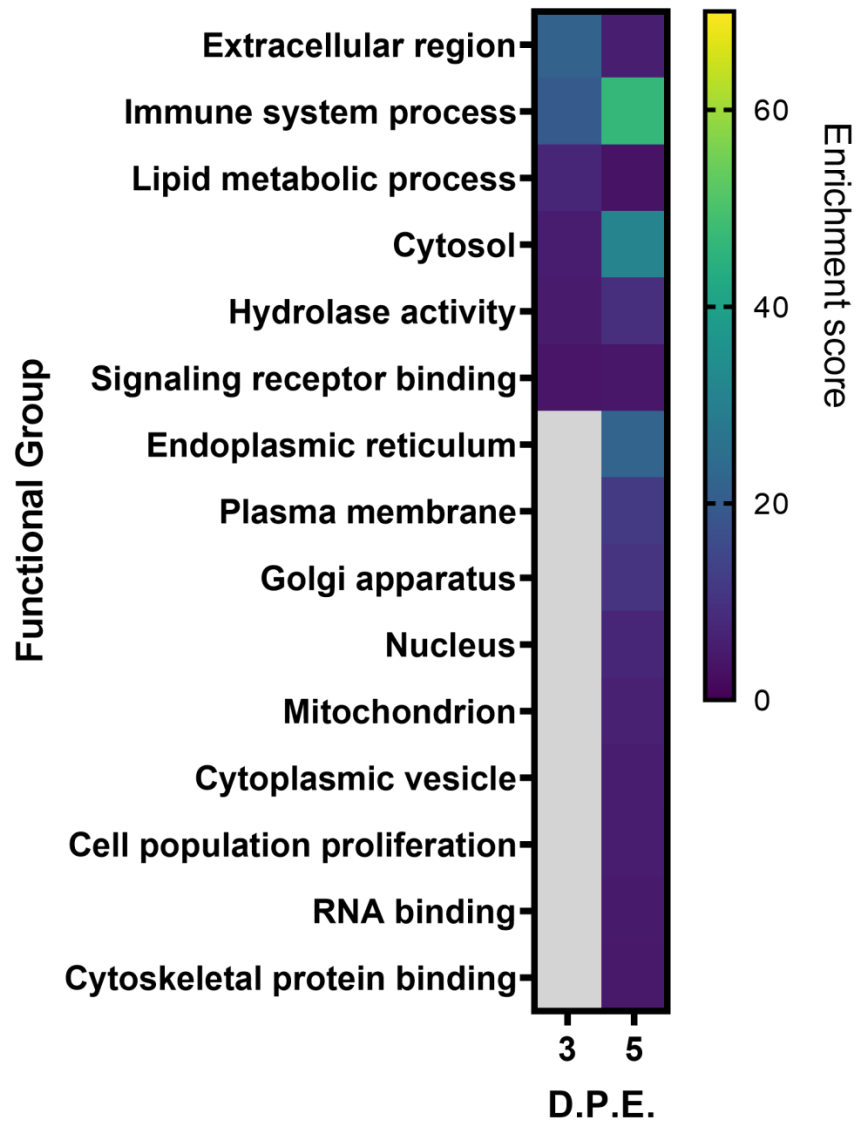


**Figure 47. Gene ontology enrichment analysis of spleen tissue**

Biological class was further broken down into function groups. Only statistically functional groups with statistically significant enrichment scores ( $p$  value  $<0.05$ ) are shown. Grey blocks indicate functional groups that were not enriched.

#### **4.3.1.4 NZW rabbits recapitulate widespread immune suppression observed in other animal models**

Acute phase reactants are a class of proteins whose plasma concentrations increase or decrease in response to inflammation. The acute phase response is characterized by fever and acceleration of peripheral leukocytes. Local inflammation results in the secretion of IL-1, IL-6, and TNF $\alpha$ , which triggers the liver to produce acute phase reactants. Increased acute phase reactant proteins may contribute to the promotion of sepsis. At 2 DPE plasma IL-6 levels are increased, but levels quickly decline by 3 DPE (Figure 48B). TNFR, IL1RA, and OSMR have a fold change increase greater than 1.5 in the liver, though only TNFR and OSMR is significantly elevated (p value = 0.0020 and 0.0001, respectively) (Figure 48A).

The acute phase response consists of a group of proteins that are upregulated and a group that are downregulated. Gene expression in the liver at 3 DPE is consistent with a typical acute phase response, though due to small sample sizes, fold changes in gene expression are not significant (Figure 48A). Albumin, tissue factor, and apolipoproteins are downregulated. Complement proteins 3 and 9, fibrinogen genes (FGA, FGB, FGG), and Factor VIII are upregulated. Orosomucoid (ORM), lipopolysaccharide binding protein (LPB), C-reactive protein (CRP), serpin family genes (SERPINA3), and ceruloplasmin (CP) are highly upregulated. This gene expression was confirmed with blood parameters. ESR is affected by the presence of positively charged proteins, which reverses the zeta potential of red blood cells causing them to stick together. Fibrinogen is a very positively charged protein. ESR increased starting at 3 DPE in S4 infected rabbits (Figure 15C). C-reactive protein levels in the plasma began increasing 2 DPE but are significantly elevated at 3 DPE (Figure 48C). Serum albumin levels began to decrease at 3 DPE (Figure 48D).

At 3 DPE, little to no upregulation is seen in the TLR response pathway (Figure 49A). Only TLR-5 and ubiquitin are slightly upregulated. *F. tularensis* has been shown to inhibit the TLR response through multiple means. The LPS has 4 acyl changes in the lipid A which allows it to escape recognition by TLR-4. *F. tularensis* lipoproteins can be recognized by TLR-2, but studies suggest the bacterium is able to inhibit the downstream signaling. Complement opsonization of *F. tularensis* increases phagocytosis without neutralizing the bacteria. Downstream signaling and subsequent cytokine response is thought to be inhibited through intracellular cross talk between C3R and TLR-2. *F. tularensis* has also been shown to prevent recognition of other pathogens that utilize TLR-2 through inhibition of TLR mRNA synthesis.

Additionally, there is no upregulation in PI3K-AKT pathway (Figure 49A). The PI3K-AKT pathway can be activated by a variety of cell surface receptors, including Fc and TLR. *F. novicida* has been shown to activate the PI3K/AKT pathway, while virulent stains of *F. tularensis* have been shown to induce increased expression of PTEN to block this pathway. While AKT is downregulated in the lung, liver, and spleen, there is no increase in PTEN gene expression within the tissue in this study (data not shown). The lack of downstream signaling in the TLR and PI3/AKT pathway was also observed in the spleen (Appendix Figure 16).

At 3 DPE in the lung, STAT1, IRF1, and TAP1 are upregulated in the lung tissue suggestive of the induction of a Type II interferon response (Figure 49B). At 5 DPE, G1P2, a negative regulator of Type I IFN signaling, is upregulated. Overall, very little interferon production and subsequent downstream signaling is observed based on gene expression. This pattern was also observed in the spleen (Appendix Figure 17). Appendix Table 18 shows the fold change for immune genes expressed in the lung at 3 and 5 DPE. The upregulation of the acute phase response and downregulation of recognition and interferon responses in the NZW rabbit

corresponds with what has been observed in other animal models and humans. Thus, the NZW rabbit model is a suitable model for studying *F. tularensis* immune responses.

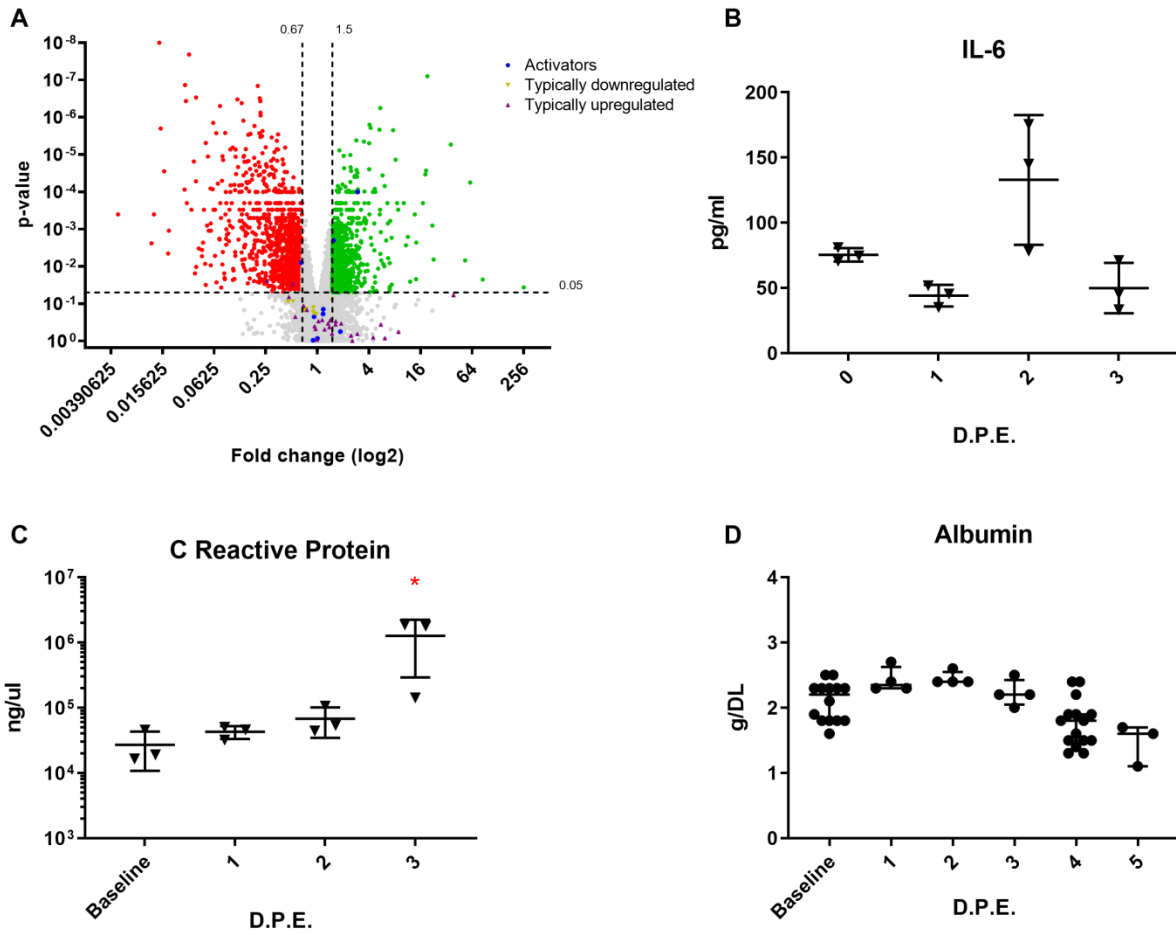


**Figure 48. Appropriate acute phase reactant response produced by the liver at 3 DPE**

NZW rabbits were exposed to virulent S4 and serially sacrificed to collect tissue and blood for A) gene expression of acute phase response, B) serum IL-6, C) serum C-reactive protein, and D) serum albumin levels.

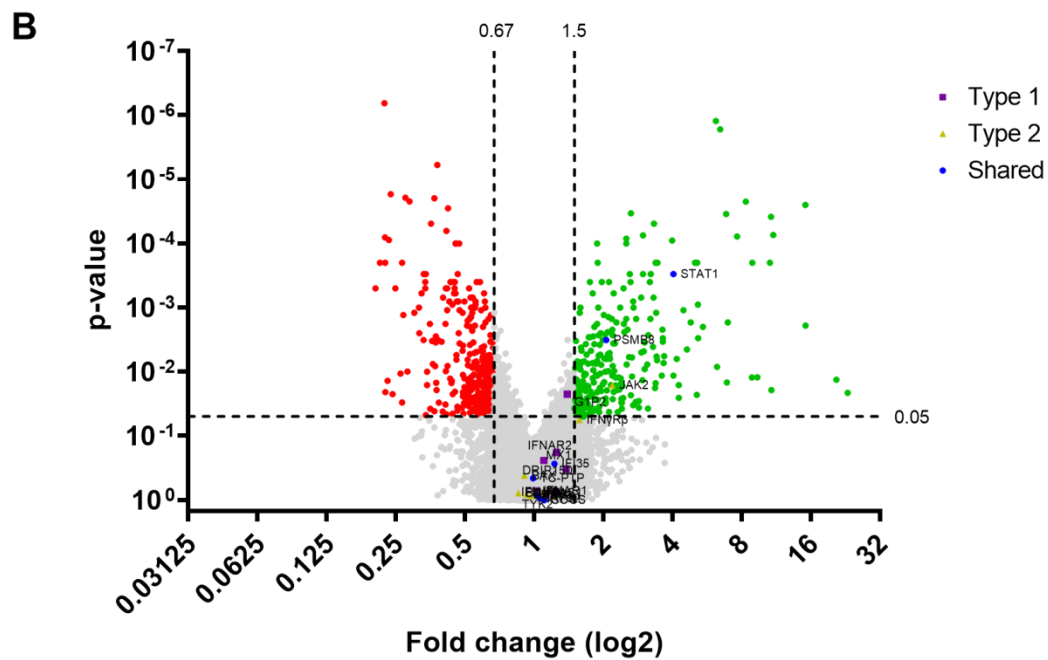
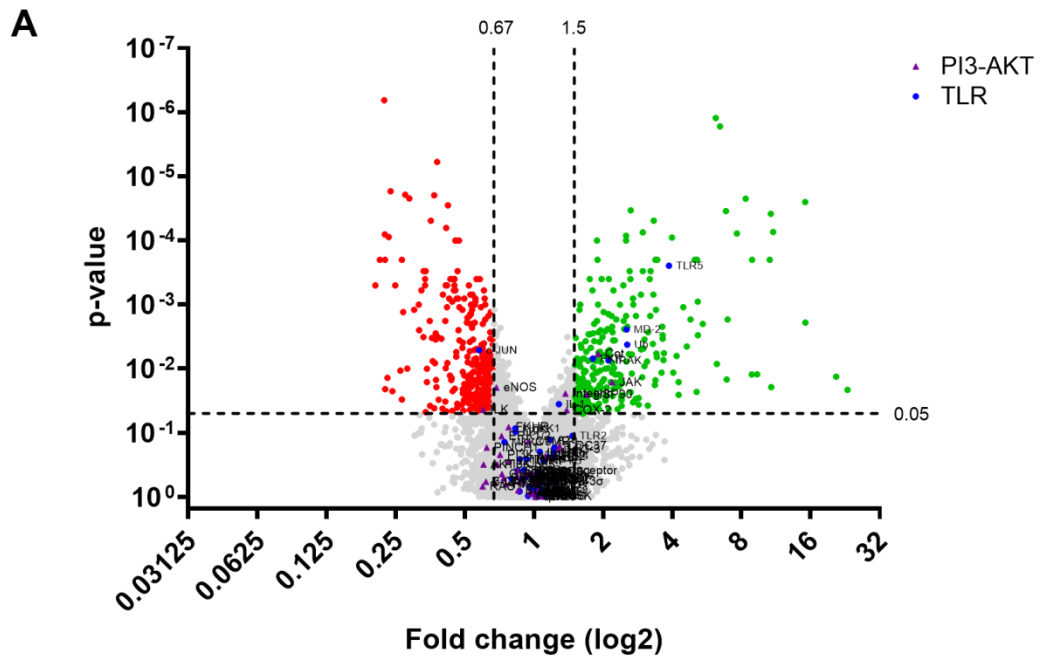


**Figure 49. No upregulation in genes related to pattern recognition pathways or interferon response in the lung at 3DPE**

NZW rabbits were exposed to virulent S4 and serially sacrificed to collect tissue for gene expression pathway analysis of A) TLR and PI3K-AKT and B) interferon signaling.

#### 4.3.1.5 Death of S4 infected rabbits is not a result of a cytokine storm event

Studies have suggested that *F. tularensis* infected animals succumb to disease to a cytokine storm like event (171, 221, 222). Here we examined genes involved with several cell death pathways, including the pyroptosis, apoptosis, and necroptosis. In the inflammasome pathway caspase-1 is upregulated at both 3 and 5 DPE (Figure 50A). There is no upregulation in NLRP3, an important component of the inflammasome complex needed to activate caspase-1. We do not see an upregulation in IL-18 or IL-1 $\beta$  genes. No changes in circulating IL-18 or IL-1 $\beta$  protein levels were observed up to 3 DPE in S4 infected rabbits (Figure 50B and 50C). Thus, in the absence of activated caspase 1, IL-18 and IL-1 $\beta$  it is not likely pyroptosis is occurring in the rabbit model. It is important to note that most research groups utilize MHb, which has been shown to result in less virulence gene expression and an impaired bacterial membrane. Additionally, many studies looking at inflammasome activation during *Francisella* infection utilize LVS, which is an attenuated strain. Thus, in vitro models and mouse models may be showing evidence of inflammasome activation due to release of double stranded DNA into the cytoplasm and the inability of an attenuated *Francisella* strain to impair the host immune response to the extent of the more virulent Type A strain.

Examination of the apoptosis pathway reveals little to no alteration in gene expression at both 3 and 5 DPE (Figure 51A). BFL1, an apoptosis regulator, is upregulated at 5 DPE. ROCK1, a serine/threonine kinase involved in the initiation of the caspase cascade, is downregulated at 5 DPE. BFL1 has been shown to mediate lipid-triggered apoptosis through the formation of pores (216). Histones are released from the nucleosome during the apoptosis process. ELISA detection of plasma for circulating histones revealed a small increase in histone 4 at 3 DPE (Figure 51B).

The lack of a cytokine response and the increase in histone 4 suggest apoptosis may be occurring in S4 infected rabbits.

Necrosis is a form of cell death induced by infection or trauma that is most often detrimental to the host. The uncontrolled release of cellular products into the extracellular space recruits leukocytes which release microbial damaging chemicals that harm host tissue, creating a cycle of tissue damage that inhibits tissue healing. AHR (aryl hydrocarbon receptor), a potent immunosuppressant, and CD36, a negative regulator of necrosis, is downregulated at both 3 and 5 DPE (Figure 52A). EGFR (epidermal growth factor receptor), a mediator of macrophage activation, and TGF $\beta$ , another immunosuppressant, is decreased at 5 DPE. Genes involved with tissue repair are upregulated at 3 and 5 DPE in the lung. IRAK3 is important for maintenance and repair of the endothelial barrier of the lung. MYC is a proliferative transcription factor. SERPINE1, or PAI-1, is important for breaking down blood clots. SFTPC and SFTPD are surfactant proteins that are necessary for proper lung function. Many genes involved in immunosuppression and wound healing are upregulated from the necrosis pathway. The observed tissue damage and the decrease in CD36 suggests necrosis pathway activation during virulent S4 infection.

Necroptosis is a programmed form of necrosis. Unlike apoptosis, it results in the release of damage associated molecular patterns that could aid in the host immune response against infection. This pathway is primarily mediated by TNF $\alpha$ . Gene expression of TNF $\alpha$  is not upregulated at either 3 or 5 DPE and there were no detectable levels of TNF $\alpha$  in the plasma of S4 infected rabbits (Figure 52B). There is a downregulation of pronecrotic proteins CaN and PELI1 at 5 DPE. The absence of PELI has been shown to promote apoptosis. ANT, a negative regulator of cell death is also downregulated at 5 DPE. EIF2AK2 (PKR), a required necroptotic

protein, was upregulated at 3 and 5 DPE. *BIRC2/3*, a negative regulator of necroptosis, was upregulated both 3 and 5 DPE. Taken together, the gene expression profile suggests necroptosis is not occurring during virulent S4 infection.

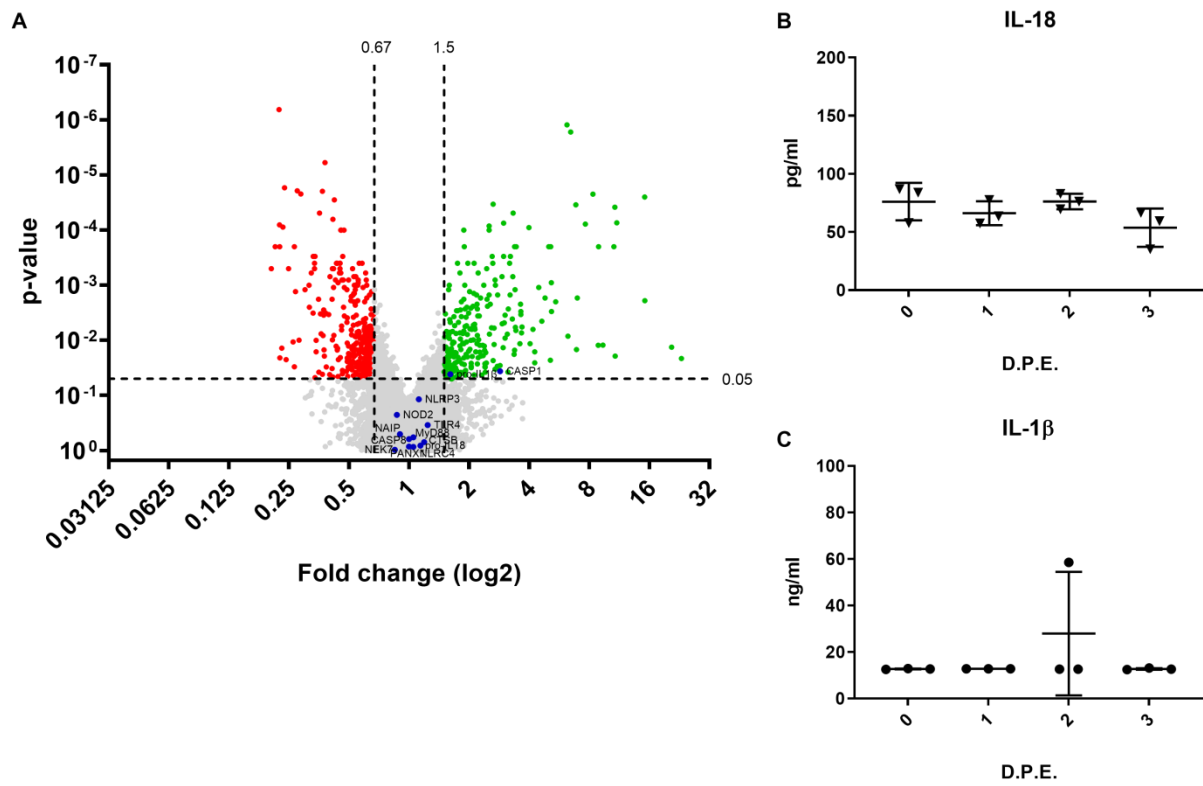


**Figure 50. No evidence of pyroptotic septic event during S4 infection**

NZW rabbits were exposed to virulent S4 and serially sacrificed to collect tissue for gene expression pathway analysis for A) the inflammasome. Plasma was taken for assessment of B) IL-18 and B) IL-1β.

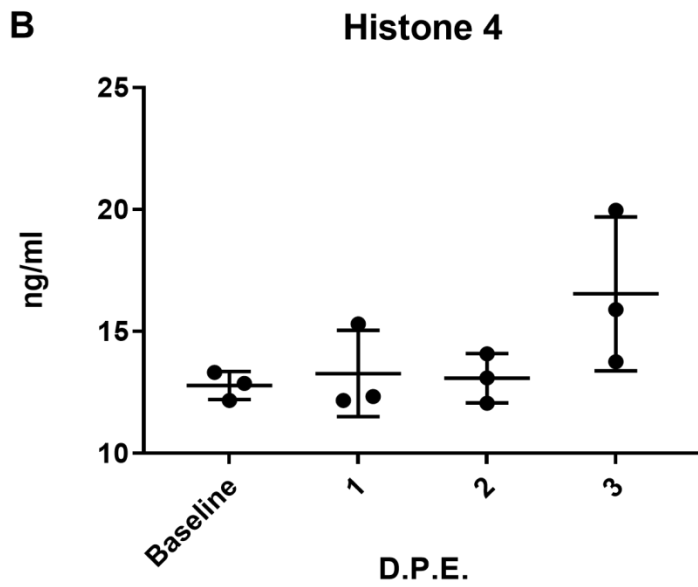
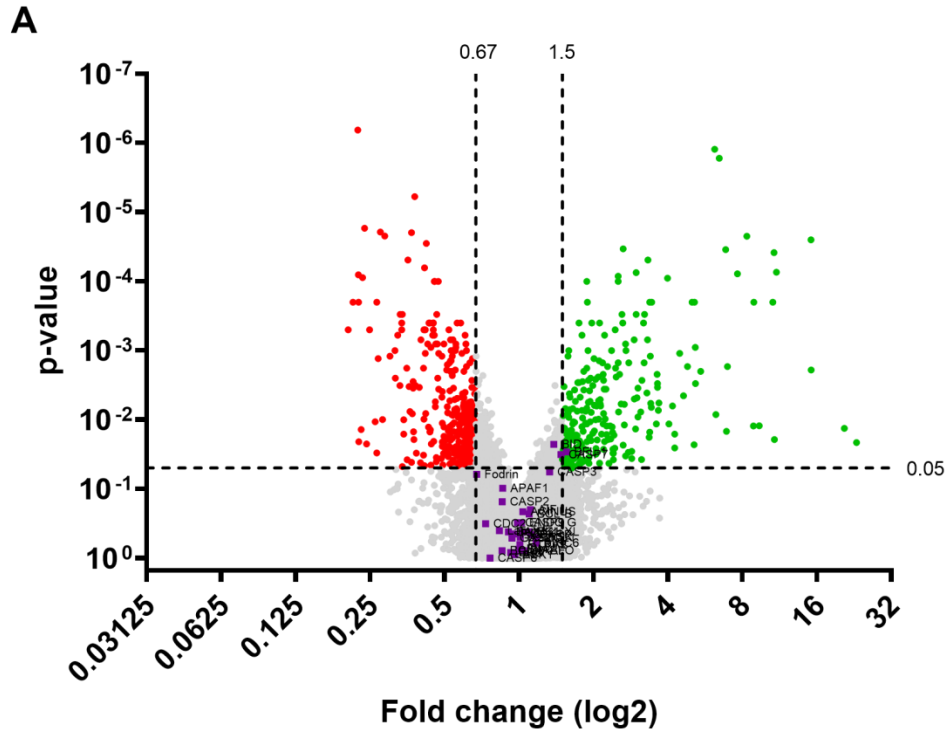


**Figure 51. No significant changes in apoptic pathway in the lung**

NZW rabbits were exposed to virulent S4 and serially sacrificed to collect tissue for gene expression pathway analysis for A) apoptosis. Plasma was taken for assessment of B) histone 4.

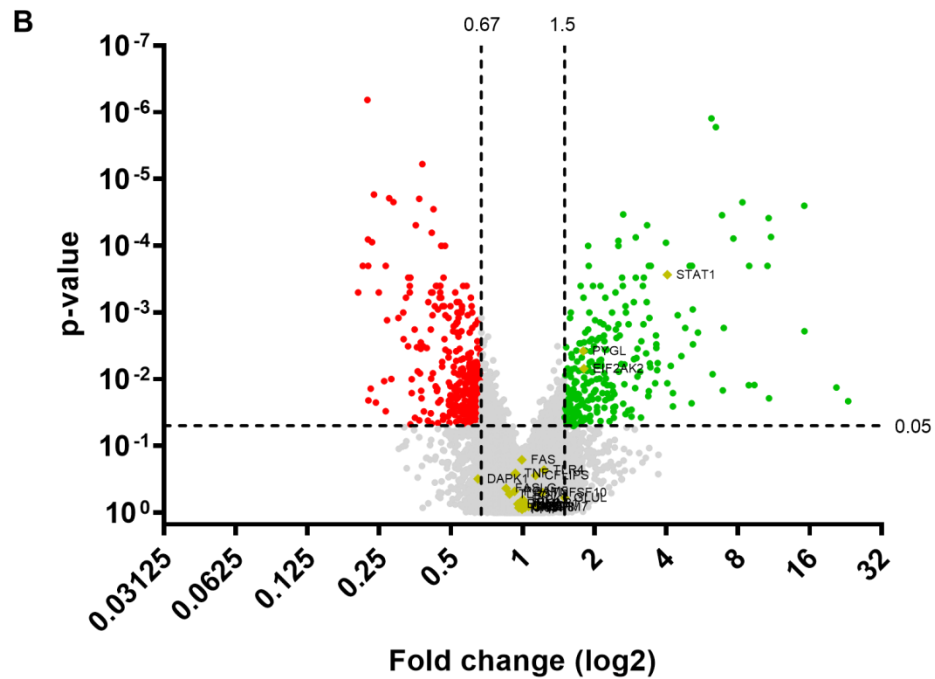
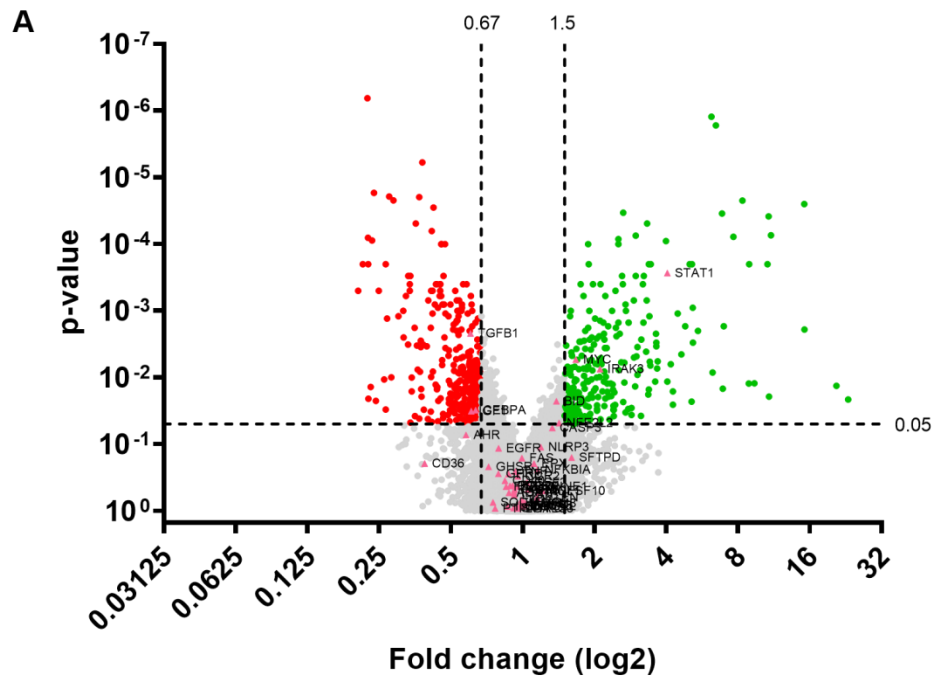


**Figure 52. Necrosis and necroptosis pathways are not upregulated in the lung of S4 infected rabbits**

NZW rabbits were exposed to virulent S4 and serially sacrificed to collect tissue for gene expression pathway analysis for A) necrosis and B) necroptosis.

#### **4.3.1.6 Virulent S4 infection results in upregulation of damaging inflammatory pathways and downregulation of wound healing pathways**

Based on the gene expression results, NZW rabbits do not appear to succumb to infection due a pyroptosis mediated cytokine storm event. To determine pathogenesis related events that may be contributing to the observed tissue damage and subsequent death of NZW rabbits infected with virulent S4, an unbiased analysis of the gene expression in the lung tissue was performed. In Figure 42, the top 10 downregulated and upregulated DEGs in the lung at 3 DPE are labelled. Fold change and *p* values for these genes are listed in Table 15. At 3 DPE, there is a downregulation of genes related to angiogenesis, including protein tyrosine phosphatase, actin alpha cardiac muscle 1, BMP binding endothelial regulator, and c-fos. There is also downregulation in genes related to cellular structure, such as proteolipid protein 1 and transgelin. Downregulation in these genes related to angiogenesis and cell structure would likely inhibit wound healing responses needed to repair the damage inflicted by host immune processes or the bacterium. There is also downregulation in calcitonin receptor, which deactivates the immune response to prevent collateral damage in wounds. Corticostatin 6 is typically induced as a defense response to bacterium, and collectin subfamily member 10 creates C4 and C2 activators. These genes are downregulated in the lungs of tularemia infected NZW rabbits. Thus, at 3 DPE we still see downregulation of wound healing processes.

Surprisingly, many of the genes upregulated at 3 DPE in the lung are immune related. Interferon stimulated genes include phospholipase A2, interferon inducible GTPase, immunity related GTPase family M, interferon induced guanylate binding protein 1, CXCL11, chitinase 3. Innate immune response genes include serum amyloid A3 and S100 calcium binding protein A8. S100 calcium binding is indicative of granulocyte infiltration. Indoleamine 2,3 dioxygenase 1 is

part of nutritional immunity and blocking immune responses. It is unclear which pathways are being altered by the host or the bacterium. Thus, there is an overall increase in genes related to immune processes and an overall decrease in genes related to wound healing.

Gene expression data was further parsed to look for trends in pathways overtime. The 366 DEGs shared between 3 and 5 DPE compared to baseline were further limited to those that had a continuous downward or upward trend over time. The top 10 genes that trended downwards and upwards are shown in Figure 53A and 53B, respectively. Similar to what was observed at 3 DPE in the lungs, genes that trended downwards were related to wound healing, while genes that trended upwards were related to inflammatory processes. Canonical pathway analysis of those DEGs that shared a trend over time show an overall decrease in pathways related to wound healing, such as HOTAIR regulatory pathway, HIF1 $\alpha$  signaling, and VEGF signaling (Figure 54). There is an upregulation in pathways related to hypercytokinemia and cardiomyopathy. There is also an upregulation in RHOGDI signaling and downregulation of Rho family GTPases. RHOGDI is an inhibitor of RhoA. RhoA is involved in a number of innate and adaptive immune responses including internalization of pathogens, migration, cell activation, antigen presentation, and activation and migration of the T and B cells of the adaptive immune response. Thus, canonical pathway analysis confirms an overall downregulation in wound healing processes and the concomitant up and downregulation of immune processes.

Predicted activation state (PAS) is a tool that helps to understand whether cellular processes are being driven up or down by correlating observed expression with reported experimental gene effects verified and stored in the IPA database. Table 16 shows the predicted activation states within the lung and their associated *p* values and z-scores. Predicted activation states correlate with the canonical pathway analysis. There is an overall decrease in

vasculogenesis, cellular organization, and quantity of cells indicating a decrease in wound healing processes. Gene expression shared between 3 and 5 DPE predicted hypertension and vascular disease, cell death, activation of leukocytes, bleeding, edema, organismal death. It is interesting to note that necrosis and apoptosis are predicted to be increased while the gene expression of mediators directly involved in those processes are not significantly altered (Figures 51 and 52A). This discrepancy is likely due what is being measured. The gene expression analysis of cell death pathways was limited to genes directly involved those processes. The predicted activation state looks at the gene expression as a whole, including events before and after activation of cell death pathways. The overall picture painted by the gene expression data is one of activation of damaging inflammatory processes, such as cellular degranulation, and a decrease in wound healing processes. Thus, NZW rabbits are likely succumbing due to the massive tissue trauma induced by *F. tularensis* infection.

**Table 15. Top 10 upregulated and downregulated genes at 3 DPE in the lung**

3 DPE	Gene	Fold change	FDR <i>p</i> value
Downregulated	proteolipid protein 1	-4.9	1.78E-01
	chromosome 13 open reading frame, human C1orf54	-4.69	1.21E-01
	protein tyrosine phosphatase, receptor type B	-4.48	1.30E-02
	actin, alpha, cardiac muscle 1	-4.46	8.74E-02
	BMP binding endothelial regulator	-4.45	1.21E-01
	calcitonin receptor-like	-4.44	1.00E+00
	corticostatin-6	-4.34	8.90E-01
	collectin sub-family member 10 (C-type lectin)	-4.29	8.74E-02
	c-fos induced growth factor (VEGF D)	-4.21	5.77E-02
	transgelin	-4.13	1.00E+00
Upregulated	serum amyloid A-3	23.19	1.00E+00
	phospholipase A2, membrane associated-like	20.67	8.75E-01
	interferon-inducible GTPase 1	15.19	3.48E-01
	indoleamine 2,3-dioxygenase 1	15.16	5.87E-02
	S100 calcium binding protein A8	11	8.74E-02
	immunity-related GTPase family, M	10.79	1.00E+00
	interferon-induced guanylate-binding protein 1-like	10.75	6.43E-02
	CXCL11	10.63	1.20E-01
	chitinase 3-like 2	9.36	8.57E-01
	guanylate-binding protein 4-like	8.91	1.20E-01

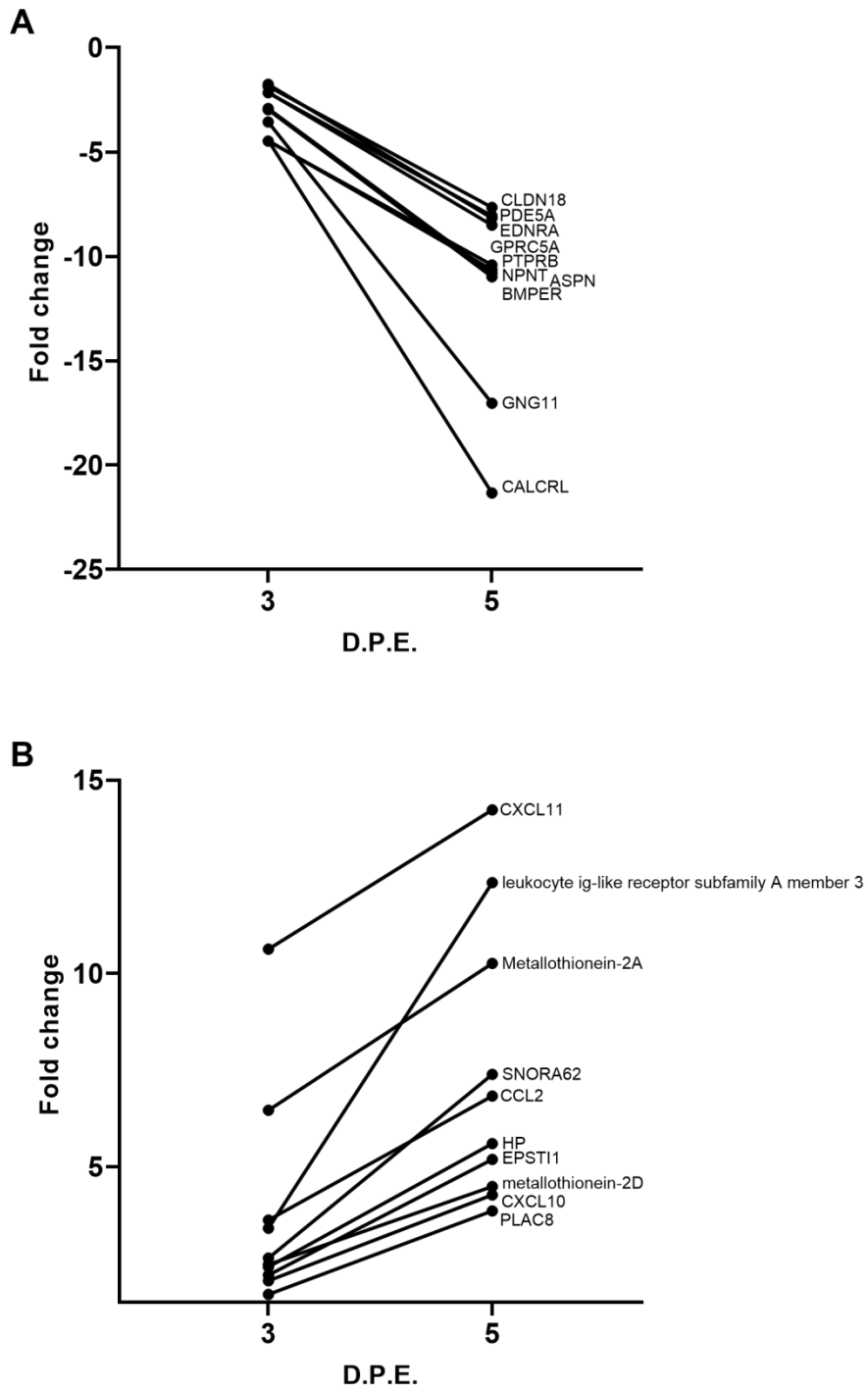


**Figure 53. The top 10 genes that trended downwards or upwards over time in the lung**

The top 10 DEGs shared between 3 and 5 DPE compared to baseline that trended A) downwards or B) upwards over time in the lung tissue of NZW rabbits infected with virulent S4.

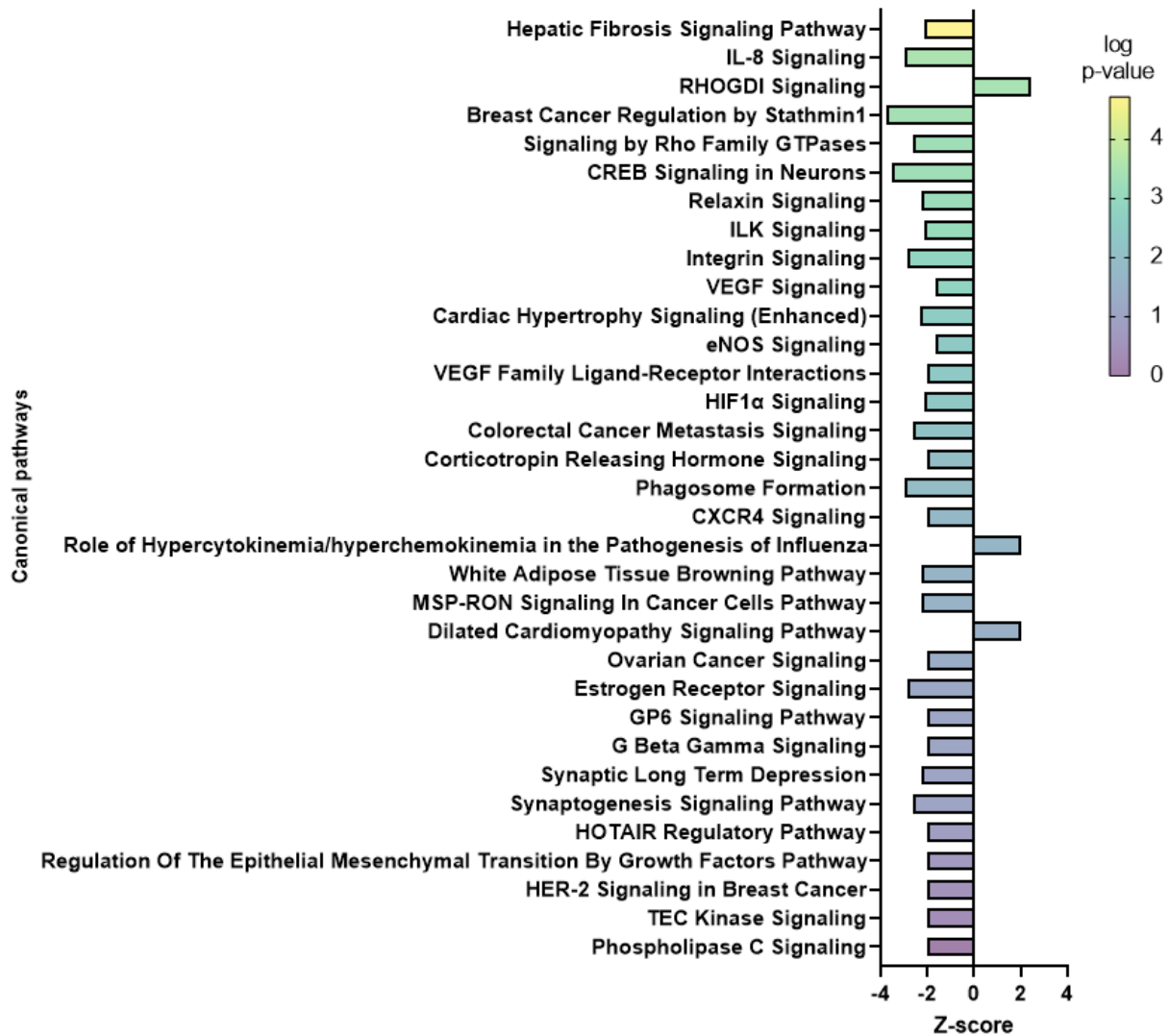


**Figure 54. Pathway analysis of DEGs that shared a trend over time in the lungs of S4 infected NZW rabbits**

Canonical pathways were limited to those that exhibited z-scores  $> 2.0$  and  $< -2.0$  and  $p$  values  $< 0.05$ . Z-scores are shown on the x-axis and  $p$  values are represented by a heatmap.

**Table 16. Predicted activation states in the lungs**

Disease/Function	PAS	Z-score	P value
Development of vasculature	↓	-2.775	2.36E-35
Branching of vasculature	↓	-2.171	3.06E-10
Tubulation of vascular endothelial cells	↓	-3.249	3.69E-08
Migration of vascular endothelial cells	↓	-3.318	3.97E-10
Vasculogenesis	↓	-2.741	1.50E-31
Angiogenesis	↓	-2.765	1.63E-32
Formation of cellular protrusions	↓	-3.188	3.85E-08
Cell spreading	↓	-2.053	3.35E-08
Organization of cytoplasm	↓	-3.084	1.28E-09
Development of neurons	↓	-2.133	3.83E-09
Invasion of cells	↓	-2.853	1.21E-14
Cell movement	↓	-2.022	3.70E-27
Quantity of cells	↓	-2.249	1.23E-13
Hypertension	↑	2.215	1.95E-20
Vascular disease	↑	2.606	3.38E-11
Necrosis	↑	3.362	2.33E-10
Apoptosis	↑	2.525	3.42E-13
Binding of leukocytes	↑	2.059	1.88E-08
Activation of blood cells	↑	2.267	4.75E-09
Degranulation of cells	↑	2.213	1.39E-11
Bleeding	↑	2.759	1.09E-07
Edema	↑	2.405	1.79E-12
Organismal death	↑	5.458	4.83E-14

### 4.3.2 Aim 3b

#### 4.3.2.1 Cell death pathways are not activated by attenuated *F. tularensis* strains

PCR was performed to assess gene expression of select proteins involved in cell death pathways from NZW rabbits exposed to virulent S4, LVS, S4 $\Delta$ aroD, or S4 $\Delta$ guaBA. Matching what was seen in the microarray from S4 infected rabbits, there was a trend for STAT1 to be elevated in the lung, liver and spleen at 3 DPE, but this difference was not significant compared to baseline (Figure 55A, 55B, and 55C). Gene expression of apoptotic markers caspase-3 and caspase-9 was not altered for LVS, S4 $\Delta$ aroD, or S4 $\Delta$ guaBA in the lung, liver, or spleen. IL-1 $\beta$ , a surrogate for inflammasome activation and pyroptosis, was similarly unchanged for all vaccine strains. STAT1 was not upregulated for the vaccine strains, as observed during virulent S4 infection. STAT1 is an important regulator for both necrosis and necroptosis but plays a role in many other immune pathways. IFN $\beta$ , a mediator of necroptosis, was also not upregulated. In the spleen, IFN $\beta$  gene expression was downregulated.

Interferons, EGF, PDGF, IL-6, and IL-27 induce STAT1. Though not significantly elevated, STAT1 gene expression in the liver and spleen correlated with vaccine efficacy ( $R^2=0.9274$  and  $R^2=0.6298$ , respectively) (Figure 56A and 56B). S4 $\Delta$ aroD exposed rabbits exhibited the highest STAT1 gene expression in the liver and were the only vaccine group that was detected to disseminate outside of the lung tissue. Overall, the gene expression does not give a clear picture of which cell death pathways are being triggered during infection for any of the vaccine strains.

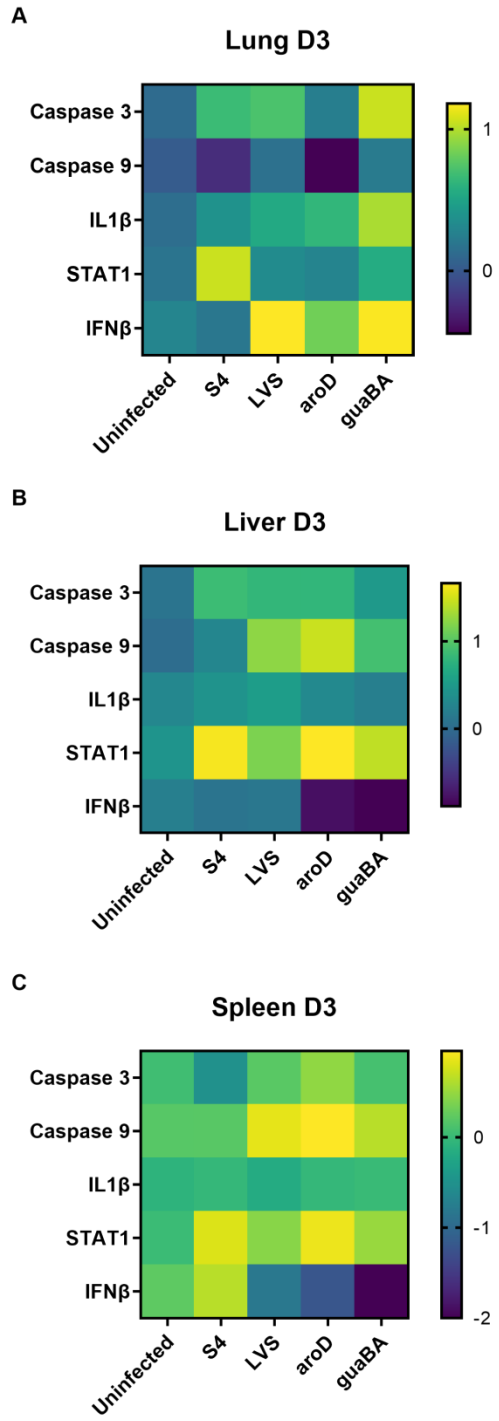


**Figure 55. IFN $\beta$  gene expression differs between vaccine strains in the lung, liver, and spleen**

NZW rabbits were exposed to S4, LVS, S4aroD, or S4guaBA and sacrificed at 3 DPE to collect tissue for assessment of cell death gene expression in the A) lung, B) liver, and C) spleen.

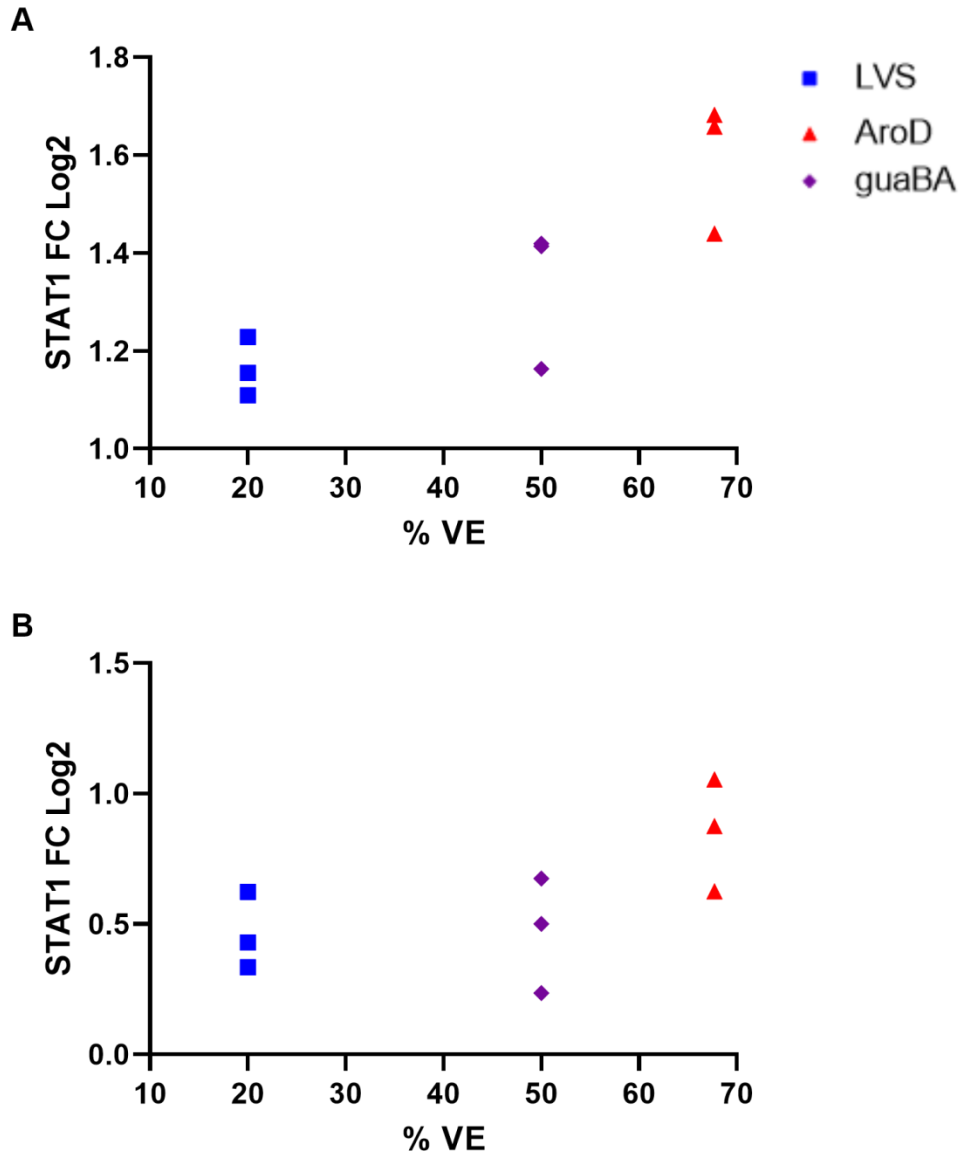


**Figure 56. STAT1 gene expression correlates with observed vaccine efficacies**

Each symbol represents a different animal. Rabbits were exposed to LVS, S4ΔaroD, or S4ΔguaBA and gene expression was assessed in the A) liver and B) spleen.

#### 4.3.2.2 Protective cytokines induced by vaccine strains

A few select genes were chosen to assess the production of a protective cytokine response 14 days following exposure to the vaccine strains. There is a trend in upregulation of gene expression of IFN $\gamma$  and CXCL10 in the lung, liver and spleen, though this upregulation is not significant (Figure 57A-57C). IFN $\gamma$  is a critical and necessary cytokine for the control of *F. tularensis* infection. CXCL10 is secreted in response to IFN $\gamma$  and is also important for recruitment of monocytes. In the lungs, IL 6 and CCL2 gene expression are significantly different between the vaccine strains based on an ANOVA analysis (Figure 57A). CCL2 recruits monocytes and has also been shown to be critical for bacterial clearance. In the spleen, IFN $\gamma$  gene expression was significantly different between vaccines strains based on ANOVA analysis (Figure 57C).

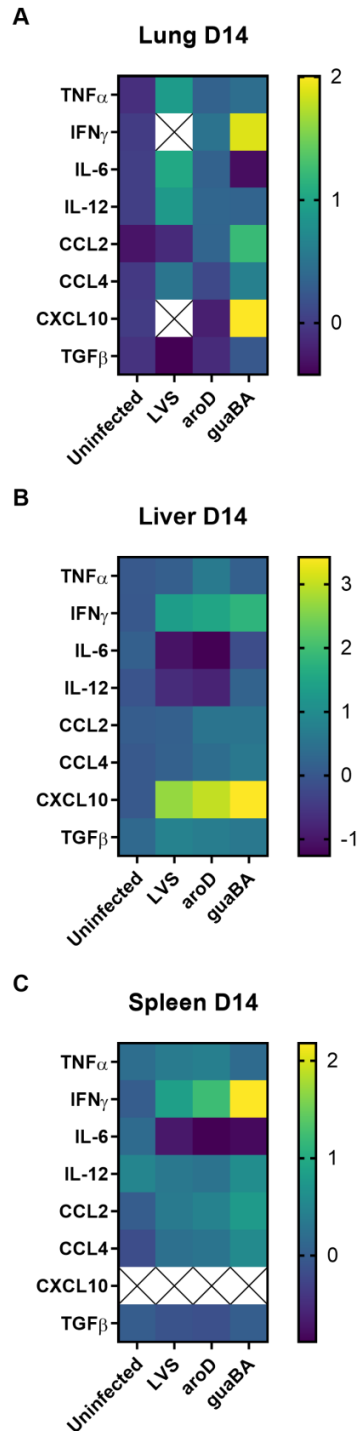


**Figure 57. Trend in upregulation of IFN $\gamma$  and CXCL10 in rabbits exposed to attenuated *F. tularensis* strains**

NZW rabbits were exposed to S4, LVS, S4 $\Delta$ aroD, or S4 $\Delta$ guaBA and sacrificed at 3 DPE to collect tissue for assessment of gene expression of protective cytokines in the A) lung, B) liver, and C) spleen.

## 5.0 Discussion

Despite the plethora of research regarding *F. tularensis*, specifics regarding host-pathogen interactions and their relevance to human disease remain elusive. This is largely due to the differences in experimental design between research laboratories. Aim 1 of this study examined only a few potential confounding factors observed in *F. tularensis* research which makes it difficult to compare results obtained in different laboratories. We have developed and standardized a nose-only inhalation exposure system of exposure of NZW rabbits to small-particle aerosols. This method provides a reproducible method of delivery of aerosolized *F. tularensis* in a relevant animal model. This experimental design was used to assess sex, choice of broth culture for growth of challenge material, vaccine schedule, and strain selection. Sex specific disease outcomes have been observed for many infectious diseases, including influenza and SARS (160-163). MHb, BHI broth, and Chamberlain chemically defined medium are common growth mediums used in *F. tularensis* studies. Each broth results in a distinct proteomic expression pattern of *F. tularensis* which can affect vaccine efficacy studies (166, 168, 169). Though *Francisella* species exhibit high genetic homology, *F. tularensis* subspecies exhibit different virulence patterns ranging from lethal infection to no clinical disease (145).

Sex was not a significant biological factor in primary virulent S4 infection as there was no difference in time to death between male and female rabbits. Female rabbits exhibited more weight loss and higher ESRs during the moribund period compared to males. There was a trend for S4 $\Delta$ aroD vaccinated males to exhibit higher vaccine efficacy compared to S4 $\Delta$ aroD vaccinated females, though this difference was not significant. There was also a trend for sex differences following vaccination with LVS. Male rabbits were more susceptible to virulent S4

challenge compared to females, but the difference in survival was not significant. This increased susceptibility of LVS vaccinated males was also observed in mice (165). These data suggest sex is a possible confounding factor for vaccine efficacy studies, and thus animals of both sexes should be included in *F. tularensis* vaccine efficacy studies.

Vaccine efficacy was not significantly different between challenge material grown in MHb and BHI, but vaccine efficacy was lower in the BHI grown S4 exposed group. Additionally, the BHI grown S4 group exhibited more severe clinical disease as measured by weight change, temperature change, and ESR. This corresponds to the differences in LD99 in mice exposed to MHb grown LVS and BHI grown LVS (166). The difference in vaccine efficacy between these groups could be due to the small sample size, but the differences in vaccine efficacy and clinical presentation indicate growth medium is an important consideration for *F. tularensis* vaccine efficacy studies. Many research groups studying *F. tularensis* use MHb. Growth of *F. tularensis* in MHb results in impaired bacterial membranes and less expression of virulence factors compared to growth in BHI broth (168). More importantly, the differences induced in the bacteria by choice of growth medium have measurable effects within the host. Use of BHI broth may represent a more robust experimental design as it results in a more rigorous challenge for *Francisella* vaccines. Use of BHI broth for growth of *F. tularensis* results in a more virulent phenotype that can affect interpretation of vaccine efficacy studies. Standardizing choice of growth medium among *Francisella* research groups will aid in selecting vaccine candidates that can protect against a more virulent phenotype, which result in costs savings. Additionally, standardizing growth medium will allow for comparison of *Francisella* pathogenesis and vaccine efficacy studies between research groups.

We have previously shown that a prime/boost vaccine regimen resulted in improved vaccine efficacy of aerosolized S4 $\Delta$ aroD compared to a single prime vaccination. For LVS, the prime/boost regimen improved VE, but this difference was not significantly different. Though animals vaccinated with the prime/boost regimen exhibited higher antibody titers, there was no difference in clinical symptoms.

A single vaccination via scarification revealed S4 $\Delta$ aroD resulted in better vaccine efficacy compared to S4 $\Delta$ guaBA in NZW (177), but how these vaccines compared when given via our current experimental design had not been assessed. Similar to what was observed with the single scarification, S4 $\Delta$ aroD resulted in better vaccine efficacy and protection from clinical disease compared to S4 $\Delta$ guaBA when given as an aerosol with a prime/boost schedule. S4 $\Delta$ aroD also resulted in superior vaccine efficacy compared to S4 $\Delta$ clpB. These data highlight the importance of strain selection as it can alter the overall virulence of the bacterium, which can affect vaccine efficacy.

Another undertaking of this work was to characterize the NZW rabbit as a model of virulent S4 infection. Mice have been used extensively to study *F. tularensis* pathogenesis and develop vaccines. Due to the hypersusceptibility of mice to *Francisella* species and differences in the immune response compared to humans, there was a need to develop an intermediate model to test *Francisella* vaccine candidates before moving into NHP studies. Similar to other animal models and humans, NZW rabbits exhibited weight loss, fever, an elevated ESR, and splenomegaly. Clinical signs of disease develop around day three of infection. In conjunction with the onset of clinical symptoms, bacteria disseminate to the liver and spleen. No hepatomegaly was observed in any of the rabbits used in these experiments. Humans can have hepatomegaly during infection, but it is not a hallmark characteristic of *F. tularensis* infection.

Hepatomegaly has also been observed to a high degree in the NHP and rat model. *F. tularensis* has been shown to primarily replicate in rat hepatocytes. Mice are also thought to succumb to *F. tularensis* infection due to liver failure. Thus, involvement of the liver during infection of NZW rabbits may set this animal model apart from others. Bacteria are consistently found in the lung, liver, and spleen of S4 exposed rabbits, which is consistent with other animal models and humans that have succumbed to infection. Lethal *F. tularensis* infection in NZW rabbits resulted in a caseous necrosis in affected tissues, consistent with other animal models. Neutrophil infiltration has been implicated as one of the causes of tissue damage during S4 infection. While neutrophils can be found within the lung tissue and it appears neutrophil numbers increase over time, neutrophils make up a very small proportion of cells seen in infected lung tissue. Neutrophil infiltration in mice and NHPs was determined via H&E staining and was not quantified. Whether the limited neutrophil infiltration observed is consistent with what was observed in other animal models or unique to this model still needs to be determined. The rabbit is a frequently used animal model due to their ease of handling, breeding, and housing. They are used to study a variety of medical conditions and infectious disease and are used as bioreactors for production of proteins. The NZW rabbit model serves as a suitable model for virulent *F. tularensis* infection but the limited reagents for use in this model can make performing experiments difficult.

Genes related to wound healing and angiogenesis comprised the majority of the top ten downregulated genes in the lung at 3 DPE. Chemotactic protein gene expression was upregulated. Several interferon-induced genes were upregulated in the lung, though upregulation of Type I and Type II interferons was not observed. Additionally, immunosuppressive genes were highly upregulated, including genes involved in suppressing the adaptive immune response.

Pro- and anti-apoptotic related genes were both upregulated, but genes directly involved in the apoptosis pathway exhibited no notable changes in gene expression. Traditional immune pathways, such as TLR and IFN signaling, and cell death pathways also showed no notable changes in gene expression. Interestingly STAT1 was upregulated in the lung tissue, but not IFN $\gamma$ . STAT1 is typically upregulated in response to increasing IFN $\gamma$ , though it can be upregulated in its absence by PDGF, IL-6, EGF, and IL-27. STAT1 is an important regulator of NK cell cytotoxicity. IFN $\gamma$  is important for maintaining NK cytolytic function and critical for controlling primary *F. tularensis* infection. *F. tularensis* may be inhibiting NK function by blocking IFN $\gamma$  production allowing for the establishment of lethal infection.

In the liver, amino acid degradation pathways were downregulated. *F. tularensis* may be exploiting this reduction in amino acid catabolism to avoid autophagy, inhibit that adaptive immune response, and aid in bacterial replication. In mice, S4 infection is thought to inhibit the immune response during early infection before leading to a cytokine storm mediated in death. The lack of upregulation of cytokine and pyroptotic genes and circulating IL-1 $\beta$  and TNF $\alpha$  suggest NZW rabbits are not succumbing to virulent S4 infection due to a cytokine storm mediated event. The inability of the microarray to distinguish the cell death pathways responsible for the necrosis observed in the tissue indicate alternative methods may need to be used to assess these pathways. A major limitation of the gene expression analysis was the lack of gene ontology files for pathway analysis. Papers performing gene expression studies in rabbits include resources that are no longer available (223-225). Thus, this work utilized gene ontology data from mice for the gene ontology portion. The IPA software also lacked rabbit reference files, and thus pathway analysis was performed using a combination of mouse, rat, and human pathways.

Aim 2 of this work also sought to characterize the clinical progression of the attenuated vaccines: LVS, S4 $\Delta$ aroD, and S4 $\Delta$ guaBA. Surprisingly, all vaccine strains resulted in a similar, but milder, clinical presentation to virulent S4. This was characterized by fever, weight loss, increased ESR, and a loss of circulating lymphocytes which all resolved within four to seven days. S4 $\Delta$ guaBA results in a more severe pathology compared to LVS and S4 $\Delta$ aroD. Rabbits exposed to S4 $\Delta$ guaBA exhibit more weight loss, higher fevers, caseous necrosis of the lung, and disruption of splenic architecture. At 14 DPE, the lung damage was not resolved and bacteria were still detectable in at least one of the lung lobes. LVS resulted in the mildest clinical presentation, with a low and short temperature increase, mild pathological changes in the lung and no splenomegaly. Though S4 $\Delta$ guaBA persisted in the lungs longer than the other vaccine strains, dissemination to the spleen was only observed in rabbits exposed to S4 $\Delta$ aroD. It is possible S4 $\Delta$ guaBA results in poorer vaccine efficacy compared to S4 $\Delta$ aroD due to the extensive lung damage. It is unclear if damage has been completely repaired by 30 DPE when rabbits would be challenged. Based on these data, it is likely that vaccine efficacy is affected by both persistence and dissemination.

There are numerous innate immune mechanisms involved in a normal host response to infectious disease. This study aimed to look only at cell death pathways initiated by attenuated *F. tularensis* strains. No outstanding changes in genes related to apoptosis, pyroptosis, or necroptosis were observed for LVS, S4 $\Delta$ aroD, or S4 $\Delta$ guaBA in the lung, liver, or spleen. STAT1 was upregulated in the lung of S4 infected rabbits, but not in rabbits exposed to the attenuated *F. tularensis* strains. However, STAT1 was upregulated in the liver and spleen for both virulent and attenuated *F. tularensis* strains. In fact, S4 $\Delta$ aroD resulted in the highest increase in STAT1 gene expression of the attenuated vaccine strains. This correlated with observed vaccine efficacy and

tissue dissemination. STAT1 is induced by interferons, and thus STAT1 gene expression may be indicative of IFN $\gamma$  production, which is key for controlling *F. tularensis* infection. Virulent *F. tularensis* has been shown to induce STAT1 gene expression, but inhibit STAT1 mediated signaling to prevent activation of antigen specific T cells (226). Thus, STAT1 mediated signaling should be explored to better understand its role in vaccine efficacy of attenuated *F. tularensis* strains.

Examination of genes that correlate with protection from S4 infection in other animal models reveal only an upregulation of IFN $\gamma$  and CXCL10. Microarrays may lack the sensitivity to detect changes in cell death pathways within tissues due to low constitutive levels of genes involved in these pathways and the inundation of DNA from normal tissue architecture. Thus, the importance of cell death pathways in the development of a protective immune response to *F. tularensis* should be explored using other means.

## **5.1 Future directions**

Differences in experimental design result in confounding factors that are muddying the interpretation of the vast body of research related to *F. tularensis* pathogenesis and vaccine development. Sex, choice of growth medium, vaccine schedule, and strain selection are just a few confounding factors explored in this work, but there are many more that need to be identified. Other confounding factors that should be further explored are the method of inoculation for pulmonary studies. Aerosol infection is often replicated using intratracheal instillation, intranasal inoculation, or aerosol delivery. A direct comparison of these inoculation methods has not been done to determine if these different methods result in the same disease

course and pathology. Time to challenge after vaccination should also be assessed. Due to costs of housing animals for long periods of time, many studies utilize relatively short times for assessing vaccine efficacy. Assessing longevity of protection is an important part of vaccine development.

The role of persistence and dissemination in vaccine efficacy should be further explored and confirmed. Antibiotics can be used to decrease the time the bacteria persist in the tissue and if given at the right time, can prevent dissemination to the liver and spleen. Rabbits would be vaccinated with LVS, S4 $\Delta$ aroD, or S4 $\Delta$ guaBA and antibiotic therapy initiated 1 to 3 DPE for several days. Optimal doses and time to initiation of treatment would need to be determined experimentally to confirm abrogation of dissemination. Rabbits would then be challenged with virulent S4 to determine if decreases in persistence or dissemination altered vaccine efficacy.

Cell culture is a useful tool for proof-of-concept studies or as a surrogate for animal studies. It would be useful to develop a primary rabbit macrophage or PBL cell culture model. Cytokine production should be compared between the cell culture models and the whole animal model to confirm comparability between these methods. Cell culture models could then be used for studies assessing the innate immune mechanisms activated by S4 and attenuated vaccine strains as they can be upscaled to reach detectable changes in these pathways.

The inflammasome was not found to be altered during infection with the attenuated vaccine strains used in this study. The inflammasome was chosen because of its ability to recognize dsDNA and the potential for attenuated strains to exhibit a compromised membrane that would result in release of dsDNA. Many other innate pathways may be playing a role in VE, such as interferon pathways and macrophage function. Flow cytometry can be used to identify early infiltrating cell types following infection and the subsequent adaptive immune cell types.

Determining the innate immune mechanisms can influence the selection of adjuvants that can stimulate an immune response that will result in the development of a protective immune response.

## **5.2 Public health significance**

### **5.2.1 Bioterrorism defense**

The value of vaccines against infectious diseases that cause severe disease, has a high incidence of cases, and is easily spread within a population is easily measured. However, the value of vaccines to protect against biological threats is not as obvious. Biological threats are infectious agents that are able to cause severe disease, but often have low case numbers and are not easily spread. Vaccination against biological threats is an effective way to counter potential bioweapon attacks against the U.S. military because high levels of vaccine coverage can be achieved.

Vaccination of the general population is unlikely due to the high costs, variety of potential biological threats, and difficulty in achieving adequate vaccine coverage. However, effective vaccines can be used to control epidemics, prevent pandemics, and protect first responders, laboratory workers, and health care providers with a high risk of exposure.

## 5.2.2 Vaccine development

Production of vaccines is a lengthy and expensive process. Only a small percentage of potential therapeutics and vaccines reach regulatory approval. Increasing research and development budgets and regulatory controls will result in significant gaps in the future therapeutic market. Understanding biological, technical, and analytical factors that can influence the interpretation of proof-of-concept studies is important for developing rigorous experimental designs and increasing reproducibility of results. Narrowing the pool of potential therapeutic drugs that are moved forward in drug development process would result in cost savings that could improve the output of future therapeutics.

LAVs are able to multiply within the human host to provide continuous antigenic stimulation over time without being pathogenic. This stimulation results in the production of a strong cellular immune and antibody response which often confers lifelong immunity with few doses. The live nature of LAVs represents a major disadvantage. Live pathogens can mutate over time which can result in reversion back to a pathogenic state or over attenuation that would fail to induce a protective immune response. People with immune deficiencies cannot safely receive LAVs. LAVs often require a cold chain to stay effective and skilled health care workers to handle them which result in added costs that can hamper their use in resource-limited areas.

Development of inactivated and components vaccines has proven difficult due to their poor immunogenic nature. This often results in the need for multiple doses to elicit and sustain a protective immune response throughout the human life span. Vaccine technology has come a long way in improving these types of vaccines. The discovery of new adjuvants has aided in pushing the immune response towards the proper T helper cell response and prolonging antigen

persistence within tissue. Vaccines can now include localization signals via proteins or nucleic acid sequence to target specific tissues that would improve vaccine efficacy.

The development of inactive *F. tularensis* vaccines has been hindered by the inability to identify a consistent set of bacterial antigens that result in a protective immune response. Inactive whole cell-based *F. tularensis* vaccines have been ineffective and produce many adverse reactions in the host. Live attenuated *F. tularensis* vaccine strains have proven more effective than their inactive counterparts, but the mechanisms important for the development of a protective immune response are still unclear. Determining the role of persistence, dissemination, and early innate immune responses in vaccine efficacy will aid in selecting adjuvants and localization signals that can improve the vaccine efficacy of inactivated *F. tularensis* vaccine strains.

## Appendix A Glossary and Abbreviations

*F. tularensis*: *Francisella tularensis*; a small, pleomorphic, gram-negative coccobacillus

*F. tularensis* subsp. *tularensis*: a type A subspecies of *F. tularensis*

*F. tularensis* subsp. *holarctica*: a Type B subspecies of *F. tularensis*

*F. tularensis* subsp. *mediastitica*: a nonvirulent subspecies of *F. tularensis*

*F. novicida*: *Francisella novicida*; a distinct subspecies of *Francisella* classified based on its clinical disease despite 99.8% sequence similarity in 16s rDNA

U.S.: United States

CFU: colony-forming units

FCP: *Francisella* containing phagosome

LPS: lipopolysaccharide

NF $\kappa$ B: Nuclear Factor kappa-light-chain-enhancer of activated B cells

Kb: kilobase

FPI: *Francisella* pathogenicity island

USSR: Union of Soviet Socialist Republics

CDC: Center for Disease Control

FDA: U.S. Food and Drug Administration

LVS: Live Vaccine Strain; an attenuated Type B strain of *F. tularensis* obtained from the USSR

WT: wild type

DPE: days post exposure

KO: knockout

S4: SchuS4; a Type A strain of *F. tularensis*

DN: double negative

PBL: peripheral blood leukocytes

LD50: lethal dose; amount of a substance that kills 50% of a test sample

CRP: C-reactive protein

ESR: erythrocyte sedimentation rate

NHP: non-human primate

LDH: lactate dehydrogenase

BUN: blood urea nitrogen

NZW: New Zealand White; a species of rabbit

LD100: lethal dose; amount of a substance to kill 100% of a test sample

MHb: Mueller Hinton Broth

BHI: Brain Heart Infusion

NR-643: a substrain of S4: produce severe infection, but is not lethal

NR-10492: a substrain of S4; produces prototypical lethal infection

VE: vaccine efficacy; in animal experiments, vaccine efficacy corresponds with percent survival of vaccinated animals following challenge

S4 $\Delta$ aroD: a strain of S4 with a deletion of the *aroD* gene which results in attenuation of the bacterium

S4 $\Delta$ aroC: a strain of S4 with a deletion of the *aroC* gene which results in attenuation of the bacterium

S4 $\Delta$ guaBA: a strain of S4 with a deletion of the guaBA operon which results in attenuation of the bacterium

S4 $\Delta$ clpB: a strain of S4 with deletion of the clpB gene which results in attenuation of the bacterium

LAV: live attenuated vaccine

VEEV: Venezuelan Equine Encephalitis Virus

RML: Rocky Mountain Lab

RML LVS: a substrain of LVS identified in the CDC's RML; the strain appears to be more virulent than traditionally used LVS strains

ATCC 29684: traditionally used strain of LVS

BCG: Bacillus Calmette-Guerin; refers to the vaccine against tuberculosis

BSL-3: biosafety level-3

RBL: Regional Biocontainment Laboratory

USDA: United States Department of Agriculture

PAPR: powered air purifying respirators

NIH: National Institutes of Health

AWA: Animal Welfare Act

AAALAC: Association for Assessment and Accreditation of Laboratory Animal Care

BAL: bronchoalveolar lavage

CHA: Cysteine heart agar

PBS: phosphate buffered saline

AGI: All glass impinger; aerosol-sampling device used to determine the aerosol concentration of a pathogen

CBC: complete blood count; includes total WBC count and differential, RBC indices, and platelet indices

PCR: polymerase chain reaction

GAPDH: glyceraldehyde-3-phosphate dehydrogenase; a housekeeping gene frequently used for normalization of gene expression studies

cDNA: complementary DNA

DEG: differentially expressed gene

PPIA: peptidylprolyl isomerase A; a housekeeping gene

IQR: interquartile range

WBC: white blood cells

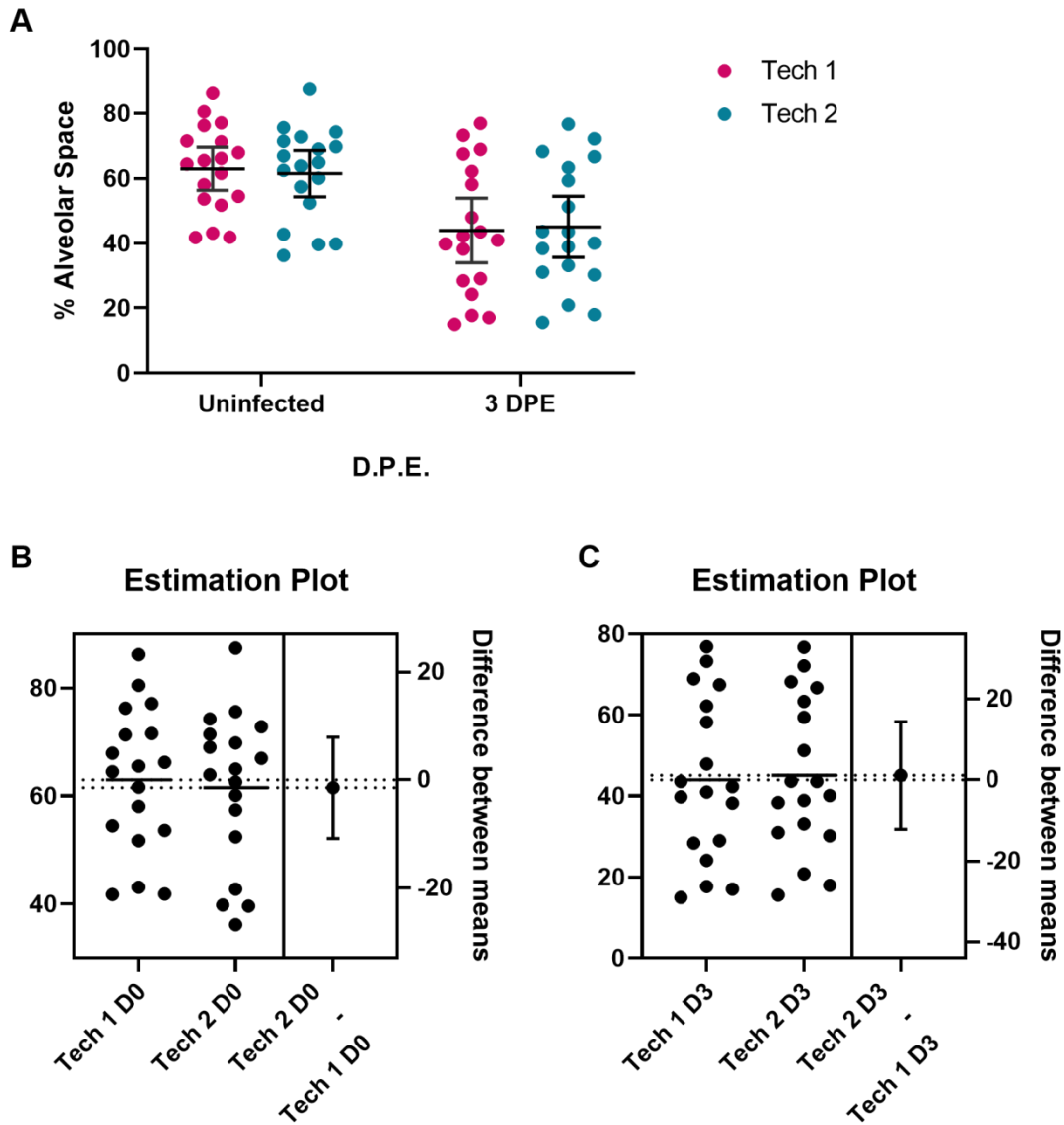
RBC: red blood cell

## **Appendix B Supplementary Figures and Tables**

### **Appendix B.1 Aim 2**

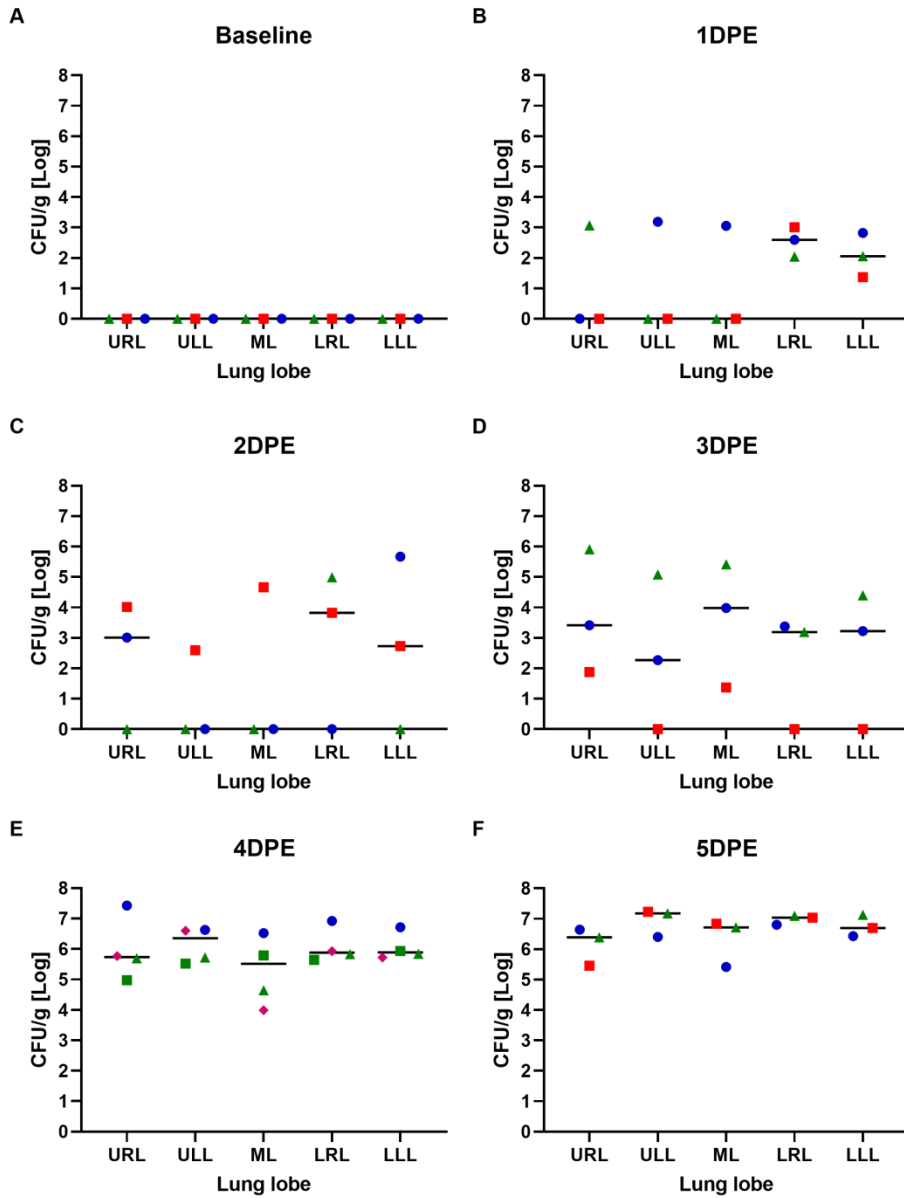
#### **Appendix B.1.1 Aim 2a**

To ensure alveolar space analysis was not influenced by personal bias, this test was performed by two technicians, one of whom was blinded to the infection status of the animals. Each individual selected regions of interest from 18 images and results were compared. Both technicians detected significant changes between uninfected and 3 DPE ( $p$  value=0.0020 for Tech 1 and  $p$  value=0.0061 for Tech 2) (Appendix Figure 1A). No differences were observed in alveolar space analysis of D0 and D3 lung tissues between technicians ( $p$  value=0.7530 and 0.8654, respectively) (Appendix Figure 1B and 1C).



**Appendix Figure 1. No significant differences were observed in alveolar space analysis between technicians**

Images of stained H&E slides of lung tissue were used to select regions of interest for alveolar space analysis. A) Results of alveolar space analysis between technicians. B) Differences in means of alveolar space analysis.

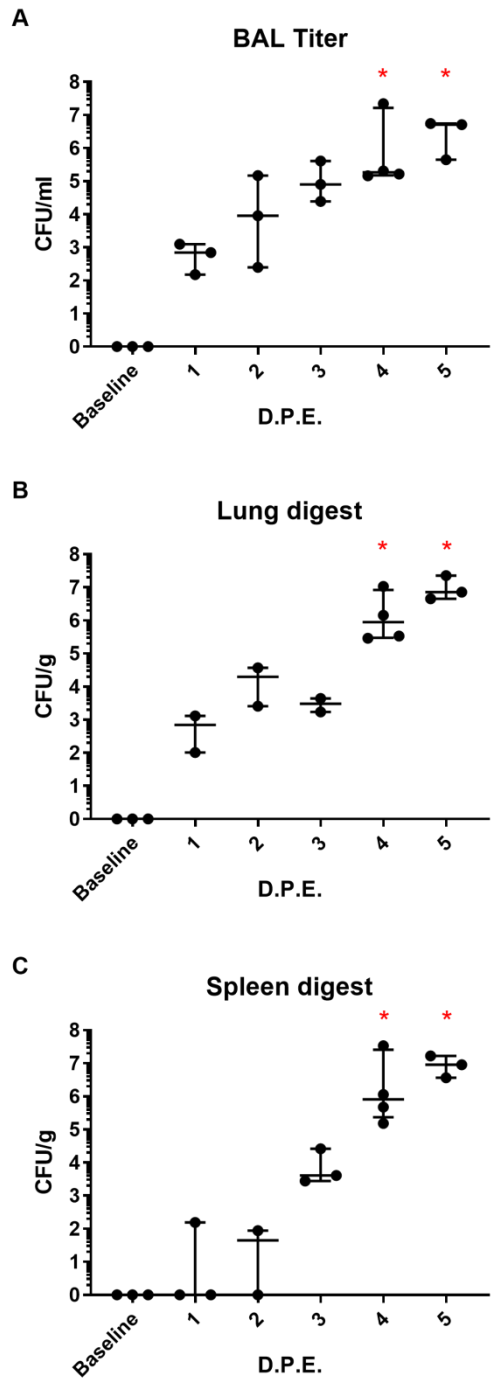


**Appendix Figure 2. Infection primarily starts in lower lungs and then spreads to upper lungs**

Color/symbols represents data points from a single animal. Symbols/colors reused between graphs, but no subjects were used on multiple days. Bar indicates median titer.

**Appendix Table 1. Dunn's multiple comparison of lung titers for each lobe compared to baseline**

	URL	ULL	ML	LRL	LLL
1 DPE	>0.9999	>0.9999	>0.9999	>0.9999	>0.9999
2 DPE	>0.9999	>0.9999	>0.9999	>0.9999	>0.9999
3 DPE	0.4866	>0.9999	0.6838	>0.9999	>0.9999
4 DPE	<b>0.0329</b>	0.0557	0.0852	<b>0.0291</b>	<b>0.0242</b>
5 DPE	<b>0.0286</b>	<b>0.0185</b>	<b>0.0146</b>	<b>0.0064</b>	<b>0.0082</b>



Appendix Figure 3. Titters taken at necropsy corroborate bacterial growth in tissues seen from frozen tissue pieces

## Appendix B.1.2 Aim 2b

**Appendix Table 2. Tukey's multiple comparison of clinical signs for vaccine strains over time**

Comparison	Parameter	Baseline	1 DPE	2 DPE	3 DPE	4 DPE	5 DPE	6 DPE	7 DPE
LVS vs S4ΔaroD	Weight	NS	0.0002	NS	NS	NS	ND	ND	NS
	Temperature	NS	NS	<0.0001	0.0008	NS	ND	ND	0.0271
	WBC	NS	NS	NS	NS	NS	NS	ND	NS
	Lymphocytes	NS	NS	NS	NS	NS	NS	ND	NS
	Granulocytes	NS	NS	NS	NS	NS	NS	ND	NS
	Monocytes	NS	NS	NS	NS	NS	NS	ND	NS
	Platelets	NS	NS	NS	NS	NS	NS	ND	NS
	RBC	NS	NS	NS	NS	NS	NS	ND	NS
	ESR	NS	NS	NS	0.0013	NS	NS	ND	NS
LVS vs S4ΔguaBA	Weight	NS	NS	NS	NS	0.0001	ND	ND	0.0038
	Temperature	NS	<0.0001	<0.0001	0.0009	0.0054	ND	ND	NS
	WBC	NS	NS	NS	NS	NS	NS	ND	NS
	Lymphocytes	NS	NS	NS	NS	NS	NS	ND	0.0385
	Granulocytes	NS	NS	NS	NS	NS	NS	ND	NS
	Monocytes	NS	NS	NS	NS	NS	NS	ND	NS
	Platelets	NS	NS	NS	NS	NS	NS	ND	NS
	RBC	NS	NS	NS	NS	NS	NS	ND	NS
	ESR	NS	NS	NS	NS	NS	NS	ND	NS
S4ΔaroD vs S4ΔguaBA	Weight	NS	NS	NS	NS	0.0010	ND	ND	0.0043
	Temperature	NS	<0.0001	NS	NS	0.0337	NS	ND	NS
	WBC	NS	0.0170	NS	NS	NS	NS	ND	NS
	Lymphocytes	NS	NS	NS	NS	NS	NS	ND	NS
	Granulocytes	NS	NS	NS	NS	NS	NS	ND	NS
	Monocytes	NS	NS	NS	NS	NS	NS	ND	NS
	Platelets	NS	NS	NS	NS	NS	NS	ND	NS
	RBC	NS	0.0138	NS	NS	NS	NS	ND	NS
	ESR	NS	NS	0.0342	NS	NS	NS	ND	NS

### Appendix B.1.3 Aim 2c

Appendix Table 3. Kruskal Wallis comparison of tissue titers between vaccine groups over time

Comparison	Tissue	3 DPE	7 DPE	14 DPE
LVS vs S4ΔaroD	Lung	NS	NS	NS
	Liver	NS	NS	NS
	Spleen	NS	0.0033	NS
LVS vs S4ΔguaBA	Lung	0.0018	NS	NS
	Liver	NS	NS	NS
	Spleen	NS	NS	NS
S4ΔaroD vs S4ΔguaBA	Lung	0.0044	NS	NS
	Liver	NS	NS	NS
	Spleen	NS	0.0033	NS

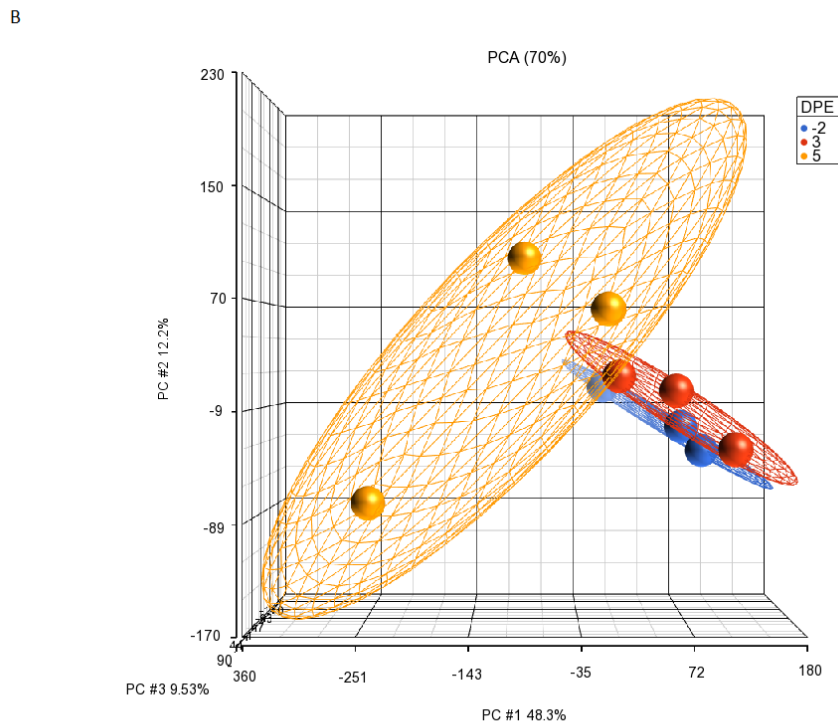
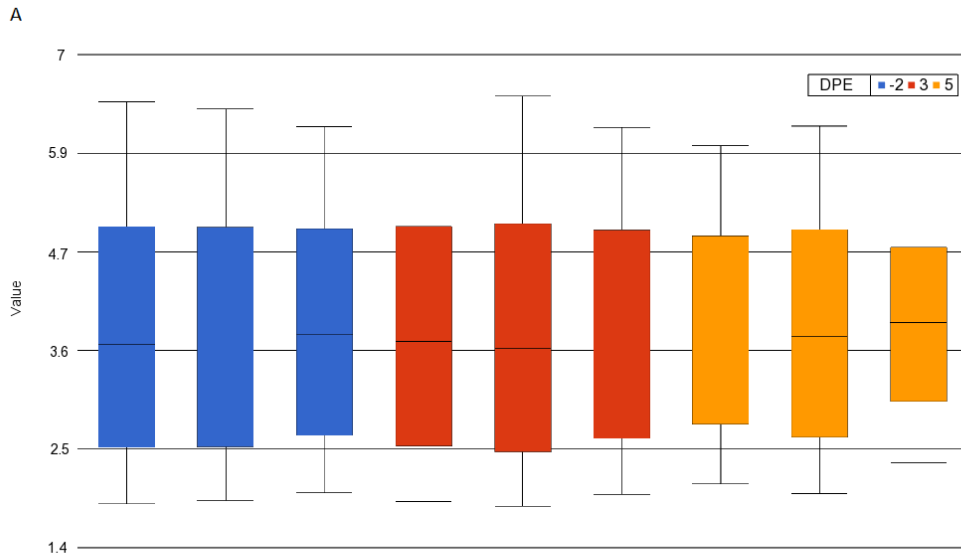
## Appendix B.2 Aim 3

### Appendix B.2.1 Aim 3a

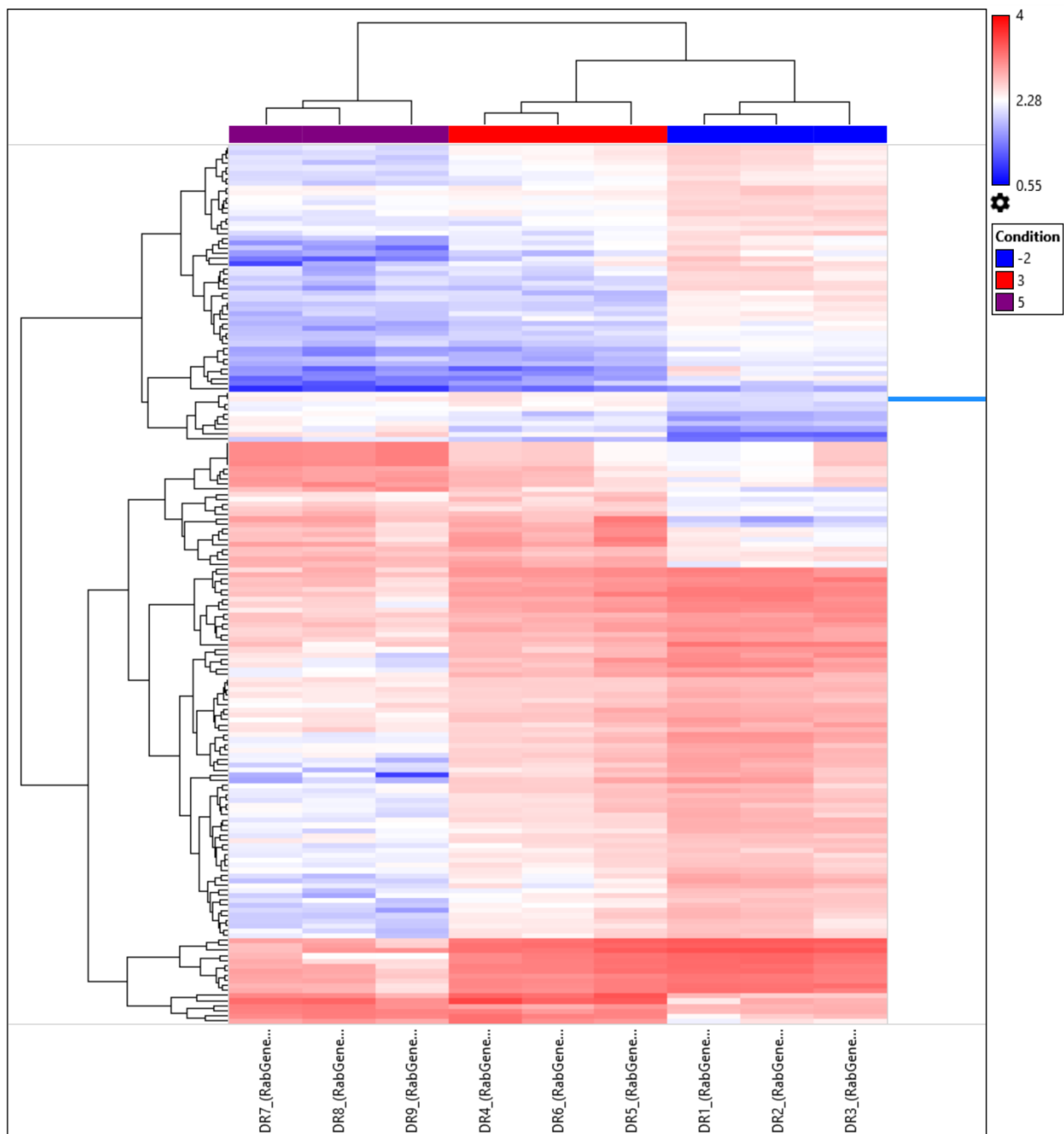
Appendix Figures 4 and 5 show the signal box plots, histograms, and hierarchical clustering for the microarray analysis performed in the lung. This QC indicates the RNA and microarray experiment was of acceptable quality. Additionally, the PCA plots and hierarchical clustering gave good separation between time points, further validating the quality of the microarray samples.

Appendix Figure 6 and 7 show pathway analysis performed on DEGs in the lung at 3 and 5 DPE using Ingenuity Pathway Analysis software. Pathways were limited to those that had z-scores greater than 1.5 or less than -1.5 and *p* values less than 0.05. Z-scores take into account the directional effect of one molecule on another molecule or process and the direction of change of genes in the data set. Several canonical pathways associated with white blood cell migration are altered (Appendix Figure 6). Leukocyte extravasation, integrin signaling, ILK signaling, IL-8 signaling are downregulated and PDGF signaling is upregulated. Pathways affected that are involved in wound healing and lung repair include HOTAIR regulatory pathway, HIF1 $\alpha$  signaling, VEGF signaling, angiogenesis, and PDGF signaling. HMGB1 signaling, DC maturation, and interferon signaling are involved in inflammatory pathways. PDGF aids in lung repair during hypoxic episodes. Pathways involved in oxidative stress that are altered at 3 DPE include eNOS signaling, and p38 MAPK signaling. At 5 DPE canonical pathways involved with cell cycle, WBC migration, lung repair, inflammation, and phagocytosis are altered (Appendix Figure 7).

Predicted activation state analysis show pathways related to clearance of cells, apoptosis of connective tissues cells, and apoptosis of fibroblasts are predicted to be increased at 3 DPE in the rabbits based on the microarray data (Appendix Table 7). Formation of lung tissue is predicted to be decreased at 5 DPE.



**Appendix Figure 4. QC and PCA plot for lung gene expression of S4 infected NZW rabbits**



**Appendix Figure 5. Hierarchical clustering reveals significant differences in gene expression at different times post infection**

Microarray data were filtered to include samples with a gene-level fold change  $<-1.5$  or  $>1.5$  and a gene-level p value  $<0.05$ .

**Appendix Table 4. Top 10 upregulated and downregulated genes at 5 DPE in the lung**

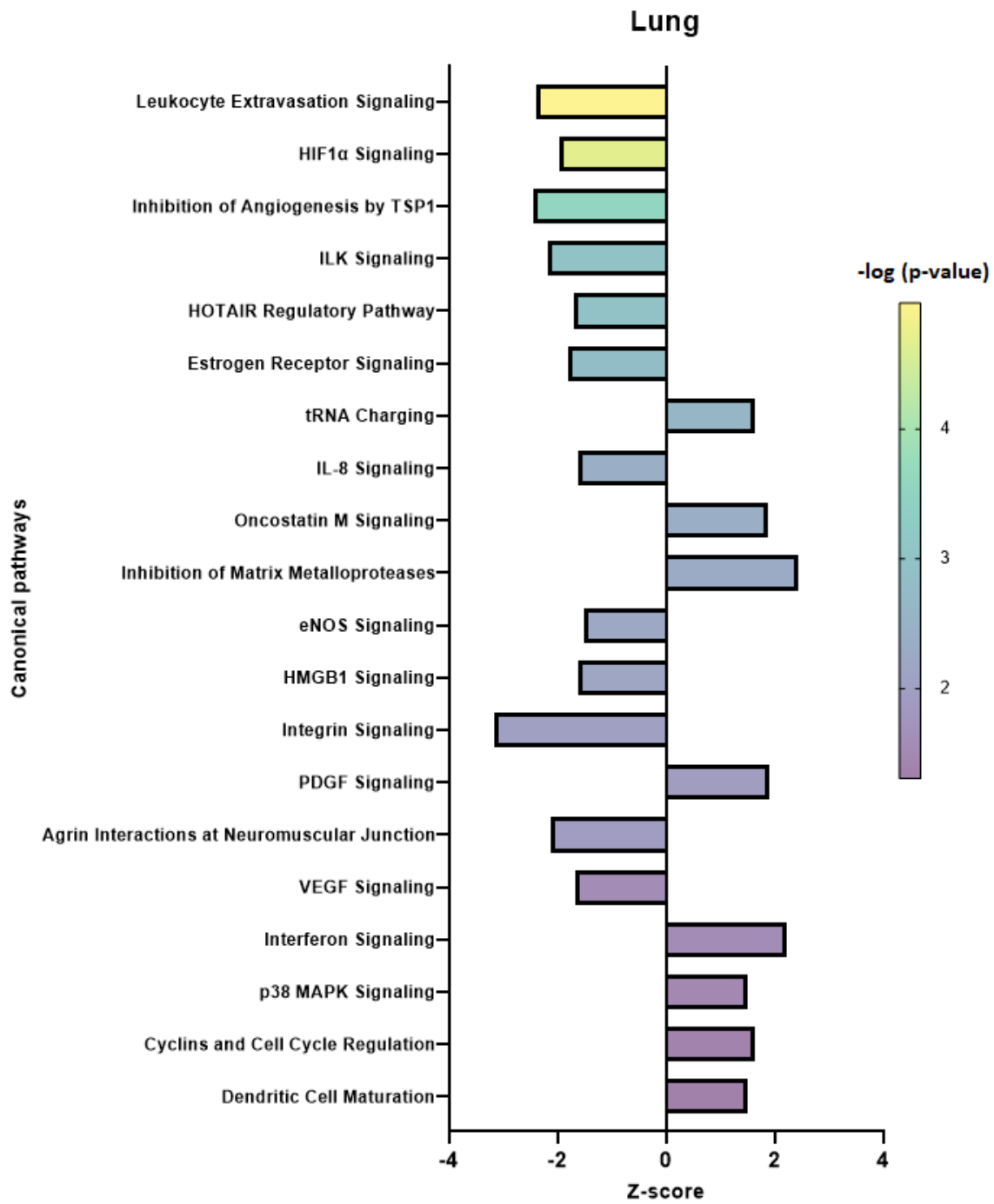
5 DPE	Gene	Fold change	FDR <i>p</i> value
Downregulated	Dermatopontin	-37.41	7.40E-03
	hemoglobin beta	-22.9	1.60E-03
	calcitonin receptor-like	-21.33	1.97E-02
	rhotekin 2	-17.59	1.74E-02
	guanine nucleotide binding protein, gamma 11	-17.04	7.90E-03
	methyltransferase-like protein 7A	-16.36	4.22E-02
	osteoglycin	-15.4	7.90E-03
	SEC14-like 3	-12.41	4.00E-03
	tubulin beta-2A chain	-12.35	2.07E-02
	caveolin 2	-11.73	1.33E-02
Upregulated	CXCL11	14.23	2.19E-02
	serum amyloid A3	12.65	1.14E-01
	leukocyte immunoglobulin-like receptor subfamily A member 3	12.35	9.10E-03
	metallothionein-2A	10.26	7.00E-04
	ADAM metalloproteinase domain 28	9.9	4.78E-02
	small nucleolar RNA, H/ACA box 62	7.39	1.82E-02
	hemopexin	7.18	8.31E-02
	S100 calcium binding protein A8	6.83	4.82E-02
	CCL2	6.83	2.35E-02
	interferon-induced guanylate-binding protein 1-like	6.65	3.14E-02

**Appendix Table 5. GO analysis of lung at 3 DPE**

Functional group	enrichment score	<i>p</i> value	% in group present	Upregulated (FDR <0.05)	Downregulated (FDR <0.05)
Extracellular region	59.41	0.00	7.62	64 (6)	66 (16)
Plasma membrane	53.83	0.00	5.29	85 (7)	141 (30)
Cytosol	37.55	0.00	5.15	111 (10)	67 (9)
Immune system process	36.99	0.00	10.7	45 (10)	7 (0)
Endoplasmic reticulum	27.21	0.00	6.07	56 (4)	37 (9)
Signaling receptor binding	15.45	0.00	7.77	10 (0)	22 (3)
Nucleus	8.06	0.00	3.43	129 (6)	78 (9)
Mitochondrion	7.78	0.00	4.13	46 (5)	27 (4)
Transferase activity	7.59	0.00	4.12	47 (3)	26 (2)
Hydrolase activity	7.1	0.00	4.14	39 (3)	26 (8)
Lipid binding	5.86	0.00	5.79	10 (0)	8 (1)
Ligase activity	5.62	0.00	7.63	8 (0)	2 (0)
Synapse	5.13	0.01	4.4	12 (0)	22 (5)
Cytoskeletal protein binding	5.06	0.01	8.86	4 (0)	3 (0)
Cell projection	4.77	0.01	4.04	15 (0)	29 (5)
Golgi apparatus	4.52	0.01	3.86	28 (1)	23 (5)
Cell differentiation	4.28	0.01	4	12 (0)	28 (9)
Cell death	3.97	0.02	10.81	0 (0)	4 (0)
Cytoplasmic vesicle	3.96	0.02	4.07	11 (1)	15 (3)
Lipid metabolic process	3.13	0.04	4.12	9 (1)	13 (3)

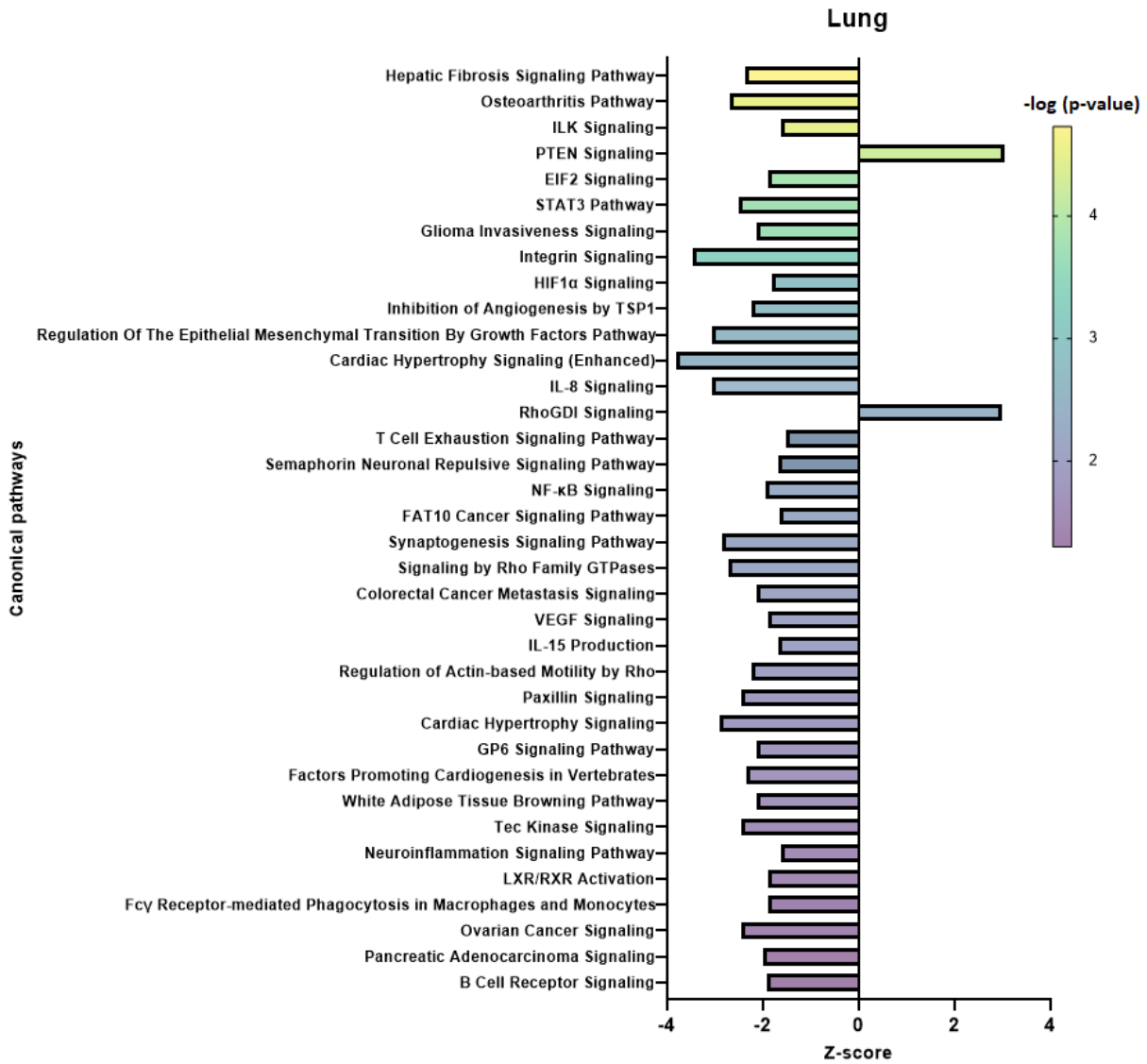
**Appendix Table 6. GO analysis of lung 5 DPE**

Functional group	enrichment score	<i>p</i> value	% in group present	Upregulated (FDR <0.05)	Downregulated (FDR <0.05)
Nucleus	28.89	0	32.78	306 (22)	1128 (113)
Cytosol	25.14	0	34.18	166 (21)	731 (94)
RNA binding	19.77	0	39.1	42 (5)	222 (9)
Endoplasmic reticulum	7.75	0	33.24	67 (7)	302 (43)
Signaling receptor binding	4.34	0.1	34.97	30 (4)	70 (23)
DNA binding	3.27	0.04	31.05	115 (5)	270 (27)
Cytoskeletal protein binding	3.18	0.04	39.39	2 (0)	25 (6)



**Appendix Figure 6. Pathway analysis of DEGs in the lung at 3 DPE**

Canonical pathways were limited to those that exhibited z-scores  $> 1.5$  and  $< -1.5$  and  $p$  values  $< 0.05$ . Z-scores are shown on the x-axis and  $p$  values are represented by a heatmap.



**Appendix Figure 7. Pathway analysis of DEGs in the lung at 5 DPE**

Canonical pathways were limited to those that exhibited z-scores  $> 1.5$  and  $< -1.5$  and  $p$  values  $< 0.05$ . Z-scores are shown on the x-axis and  $p$  values are represented by a heatmap.

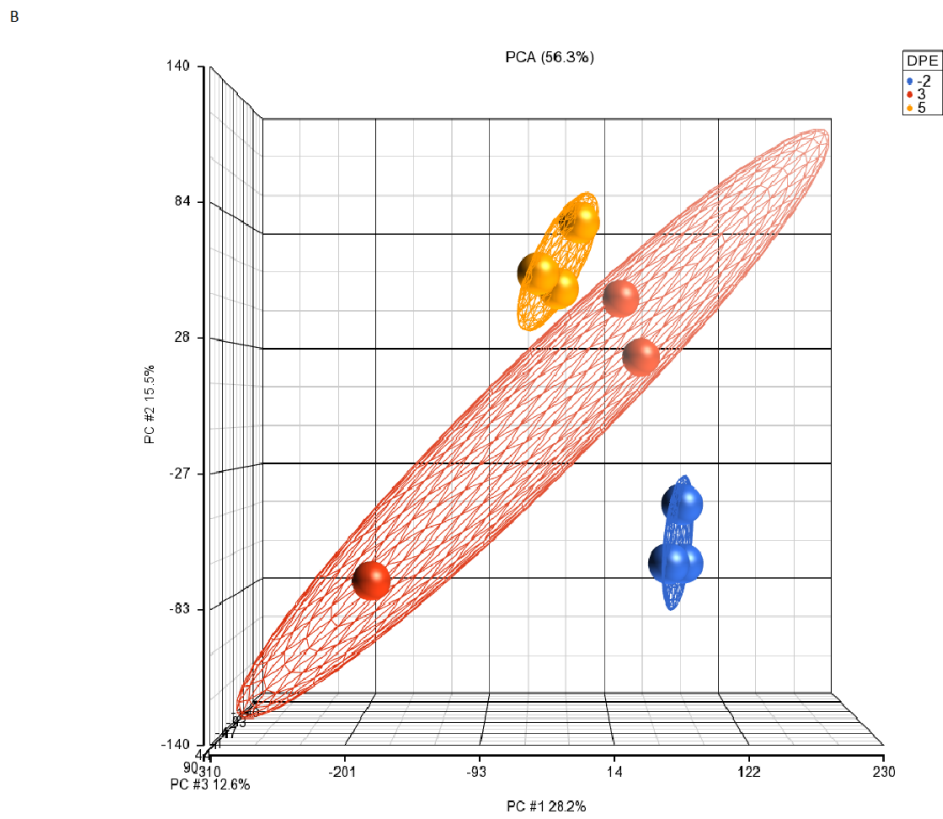
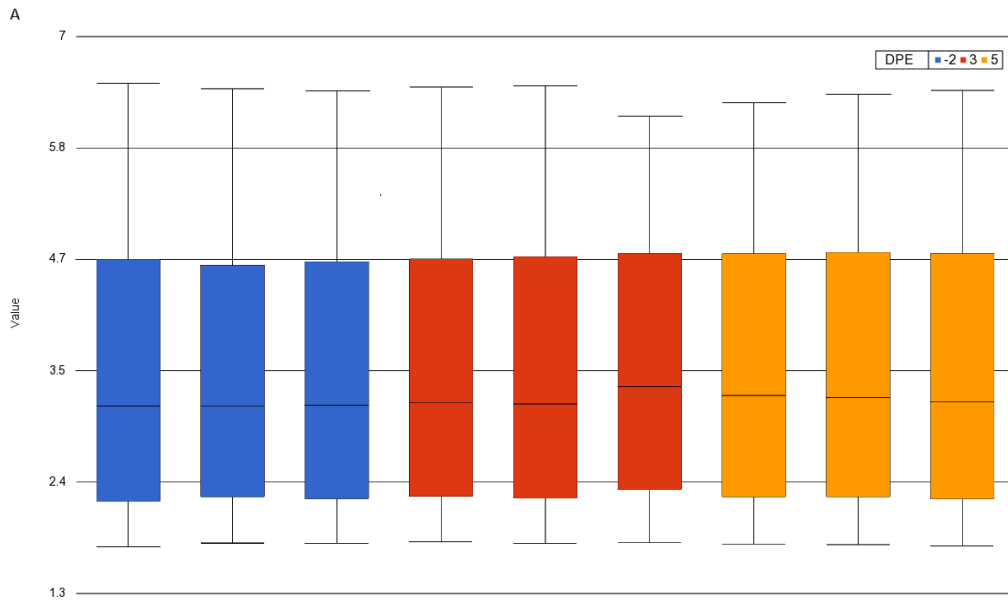
**Appendix Table 7. Predicted activation states in the lung tissue of S4 infected rabbits**

Disease/Function	PAS	Z-score	<i>P</i> value
<b>3 DPE</b>			
Clearance of cells	↑	2.219	1.07E-05
Apoptosis of connective tissue cells	↑	2.236	1.69E-04
Apoptosis of fibroblasts	↑	2.000	6.72E-04
<b>5 DPE</b>			
Formation of lung	↓	-2.376	3.68E-11

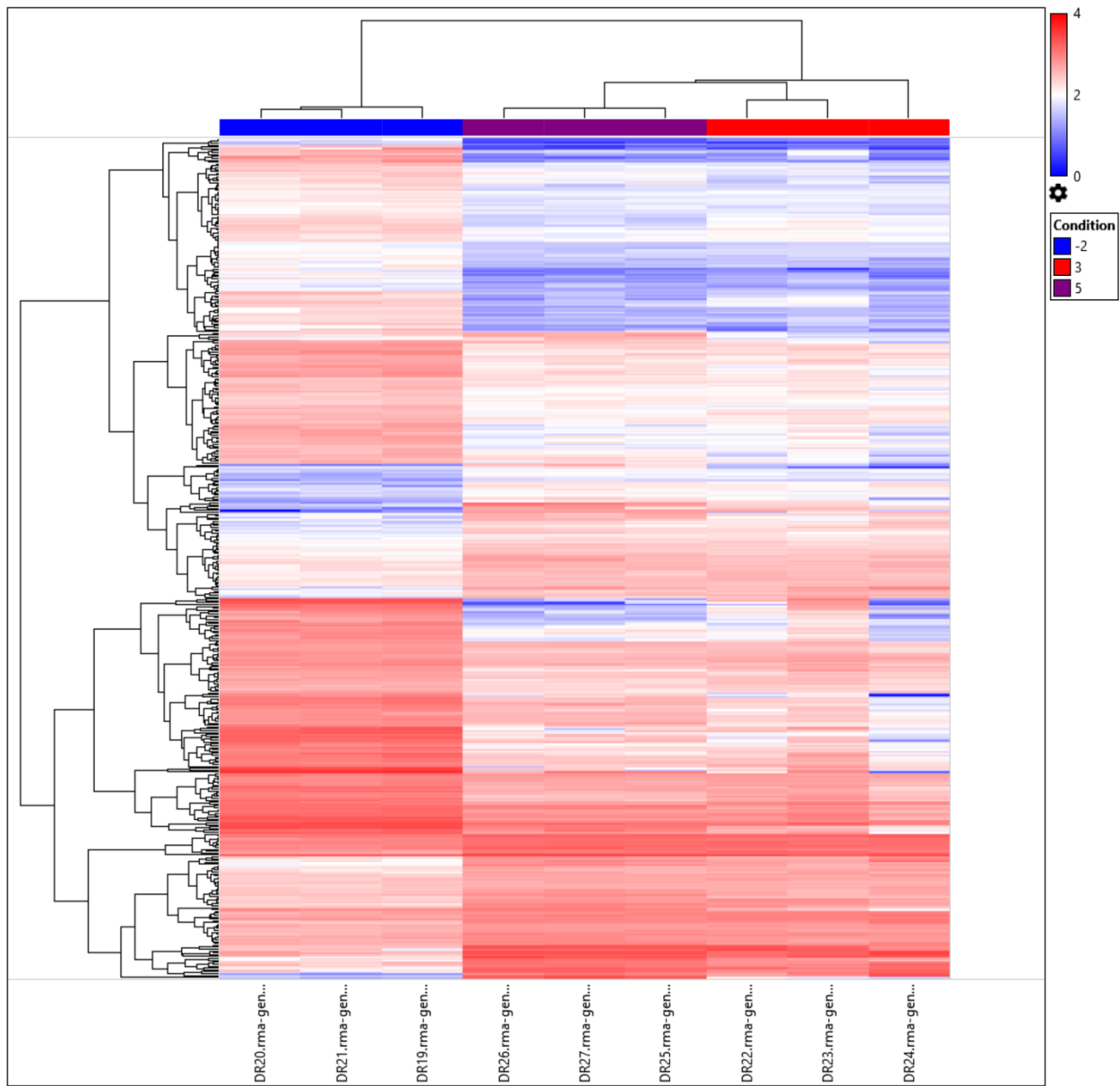
Appendix Figures 8 and 9 show the signal box plots, histograms, and hierarchical clustering for the microarray analysis performed in the lung. This QC indicates the RNA and microarray experiment was of acceptable quality. Additionally, the PCA plots and hierarchical clustering gave good separation between time points, further validating the quality of the microarray samples. Appendix Table 8 and Appendix Table 9 show the top 10 upregulated and downregulated genes at 3 and 5 DPE, respectively.

Appendix Figure 10 and 11 show canonical pathways that are altered in the liver at 3 and 5 DPE. At 3 DPE, several lipid pathways are downregulated such as the superpathway of cholesterol biosynthesis, cholesterol biosynthesis, and fatty acid oxidation. Amino acid degradation pathways are also downregulated, including methionine, tryptophan, tyrosine, isoleucine, phenylalanine, valine, and leucine. At 5 DPE canonical pathways involved with amino acid degradation, lipids, and inflammation are significantly altered. Amino acid degradation and lipid synthesis pathways are downregulated. Inflammatory signaling pathways are upregulated, such as interferon, necroptosis, and iNOS.

Significant PAS of the liver are shown in Appendix Table 12. Several functions involved with lipid transport are predicted to be downregulated. Additionally, fatty acid metabolism and gluconeogenesis is downregulated. Colonization and quantity of cells is predicted to decrease. Concomitant with decreases in lipid transport pathways, accumulation of lipids is expected to increase. Pathways associated with necrosis and cell death were predicted to be upregulated.



Appendix Figure 8. QC and PCA plot for liver gene expression of S4 infected NZW rabbits



**Appendix Figure 9. Significant differences in gene expression at different times post infection**

Microarray data were filtered to include samples with a gene-level fold change  $<-1.5$  or  $>1.5$  and a gene-level  $p$  value  $<0.05$ .

**Appendix Table 8. Top 10 upregulated and downregulated genes at 3 DPE in the liver**

3 DPE	Gene	Fold change	FDR <i>p</i> value
Downregulated	fatty acid binding protein 1, liver	-211.47	2.92E-02
	UDP-glucuronosyltransferase 2B16	-85.65	8.23E-02
	acyl-CoA desaturase-like	-80.42	3.27E-02
	polycyclic hydrocarbon-inducible cytochrom P450c	-69.68	2.00E-04
	methyltransferase-like protein 7A	-67.28	2.20E-03
	ornithine carbamoyltransferase	-61.13	7.30E-03
	glutathione S-transferase Yc-like	-54.89	1.16E-01
	alcohol dehydrogenase class-2 isozyme 2	-53.93	5.53E-02
	solute carrier family 22 member 24-like	-35.37	1.37E-02
	uridine phosphorylase 2	-34.86	7.00E-04
Upregulated	phospholipase A2, membrane associated-like	256.47	3.26E-01
	serum amyloid protein A	85.14	2.65E-01
	CXCL11	61.03	1.08E-02
	transcobalamin I (Vitamin B12 binding protein)	53.09	1.46E-01
	interferon-induced guanylate-binding protein 1-like	36.16	3.20E-03
	metallothionein-2A	22.81	1.43E-01
	STEAP family member 4	22.05	4.67E-02
	proteasome subunit, beta type, 9	19.24	6.00E-04
	serum amyloid A-3	18.63	7.20E-03
	interferon-induced very large GTPase 1-like	18.24	8.00E-03

**Appendix Table 9. Top 10 upregulated and downregulated genes at 5 DPE in the liver**

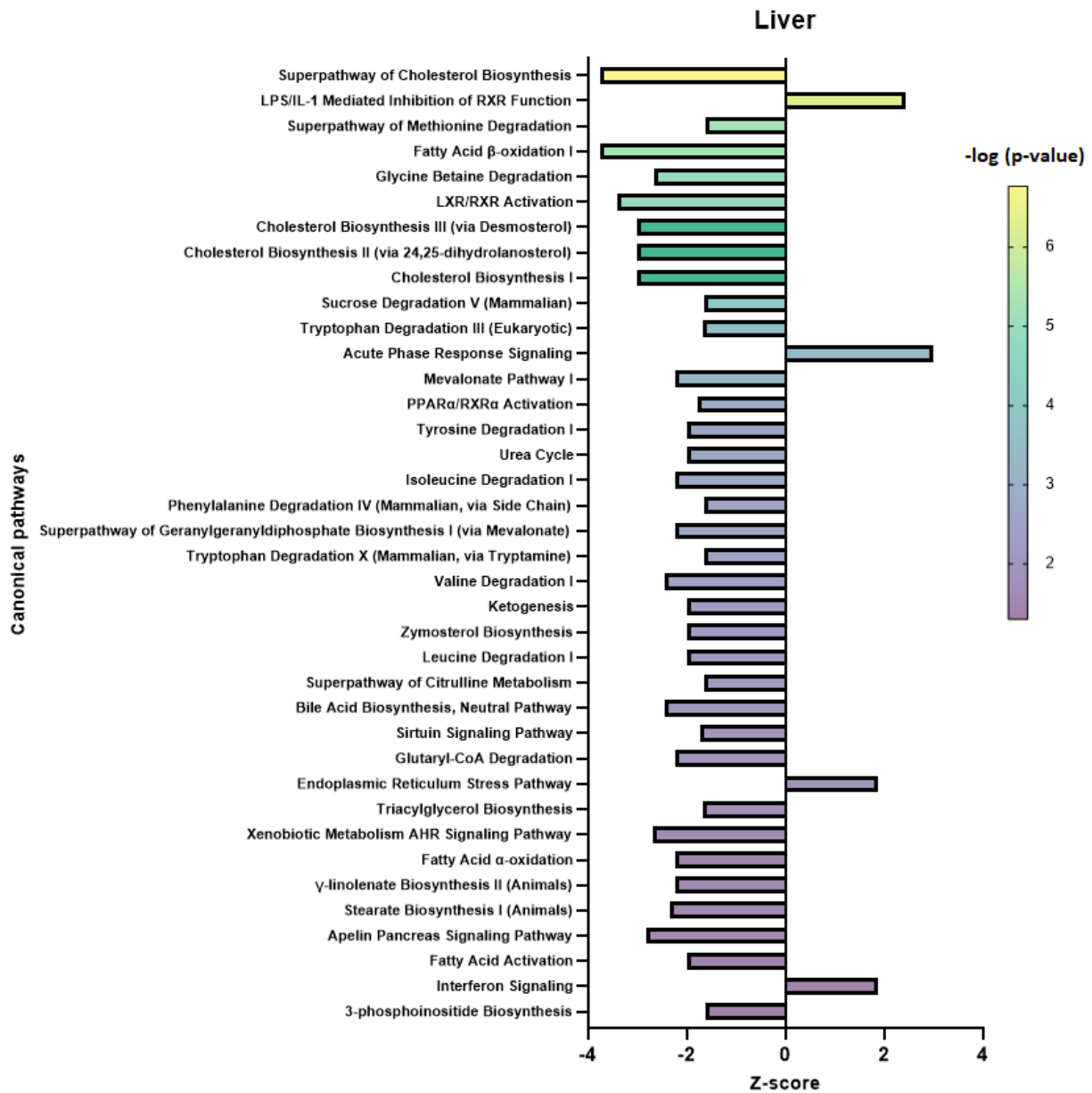
5 DPE	Gene	Fold change	FDR <i>p</i> value
Downregulated	acyl-CoA desaturase-like	-522.07	1.07E-02
	alcohol dehydrogenase class-2 isozyme 2	-378.21	1.38E-02
	hydroxysteroid (17-beta) dehydrogenase 13	-200.59	1.76E-02
	ST3A1	-175.05	1.90E-02
	UDP-glucuronosyltransferase 2B16	-106.97	2.31E-02
	glutathione S-transferase Yc-like	-90.44	5.54E-02
	cytochrome P450 2E1	-89.98	1.51E-01
	polycyclic hydrocarbon-inducible cytochrome P450c	-78.13	1.00E-04
	UDP-glucuronosyltransferase 2B31-like	-65.35	1.06E-02
	glutathione S-transferase alpha I	-54.98	1.79E-01
Upregulated	phospholipase A2, membrane associated-like	168.89	1.60E-01
	serum amyloid protein A	142.11	1.02E-01
	S100 calcium binding protein A8	122.61	1.68E-02
	solute carrier family 51, beta subunit	121.88	3.00E-04
	orosomucoid 1	81.1	6.96E-02
	serum amyloid A-3	79.23	1.40E-03
	chitinase 3-like 2	59.33	1.30E-03
	interferon-induced guanylate-binding protein 1-like	56.85	1.70E-03
	placenta-specific 8	56.29	4.29E-02
	transcobalamin I (vitamin B12 binding protein)	54.77	4.69E-02

**Appendix Table 10. GO analysis of liver at 3 DPE**

Functional group	enrichment score	<i>p</i> value	% in group present	Upregulated (FDR<0.05)	Downregulated (FDR<0.05)
Oxidoreductase activity	67.86	0	42.03	22 (5)	146 (61)
Mitochondrion	62.97	0	29.69	88 (14)	293 (99)
Lipid metabolic process	40.64	0	35.84	29 (4)	115 (39)
Endoplasmic reticulum	36.75	0	27.37	129 (25)	174 (58)
Immune system process	35.15	0	36.71	94 (18)	24 (3)
Cytosol	16.76	0	21.47	272 (67)	289 (94)
Transferase activity	11.08	0	22.01	136 (35)	170 (58)
Lipid binding	8.82	0	27.24	22 (3)	45 (14)
Ligase activity	6.17	0	29.36	7 (2)	25 (6)
Signaling receptor binding	5.94	0	24.48	34 (2)	36 (8)
Plasma membrane	5.39	0	19.43	306 (32)	290 (93)
Hydrolase activity	5.05	0.01	20.56	94 (19)	147 (44)
Cytoskeletal protein binding	4.69	0.01	30.3	8 (0)	12 (4)
Extracellular region	3.84	0.02	20.11	99 (15)	129 (25)
Enzyme regulator activity	3.24	0.04	36.84	1 (1)	6 (0)

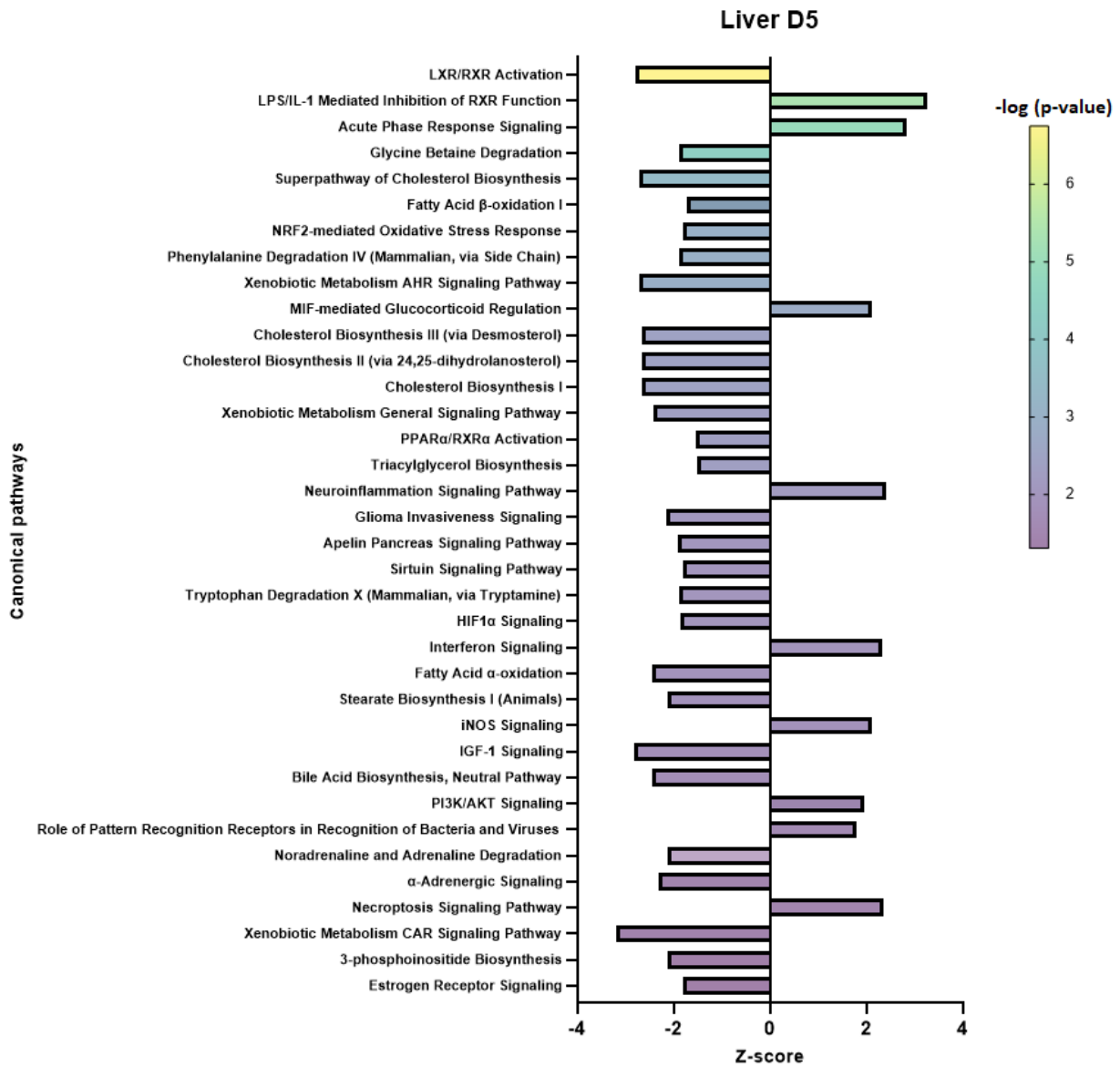
**Appendix Table 11. GO analysis of liver at 5 DPE**

Functional group	enrichment score	<i>p</i> value	% in group present	Upregulated (FDR<0.05)	Downregulated (FDR<0.5)
Oxidoreductase activity	55.69	0	38.99	36 (12)	119 (59)
Mitochondrion	53.84	0	28.27	123 (42)	239 (95)
Endoplasmic reticulum	41.11	0	27.55	147 (47)	159 (55)
Lipid metabolic process	31.14	0	32.83	37 (9)	95 (26)
Immune system process	25.12	0	32.91	87 (27)	18 (6)
Cytosol	15.33	0	20.89	263 (114)	283 (128)
Transferase activity	11.23	0	21.65	119 (49)	181 (70)
Golgi apparatus	8.09	0	21.51	101 (34)	120 (43)
Hydrolase activity	6.1	0	20.56	100 (32)	141 (55)
Transporter activity	5.15	0.01	33.33	11 (6)	5 (1)
Lipid binding	4.77	0.01	23.58	25 (10)	33 (13)
Plasma membrane	4.29	0.01	18.81	291 (84)	287 (124)
Cytoskeletal protein binding	4.16	0.02	28.79	7 (1)	12 (4)
Cytoplasmic vesicle	3.42	0.03	20.32	59 (26)	59 (24)
Enzyme regulator activity	3.34	0.04	36.84	1 (1)	6 (1)



**Appendix Figure 10. Pathway analysis of DEGs in the liver at 3 DPE**

Canonical pathways were limited to those that exhibited z-scores  $> 1.5$  and  $< -1.5$  and  $p$  values  $< 0.05$ . Z-scores are shown on the x-axis and  $p$  values are represented by a heatmap.



**Appendix Figure 11. Pathway analysis of DEGs in the liver at 5 DPE**

Canonical pathways were limited to those that exhibited z-scores  $> 1.5$  and  $< -1.5$  and  $p$  values  $< 0.05$ . Z-scores are shown on the x-axis and  $p$  values are represented by a heatmap.

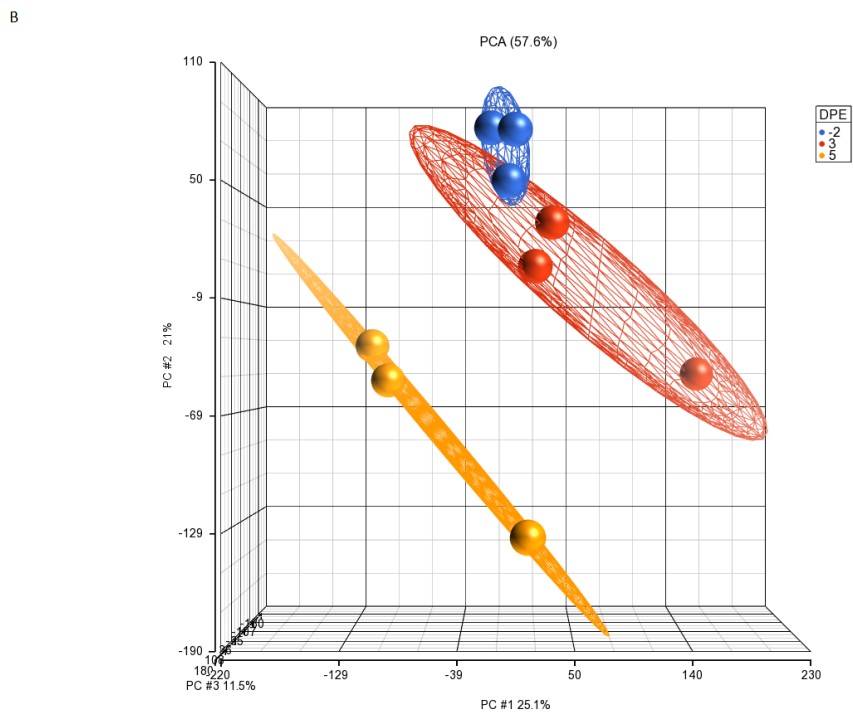
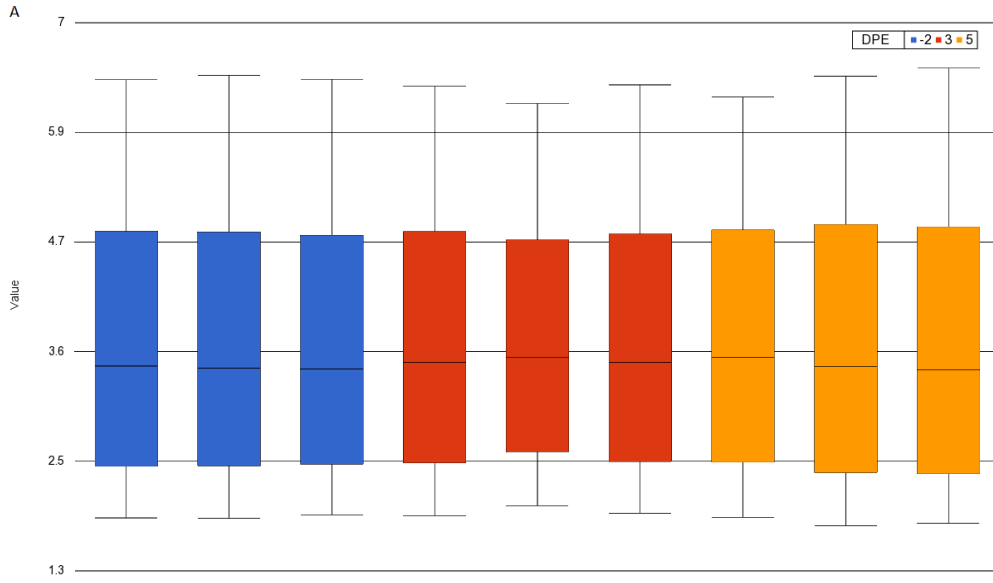
**Appendix Table 12. Predicted activation states in the liver tissue of S4 infected rabbits**

Disease/Function	PAS	Z-Score	<i>p</i> value
<b>3 DPE</b>			
Transport of molecule	↓	-2.323	3.29E-09
Transport of lipid	↓	-3.060	1.99E-06
Cholesterol transport	↓	-2.619	1.70E-05
Transport of steroid	↓	-3.112	3.84E-05
Fatty acid metabolism	↓	-2.683	7.88E-05
Export of lipid	↓	-2.000	5.96E-03
<b>5 DPE</b>			
Gluconeogenesis of hepatocytes	↓	-2.195	2.13E-04
Quantity of glycogen	↓	-2.199	2.79E-03
Colonization	↓	-2.000	1.20E-02
Quantity of cells	↓	-2.489	1.93E-02
Necrosis	↑	2.492	1.03E-08
Cell death of liver	↑	2.444	4.62E-08
Necrosis of liver	↑	2.354	7.01E-08
Accumulation of lipid	↑	2.410	5.52E-07
Cell death of liver cells	↑	2.370	3.49E-05
Liver lesion	↑	2.392	4.71E-04
Cellular infiltration by mononuclear lymphocytes	↑	2.186	2.22E-02

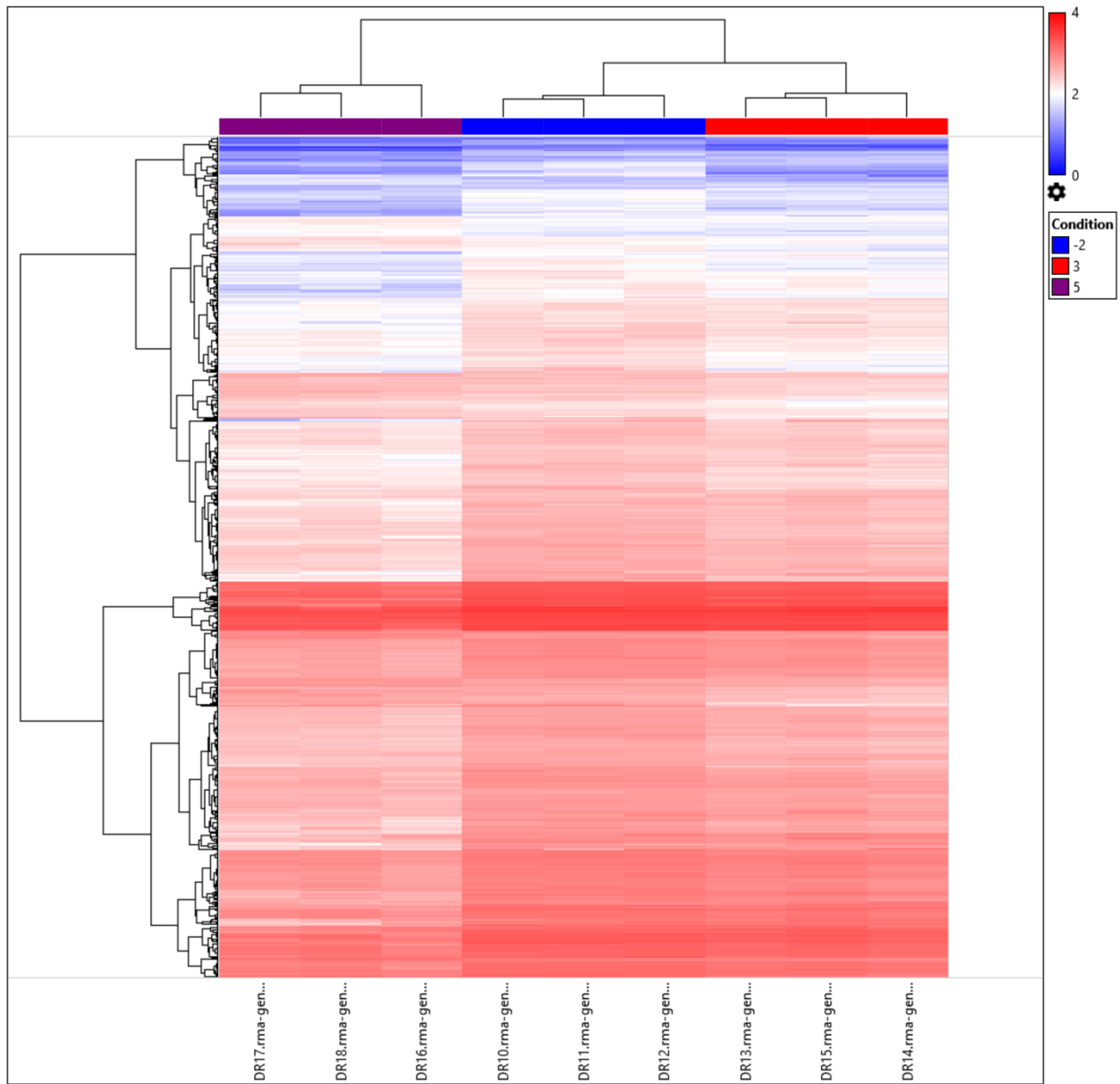
Appendix Figures 12 and 13 show the signal box plots, histograms, and hierarchical clustering for the microarray analysis performed in the lung. This QC indicates the RNA and microarray experiment was of acceptable quality. Additionally, the PCA plots and hierarchical clustering gave good separation between time points, further validating the quality of the microarray samples. Appendix Table 13 and Appendix Table 14 show the top 10 upregulated and downregulated genes at 3 and 5 DPE, respectively.

Pathway analysis shows an upregulation in canonical pathways associated with the immune response at 3 DPE, including interferon signaling, TREM1 signaling, and MIF regulation of innate immunity (Appendix Figure 14). The 14-3-3 mediated signaling pathway, which is involved in class switching, is downregulated. Lipid synthesis pathways are downregulated, similar to what was observed in the liver. At 5 DPE, more pathways associated with the immune response are significantly upregulated, such as IL-6 signaling, necroptosis signaling, inflammasome pathway, and PKR induced interferon induction, and toll like receptor signaling (Appendix Figure 15). Pathways involved in wound healing and the cell cycle are also upregulated.

Based on the microarray data, cell death of immune cells is predicted to be decreased in the spleen (Appendix Table 17). Hyperplasia of the spleen is predicted to be decreased. Quantity of mononuclear leukocytes and formation of germinal centers is predicted to be increased. Concomitantly, immune response of T lymphocytes is expected to be increased post exposure.



Appendix Figure 12. QC and PCA plot for spleen gene expression of S4 infected NZW rabbits



1

**Appendix Figure 13. Significant differences in gene expression at different times post infection**

Microarray data were filtered to include samples with a gene-level fold change  $<-1.5$  or  $>1.5$  and a gene-level p value  $<0.05$ .

**Appendix Table 13. Top 10 upregulated and downregulated genes at 3 DPE in the spleen**

3 DPE Gene	Fold change	FDR <i>p</i> value
Downregulated	selenoprotein P, plasma 1	-7.46 2.80E-03
	acyl-CoA desaturase-like	-6.5 1.20E-01
	solute carrier family, iron-regulated transporter	-6.26 7.00E-04
	deoxyribonuclease I-like 3	-6.13 7.68E-02
	corticostatin-6	-4.99 3.38E-01
	purinergic receptor P2Y, G protein coupled, 14	-3.96 2.25E-02
	asporin	-3.74 2.25E-02
	collagen, type XIV, alpha 1	-3.71 2.46E-02
	spermatogenesis associated 6	-3.58 2.25E-02
	melan-A	-3.31 1.80E-02
Upregulated	CXCL11	16.22 3.70E-03
	immunity-related GTPase family, M	10.33 4.11E-01
	interferon-induced guanylate-binding protein 1-like	8.21 6.29E-05
	interferon-induced very large GTPase 1-like	7.85 7.00E-04
	interferon-inducible GTPase 1	5.99 3.48E-01
	S100 calcium binding protein A8	5.49 3.18E-01
	leucine aminopeptidase 3	5.08 2.00E-04
	immunoresponsive 1 homolog	4.96 2.25E-02
	retinoic acid receptor responder protein 3-like	4.78 2.50E-01
	CXCL8	4.7 2.03E-01

**Appendix Table 14. Top 10 upregulated and downregulated genes at 5 DPE in the spleen**

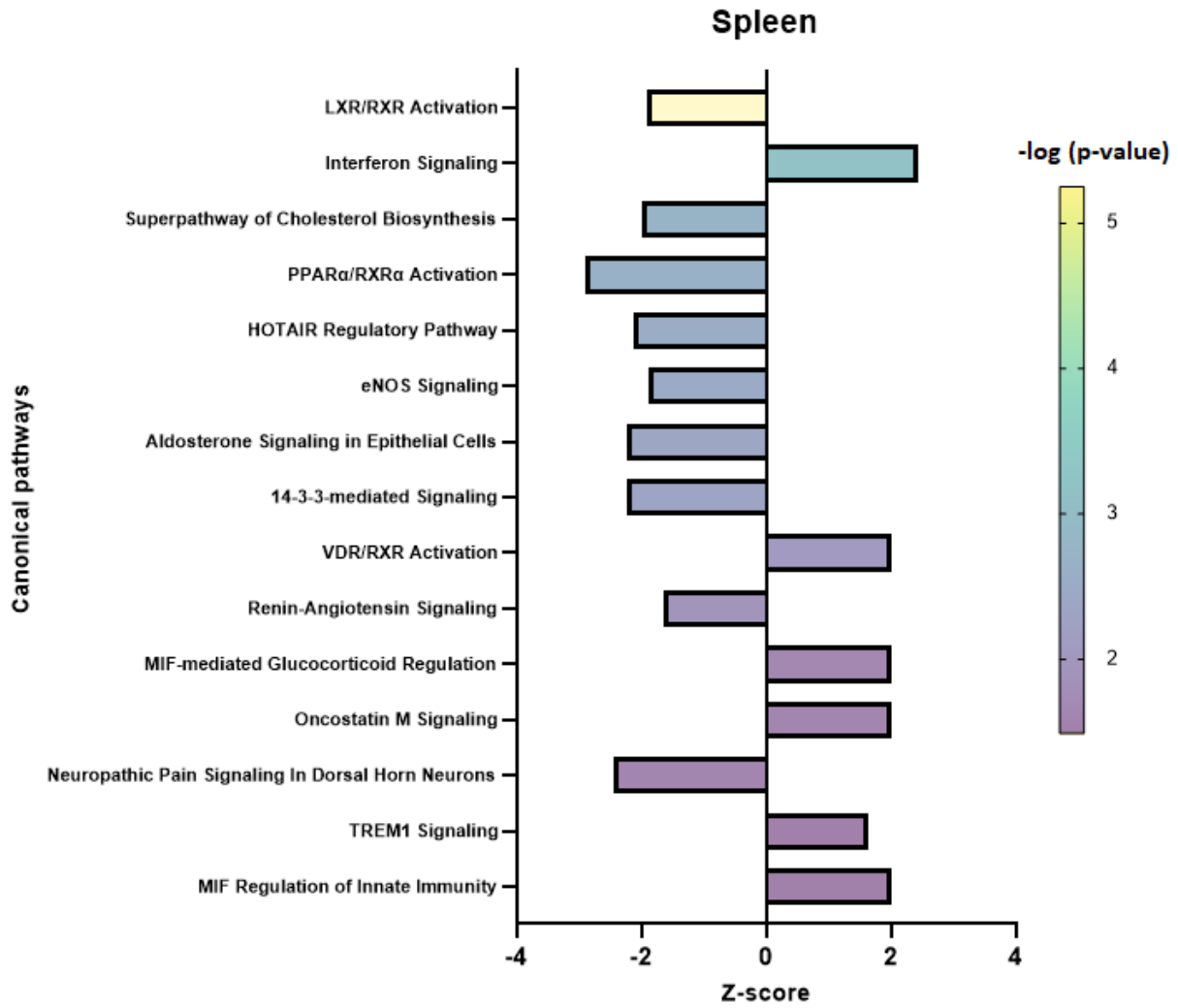
5 DPE Gene	Fold change	FDR <i>p</i> value
corticostatin-6	-22.35	3.91E-02
defensin NP-4	-20.36	1.73E-01
C-type lectin domain family 12, member A	-8.76	4.00E-04
neutrophil antibiotic peptide NP-5 like	-7.63	2.25E-02
vascular non-inflammatory molecule 2	-6.04	2.00E-04
transmembrane protein 107	-5.2	7.07E-02
G protein-coupled receptor 183	-5.15	8.00E-04
serine/threonine kinase 17b	-5	1.72E-05
squalene epoxidase	-4.86	3.80E-03
chromosome unknown open reading frame, human C16orf87	-4.64	8.00E-04
CXCL11	137.66	1.53E-05
serum amyloid A-3	45.01	7.47E-06
immunoresponsive 1 homolog	34.57	9.64E-06
interferon-induced guanylate-binding protein 1-like	33.29	7.30E-07
retinoic acid receptor responder protein 3-like	32.23	4.10E-03
V-set and immunoglobulin domain containing 4	29.35	7.47E-06
interferon-inducible GTPase 1	28.83	2.39E-02
S100 calcium binding protein A8	28.76	1.10E-03
TIMP metalloproteinase inhibitor 1	27.04	8.58E-05
formyl peptide receptor 2	23.01	2.42E-05

**Appendix Table 15. GO analysis of spleen at 3 DPE**

Functional group	enrichment score	p value	% in group present	Upregulated (FDR<0.05)	Downregulated (FDR<0.05)
Extracellular region	21.79	0	8.36	49 (6)	45 (18)
Immune system process	19.35	0	12.34	23 (7)	16 (2)
Lipid metabolic process	7.31	0	8.02	10 (1)	22 (3)
Cytosol	5.15	0.01	5.3	51 (16)	87 (18)
Hydrolase activity	4.74	0.01	5.8	23 (4)	45 (14)
Signaling receptor binding	3.66	0.03	6.99	8 (1)	12 (1)

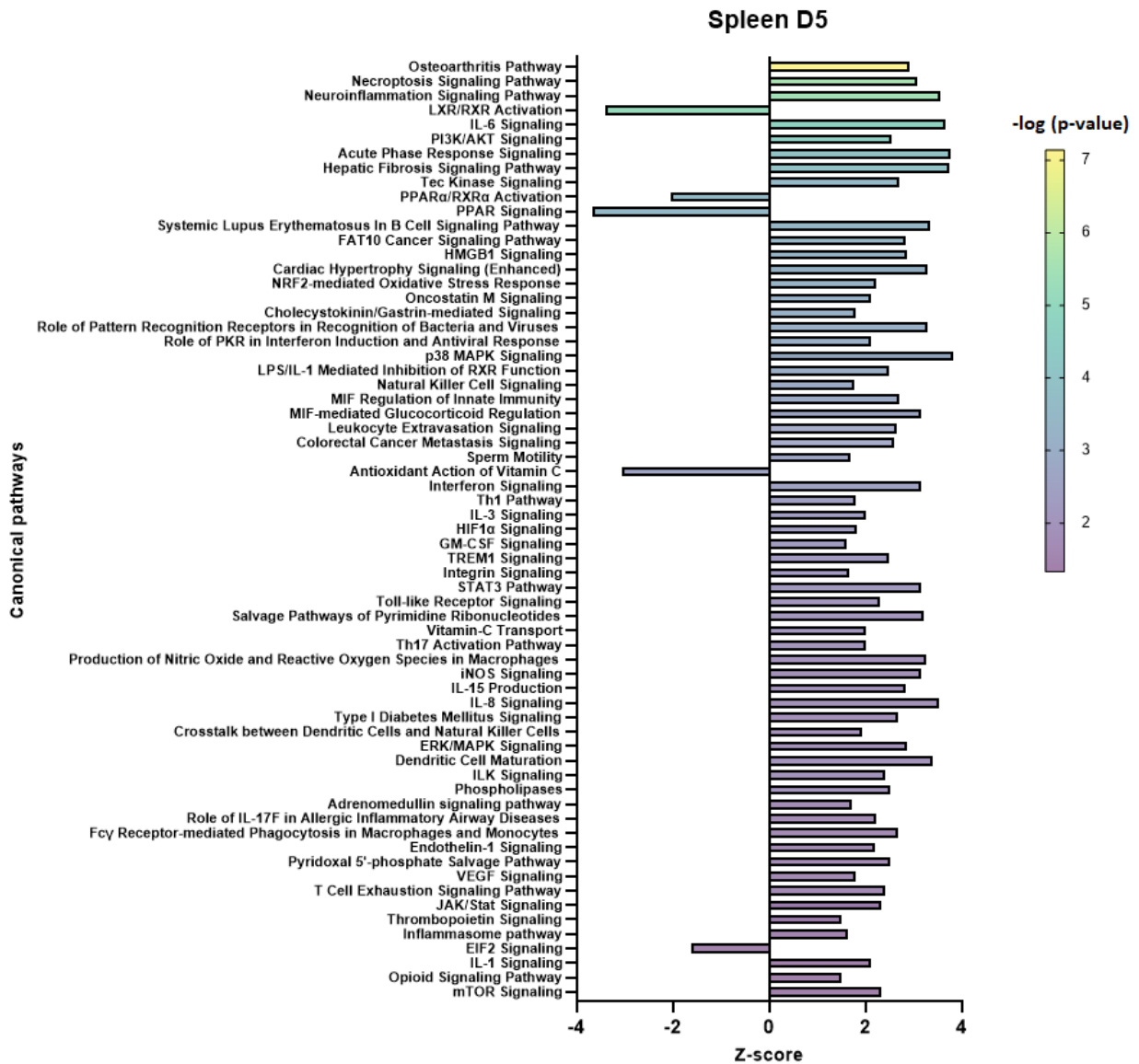
**Appendix Table 16. GO analysis of spleen at 5 DPE**

Functional group	enrichment score	<i>p</i> value	% in group present	Upregulated (FDR<0.05)	Downregulated (FDR<0.05)
Immune system process	46.55	0	37.03	95 (77)	22 (19)
Cytosol	31.46	0	20.62	320 (260)	221 (182)
Endoplasmic reticulum	22.02	0	22.49	176 (150)	73 (59)
Plasma membrane	11.42	0	18.16	404 (322)	152 (128)
Golgi apparatus	10.42	0	20.23	134 (110)	73 (64)
Hydrolase activity	9.06	0	19.54	131 (119)	98 (78)
Nucleus	7.18	0	17.12	361 (284)	385 (322)
Mitochondrion	6.06	0	18.5	156 (111)	83 (66)
Extracellular region	5.74	0	18.59	174 (143)	35 (24)
Cytoplasmic vesicle	5.3	0	19.52	85 (74)	33 (26)
Cell population proliferation	5.04	0.01	23.94	26 (23)	9 (8)
RNA binding	4.53	0.01	18.96	44 (38)	84 (61)
Cytoskeletal protein binding	4.5	0.01	27.27	15 (9)	3 (3)
Signaling receptor binding	3.86	0.02	20.28	42 (33)	16 (11)
Lipid metabolic process	3.28	0.04	19.05	49 (42)	28 (24)



**Appendix Figure 14. Pathway analysis of DEGs in the spleen at 3 DPE**

Canonical pathways were limited to those that exhibited z-scores  $> 1.5$  and  $< -1.5$  and  $p$  values  $< 0.05$ . Z-scores are shown on the x-axis and  $p$  values are represented by a heatmap.

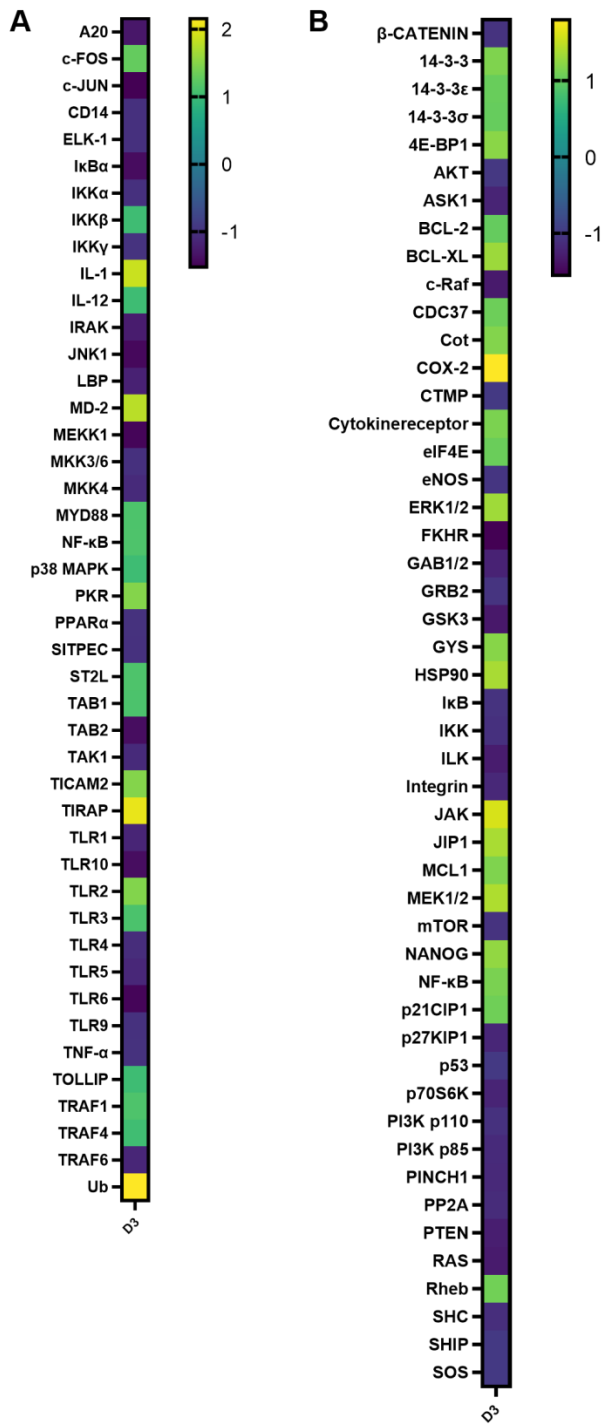


**Appendix Figure 15. Pathway analysis of DEGs in the spleen at 5 DPE**

Canonical pathways were limited to those that exhibited z-scores  $> 1.5$  and  $< -1.5$  and  $p$  values  $< 0.05$ . Z-scores are shown on the x-axis and  $p$  values are represented by a heatmap.

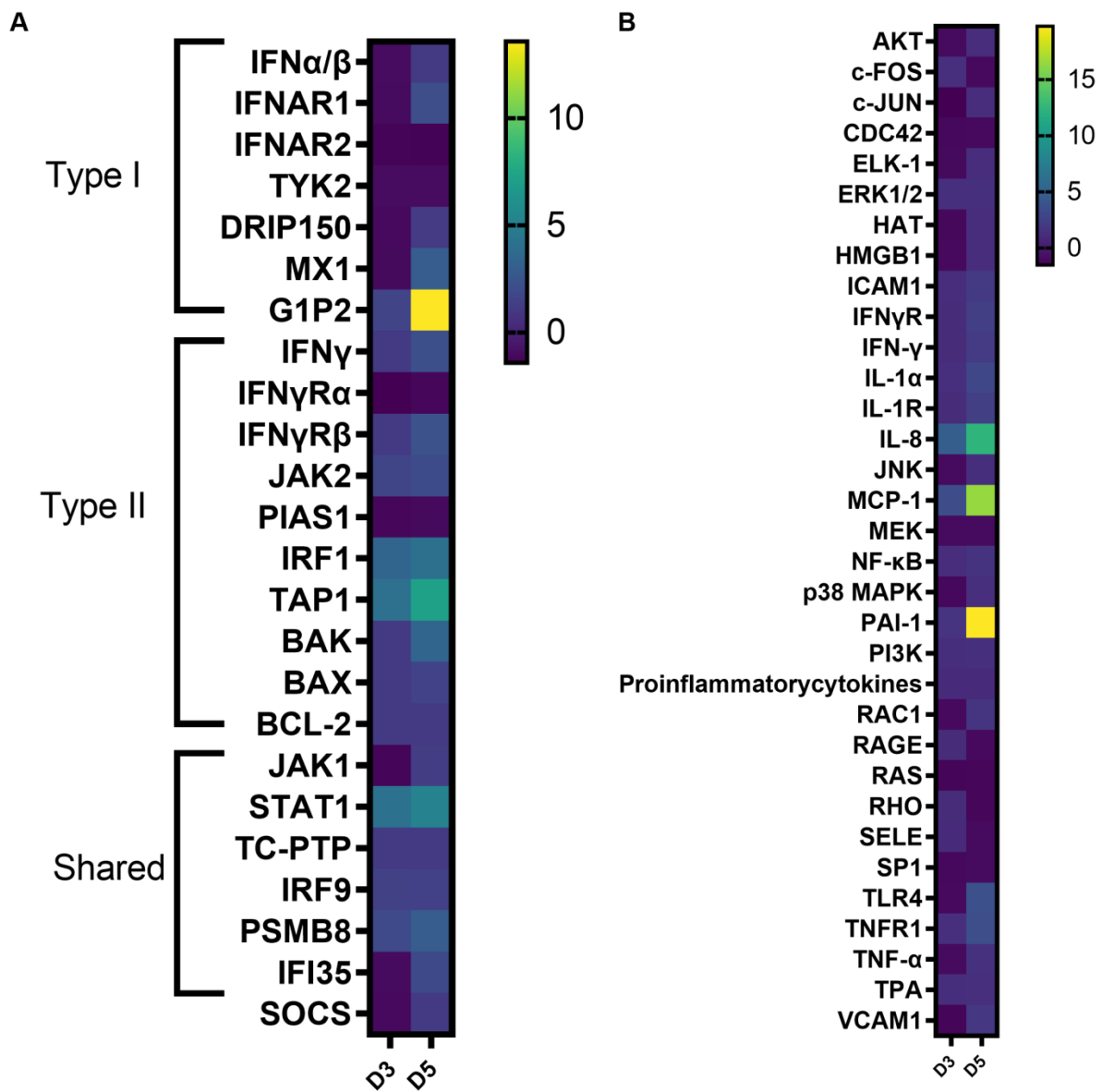
**Appendix Table 17. Predicted activation states in the spleen**

Disease/Function	PAS	Z-score	<i>p</i> value
<b>3 DPE</b>			
Cell death of immune cells	↓	-2.249	3.72E-02
<b>5 DPE</b>			
Hyperplasia of spleen	↓	-2.350	1.85E-02
Quantity of mononuclear leukocytes	↑	2.138	1.84E-05
Formation of germinal center	↑	2.138	5.70E-04
Immune response of T lymphocytes	↑	2.135	2.53E-02



**Appendix Figure 16. Gene expression of PRR pathways in the liver**

NZW rabbits were exposed to virulent S4 and serially sacrificed to collect tissue for gene expression pathway analysis for A) TLR and B) PI3K-AKT.



**Appendix Figure 17. Interferon and HMGB1 signaling gene expression in the spleen**

NZW rabbits were exposed to virulent S4 and serially sacrificed to collect tissue for gene expression pathway analysis for A) interferon and B) HMGB1.

**Appendix Table 18. Fold change of immune genes in the lung**

Gene	3 DPE	5 DPE	Gene	3 DPE	5 DPE	Gene	3 DPE	5 DPE
CCL14	-1.02	1.07	IL6	1.25	3.10	IL37	-1.16	1.37
CCL2	3.62	6.83	IL6R	-1.00	-1.10	IL3RA	-1.01	1.02
CCL20	1.86	-1.50	IL6ST	1.66	-1.30	ILDR1	1.01	1.25
CCL21	-1.20	1.34	IL7R	-1.78	-1.64	ILDR2	1.04	1.67
CCL22	-1.05	1.14	IL9	1.27	2.27	ILF2	-1.53	-3.42
CCL27	-1.01	1.39	IL10	-1.08	1.58	ILF3	1.06	-1.05
CCL4	-1.06	1.67	IL10RA	1.03	1.02	NOS2	-2.05	-2.53
CD14	1.03	1.43	IL12A	1.02	1.09	STAT1	4.04	1.87
CSF2	1.03	-1.21	IL12RB2	-1.05	-1.17	STAT4	-1.61	-1.67
CXCL10	2.47	4.49	IL13	-1.01	1.22	STAT5B	-1.13	-1.26
CXCL11	10.63	14.23	IL13RA1	1.48	1.20	TBX21	1.15	1.62
CXCL9	-1.11	1.14	IL15	1.75	1.03	THBS1	-1.16	-1.52
CXCR4	-1.23	-3.19	IL16	1.16	1.57	TNF	-1.09	1.11
GATA1	1.05	1.41	IL17A	1.07	1.57	TNFAIP3	1.24	1.5
GATA2	1.00	1.09	IL17F	-1.03	1.76	TNFAIP8L2	-1.45	-1.27
GATAD2B	-1.54	-2.47	IL17RA	-1.01	-1.07	TNFAIP8L3	1.22	1.62
IFNAR1	1.01	-2.51	IL17RE	-1.00	1.36	TNFRSF11B	1.09	1.03
IFNAR2	1.31	-1.96	IL18	1.14	-1.73	TNFRSF17	1.08	-1.83
IFN $\gamma$	1.01	1.18	IL18BP	2.71	2.59	TNFRSF1A	1.64	1.14
IFNGR1	-1.07	-1.41	IL18R1	1.01	1.25	TNFRSF1B	-1.01	1.03
IFNGR2	1.61	-1.04	IL18RAP	-1.07	-1.03	TNFRSF21	1.76	1.10
IL1a	1.06	1.24	IL21	-1.08	1.18	TNFRSF25	1.01	1.38
IL1b	1.61	-1.24	IL22	1.03	1.52	TNFRSF8	1.20	1.60
IL1R2	1.11	4.48	IL22RA2	1.10	1.37	TNFRSF9	1.14	1.24
IL1RAP	2.37	2.08	IL23R	-1.05	1.00	TNFSF10	1.18	-2.64
IL1RAPL2	-1.01	1.35	IL27RA	-1.05	1.13	TNFSF11	1.03	1.30
IL1RL1	1	1.03	IL31	-1.19	1.06	TNFSF13	-1.08	1.08
IL1RN	1.27	2.41	IL33	3.38	1.32	TNFSF8	-1.00	1.11
IL2	-1.05	1.07	IL34	1.09	1.05			
IL4	1.02	1.11	IL36G	-1.02	1.85			

## Bibliography

1. Christopher LGW, Cieslak LTJ, Pavlin JA, Eitzen EM. 1997. Biological warfare: a historical perspective. *Jama* 278:412-417.
2. Council NR. 2006. *Overcoming Challenges to Develop Countermeasures Against Aerosolized Bioterrorism Agents: Appropriate Use of Animal Models*. National Academies Press.
3. Russell PK. 1999. Vaccines in civilian defense against bioterrorism. *Emerging infectious diseases* 5:531.
4. Matz L, Kamdar K, Holder M, Metcalf G, Weissenberger G, Meng Q, Vee V, Han Y, Muzny D, Gibbs R. 2018. Challenges of *Francisella* classification exemplified by an atypical clinical isolate. *Diagnostic microbiology and infectious disease* 90:241-247.
5. Brown VR, Adney DR, Olea-Popelka F, Bowen RA. 2015. Prior Inoculation with Type B Strains of *Francisella tularensis* Provides Partial Protection against Virulent Type A Strains in Cottontail Rabbits. *PLoS One* 10:e0140723.
6. Dakota S. 2015. Update on Emerging Infections: News From the Centers for Disease Control and Prevention. *MMWR Morb Mortal Wkly Rep* 64:1317-1318.
7. Dinc G, Demiraslan H, Doganay M. 2017. Unexpected risks for campers and hikers: Tick-borne infections. *International Journal of Travel Medicine and Global Health* 5:5-13.
8. Büyük F, Çelebi Ö, Celik E, Çelebi B, Kilic S, Sağlam AG, Akça D, Doğanay M, Otlı S, Şahin M. 2016. The prevalence of tularemia in occupational groups that have contact with animals. *Turkish journal of medical sciences* 46:451-456.
9. Christenson B. 1984. An outbreak of tularemia in the northern part of central Sweden. *Scandinavian journal of infectious diseases* 16:285-290.
10. Evans ME, Gregory DW, Schaffner W, McGee ZA. 1985. Tularemia: a 30-year experience with 88 cases. *Medicine* 64:251-269.
11. McClellan G, Coleman M, Crary D, Thurman A, Thran B. 2018. Human Dose–Response Data for *Francisella tularensis* and a Dose-and Time-Dependent Mathematical Model of Early-Phase Fever Associated with Tularemia After Inhalation Exposure. *Risk Analysis* 38:1685-1700.
12. Burckhardt F, Hoffmann D, Jahn K, Heuner K, Jacob D, Vogt M, Bent S, Grunow R, Zanger P. 2018. Oropharyngeal tularemia from freshly pressed grape must. *New England Journal of Medicine* 379:197-199.
13. Feldman KA, Ensore RE, Lathrop SL, Matyas BT, McGuill M, Schriefer ME, Stiles-Enos D, Dennis DT, Petersen LR, Hayes EB. 2001. An outbreak of primary pneumonic tularemia on Martha's Vineyard. *New England Journal of Medicine* 345:1601-1606.
14. Faucher J, Chirouze C, Coutris C, Fery-Blanco C, Maurin M, Hoen B. 2012. Typhoidal tularemia: 2 familial cases. *Case reports in infectious diseases* 2012.
15. Tärnvik A, Berglund L. 2003. Tularaemia. *European Respiratory Journal* 21:361-373.
16. Limaye AP, Hooper CJ. 1999. Treatment of tularemia with fluoroquinolones: two cases and review. *Clinical infectious diseases* 29:922-924.

17. Tulkens PM. 1989. Nephrotoxicity of aminoglycoside antibiotics. *Toxicology letters* 46:107-123.
18. Santic M, Al-Khodori S, Abu Kwaik Y. 2010. Cell biology and molecular ecology of *Francisella tularensis*. *Cellular microbiology* 12:129-139.
19. Balagopal A, MacFarlane AS, Mohapatra N, Soni S, Gunn JS, Schlesinger LS. 2006. Characterization of the receptor-ligand pathways important for entry and survival of *Francisella tularensis* in human macrophages. *Infection and immunity* 74:5114-5125.
20. Schulert GS, Allen LAH. 2006. Differential infection of mononuclear phagocytes by *Francisella tularensis*: role of the macrophage mannose receptor. *Journal of leukocyte biology* 80:563-571.
21. Geier H, Celli J. 2011. Phagocytic receptors dictate phagosomal escape and intracellular proliferation of *Francisella tularensis*. *Infection and immunity* 79:2204-2214.
22. Ben Nasr A, Haithcoat J, Masterson JE, Gunn JS, Eaves-Pyles T, Klimpel GR. 2006. Critical role for serum opsonins and complement receptors CR3 (CD11b/CD18) and CR4 (CD11c/CD18) in phagocytosis of *Francisella tularensis* by human dendritic cells (DC): uptake of *Francisella* leads to activation of immature DC and intracellular survival of the bacteria. *Journal of leukocyte biology* 80:774-786.
23. Barker JR, Chong A, Wehrly TD, Yu JJ, Rodriguez SA, Liu J, Celli J, Arulanandam BP, Klose KE. 2009. The *Francisella tularensis* pathogenicity island encodes a secretion system that is required for phagosome escape and virulence. *Molecular microbiology* 74:1459-1470.
24. Pierini LM. 2006. Uptake of serum-opsonized *Francisella tularensis* by macrophages can be mediated by class A scavenger receptors. *Cellular microbiology* 8:1361-1370.
25. Clemens DL, Lee B-Y, Horwitz MA. 2005. *Francisella tularensis* enters macrophages via a novel process involving pseudopod loops. *Infection and immunity* 73:5892.
26. Santic M, Asare R, Skrobonja I, Jones S, Kwaik YA. 2008. Acquisition of the vacuolar ATPase proton pump and phagosome acidification are essential for escape of *Francisella tularensis* into the macrophage cytosol. *Infection and immunity* 76:2671-2677.
27. Chong A, Wehrly TD, Nair V, Fischer ER, Barker JR, Klose KE, Celli J. 2008. The early phagosomal stage of *Francisella tularensis* determines optimal phagosomal escape and *Francisella* pathogenicity island protein expression. *Infection and immunity* 76:5488-5499.
28. Golovliov I, Twine SM, Shen H, Sjöstedt A, Conlan W. 2013. A  $\Delta$ clpB mutant of *Francisella tularensis* subspecies *holarctica* strain, FSC200, is a more effective live vaccine than *F. tularensis* LVS in a mouse respiratory challenge model of tularemia. *PLoS One* 8.
29. Lindgren H, Golovliov I, Baranov V, Ernst RK, Telepnev M, Sjöstedt A. 2004. Factors affecting the escape of *Francisella tularensis* from the phagolysosome. *Journal of medical microbiology* 53:953-958.
30. Santic M, Molmeret M, Klose KE, Jones S, Kwaik YA. 2005. The *Francisella tularensis* pathogenicity island protein IglC and its regulator MglA are essential for modulating phagosome biogenesis and subsequent bacterial escape into the cytoplasm. *Cellular microbiology* 7:969-979.
31. Bönquist L, Lindgren H, Golovliov I, Guina T, Sjöstedt A. 2008. MglA and Igl proteins contribute to the modulation of *Francisella tularensis* live vaccine strain-containing phagosomes in murine macrophages. *Infection and immunity* 76:3502-3510.

32. Schmerk CL, Duplantis BN, Howard PL, Nano FE. 2009. A *Francisella novicida* pdpA mutant exhibits limited intracellular replication and remains associated with the lysosomal marker LAMP-1. *Microbiology* 155:1498.
33. McCaffrey RL, Schwartz JT, Lindemann SR, Moreland JG, Buchan BW, Jones BD, Allen LAH. 2010. Multiple mechanisms of NADPH oxidase inhibition by type A and type B *Francisella tularensis*. *Journal of leukocyte biology* 88:791-805.
34. Bröms JE, Meyer L, Sun K, Lavander M, Sjöstedt A. 2012. Unique substrates secreted by the type VI secretion system of *Francisella tularensis* during intramacrophage infection. *PloS one* 7.
35. Baron GS, Nano FE. 1998. MglA and MglB are required for the intramacrophage growth of *Francisella novicida*. *Molecular microbiology* 29:247-259.
36. Brotcke A, Monack DM. 2008. Identification of fevR, a novel regulator of virulence gene expression in *Francisella novicida*. *Infection and immunity* 76:3473-3480.
37. Buchan BW, McCaffrey RL, Lindemann SR, Allen L-AH, Jones BD. 2009. Identification of migR, a regulatory element of the *Francisella tularensis* live vaccine strain iglABCD virulence operon required for normal replication and trafficking in macrophages. *Infection and immunity* 77:2517-2529.
38. Lai X-H, Golovliov I, Sjöstedt A. 2001. *Francisella tularensis* induces cytopathogenicity and apoptosis in murine macrophages via a mechanism that requires intracellular bacterial multiplication. *Infection and immunity* 69:4691.
39. Wickstrum JR, Bokhari SM, Fischer JL, Pinson DM, Yeh H-W, Horvat RT, Parmely MJ. 2009. *Francisella tularensis* induces extensive caspase-3 activation and apoptotic cell death in the tissues of infected mice. *Infection and immunity* 77:4827-4836.
40. Zhang J, Tachado SD, Patel N, Zhu J, Imrich A, Manfruelli P, Cushion M, Kinane TB, Koziel H. 2005. Negative regulatory role of mannose receptors on human alveolar macrophage proinflammatory cytokine release in vitro. *Journal of leukocyte biology* 78:665-674.
41. Duenas AI, Aceves M, Orduña A, Díaz R, Sánchez Crespo M, García-Rodríguez C. 2006. *Francisella tularensis* LPS induces the production of cytokines in human monocytes and signals via Toll-like receptor 4 with much lower potency than *E. coli* LPS. *International immunology* 18:785-795.
42. Phillips NJ, Schilling B, McLendon MK, Apicella MA, Gibson BW. 2004. Novel modification of lipid A of *Francisella tularensis*. *Infection and immunity* 72:5340.
43. Lindemann SR, Peng K, Long ME, Hunt JR, Apicella MA, Monack DM, Allen L-AH, Jones BD. 2011. *Francisella tularensis* Schu S4 O-antigen and capsule biosynthesis gene mutants induce early cell death in human macrophages. *Infection and immunity* 79:581.
44. Case EDR, Chong A, Wehrly TD, Hansen B, Child R, Hwang S, Virgin HW, Celli J. 2014. The *Francisella* O-antigen mediates survival in the macrophage cytosol via autophagy avoidance. *Cellular microbiology* 16:862-877.
45. Katz J, Zhang P, Martin M, Vogel SN, Michalek SM. 2006. Toll-like receptor 2 is required for inflammatory responses to *Francisella tularensis* LVS. *Infection and immunity* 74:2809-2816.
46. Thakran S, Li H, Lavine CL, Miller MA, Bina JE, Bina XR, Re F. 2008. Identification of *Francisella tularensis* lipoproteins that stimulate the toll-like receptor (TLR) 2/TLR1 heterodimer. *Journal of Biological chemistry* 283:3751-3760.

47. Li H, Nookala S, Bina XR, Bina JE, Re F. 2006. Innate immune response to *Francisella tularensis* is mediated by TLR2 and caspase-1 activation. *Journal of leukocyte biology* 80:766-773.
48. Dai S, Rajaram MV, Curry HM, Leander R, Schlesinger LS. 2013. Fine tuning inflammation at the front door: macrophage complement receptor 3-mediates phagocytosis and immune suppression for *Francisella tularensis*. *PLoS pathogens* 9.
49. Leander R, Dai S, Schlesinger LS, Friedman A. 2012. A mathematical model of CR3/TLR2 crosstalk in the context of *Francisella tularensis* infection. *PLoS computational biology* 8.
50. Mohapatra NP, Soni S, Rajaram MV, Dang PM-C, Reilly TJ, El-Benna J, Clay CD, Schlesinger LS, Gunn JS. 2010. *Francisella* acid phosphatases inactivate the NADPH oxidase in human phagocytes. *The Journal of Immunology* 184:5141-5150.
51. Schulert GS, McCaffrey RL, Buchan BW, Lindemann SR, Hollenback C, Jones BD, Allen L-AH. 2009. *Francisella tularensis* genes required for inhibition of the neutrophil respiratory burst and intramacrophage growth identified by random transposon mutagenesis of strain LVS. *Infection and immunity* 77:1324-1336.
52. Lindgren H, Shen H, Zingmark C, Golovliov I, Conlan W, Sjöstedt A. 2007. Resistance of *Francisella tularensis* strains against reactive nitrogen and oxygen species with special reference to the role of KatG. *Infection and immunity* 75:1303.
53. Melillo AA, Mahawar M, Sellati TJ, Malik M, Metzger DW, Melendez JA, Bakshi CS. 2009. Identification of *Francisella tularensis* live vaccine strain CuZn superoxide dismutase as critical for resistance to extracellularly generated reactive oxygen species. *Journal of bacteriology* 191:6447.
54. Bosio CM, Dow SW. 2005. *Francisella tularensis* induces aberrant activation of pulmonary dendritic cells. *The Journal of Immunology* 175:6792-6801.
55. Atkins HS, Dassa E, Walker NJ, Griffin KF, Harland DN, Taylor RR, Duffield ML, Titball RW. 2006. The identification and evaluation of ATP binding cassette systems in the intracellular bacterium *Francisella tularensis*. *Research in microbiology* 157:593-604.
56. Maier TM, Casey MS, Becker RH, Dorsey CW, Glass EM, Maltsev N, Zahrt TC, Frank DW. 2007. Identification of *Francisella tularensis* Himar1-based transposon mutants defective for replication in macrophages. *Infection and immunity* 75:5376.
57. Su J, Yang J, Zhao D, Kawula TH, Banas JA, Zhang J-R. 2007. Genome-wide identification of *Francisella tularensis* virulence determinants. *Infection and immunity* 75:3089.
58. Alkhuder K, Meibom KL, Dubail I, Dupuis M, Charbit A. 2009. Glutathione provides a source of cysteine essential for intracellular multiplication of *Francisella tularensis*. *PLoS Pathog* 5:e1000284.
59. Herzenberg LA, De Rosa SC, Dubs JG, Roederer M, Anderson MT, Ela SW, Deresinski SC, Herzenberg LA. 1997. Glutathione deficiency is associated with impaired survival in HIV disease. *Proceedings of the National Academy of Sciences* 94:1967-1972.
60. Steele S, Brunton J, Ziehr B, Taft-Benz S, Moorman N, Kawula T. 2013. *Francisella tularensis* harvests nutrients derived via ATG5-independent autophagy to support intracellular growth. *PLoS Pathog* 9:e1003562.
61. Woolard MD, Wilson JE, Hensley LL, Jania LA, Kawula TH, Drake JR, Frelinger JA. 2007. *Francisella tularensis*-infected macrophages release prostaglandin E2 that blocks T

- cell proliferation and promotes a Th2-like response. *The Journal of Immunology* 178:2065-2074.
62. Wilson JE, Katkere B, Drake JR. 2009. *Francisella tularensis* induces ubiquitin-dependent major histocompatibility complex class II degradation in activated macrophages. *Infection and immunity* 77:4953.
  63. Harris S. 1992. Japanese biological warfare research on humans: a case study of microbiology and ethics. *Annals of the New York Academy of Sciences* 666:21-52.
  64. Organization WH. 1970. Health aspects of chemical and biological weapons: report of a WHO group of consultants.
  65. Kaufmann AF, Meltzer MI, Schmid GP. 1997. The economic impact of a bioterrorist attack: are prevention and postattack intervention programs justifiable? *Emerging infectious diseases* 3:83.
  66. Foshay L, Hesselbrock W, Wittenberg H, Rodenberg A. 1942. Vaccine prophylaxis against tularemia in man. *American Journal of Public Health and the Nations Health* 32:1131-1145.
  67. Coriell LL, King EO, Smith MG. 1948. Studies on Tularemia. IV. Observations on Tularemia in Normal and Vaccinated Monkeys. *Journal of Immunology* 58:183-202.
  68. SASLAW S, EIGELSBACH HT, PRIOR JA, WILSON HE, CARHART S. 1961. Tularemia vaccine study: II. Respiratory challenge. *Archives of internal medicine* 107:702-714.
  69. Conlan JW, Shen H, Webb A, Perry MB. 2002. Mice vaccinated with the O-antigen of *Francisella tularensis* LVS lipopolysaccharide conjugated to bovine serum albumin develop varying degrees of protective immunity against systemic or aerosol challenge with virulent type A and type B strains of the pathogen. *Vaccine* 20:3465-3471.
  70. Fulop M, Manchee R, Titball R. 1995. Role of lipopolysaccharide and a major outer membrane protein from *Francisella tularensis* in the induction of immunity against tularemia. *Vaccine* 13:1220-1225.
  71. Surcel H-M, Sarvas M, Helander I, Herva E. 1989. Membrane proteins of *Francisella tularensis* LVS differ in ability to induce proliferation of lymphocytes from tularemia-vaccinated individuals. *Microbial pathogenesis* 7:411-419.
  72. Fulton KM, Zhao X, Petit MD, Kilmury SL, Wolfraim LA, House RV, Sjostedt A, Twine SM. 2011. Immunoproteomic analysis of the human antibody response to natural tularemia infection with Type A or Type B strains or LVS vaccination. *Int J Med Microbiol* 301:591-601.
  73. Sundaresh S, Randall A, Unal B, Petersen JM, Belisle JT, Gill Hartley M, Duffield M, Titball RW, Davies DH, Felgner PL. 2007. From protein microarrays to diagnostic antigen discovery: a study of the pathogen *Francisella tularensis*. *Bioinformatics* 23:i508-i518.
  74. Gaur R, Alam SI, Kamboj DV. 2017. Immunoproteomic Analysis of Antibody Response of Rabbit Host Against Heat-Killed *Francisella tularensis* Live Vaccine Strain. *Curr Microbiol* 74:499-507.
  75. Huntley JF, Conley PG, Rasko DA, Hagman KE, Apicella MA, Norgard MV. 2008. Native outer membrane proteins protect mice against pulmonary challenge with virulent type A *Francisella tularensis*. *Infection and immunity* 76:3664-3671.
  76. Chu P, Cunningham AL, Yu J-J, Nguyen JQ, Barker JR, Lyons CR, Wilder J, Valderas M, Sherwood RL, Arulanandam BP. 2014. Live attenuated *Francisella novicida* vaccine

- protects against *Francisella tularensis* pulmonary challenge in rats and non-human primates. *PLoS pathogens* 10:e1004439.
77. Andersson H, Hartmanová B, Bäck E, Eliasson H, Landfors M, Näslund L, Ryden P, Sjöstedt A. 2006. Transcriptional profiling of the peripheral blood response during tularemia. *Genes & Immunity* 7:503-513.
  78. Conlan JW, Zhao X, Harris G, Shen H, Bolanowski M, Rietz C, Sjöstedt A, Chen W. 2008. Molecular immunology of experimental primary tularemia in mice infected by respiratory or intradermal routes with type A *Francisella tularensis*. *Molecular immunology* 45:2962-2969.
  79. Elkins KL, Rhinehart-Jones TR, Culkin SJ, Yee D, Winegar RK. 1996. Minimal requirements for murine resistance to infection with *Francisella tularensis* LVS. *Infection and immunity* 64:3288.
  80. Leiby D, Fortier A, Crawford R, Schreiber R, Nacy C. 1992. In vivo modulation of the murine immune response to *Francisella tularensis* LVS by administration of anticytokine antibodies. *Infection and immunity* 60:84.
  81. Surcel H, Syrjälä H, Karttunen R, Tapaninaho S, Herva E. 1991. Development of *Francisella tularensis* antigen responses measured as T-lymphocyte proliferation and cytokine production (tumor necrosis factor alpha, gamma interferon, and interleukin-2 and-4) during human tularemia. *Infection and immunity* 59:1948-1953.
  82. Koskela P, Salminen A. 1985. Humoral immunity against *Francisella tularensis* after natural infection. *J Clin Microbiol* 22:973-9.
  83. Andersson H, Hartmanova B, KuoLee R, Ryden P, Conlan W, Chen W, Sjöstedt A. 2006. Transcriptional profiling of host responses in mouse lungs following aerosol infection with type A *Francisella tularensis*. *Journal of medical microbiology* 55:263-271.
  84. Anthony LS, Ghadirian E, Nestel FP, Kongshavn PA. 1989. The requirement for gamma interferon in resistance of mice to experimental tularemia. *Microbial pathogenesis* 7:421-428.
  85. De Pascalis R, Taylor BC, Elkins KL. 2008. Diverse myeloid and lymphoid cell subpopulations produce gamma interferon during early innate immune responses to *Francisella tularensis* live vaccine strain. *Infection and immunity* 76:4311.
  86. López MC, Duckett NS, Baron SD, Metzger DW. 2004. Early activation of NK cells after lung infection with the intracellular bacterium, *Francisella tularensis* LVS. *Cellular immunology* 232:75-85.
  87. Bokhari SM, Kim K-J, Pinson DM, Slusser J, Yeh H-W, Parmely MJ. 2008. NK cells and gamma interferon coordinate the formation and function of hepatic granulomas in mice infected with the *Francisella tularensis* live vaccine strain. *Infection and immunity* 76:1379.
  88. Fortier AH, Polsinelli T, Green SJ, Nacy CA. 1992. Activation of macrophages for destruction of *Francisella tularensis*: identification of cytokines, effector cells, and effector molecules. *Infection and immunity* 60:817.
  89. Anthony L, Morrissey P, Nano F. 1992. Growth inhibition of *Francisella tularensis* live vaccine strain by IFN-gamma-activated macrophages is mediated by reactive nitrogen intermediates derived from L-arginine metabolism. *The Journal of Immunology* 148:1829-1834.

90. Lindgren H, Stenmark S, Chen W, Tärnvik A, Sjöstedt A. 2004. Distinct roles of reactive nitrogen and oxygen species to control infection with the facultative intracellular bacterium *Francisella tularensis*. *Infection and immunity* 72:7172.
91. Sjöstedt A, Conlan JW, North RJ. 1994. Neutrophils are critical for host defense against primary infection with the facultative intracellular bacterium *Francisella tularensis* in mice and participate in defense against reinfection. *Infection and immunity* 62:2779.
92. Conlan JW, KuoLee R, Shen H, Webb A. 2002. Different host defences are required to protect mice from primary systemic vs pulmonary infection with the facultative intracellular bacterial pathogen, *Francisella tularensis* LVS. *Microbial pathogenesis* 32:127-134.
93. Fernandes-Alnemri T, Yu J-W, Juliana C, Solorzano L, Kang S, Wu J, Datta P, McCormick M, Huang L, McDermott E. 2010. The AIM2 inflammasome is critical for innate immunity to *Francisella tularensis*. *Nature immunology* 11:385.
94. Mariathasan S, Weiss DS, Dixit VM, Monack DM. 2005. Innate immunity against *Francisella tularensis* is dependent on the ASC/caspase-1 axis. *The Journal of experimental medicine* 202:1043-1049.
95. Lavine CL, Clinton SR, Angelova-Fischer I, Marion TN, Bina XR, Bina JE, Whitt MA, Miller MA. 2007. Immunization with heat-killed *Francisella tularensis* LVS elicits protective antibody-mediated immunity. *Eur J Immunol* 37:3007-20.
96. Green TW, Eigelsbach HT. 1950. Immunity in tularemia; report of 2 cases of proved reinfection. *Arch Intern Med (Chic)* 85:777-82.
97. Twine SM, Petit MD, Shen H, Mykytczuk NC, Kelly JF, Conlan JW. 2006. Immunoproteomic analysis of the murine antibody response to successful and failed immunization with live anti-*Francisella* vaccines. *Biochemical and biophysical research communications* 346:999-1008.
98. Elkins KL, Bosio CM, Rhinehart-Jones TR. 1999. Importance of B cells, but not specific antibodies, in primary and secondary protective immunity to the intracellular bacterium *Francisella tularensis* live vaccine strain. *Infection and immunity* 67:6002.
99. Chen W, KuoLee R, Shen H, Conlan JW. 2004. Susceptibility of immunodeficient mice to aerosol and systemic infection with virulent strains of *Francisella tularensis*. *Microbial pathogenesis* 36:311-318.
100. Bosio CM, Elkins KL. 2001. Susceptibility to secondary *Francisella tularensis* live vaccine strain infection in B-cell-deficient mice is associated with neutrophilia but not with defects in specific T-cell-mediated immunity. *Infection and Immunity* 69:194.
101. Cowley SC, Meierovics AI, Frelinger JA, Iwakura Y, Elkins KL. 2010. Lung CD4<sup>-</sup>CD8<sup>-</sup> double-negative T cells are prominent producers of IL-17A and IFN- $\gamma$  during primary respiratory murine infection with *Francisella tularensis* live vaccine strain. *The Journal of Immunology* 184:5791-5801.
102. Cowley SC, Hamilton E, Frelinger JA, Su J, Forman J, Elkins KL. 2005. CD4<sup>-</sup>CD8<sup>-</sup> T cells control intracellular bacterial infections both in vitro and in vivo. *The Journal of experimental medicine* 202:309-319.
103. Woolard MD, Hensley LL, Kawula TH, Frelinger JA. 2008. Respiratory *Francisella tularensis* live vaccine strain infection induces Th17 cells and prostaglandin E2, which inhibits generation of gamma interferon-positive T cells. *Infection and immunity* 76:2651-2659.

104. Sjöstedt A, North RJ, Conlan JW. 1996. The requirement of tumour necrosis factor- $\alpha$  and interferon- $\gamma$  for the expression of protective immunity to secondary murine tularaemia depends on the size of the challenge inoculum. *Microbiology* 142:1369-1374.
105. Cowley SC, Elkins KL. 2003. Multiple T cell subsets control *Francisella tularensis* LVS intracellular growth without stimulation through macrophage interferon  $\gamma$  receptors. *The Journal of experimental medicine* 198:379-389.
106. Cowley SC, Sedgwick JD, Elkins KL. 2007. Differential requirements by CD4+ and CD8+ T cells for soluble and membrane TNF in control of *Francisella tularensis* live vaccine strain intramacrophage growth. *The Journal of Immunology* 179:7709-7719.
107. Elkins KL, Colombini SM, Meierovics AI, Chu MC, Chou AY, Cowley SC. 2010. Survival of secondary lethal systemic *Francisella* LVS challenge depends largely on interferon gamma. *Microbes and infection* 12:28-36.
108. Conlan JW, Shen H, KuoLee R, Zhao X, Chen W. 2005. Aerosol-, but not intradermal-immunization with the live vaccine strain of *Francisella tularensis* protects mice against subsequent aerosol challenge with a highly virulent type A strain of the pathogen by an  $\alpha\beta$  T cell-and interferon gamma-dependent mechanism. *Vaccine* 23:2477-2485.
109. Wu TH, Hutt JA, Garrison KA, Berliba LS, Zhou Y, Lyons CR. 2005. Intranasal vaccination induces protective immunity against intranasal infection with virulent *Francisella tularensis* biovar A. *Infection and immunity* 73:2644-2654.
110. Bakshi CS, Malik M, Mahawar M, Kirimanjeswara GS, Hazlett KR, Palmer LE, Furie MB, Singh R, Melendez JA, Sellati TJ. 2008. An improved vaccine for prevention of respiratory tularemia caused by *Francisella tularensis* SchuS4 strain. *Vaccine* 26:5276-5288.
111. Salerno-Gonçalves R, Hepburn MJ, Bavari S, Sztejn MB. 2009. Generation of heterogeneous memory T cells by live attenuated tularemia vaccine in humans. *Vaccine* 28:195-206.
112. Griffin AJ, Crane DD, Wehrly TD, Bosio CMJC, Immunology V. 2015. Successful protection against tularemia in C57BL/6 mice is correlated with expansion of *Francisella tularensis*-specific effector T cells. 22:119-128.
113. Cunningham AL, Mann BJ, Qin A, Santiago AE, Grassel C, Lipsky M, Vogel SN, Barry EM. 2020. Characterization of Schu S4 aro mutants as live attenuated tularemia vaccine candidates. *Virulence* 11:283-294.
114. Aebersold P. 2011. FDA experience with medical countermeasures under the animal rule. *Advances in preventive medicine* 2012.
115. Snoy P. 2010. Establishing Efficacy of Human Products Using Animals The US Food and Drug Administration's "Animal Rule". *Veterinary Pathology Online* 47:774-778.
116. Burns DL. 2012. Licensure of vaccines using the Animal Rule. *Current opinion in virology* 2:353-356.
117. Food and Drug Administration. 2014. Guidance for Industry: Product Development Under the Animal Rule.
118. Ancuta P, Pedron T, Girard R, Sandström G, Chaby R. 1996. Inability of the *Francisella tularensis* lipopolysaccharide to mimic or to antagonize the induction of cell activation by endotoxins. *Infection and immunity* 64:2041-2046.
119. Matyas BT, Nieder HS, TELFORD III SR. 2007. Pneumonic tularemia on Martha's Vineyard: clinical, epidemiologic, and ecological characteristics. *Annals of the New York Academy of Sciences* 1105:351-377.

120. McCrumb Jr FR. 1961. Aerosol infection of man with *Pasteurella tularensis*. *Bacteriological reviews* 25:262.
121. Stuart B, Pullen R. 1945. Tularemic Pneumonia. Review of American Literature and Report of 15 Additional Cases. *American Journal of Medical Sciences* 210:223-36.
122. Dembek ZF, Buckman RL, Fowler SK, Hadler JL. 2003. Missed sentinel case of naturally occurring pneumonic tularemia outbreak: lessons for detection of bioterrorism. *The Journal of the American Board of Family Practice* 16:339-342.
123. Fredricks DN, Remington JS. 1996. Tularemia presenting as community-acquired pneumonia: implications in the era of managed care. *Archives of internal medicine* 156:2137-2140.
124. Francis E. 1928. Symptoms, diagnosis and pathology of tularemia. *Journal of the American Medical Association* 91:1155-1161.
125. Westerman E, McDONALD J. 1983. Tularemia pneumonia mimicking legionnaires' disease: isolation of organism on CYE agar and successful treatment with erythromycin. *Southern medical journal* 76:1169-1170.
126. Baskerville A, Hambleton P, Dowsett A. 1978. The pathology of untreated and antibiotic-treated experimental tularaemia in monkeys. *British journal of experimental pathology* 59:615.
127. Day WC, Berendt RF. 1972. Experimental tularemia in *Macaca mulatta*: relationship of aerosol particle size to the infectivity of airborne *Pasteurella tularensis*. *Infection and immunity* 5:77-82.
128. Nelson M, Lever MS, Savage VL, Salguero FJ, Pearce PC, Stevens DJ, Simpson AJ. 2009. Establishment of lethal inhalational infection with *Francisella tularensis* (tularaemia) in the common marmoset (*Callithrix jacchus*). *International journal of experimental pathology* 90:109-118.
129. Glynn AR, Alves DA, Frick O, Erwin-Cohen R, Porter A, Norris S, Waag D, Nalca A. 2015. Comparison of experimental respiratory tularemia in three nonhuman primate species. *Comparative immunology, microbiology and infectious diseases* 39:13-24.
130. Valderas M, Zinter E, Brasel T, Barr E, Hutt J. Characterization of aerosol infection with *F. tularensis* Schu S4 in cynomolgus macaques and LD50 determination, p. *In* (ed),
131. Hambleton P, Baskerville A, Harris-Smith P, Bailey N. 1978. Changes in whole blood and serum components of grivet monkeys with experimental respiratory *Francisella tularensis* infection. *British journal of experimental pathology* 59:630.
132. Sawyer WD, Dangerfield HG, Hogge AL, Crozier D. 1966. Antibiotic prophylaxis and therapy of airborne tularemia. *Bacteriological reviews* 30:542.
133. White JD, Rooney JR, Prickett PA, Derrenbacher EB, Beard CW, Griffith WR. 1964. Pathogenesis of experimental respiratory tularemia in monkeys. *The Journal of infectious diseases*:277-283.
134. Nelson M, Lever MS, Dean RE, Savage VL, Salguero FJ, Pearce PC, Stevens DJ, Simpson AJ. 2010. Characterization of lethal inhalational infection with *Francisella tularensis* in the common marmoset (*Callithrix jacchus*). *Journal of medical microbiology* 59:1107.
135. Guina T, Lanning LL, Omland KS, Williams MS, Wolfraim LA, Heyse SP, Houchens CR, Sanz P, Hewitt JA. 2018. The cynomolgus macaque natural history model of pneumonic tularemia for predicting clinical efficacy under the animal rule. *Frontiers in cellular and infection microbiology* 8:99.

136. Frick OM, Livingston VA, Whitehouse CA, Norris SL, Alves DA, Facemire PR, Reed DS, Nalca A. 2021. The Natural History of Aerosolized *Francisella tularensis* Infection in *Cynomolgus* Macaques. *Pathogens* 10:597.
137. Twine SM, Shen H, Kelly JF, Chen W, Sjöstedt A, Conlan JW. 2006. Virulence comparison in mice of distinct isolates of type A *Francisella tularensis*. *Microbial pathogenesis* 40:133-138.
138. Conlan JW, Shen H, Golovliov I, Zingmark C, Oyston PC, Chen W, House RV, Sjöstedt A. 2010. Differential ability of novel attenuated targeted deletion mutants of *Francisella tularensis* subspecies *tularensis* strain SCHU S4 to protect mice against aerosol challenge with virulent bacteria: effects of host background and route of immunization. *Vaccine* 28:1824-1831.
139. Shen H, Harris G, Chen W, Sjöstedt A, Ryden P, Conlan W. 2010. Molecular immune responses to aerosol challenge with *Francisella tularensis* in mice inoculated with live vaccine candidates of varying efficacy. *PloS one* 5:e13349.
140. Conlan JW, Chen W, Shen H, Webb A, KuoLee R. 2003. Experimental tularemia in mice challenged by aerosol or intradermally with virulent strains of *Francisella tularensis*: bacteriologic and histopathologic studies. *Microbial pathogenesis* 34:239-248.
141. Forestal CA, Malik M, Catlett SV, Savitt AG, Benach JL, Sellati TJ, Furie MB. 2007. *Francisella tularensis* has a significant extracellular phase in infected mice. *The Journal of infectious diseases* 196:134-137.
142. Raymond CR, Conlan JW. 2009. Differential susceptibility of Sprague–Dawley and Fischer 344 rats to infection by *Francisella tularensis*. *Microbial pathogenesis* 46:231-234.
143. Ray HJ, Chu P, Wu TH, Lyons CR, Murthy AK, Guentzel MN, Klose KE, Arulanandam BP. 2010. The Fischer 344 rat reflects human susceptibility to *Francisella* pulmonary challenge and provides a new platform for virulence and protection studies. *PLoS One* 5:e9952.
144. Hutt JA, Lovchik JA, Dekonenko A, Hahn AC, Wu TH. 2017. The Natural History of Pneumonic Tularemia in Female Fischer 344 Rats after Inhalational Exposure to Aerosolized *Francisella tularensis* Subspecies *tularensis* Strain SCHU S4. *Am J Pathol* 187:252-267.
145. Olsufiev N, Emelyanova O, Dunayeva T. 1959. Comparative study of strains of *B. tularensis* in the old and new world and their taxonomy. *J Hyg, Epidemiol, Microbiol & Immunol* 3:138-49.
146. Reed DS, Smith LK, Dunsmore T, Trichel A, Ortiz LA, Cole KS, Barry EJ. 2011. Pneumonic tularemia in rabbits resembles the human disease as illustrated by radiographic and hematological changes after infection. *PLoS one* 6:e24654.
147. Baskerville A, Hambleton P. 1976. Pathogenesis and pathology of respiratory tularaemia in the rabbit. *British journal of experimental pathology* 57:339.
148. Yamane K, Leung KP. 2016. Rabbit M1 and M2 macrophages can be induced by human recombinant GM-CSF and M-CSF. *FEBS Open Bio* 6:945-53.
149. Kamaruzaman NA, Kardia E, Kamaldin N, Latahir AZ, Yahaya BH. 2013. The rabbit as a model for studying lung disease and stem cell therapy. *Biomed Res Int* 2013:691830.
150. Textoris J, Ban LH, Capo C, Raoult D, Leone M, Mege J-L. 2010. Sex-related differences in gene expression following *Coxiella burnetii* infection in mice: potential role of circadian rhythm. *PloS one* 5.

151. Queen AE, Moerdyk-Schauwecker M, McKee LM, Leamy LJ, Huet YM. 2016. Differential expression of inflammatory cytokines and stress genes in male and female mice in response to a lipopolysaccharide challenge. *PLoS One* 11.
152. Rathod KS, Kapil V, Velmurugan S, Khambata RS, Siddique U, Khan S, Van Eijl S, Gee LC, Bansal J, Pitrola K. 2017. Accelerated resolution of inflammation underlies sex differences in inflammatory responses in humans. *The Journal of clinical investigation* 127:169-182.
153. Maret A, Coudert JD, Garidou L, Foucras G, Gourdy P, Krust A, Dupont S, Chambon P, Druet P, Bayard F. 2003. Estradiol enhances primary antigen-specific CD4 T cell responses and Th1 development in vivo. Essential role of estrogen receptor  $\alpha$  expression in hematopoietic cells. *European journal of immunology* 33:512-521.
154. Soucy G, Boivin G, Labrie F, Rivest S. 2005. Estradiol is required for a proper immune response to bacterial and viral pathogens in the female brain. *The Journal of Immunology* 174:6391-6398.
155. Butts CL, Shukair SA, Duncan KM, Bowers E, Horn C, Belyavskaya E, Tonelli L, Sternberg EM. 2007. Progesterone inhibits mature rat dendritic cells in a receptor-mediated fashion. *International immunology* 19:287-296.
156. Zhao X, Liu L, Liu D, Fan H, Wang Y, Hu Y, Hou Y. 2012. Progesterone Enhances Immunoregulatory Activity of Human Mesenchymal Stem Cells Via PGE 2 and IL-6. *American Journal of Reproductive Immunology* 68:290-300.
157. Lai J-J, Lai K-P, Chuang K-H, Chang P, Yu I-C, Lin W-J, Chang C. 2009. Monocyte/macrophage androgen receptor suppresses cutaneous wound healing in mice by enhancing local TNF- $\alpha$  expression. *The Journal of clinical investigation* 119:3739-3751.
158. Roden AC, Moser MT, Tri SD, Mercader M, Kuntz SM, Dong H, Hurwitz AA, McKean DJ, Celis E, Leibovich BC. 2004. Augmentation of T cell levels and responses induced by androgen deprivation. *The Journal of Immunology* 173:6098-6108.
159. Page ST, Plymate SR, Bremner WJ, Matsumoto AM, Hess DL, Lin DW, Amory JK, Nelson PS, Wu JD. 2006. Effect of medical castration on CD4+ CD25+ T cells, CD8+ T cell IFN- $\gamma$  expression, and NK cells: a physiological role for testosterone and/or its metabolites. *American Journal of Physiology-Endocrinology and Metabolism* 290:E856-E863.
160. Robinson DP, Lorenzo ME, Jian W, Klein SL. 2011. Elevated 17 $\beta$ -estradiol protects females from influenza A virus pathogenesis by suppressing inflammatory responses. *PLoS pathogens* 7.
161. Lyden D, Olszewski J, Feran M, Job L, Huber S. 1987. Coxsackievirus B-3-induced myocarditis. Effect of sex steroids on viremia and infectivity of cardiocytes. *The American journal of pathology* 126:432.
162. Klingström J, Lindgren T, Ahlm C. 2008. Sex-dependent differences in plasma cytokine responses to hantavirus infection. *Clin Vaccine Immunol* 15:885-887.
163. Channappanavar R, Fett C, Mack M, Ten Eyck PP, Meyerholz DK, Perlman S. 2017. Sex-based differences in susceptibility to severe acute respiratory syndrome coronavirus infection. *The Journal of Immunology* 198:4046-4053.
164. Ashtekar AR, Zhang P, Katz J, Deivanayagam CC, Rallabhandi P, Vogel SN, Michalek SM. 2008. TLR4-mediated activation of dendritic cells by the heat shock protein DnaK from *Francisella tularensis*. *Journal of leukocyte biology* 84:1434-1446.

165. Sunagar R, Kumar S, Franz BJ, Gosselin EJ. 2016. Vaccination evokes gender-dependent protection against tularemia infection in C57BL/6Tac mice. *Vaccine* 34:3396-3404.
166. Faith S, Smith LK, Swatland A, Reed DS. 2012. Growth conditions and environmental factors impact aerosolization but not virulence of *Francisella tularensis* infection in mice. *Frontiers in cellular and infection microbiology* 2:126.
167. Wu TH, Zsemlye JL, Statom GL, Hutt JA, Schrader RM, Scrymgeour AA, Lyons CR. 2009. Vaccination of Fischer 344 rats against pulmonary infections by *Francisella tularensis* type A strains. *Vaccine* 27:4684-4693.
168. Hazlett KR, Caldon SD, McArthur DG, Cirillo KA, Kirimanjeswara GS, Magguilli ML, Malik M, Shah A, Broderick S, Golovliov I. 2008. Adaptation of *Francisella tularensis* to the mammalian environment is governed by cues which can be mimicked in vitro. *Infection and immunity* 76:4479-4488.
169. Holland KM, Rosa SJ, Kristjansdottir K, Wolfgeher D, Franz BJ, Zarrella TM, Kumar S, Sunagar R, Singh A, Bakshi CS. 2017. Differential growth of *Francisella tularensis*, which alters expression of virulence factors, dominant antigens, and surface-carbohydrate synthases, governs the apparent virulence of Ft SchuS4 to immunized animals. *Frontiers in microbiology* 8:1158.
170. Johansson A, Farlow J, Larsson P, Dukerich M, Chambers E, Byström M, Fox J, Chu M, Forsman M, Sjöstedt A. 2004. Worldwide genetic relationships among *Francisella tularensis* isolates determined by multiple-locus variable-number tandem repeat analysis. *Journal of bacteriology* 186:5808-5818.
171. Mares CA, Ojeda SS, Morris EG, Li Q, Teale JM. 2008. Initial delay in the immune response to *Francisella tularensis* is followed by hypercytokinemia characteristic of severe sepsis and correlating with upregulation and release of damage-associated molecular patterns. *Infection and immunity* 76:3001-3010.
172. Kugeler KJ, Mead PS, Janusz AM, Staples JE, Kubota KA, Chalcraft LG, Petersen JM. 2009. Molecular epidemiology of *Francisella tularensis* in the United States. *Clinical Infectious Diseases* 48:863-870.
173. Molins CR, Delorey MJ, Yockey BM, Young JW, Sheldon SW, Reese SM, Schriefer ME, Petersen JM. 2010. Virulence differences among *Francisella tularensis* subsp. *tularensis* clades in mice. *PLoS One* 5:e10205.
174. Champion MD, Zeng Q, Nix EB, Nano FE, Keim P, Kodira CD, Borowsky M, Young S, Koehrsen M, Engels R. 2009. Comparative genomic characterization of *Francisella tularensis* strains belonging to low and high virulence subspecies. *PLoS Pathog* 5:e1000459.
175. Lovchik JA, Reed DS, Hutt JA, Xia F, Stevens RL, Modise T, Barry EM, Wu TH. 2021. Identification of an Attenuated Substrain of *Francisella tularensis* SCHU S4 by Phenotypic and Genotypic Analyses. *Pathogens* 10:638.
176. Chen W, Shen H, Webb A, KuoLee R, Conlan JW. 2003. Tularemia in BALB/c and C57BL/6 mice vaccinated with *Francisella tularensis* LVS and challenged intradermally, or by aerosol with virulent isolates of the pathogen: protection varies depending on pathogen virulence, route of exposure, and host genetic background. *Vaccine* 21:3690-3700.
177. Reed DS, Le’Kneitah PS, Cole KS, Santiago AE, Mann BJ, Barry EMJI, immunity. 2014. Live attenuated mutants of *Francisella tularensis* protect rabbits against aerosol challenge with a virulent type A strain. *IAI*. 01498-14.

178. Pasetti MF, Cuberos L, Horn TL, Shearer JD, Matthews SJ, House RV, Sztein MB. 2008. An improved *Francisella tularensis* live vaccine strain (LVS) is well tolerated and highly immunogenic when administered to rabbits in escalating doses using various immunization routes. *Vaccine* 26:1773-1785.
179. Lowe DC, Savidge TC, Pickard D, Eckmann L, Kagnoff MF, Dougan G, Chatfield SN. 1999. Characterization of candidate live oral *Salmonella typhi* vaccine strains harboring defined mutations in *aroA*, *aroC*, and *htrA*. *Infection and immunity* 67:700.
180. O'Malley KJ, Bowling JL, Stinson E, Cole KS, Mann BJ, Namjoshi P, Hazlett KR, Barry EM, Reed DSJ. 2018. Aerosol prime-boost vaccination provides strong protection in outbred rabbits against virulent type A *Francisella tularensis*. *PLoS Pathogens* 13:e0205928.
181. Tesfa-Selase F, Drabble WT. 1992. Regulation of the *gua* operon of *Escherichia coli* by the DnaA protein. *Molecular and General Genetics* 231:256-264.
182. Santiago AE, Mann BJ, Qin A, Cunningham AL, Cole LE, Grassel C, Vogel SN, Levine MM, Barry EM. 2015. Characterization of *Francisella tularensis* Schu S4 defined mutants as live-attenuated vaccine candidates. *Pathogens and disease* 73.
183. Turner AK, Lovell MA, Hulme SD, Zhang-Barber L, Barrow PA. 1998. Identification of *Salmonella typhimurium* genes required for colonization of the chicken alimentary tract and for virulence in newly hatched chicks. *Infection and immunity* 66:2099-2106.
184. Chastanet A, Derre I, Nair S, Msadek T. 2004. *clpB*, a novel member of the *Listeria monocytogenes* CtsR regulon, is involved in virulence but not in general stress tolerance. *Am Soc Microbiol*.
185. Alam A, Golovliov I, Javed E, Kumar R, Ådén J, Sjöstedt A. 2020. Dissociation between the critical role of ClpB of *Francisella tularensis* for the heat shock response and the DnaK interaction and its important role for efficient type VI secretion and bacterial virulence. *PLoS pathogens* 16:e1008466.
186. Meibom KL, Dubail I, Dupuis M, Barel M, Lenco J, Stulik J, Golovliov I, Sjöstedt A, Charbit A. 2008. The heat-shock protein ClpB of *Francisella tularensis* is involved in stress tolerance and is required for multiplication in target organs of infected mice. *Molecular microbiology* 67:1384-1401.
187. Ryden P, Twine S, Shen H, Harris G, Chen W, Sjöstedt A, Conlan W. 2013. Correlates of protection following vaccination of mice with gene deletion mutants of *Francisella tularensis* subspecies *tularensis* strain, SCHU S4 that elicit varying degrees of immunity to systemic and respiratory challenge with wild-type bacteria. *Molecular Immunology* 54:58-67.
188. Clements M, Murphy BR. 1986. Development and persistence of local and systemic antibody responses in adults given live attenuated or inactivated influenza A virus vaccine. *Vaccine* 23:66-72.
189. Belshe RB, Edwards KM, Vesikari T, Black SV, Walker RE, Hultquist M, Kemble G, Connor EM. 2007. Live attenuated versus inactivated influenza vaccine in infants and young children. *Vaccine* 25:685-696.
190. Faden H, Modlin JF, Thoms ML, McBean AM, Ferdon MB, Ogra PL. 1990. Comparative evaluation of immunization with live attenuated and enhanced-potency inactivated trivalent poliovirus vaccines in childhood: systemic and local immune responses. *Vaccine* 16:1291-1297.

191. Jahrling PB, Stephenson EHJocm. 1984. Protective efficacies of live attenuated and formaldehyde-inactivated Venezuelan equine encephalitis virus vaccines against aerosol challenge in hamsters. 19:429-431.
192. Putnak JR, Collier B-A, Voss G, Vaughn DW, Clements D, Peters I, Bignami G, Hough H-S, Chen RC-M, Barvir DAJV. 2005. An evaluation of dengue type-2 inactivated, recombinant subunit, and live-attenuated vaccine candidates in the rhesus macaque model. 23:4442-4452.
193. Kadull PJ, Reames HR, Coriell LL, Foshay L. 1950. Studies on tularemia. V. Immunization of man. *Journal of Immunology* 65:425-35.
194. Baron SD, Singh R, Metzger DW. 2007. Inactivated *Francisella tularensis* live vaccine strain protects against respiratory tularemia by intranasal vaccination in an immunoglobulin A-dependent fashion. *Infection and immunity* 75:2152-2162.
195. Gordon M, Donaldson DM, Wright GG. 1964. Immunization of mice with irradiated *Pasteurella tularensis*. *The Journal of infectious diseases*:435-440.
196. Klimpel GR, Eaves-Pyles T, Moen ST, Taormina J, Peterson JW, Chopra AK, Niesel DW, Carness P, Haithcoat JL, Kirtley M. 2008. Levofloxacin rescues mice from lethal intra-nasal infections with virulent *Francisella tularensis* and induces immunity and production of protective antibody. *Vaccine* 26:6874-6882.
197. Demento SL, Eisenbarth SC, Foellmer HG, Platt C, Caplan MJ, Saltzman WM, Mellman I, Ledizet M, Fikrig E, Flavell RA. 2009. Inflammasome-activating nanoparticles as modular systems for optimizing vaccine efficacy. *Vaccine* 27:3013-3021.
198. Dotson RJ, Rabadi SM, Westcott EL, Bradley S, Catlett SV, Banik S, Harton JA, Bakshi CS, Malik M. 2013. Repression of inflammasome by *Francisella tularensis* during early stages of infection. *Journal of Biological Chemistry* 288:23844-23857.
199. Li H, Willingham SB, Ting JP-Y, Re F. 2008. Cutting edge: inflammasome activation by alum and alum's adjuvant effect are mediated by NLRP3. *The Journal of Immunology* 181:17-21.
200. van de Veerdonk FL, Joosten LA, Shaw PJ, Smeekens SP, Malireddi RS, van der Meer JW, Kullberg BJ, Netea MG, Kanneganti TD. 2011. The inflammasome drives protective Th1 and Th17 cellular responses in disseminated candidiasis. *European journal of immunology* 41:2260-2268.
201. Saiga H, Nieuwenhuizen N, Gengenbacher M, Koehler A-B, Schuerer S, Moura-Alves P, Wagner I, Mollenkopf H-J, Dorhoi A, Kaufmann SH. 2015. The Recombinant BCG  $\Delta$ ureC::hly vaccine targets the AIM2 inflammasome to induce autophagy and inflammation. *The Journal of infectious diseases* 211:1831-1841.
202. Tsuchiya K, Hara H, Kawamura I, Nomura T, Yamamoto T, Daim S, Dewamitta SR, Shen Y, Fang R, Mitsuyama M. 2010. Involvement of absent in melanoma 2 in inflammasome activation in macrophages infected with *Listeria monocytogenes*. *The Journal of Immunology* 185:1186-1195.
203. Warren SE, Armstrong A, Hamilton MK, Mao DP, Leaf IA, Miao EA, Aderem A. 2010. Cutting edge: Cytosolic bacterial DNA activates the inflammasome via Aim2. *The Journal of Immunology* 185:818-821.
204. Sauer J-D, Pereyre S, Archer KA, Burke TP, Hanson B, Lauer P, Portnoy DA. 2011. *Listeria monocytogenes* engineered to activate the Nlrc4 inflammasome are severely attenuated and are poor inducers of protective immunity. *Proceedings of the National Academy of Sciences* 108:12419-12424.

205. Henry T, Brotcke A, Weiss DS, Thompson LJ, Monack DM. 2007. Type I interferon signaling is required for activation of the inflammasome during *Francisella* infection. *The Journal of experimental medicine* 204:987-994.
206. Jones JW, Kayagaki N, Broz P, Henry T, Newton K, O'Rourke K, Chan S, Dong J, Qu Y, Roose-Girma M. 2010. Absent in melanoma 2 is required for innate immune recognition of *Francisella tularensis*. *Proceedings of the National Academy of Sciences* 107:9771-9776.
207. Wickstrum JR, Hong K-J, Bokhari S, Reed N, McWilliams N, Horvat RT, Parmely MJ. 2007. Coactivating signals for the hepatic lymphocyte gamma interferon response to *Francisella tularensis*. *Infection and immunity* 75:1335-1342.
208. del Barrio L, Sahoo M, Lantier L, Reynolds JM, Ceballos-Olvera I, Re F. 2015. Production of anti-LPS IgM by B1a B cells depends on IL-1 $\beta$  and is protective against lung infection with *Francisella tularensis* LVS. *PLoS pathogens* 11.
209. Atianand MK, Duffy EB, Shah A, Kar S, Malik M, Harton JA. 2011. *Francisella tularensis* reveals a disparity between human and mouse NLRP3 inflammasome activation. *Journal of Biological Chemistry* 286:39033-39042.
210. Roy CJ, Pitt ML. 2012. Infectious Disease Aerobiology: Aerosol Challenge Methods, p 65-79. *In* Swearingen JR (ed), *Biodefense Research Methodology and Animal Models*, 2 ed. CRC Press.
211. Saini D, Hopkins GW, Chen C-j, Seay SA, Click EM, Lee S, Hartings JM, Frothingham R. 2011. Sampling port for real-time analysis of bioaerosol in whole body exposure system for animal aerosol model development. *Journal of pharmacological and toxicological methods* 63:143-149.
212. Schnupf P, Sansonetti PJ. 2012. Quantitative RT-PCR profiling of the rabbit immune response: assessment of acute *Shigella flexneri* infection. *PLoS One* 7:e36446.
213. Uddin MJ, Suen WW, Prow NA, Hall RA, Bielefeldt-Ohmann H. 2015. West Nile virus challenge alters the transcription profiles of innate immune genes in rabbit peripheral blood mononuclear cells. *Frontiers in veterinary science* 2:76.
214. Lee C-H, Jeong T-S, Choi Y-K, Hyun B-H, Oh G-T, Kim E-H, Kim J-R, Han J-I, Bok S-H. 2001. Anti-atherogenic effect of citrus flavonoids, naringin and naringenin, associated with hepatic ACAT and aortic VCAM-1 and MCP-1 in high cholesterol-fed rabbits. *Biochemical and biophysical research communications* 284:681-688.
215. O'Malley KJ, Bowling JD, Barry EM, Hazlett KRO, Reed DS. 2019. Development, characterization and standardization of a nose-only inhalation exposure system for exposure of rabbits to small particle aerosols containing *Francisella tularensis*. *Infection and Immunity* doi:10.1128/iai.00198-19:IAI.00198-19.
216. Stinson E, Smith LP, Cole KS, Barry EM, Reed DS. 2016. Respiratory and oral vaccination improves protection conferred by the live vaccine strain against pneumonic tularemia in the rabbit model. *Pathog Dis* 74.
217. Conlan JW, Sjöstedt A, Gelhaus HC, Fleming P, McRae K, Cobb RR, De Pascalis R, Elkins KL. 2021. Modern Development and Production of a New Live Attenuated Bacterial Vaccine, SCHU S4  $\Delta$ clpB, to Prevent Tularemia. *Pathogens* 10:795.
218. Budak YU, Polat M, Huysal K. 2016. The use of platelet indices, plateletcrit, mean platelet volume and platelet distribution width in emergency non-traumatic abdominal surgery: a systematic review. *Biochemia medica* 26:178-193.

219. Zhang S, Cui Y-L, Diao M-Y, Chen D-C, Lin Z-F. 2015. Use of platelet indices for determining illness severity and predicting prognosis in critically ill patients. *Chinese medical journal* 128:2012.
220. Horzempa J, O'Dee DM, Stolz DB, Franks JM, Clay D, Nau GJ. 2011. Invasion of erythrocytes by *Francisella tularensis*. *Journal of Infectious Diseases* 204:51-59.
221. Ramos Muniz MG, Palfreeman M, Setzu N, Sanchez MA, Saenz Portillo P, Garza KM, Gosselink KL, Spencer CT. 2018. Obesity Exacerbates the Cytokine Storm Elicited by *Francisella tularensis* Infection of Females and Is Associated with Increased Mortality. *Biomed Res Int* 2018:3412732.
222. D'Elia RV, Harrison K, Oyston PC, Lukaszewski RA, Clark GC. 2013. Targeting the “cytokine storm” for therapeutic benefit. *Clinical and Vaccine Immunology* 20:319-327.
223. Wang Z, Zhang J, Li H, Li J, Niimi M, Ding G, Chen H, Xu J, Zhang H, Xu Z. 2016. Hyperlipidemia-associated gene variations and expression patterns revealed by whole-genome and transcriptome sequencing of rabbit models. *Scientific reports* 6:1-10.
224. Zhou L, Xiao Q, Bi J, Wang Z, Li Y. 2018. RabGTD: a comprehensive database of rabbit genome and transcriptome. *Database* 2018.
225. Fontanesi L, Martelli P, Scotti E, Russo V, Rogel-Gaillard C, Casadio R, Vernesi C. 2012. Exploring copy number variation in the rabbit (*Oryctolagus cuniculus*) genome by array comparative genome hybridization. *Genomics* 100:245-251.
226. Roth KM, Gunn JS, Lafuse W, Satoskar AR. 2009. *Francisella* inhibits STAT1-mediated signaling in macrophages and prevents activation of antigen-specific T cells. *International immunology* 21:19-28.